



جامعة بيروت العربية  
BEIRUT ARAB UNIVERSITY

# **Multiple-Valued Logic Circuit Design and Data Transmission Intended for Embedded Systems**

by

**RAMZI ALI JABER**

**Thesis**

*Submitted in Partial Fulfilment of the Requirements for the degree of  
PhD in Computer Engineering*

Department of [Electrical & Computer Engineering](#)  
Faculty of [Engineering](#)

2020



جامعة بيروت العربية  
BEIRUT ARAB UNIVERSITY

# **Multiple-Valued Logic Circuit Design and Data Transmission Intended for Embedded Systems**

by

**RAMZI ALI JABER**

**Thesis**

*Submitted in Partial Fulfilment of the Requirements for the degree of  
PhD in Computer Engineering*

Department of [Electrical & Computer Engineering](#)  
Faculty of [Engineering](#)

Supervised by

Dr. Ali Massoud HAIDAR  
Professor  
Faculty of Engineering  
Electrical & Computer Eng. Dept.  
Beirut Arab University

Dr. Lina EL-NIMRI  
Associate Professor  
Faculty of Economics and Business Administration  
Computer Dept.  
Lebanese University

2020



جامعة بيروت العربية  
BEIRUT ARAB UNIVERSITY

The Thesis Defense Committee for **RAMZI ALI JABER**  
Certifies that this is the approved version of the following thesis

## **Multiple-Valued Logic Circuit Design and Data Transmission Intended for Embedded Systems**

APPROVED BY:

**Supervisor Signature:** \_\_\_\_\_

**Prof. Ali Haidar**

**Examiner Signature:** \_\_\_\_\_

**Prof. Ziad Osman**

**Examiner Signature:** \_\_\_\_\_

**Associate Prof. Issam Damaj**

**Examiner Signature:** \_\_\_\_\_

**Prof. Mohamed Dbouk**

**Examiner Signature:** \_\_\_\_\_

**Prof. Mohamad Sawan**

# ACKNOWLEDGEMENT

First of all, I thank my God (ALLAH) for protecting and giving me the ability to do this hard work.

Secondly, it is my pleasure to thank all the people who helped me throughout the achievement of this thesis. Special thanks and appreciations to my supervisor Prof. Dr. Ali Haidar and Dr. Ahmad El-Hajj for granting me the opportunity to carry out this research and for their constant encouragement and valuable guidance during this thesis work.

Also, I would like to thank my co-supervisor Dr. Lina El-Nimri, Dr. Abdallah Kassem, and Dr. Ziad Osman for their trust and very kind support.

I would also like to say thanks to my friends and research colleagues for their constant support and encouragement: Dr. Bilal Owaidat, Eng. Imane Haidar, Eng. Hamza Damaj, and Eng. Abdallah Salem.

Most importantly, none of this would have been possible without the love and patience of my family. I am eternally grateful to them, for their careful considerations and high confidence in me through all these years.

Finally, I am grateful to the jury members:

1. **Prof. Ali Haidar:** Committee Chair and Computer Eng. undergraduate & graduate Program Coordinator at BAU
2. **Prof. Ziad Osman:** Chair of Electrical & Computer Eng. Dept. at BAU
3. **Associate Prof. Issam Damaj:** Director of the Center for Quality Assurance at BAU
4. **Prof. Mohamed Dbouk:** Director of L'ARiCoD: Lab of Advanced Research in Intelligent Computing & Data and Master Coordinator at Lebanese Univ.
5. **Prof. Mohamad Sawan:** Chair Professor at Westlake University, Hangzhou, China and Canada Research Chair at Polytechnique Montreal, Canada

## Abstract

Recently, the demand for portable electronics and embedded systems has increased. These devices need low-power circuit designs because they depend on batteries as an energy resource. Moreover, Multi-Valued Logic (MVL) circuits provide notable improvements over binary circuits in terms of interconnect complexity, chip area, propagation delay, and energy consumption. Therefore, this thesis proposes novel ternary circuits aiming to reduce the energy (Power Delay Product (PDP)) to preserve battery consumption.

The proposed designs include eight ternary logic gates, three ternary combinational circuits, and six Ternary Arithmetic Logic Units (TALU). The ternary logic gates are seven unary operators of the ternary system ( $A^1$ ,  $A^2$ ,  $\bar{A}^2$ ,  $A_1$ ,  $1.\bar{A}_n$ ,  $1.\bar{A}_p$ , and the Standard Ternary Inverter (STI)  $\bar{A}$ ), and Ternary NAND based on Carbon Nanotube Field-Effect Transistor (CNFET). Ternary combinational circuits, two different designs for Ternary Decoders (TDecoder) and Ternary Multiplexer (TMUX): (1) TDecoder1 using CNFET-based proposed unary operators and TDecoder2 using Double-Pass Logic (DPL) binary gates. (2) TMUX using CNFET-based proposed unary operators. And Ternary Arithmetic Logic Units are three different designs for Ternary Half-Adders (THA) and Ternary Multipliers (TMUL): (1) The first design uses the proposed TDecoder1, STI, and TNAND. (2) While the second design uses the cascading proposed TMUX. (3) As for the third design, it uses the proposed unary operators and TMUX.

This thesis applies the best trade-off between reducing the number of used transistors, utilizing energy-efficient transistor arrangement such as transmission gate and applying the dual supply voltages ( $V_{dd}$ , and  $V_{dd}/2$ ) to achieve its objective. The proposed designs are compared to the latest ternary circuits using the HSPICE simulator for different supply voltages, different temperatures, and different frequencies. Simulations are performed to prove the efficiency of the proposed designs. The results demonstrate the advantage of the proposed designs with a reduction over 73% in terms of transistors count for the THA and over 88%,

99%, 98%, 84%, 98%, and 99% in energy consumption for the STI, TNAND, TDecoder, TMUX, THA, and TMUL, respectively.

Moreover, the noise immunity curve (NIC) and Monte Carlo analysis for major process variations (TOX, CNT Diameter, CNT's Count, and Channel length) were studied. The results confirmed that the third proposed THA3 and TMUL3 had higher strength and higher noise tolerance, among other designs.

In addition, the second objective is using ternary data transmission to improve data communications between computer hosts. Also, this thesis proposes a bi-directional circuit that contains two converters: (1) A binary-to-ternary converter and (2) a ternary-to-binary converter.

Finally, logical analysis and simulation results prove the merits of the approaches compared to existing designs in terms of transistor count, reduced latency, and energy efficiency.

# Contents

<b>Contents</b>	<b>vii</b>
<b>List of Tables</b>	<b>xi</b>
<b>List of Figures</b>	<b>xiv</b>
<b>Abbreviations</b>	<b>xvii</b>
<b>Symbols</b>	<b>xix</b>
<b>1 Introduction</b>	<b>1</b>
1.1 Binary Logic System . . . . .	1
1.2 Multi-Valued Logic (MVL) System . . . . .	1
1.3 Ternary Logic System . . . . .	3
1.3.1 Relation between Binary and Ternary Digit . . . . .	4
1.4 Transistor Technologies . . . . .	5
1.4.1 BJT . . . . .	5
1.4.2 FET . . . . .	6
1.4.2.1 MOSFET . . . . .	6
1.4.2.2 CMOS . . . . .	7
1.4.2.3 FinFET . . . . .	8
1.4.2.4 CNFET . . . . .	8
1.5 Power Consumption . . . . .	12
1.6 Logic Gates . . . . .	13
1.6.1 Unary Operators of MVL Systems . . . . .	13
1.6.2 Binary Logic Gates . . . . .	14
1.6.2.1 Inverter Gate . . . . .	14
1.6.2.2 AND Gate (Minimum function) . . . . .	14
1.6.2.3 NAND Gate . . . . .	15
1.6.2.4 OR Gate (Maximum function) . . . . .	15
1.6.2.5 NOR Gate . . . . .	15
1.6.3 Ternary Logic Gates . . . . .	17
1.6.3.1 Ternary Inverter Gates . . . . .	17

1.6.3.2	Other Ternary Logic Gates . . . . .	18
1.6.4	Double Pass-transistor Logic (DPL) . . . . .	20
1.7	Objectives . . . . .	21
1.7.1	The First Objective . . . . .	21
1.7.2	The Second Objective . . . . .	21
1.8	Methodology . . . . .	21
1.8.1	Choosing the High-Performance Transistor Technology . . . . .	21
1.8.2	Utilizing Ternary Logic System . . . . .	22
1.8.3	Applying the Dual Supply Voltages . . . . .	22
1.8.4	Implementing Energy-Efficient Transistor Arrangement . . . . .	22
1.8.5	Reducing the number of used transistors . . . . .	23
1.9	Thesis Outline . . . . .	24
<b>2</b>	<b>Ternary Logic Gates</b>	<b>25</b>
2.1	Literature Review . . . . .	25
2.2	The Proposed Unary Operators of Ternary Systems . . . . .	26
2.2.1	State of CNFETs with Different Diameters . . . . .	29
2.3	The Proposed STI & TNAND Logic Gates . . . . .	32
2.3.1	The Proposed STI . . . . .	33
2.3.2	The Proposed TNAND . . . . .	34
2.4	Simulation Results and Comparisons . . . . .	38
2.4.1	Comparison of Transistors Count Of All Circuits . . . . .	42
2.4.2	Comparison of the Unary Operators Circuits . . . . .	43
2.4.3	Comparison of Different STI Circuits . . . . .	44
2.4.3.1	Impact of Different Power Supplies . . . . .	44
2.4.3.2	Impact of Different Temperatures . . . . .	44
2.4.3.3	The Impact of Different Frequencies . . . . .	46
2.4.4	Comparison of Different TNAND Circuits . . . . .	46
2.4.4.1	Impact of Different Power Supplies . . . . .	47
2.4.4.2	Impact of Different Temperatures . . . . .	48
2.4.4.3	Impact of Different Frequencies . . . . .	48
2.5	Conclusion . . . . .	49
<b>3</b>	<b>Ternary Combinational Logic Circuits</b>	<b>50</b>
3.1	Introduction and Literature Review . . . . .	50
3.2	The Proposed Ternary Decoders . . . . .	51
3.2.1	The Proposed TDecoder1 using CNFET . . . . .	52
3.2.2	The Proposed TDecoder2 using DPL Binary Gates . . . . .	55
3.3	The Proposed Ternary Multiplexer . . . . .	57
3.4	Simulation Results and Comparisons . . . . .	62
3.4.1	Comparison of Transistors Count of All Circuits . . . . .	64
3.4.2	Comparison of Different TDecoder Circuits . . . . .	64

3.4.2.1	The Impact of Different Power Supplies . . . . .	64
3.4.2.2	Impact of Different Temperatures . . . . .	66
3.4.2.3	The Impact of Different Frequencies . . . . .	66
3.4.3	Comparison between the Proposed TDecoders Circuits . . . . .	67
3.4.4	Comparison of Different TMUX Circuits . . . . .	68
3.5	Conclusion . . . . .	70
<b>4</b>	<b>Ternary Arithmetic Logic Units (TALU)</b>	<b>71</b>
4.1	Introduction and Literature Review . . . . .	71
4.2	The Proposed Ternary Half Adders . . . . .	72
4.2.1	The proposed THA1 . . . . .	78
4.2.2	The proposed THA2 . . . . .	80
4.2.3	The proposed THA3 . . . . .	82
4.3	The proposed Ternary Multipliers . . . . .	84
4.3.1	The proposed TMUL1 . . . . .	88
4.3.2	The proposed TMUL2 . . . . .	90
4.3.3	The proposed TMUL3 . . . . .	92
4.4	Simulation Results and Comparisons . . . . .	94
4.4.1	Comparison of Transistors Count . . . . .	96
4.4.2	Comparison of Different THA Circuits . . . . .	97
4.4.2.1	Comparison at Different Power Supplies . . . . .	97
4.4.2.2	Comparison at Different Temperatures . . . . .	98
4.4.2.3	Comparison at Different Frequencies . . . . .	99
4.4.3	Comparison at Different TMUL Circuits . . . . .	101
4.4.3.1	Comparison to Different Power Supplies . . . . .	101
4.4.3.2	Comparison at Different Temperatures . . . . .	102
4.4.3.3	Comparison at Different Frequencies . . . . .	103
4.4.4	Process Variations . . . . .	105
4.4.5	Noise Effect . . . . .	107
4.5	Conclusion . . . . .	110
<b>5</b>	<b>Ternary Data Transmission</b>	<b>111</b>
5.1	Introduction and Literature Review . . . . .	111
5.2	The Proposed Binary-to-Ternary Converter using CMOS DPL Gates . . . . .	113
5.2.1	Simulation Results and Comparisons . . . . .	119
5.3	The Proposed Ternary-to-Binary Converter using CNFET . . . . .	121
5.3.1	The Novel Sub-Circuit-One Design . . . . .	122
5.3.2	The Sub-Circuit-Two Design . . . . .	123
5.3.3	Simulation Results and Comparisons . . . . .	125
5.4	Conclusion . . . . .	127
<b>6</b>	<b>Conclusion and Perspectives</b>	<b>128</b>
6.1	Conclusion . . . . .	128

6.2 Perspectives . . . . .	130
<b>Appendix A High-Performance and Energy-Efficient CNFET-Based Designs for Ternary Logic Circuits</b>	<b>131</b>
<b>Appendix B CNFET-Based Designs of Ternary Half-Adder using a Novel “Decoder-less” Ternary Multiplexer based on Unary Operators</b>	<b>148</b>
<b>Appendix C A Novel Implementation of Ternary Decoder Using CMOS DPL Binary Gates</b>	<b>159</b>
<b>Appendix D A Novel Binary to Ternary Converter using Double Pass-Transistor Logic</b>	<b>164</b>
<b>Appendix E Ternary Data Transmission Between Hosts</b>	<b>170</b>
<b>Bibliography</b>	<b>174</b>

# List of Tables

1.1	The relation between the chirality, diameter, and threshold voltage. . . . .	10
1.2	CNFET model parameters . . . . .	11
1.3	Unary operators of binary logic system . . . . .	13
1.4	Unary operators of ternary logic system . . . . .	13
1.5	Binary NOT truth table . . . . .	14
1.6	Truth table of some basic binary gates . . . . .	15
1.7	Ternary inverters truth table . . . . .	18
1.8	Truth table of some basic ternary gates . . . . .	18
2.1	Truth table of the selected nine unary operators . . . . .	26
2.2	The chirality, diameter, and threshold voltage of the CNTs used in the proposed six unary operators . . . . .	30
2.3	The state of CNFETs with D1=1.487 nm and D2=0.783 nm . . . . .	30
2.4	The detailed operation of the proposed six unary operators with D1=1.487 nm and D2=0.783 nm . . . . .	31
2.5	The chirality, diameter, and threshold voltage of the CNTs used in the proposed STI . . . . .	33
2.6	The detailed operation of the STI . . . . .	34
2.7	The chirality, diameter, and threshold voltage of the CNTs used in the proposed TNAND . . . . .	34
2.8	The detailed operation of the TNAND with selected inputs . . . . .	35
2.9	The advantage of proposed STI & TNAND logic gates . . . . .	37
2.10	Comparison of Transistors Count of All Circuits . . . . .	42
2.11	Comparison between the six unary operators to [27, 36] in terms of the average power consumption, maximum propagation delay, and maximum PDP at Vdd (0.9V), temperature (27 ° C), and frequency (1 GHz) . . . . .	43
3.1	Ternary Decoder truth table . . . . .	51
3.2	The chirality, diameter, and threshold voltage of the CNTs used in the proposed TDecoder1 . . . . .	52
3.3	The detailed operation of the proposed TDecoder1 . . . . .	54
3.4	The advantage of the proposed TDecoder1 . . . . .	55
3.5	The detailed operation of the proposed TDecoder2 . . . . .	56
3.6	The diameter, and threshold voltage of the CNTs used in the proposed TMUX . . . . .	58

3.7	The operation of the proposed TMUX . . . . .	59
3.8	Comparison of Transistors Count of All Circuits . . . . .	64
3.9	Comparison of average power ( $\mu\text{w}$ ), maximum delay (ps), and maximum PDP ( $\times 10^{-17}$ J) of 4 TDecoders at $T=27^\circ\text{C}$ , $F=1$ GHz, and for different supply voltages . . . . .	65
3.10	Comparison of average power ( $\mu\text{w}$ ), maximum delay (ps), and maximum PDP ( $\times 10^{-17}$ J) of 4 TDecoders at $V_{\text{dd}}=0.9$ V, $F=1$ GHz, and for different Temperatures . . . . .	65
3.11	Comparison of average power ( $\mu\text{w}$ ), maximum delay (ps), and maximum PDP ( $\times 10^{-17}$ J) of 4 TDecoders at $T=27^\circ\text{C}$ , $V_{\text{dd}}=0.9$ V, and for different frequencies . . . . .	65
3.12	Comparison of average power ( $\mu\text{w}$ ), maximum delay (ps), and maximum PDP ( $\times 10^{-17}$ J) of the two proposed TDecoders . . . . .	67
3.13	Comparison between three TMUXs at $V_{\text{dd}}$ (0.9 V), temperature ( $27^\circ\text{C}$ ), and frequency (1 GHz) . . . . .	68
4.1	Truth table of THA . . . . .	73
4.2	Total transistors count of the proposed THA1 . . . . .	79
4.3	Total transistors count of the proposed THA3 . . . . .	83
4.4	Truth table of TMUL . . . . .	84
4.5	Total transistors count of the proposed TMUL1 . . . . .	89
4.6	Total transistors count of the proposed TMUL3 . . . . .	93
4.7	Comparison of Transistors Count . . . . .	96
4.8	Comparison of average power ( $\mu\text{W}$ ), maximum delay (ps), and maximum PDP ( $\times 10^{-18}$ J) for 8 THAs at $T=27^\circ\text{C}$ , $F=1$ GHz, and for different supply voltages . . . . .	97
4.9	Comparison of average power ( $\mu\text{W}$ ), maximum delay (ps), and maximum PDP ( $\times 10^{-18}$ J) for 8 THAs at $V_{\text{dd}}=0.9$ V, $F=1$ GHz, and for different temperatures . . . . .	98
4.10	Comparison of average power ( $\mu\text{W}$ ), maximum delay (ps), and maximum PDP ( $\times 10^{-18}$ J) for 8 THAs at $T=27^\circ\text{C}$ , $V_{\text{dd}}=0.9$ V, and for different frequencies . . . . .	100
4.11	Comparison of average power ( $\mu\text{W}$ ), maximum delay (ps), and maximum PDP ( $\times 10^{-18}$ J) for 8 TMULs at $T=27^\circ\text{C}$ , $F=1$ GHz, and for different supply voltages . . . . .	101
4.12	Comparison of average power ( $\mu\text{W}$ ), maximum delay (ps), and maximum PDP ( $\times 10^{-18}$ J) for 8 TMULs at $V_{\text{dd}}=0.9$ V, $F=1$ GHz, and at different temperatures . . . . .	102
4.13	Comparison of average power ( $\mu\text{W}$ ), maximum delay (ps), and maximum PDP ( $\times 10^{-18}$ J) for 8 TMULs at $T=27^\circ\text{C}$ , $V_{\text{dd}}=0.9$ V, and at different frequencies . . . . .	104
5.1	Binary-to-Ternary truth table . . . . .	114
5.2	Decomposition of O1 to two intermediate Binary Outputs . . . . .	115

5.3	Decomposition of the three ternary outputs . . . . .	115
5.4	Combination of Ternary Output O1 . . . . .	118
5.5	Device count in the proposed circuit (Fig.5.3) . . . . .	118
5.6	Comparison to the latest novel converter in [57] . . . . .	120
5.7	Convert 2 trits to 4 intermediate bits then final 4 bits . . . . .	122
5.8	The Sub-Circuit-One detailed truth table . . . . .	123
5.9	Total transistors count in the Ternary-to-Binary converter circuit . . . . .	125
5.10	Comparison between the three converter circuits . . . . .	125

# List of Figures

1.1	Limitation of the CPU Clock Speed and its power consumption. . . . .	2
1.2	BJT Transistor schematic symbols. . . . .	5
1.3	MOSFET Transistor schematic symbols. . . . .	7
1.4	(a) Unrolled graphite sheet and (b) the rolled carbon nanotube lattice structure. . . . .	10
1.5	Basic CMOS Binary Logic Gates. . . . .	16
1.6	Basic Ternary Logic Gates [27] using CNFET. . . . .	19
1.7	DPL Gates Design [28] . . . . .	20
2.1	The Existing unary operators (a) in [27], $A_p$ , $A_n$ , $\bar{A}$ , $A_0$ , $A_1$ , and $A_2$ (b) in [36], $A^1$ , $A^2$ , $1 \cdot \bar{A}_n$ , and $1 \cdot \bar{A}_p$ . . . . .	28
2.2	The transistor level of the proposed six unary operators: (a) $A^1$ , (b) $A^2$ , (c) $1 \cdot \bar{A}_n$ , (d) $1 \cdot \bar{A}_p$ , (e) $\bar{A}^2$ , and (f) $A_1$ . . . . .	29
2.3	The Existing STI in (a) [27], (b) [37], and (c) [38]. . . . .	32
2.4	The Existing TNAND in (a) [27], (b) [37], and (c) [38]. . . . .	32
2.5	Transistor level of the proposed STI. . . . .	33
2.6	Transistor level of the proposed TNAND. . . . .	35
2.7	Transient analysis of the proposed $A^1$ . . . . .	38
2.8	Transient analysis of the proposed $A^2$ . . . . .	39
2.9	Transient analysis of the proposed $\bar{A}^2$ . . . . .	39
2.10	Transient analysis of the proposed $1 \cdot \bar{A}_n$ . . . . .	40
2.11	Transient analysis of the proposed $1 \cdot \bar{A}_p$ . . . . .	40
2.12	Transient analysis of the proposed $A_1$ . . . . .	41
2.13	Transient analysis of the proposed STI. . . . .	41
2.14	Transient analysis of the proposed TNAND. . . . .	41
2.15	PDP Comparison of the investigated STI for: (a) Different Power Supplies, (b) Different Temperatures, and (c) Different Frequencies. . . . .	45
2.16	PDP Comparison of the investigated TNAND at: (a) Different Power Supplies, (b) Different Temperatures, and (c) Different Frequencies. . . . .	47
3.1	The Existing TDecoder in (a) [27] with 16 CNFETs, (b) [40] with 10 CNFETs, and (c) [41] with 11 CNFETs. . . . .	53
3.2	Transistor level of the proposed TDecoder1 with 9 CNFETs. . . . .	54
3.3	Transistor and Gate level of the proposed TDecoder2 with 12 transistors. . . . .	56
3.4	The model of 3:1 TMUX . . . . .	57

3.5	The Existing 3:1 TMUX in (a) [42] with 28 transistors, (b) [36] with 18 transistors. . . . .	60
3.6	Transistor level of the proposed TMUX with 15 CNFETs. . . . .	61
3.7	Transient analysis of the proposed TDecoder1. . . . .	63
3.8	Transient analysis of the proposed TDecoder2. . . . .	63
3.9	Transient analysis of the proposed 3:1 TMUX (dotted rectangle corresponds to input selected according to S). . . . .	69
4.1	The Existing THA in [36] with 64 CNFETs. . . . .	74
4.2	The Existing THA in [27] with 136 CNFETs. . . . .	75
4.3	The Existing THA in [46] with 112 CNFETs. . . . .	76
4.4	The Existing THA in [37] with 112 CNFETs. . . . .	77
4.5	The proposed THA1 with 85 CNFETs using the proposed TDecoder1, STI, and TNAND. . . . .	78
4.6	The proposed THA2 with 90 CNFETs using cascading the proposed TMUX. . . . .	80
4.7	The proposed THA3 with 45 CNFETs using the proposed TMUX and Unary Operators. . . . .	82
4.8	The Existing TMUL in (a) [27] with 100 CNFETs, (b)[46] with 86 CNFETs, and (b) [37] with 76 CNFETs. . . . .	86
4.9	The Existing TMUL in [36] with 58 CNFETs. . . . .	87
4.10	The proposed TMUL1 with 61 transistors using the proposed TDecoder1, a STI, and TNANDs. . . . .	88
4.11	The proposed TMUL2 with 60 CNFETs using cascading the proposed TMUXs. . . . .	90
4.12	The proposed TMUL3 with 40 CNFETs using the proposed TMUX and Unary Operators. . . . .	92
4.13	Transient analysis of the proposed THA1. . . . .	94
4.14	Transient analysis of the proposed TMUL1. . . . .	95
4.15	Stanford CNFET Model. . . . .	105
4.16	THAs Major Process Variations: TOX, CNT Diameter, CNT's Count, and Channel length. . . . .	106
4.17	TMULs Major Process Variations: TOX, CNT Diameter, CNT's Count, and Channel length. . . . .	107
4.18	Noise Signal. . . . .	107
4.19	THAs Noise Immunity Curve (NIC). . . . .	108
4.20	TMULs Noise Immunity Curve (NIC). . . . .	109
5.1	The proposed Data Transmission model between routers. . . . .	112
5.2	Binary-to-Ternary model . . . . .	113
5.3	The Proposed binary-to-ternary Converter Circuit . . . . .	117
5.4	The simulation transient analysis of the proposed circuit . . . . .	119
5.5	Ternary-to-Binary model . . . . .	121
5.6	Ternary-to-Binary model . . . . .	121
5.7	Novel transistor level for 1-trit input to 2-intermediate bits outputs . . . . .	123

5.8	The proposed schematic Ternary-to-Binary Converter. . . . .	124
5.9	Transient analysis of the proposed Ternary-to-Binary converter. . . . .	126

# Abbreviations

<b>BJT</b>	<b>Bipolar Junction Transistor</b>
<b>CMOS</b>	<b>Complementary MOSFET</b>
<b>CNT</b>	<b>Carbon Nanotube Tube</b>
<b>CNFET</b>	<b>Carbon Nanotube FET</b>
<b>CPL</b>	<b>Complementary Pass transistor Logic</b>
<b>CPU</b>	<b>Central Processing Unit</b>
<b>DPL</b>	<b>Double Pass transistor Logic</b>
<b>FET</b>	<b>Field Effect Transistor</b>
<b>FinFET</b>	<b>Fin FET</b>
<b>HDD</b>	<b>Hard Disk Drive</b>
<b>MOSFET</b>	<b>Metal Oxide Semiconductor FET</b>
<b>MVL</b>	<b>Multi-Valued Logic</b>
<b>NIC</b>	<b>Noise Immunity Curve</b>
<b>NTI</b>	<b>Negative Ternary Inverter</b>
<b>PTI</b>	<b>Positive Ternary Inverter</b>
<b>RAM</b>	<b>Random Access Memory</b>
<b>STI (TNOT)</b>	<b>Standard Ternary Inverter</b>
<b>TAND</b>	<b>Ternary AND</b>
<b>TNAND</b>	<b>Ternary NAND</b>
<b>TOR</b>	<b>Ternary OR</b>
<b>TNOR</b>	<b>Ternary NOR</b>
<b>TDecoder</b>	<b>Ternary Decoder</b>

<b>TMUX</b>	<b>Ternary Multiplexer</b>
<b>TALU</b>	<b>Ternary Arithmetic Logic Unit</b>
<b>THA</b>	<b>Ternary Half Adder</b>
<b>TMUL</b>	<b>Ternary Multiplier</b>
<b>PDP</b>	<b>Power Delay Product (Energy Consumption)</b>

# Symbols

$a_0$	The inter-atomic distance between each carbon atom and its neighbor
$a$	The carbon to carbon atom distance
$b$	bit (Binary digit)
$d$	The number of digits
$D_{cnt}$	The CNT diameter
$e$	The electron charge unit
$R$	The base or radix of the numerical system
$t$	trit (Ternary digit)
$V\pi$	The carbon bond energy

# Chapter 1

## Introduction

“If it would have been possible to build reliable ternary architecture, everybody would be using it.” - Donald Ervin Knuth, a famous computer scientist at Stanford University [1].

### 1.1 Binary Logic System

The two-valued logic system (Binary) dominates in circuit designs because the transistor has two states “ON” or “OFF”. However, Binary systems have disadvantages in the design, which require a large number of interconnections around 70% of the total area, 20% for insulation, and only 10% for components [2]. Therefore, Binary systems suffer from high-power consumption. Whereas, Multi-Valued Logic (MVL) circuits have more than two-valued logic, which reduces the interconnections, chip area, and power consumption [3].

### 1.2 Multi-Valued Logic (MVL) System

Multi-Valued Logic (MVL) returns to ancient Mesopotamian cultures. Five thousand years ago, the Babylonians and Sumerians used the sexagesimal system (base 60) [4].

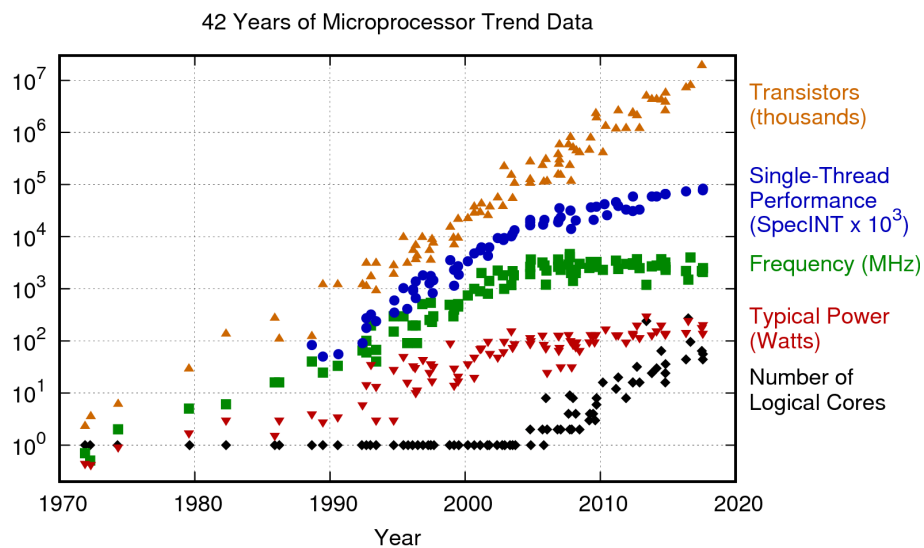


FIGURE 1.1: Limitation of the CPU Clock Speed and its power consumption.

The first algebra of  $k$ -valued logic corresponding to the work of Post was known as Post Algebra of order  $k$ , where  $k \geq 2$  [5]. Post algebra coincides with Boolean algebra for  $k=2$ .

In 1958, Nikolai P. Brusenzov and his team constructed the world's first and still unique ternary computer (called Setun) at the University of Moscow [6]. Setun gained much interest among scientists. Unfortunately, the development of ternary architectures was not keeping up with the speed of the binary counterparts because a transistor has two stable states: "ON" or "OFF".

Nowadays, many researchers believe that binary logic is doomed because of:

1. Moore's Law 1965 (transistors will double every two years) [7] is stopped because the shrinkage sizes of transistors indefinitely is not possible
2. Limitation of CPU Clock Speed and its power consumption are shown in Fig. 1.1

As shown in Fig. 1.1, Since 2011, the transistor count inside the CPU core can not exceed 10 million transistors, and the CPU clock speed and power consumption remain constant since 2010.

Therefore recently, MVL has attracted researchers' attention again over binary logic. MVL can be implemented almost in all topics. For example, in Algorithm (software), Artificial Intelligence, Big Data [8], MV-Quantum Logic [9], Wireless Sensor Networks [10], Cloud Vehicular Networks [11], Communication systems [12], Programmable Logic Arrays (PLAs), and circuit designs like Logic Gates, Arithmetic, Memory, and Memristor circuits [13–15].

Example of MVL, Samsung Ternary Memory (1995), Intel Strata Flash Memory ( 2 bits per cell) (1997), Sony Ternary Flash Memory (2010), Samsung Multi-Level Cell NAND Flash Memory (2013), CISCO SF/SG 300 Series Managed Switches (2018), TOSHIBA hexa-valued logic memory (2018), Intel and Micron hexa-valued logic SSD 1 TB (2018), Samsung hexa-valued logic SSD 1 TB (2020).

### 1.3 Ternary Logic System

The number to represent the range  $N$  from 0 to  $R^{d-1}$  of any numerical system is given by the equation (1.1):

$$N = R^d \quad (1.1)$$

Where  $R$  is the base or radix of the numerical system and  $d$  is the number of digits.

The cost and complexity  $C$  of the system is proportional to the digit. The capacity of the digits is  $(R \cdot d)$  then  $C$  is given by the equation (1.2):

$$C = k(R \cdot d) = k\left(R \cdot \frac{\log N}{\log R}\right) = k \log N \left(\frac{R}{\log R}\right) \quad (1.2)$$

Where  $k$  and  $\log N$  are constant numbers.

To minimize the cost and complexity  $C$ , we must differentiate the equation (1.2) with respect to  $R$  and set it to zero, then:

$$\frac{\partial C}{\partial R} = \frac{\partial R}{\partial \log R} = \frac{\frac{\partial R}{\partial R} \log R - R \frac{\partial \log R}{\partial R}}{(\log R)^2} = \frac{\log R - R(1/R)}{(\log R)^2} = \frac{\log R - 1}{(\log R)^2} = 0$$

then  $\log R - 1 = 0$  implies that  $R = e = 2.718$ .

Since radix  $R$  is an integer, then  $R = 3$ . Therefore, the ternary logic system is the most efficient in circuit complexity and cost compared to other bases [16].

Ternary digit, called trit, can be represented in two ways: balanced ternary logic (-1, 0, 1) corresponding to (-Vdd, 0, Vdd), and standard (unbalanced) ternary logic (0, 1, 2) corresponding to (0, Vdd/2, Vdd).

### 1.3.1 Relation between Binary and Ternary Digit

For the same amount of data,  $n$ -bits or  $m$ -trits are represented in the equation (1.3):

$$2^n = 3^m \tag{1.3}$$

This implies that

$$n = \frac{\log 3}{\log 2} m = 1.585m \tag{1.4}$$

Thus, the equation (1.4) shows that a single trit can represent 58.5% more data than a single bit.

For example, a decimal number 2186 is 1000 1000 1010 (12 bits) in binary whereas, in ternary equivalent is 2 222 222 (7 trits). Conclude that the ternary system has a notable reduction in wires around 41.7% [(12-7)\*100/12] compared to the binary system.

Therefore, Ternary systems can help to solve the problem of “ Cloud storage, big data, artificial intelligence, technical computing, and ever-richer digital content demand massive storage capacity and exceptional performance.”

## 1.4 Transistor Technologies

This section is summarizing the transistor technologies [17]. The transistor, a semiconductor, is one of the most important devices used in electronic applications. It is mainly applied in two ways: (1) amplification, and (2) switching. In digital logic circuits, like in this thesis, it will be used as a switch.

Transistor has at least three terminals: The first one is for voltage supply or output [called Drain (D) or Collector (C)], the second one is for input voltage or controller [called Gate (G) or Base (B)], and the third one is for the output or ground [called Source (S) or Emitter (E)]. The terminals names depend on the transistor technology which will be discussed later.

Transistor is manufactured from a material like Silicon, Germanium, Carbon, or others.

### 1.4.1 BJT

The Bipolar Junction Transistor (BJT) invented in 1947 at the Bell Telephone Laboratories. The BJT is a three-layer device. It is classified according to the types of the layers as NPN or PNP transistors. NPN transistors are constructed by sandwiching P-type layer between two N-type layers, while PNP transistors are constructed by sandwiching N-type layer between two P-type layers, as shown in Fig. 1.2:

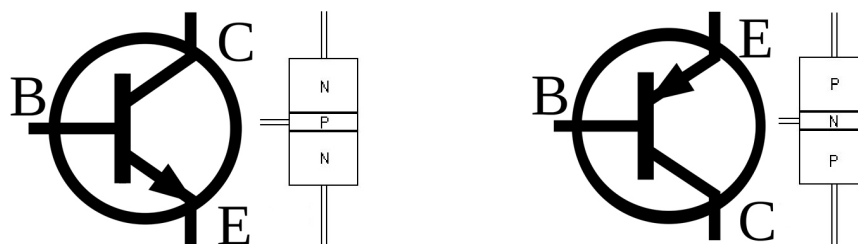


FIGURE 1.2: BJT Transistor schematic symbols.

**Advantages:**

1. BJT has a large gain bandwidth.
2. It shows better performance at high frequency.
3. It has a better voltage gain.
4. It can be operated in low or high power applications.
5. It has a high current density.
6. There is a low forward voltage drop.

**Disadvantages:**

1. BJT is sensitive of radiation.
2. It has a very complex base control. So it may lead to confusion and requires skillful handling.
3. The switching speed of a BJT is low.
4. It produce more noise.
5. It has low thermal stability.

## 1.4.2 FET

Julius Edgar Lilienfeld first patented the concept of a Field-Effect Transistor (FET) in 1925. The first FET device to be successfully built was the Junction Field-Effect Transistor (JFET) by Heinrich Welker in 1945 [18].

### 1.4.2.1 MOSFET

The Metal–Oxide–Semiconductor Field-Effect Transistor (MOSFET), unipolar transistor, was invented by Mohamed Atalla and Dawon Kahng in 1959. The MOSFET largely superseded both the BJT and the JFET. Apart from the terminals (Drain, Gate, Source), there is a substrate (Sub) or a body.

MOSFET utilizes an insulator (typically SiO<sub>2</sub>) between the gate and the body which provides high input impedance, thus capturing all the input signal.

MOSFET schematic symbols are shown in Fig. 1.3.

### 1.4.2.2 CMOS

CMOS (Complementary MOS) technology was invented at Fairchild Semiconductor in 1963 [19]. It is used in microprocessors, microcontrollers, memory chips, and other digital logic circuits. Also, It is used in several analog circuits such as data converters and image sensors (CMOS sensor).

#### CMOS Advantages:

1. MOSFETs provide greater efficiency while operating at lower voltages.
2. Absence of gate current results in high input impedance producing high switching speed.
3. Lowest power dissipation of all gates (a few nW).
4. Huge fan-out capability (>50).

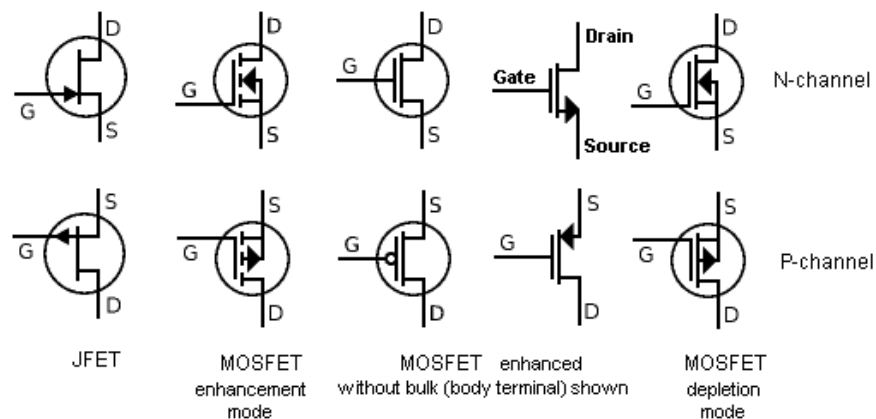


FIGURE 1.3: MOSFET Transistor schematic symbols.

5. Very high noise-immunity and noise-margin (typically,  $V_{DD}/2$ ).
6. Lower propagation delay than NMOS.
7. Temperature stability is excellent.

**CMOS Disadvantages:**

1. The thin oxide layer makes the MOSFETs vulnerable to permanent damage when evoked by electrostatic charges.
2. Overload voltages make it unstable.

**1.4.2.3 FinFET**

Hitachi Central Research Laboratory in 1989 first fabricated a Fin Field-Effect Transistor (FinFET) [20]. It is a multigate device and has faster switching times than the CMOS.

FinFET is a "3D" transistor or a type of non-planar transistor. It is the basis for nanoelectronic and becomes the dominant gate design at 14 nm, 10 nm, and 7 nm process nodes.

**1.4.2.4 CNFET**

A Carbon Nanotube Field-Effect Transistor (CNFET) was first demonstrated in 1998. It refers to a FET that uses a single carbon nanotube or more as the channel material instead of bulk silicon in the traditional MOSFET structure.

**CNFET Advantages:**

1. Very fast switching time
2. Better control over channel formation
3. Customize the threshold voltage by changing CNT diameter

4. High electron mobility
5. High current density
6. High transconductance
7. High linearity

### **CNFET Disadvantages:**

1. Lifetime (degradation): Carbon nanotubes degrade in a few months.
2. Reliability issues when operated under high electric field or temperature gradients.
3. Production cost.

Among the techniques mentioned above, CNFET provides the best trade-off in terms of energy efficiency and circuit speed [21].

Details about the Stanford CNFET model used in this thesis can be found in [22–24]. However, it is worth mentioning that the CNFETs use a semiconducting single-walled CNT as a channel for conduction with high drive current  $35 \mu\text{ A}$  when the supply voltage  $V_{\text{dd}}$  is equal to  $0.9\text{ V}$ .

A single-walled carbon nanotube (SWCNT) can be visualized as a sheet of graphite which is rolled up and joined together along a wrapping vector  $C_h = i \cdot \bar{a}_1 + j \cdot \bar{a}_2$ , where  $[\bar{a}_1, \bar{a}_2]$  are lattice unit vectors as shown by Fig. 1.4, and the indices  $(i, j)$  are positive integers that specify the chirality of the tube.

This chirality vector determines if the CNT is metallic or semiconducting; if  $i = j$  or  $i - j = 3t$ , where  $t$  is an integer, then the nanotube is metallic else it is semiconducting.

The CNFET diameter can be calculated from equation (1.5):

$$D_{\text{cnt}} = \frac{\sqrt{3} \cdot a_0}{\pi} \sqrt{i^2 + j^2 + ij} \quad (1.5)$$

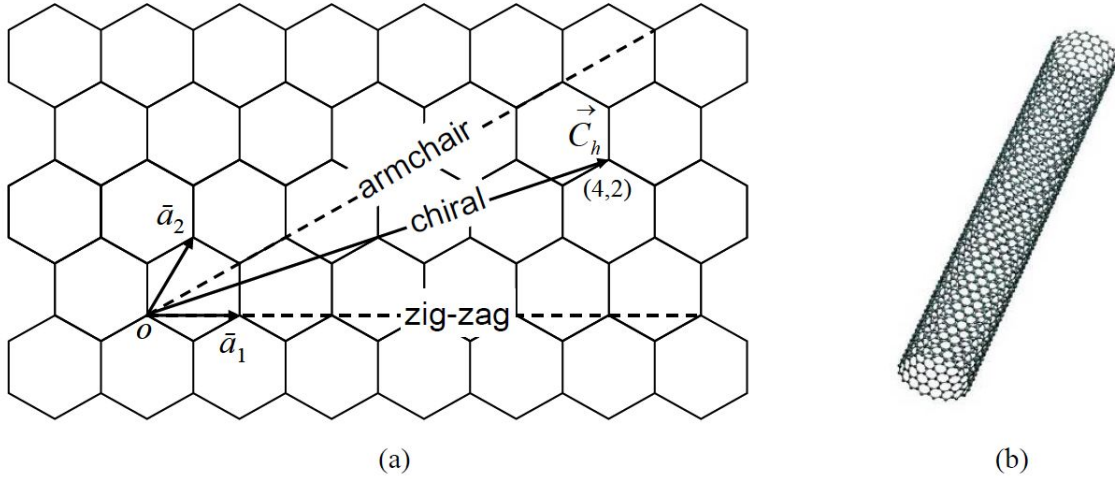


FIGURE 1.4: (a) Unrolled graphite sheet and (b) the rolled carbon nanotube lattice structure.

TABLE 1.1: The relation between the chirality, diameter, and threshold voltage.

Chirality	CNT diameter	Threshold voltage	
		N-CNFET	P-CNFET
(10,0)	0.783nm	0.559V	- 0.559V
(13,0)	1.018nm	0.428V	- 0.428V
(19,0)	1.487nm	0.289V	- 0.289V

Where  $a_0 = 0.142$  nm is the inter-atomic distance between each carbon atom and its neighbor, and the integer pair  $(i, j)$  represents the chirality vector.

The characteristics of the CNFET model are similar to traditional MOSFETs. Except for the threshold voltage, which is calculated by the equation (1.6):

$$V_{th} = \frac{\sqrt{3}}{3} \frac{a \cdot V\pi}{e \cdot D_{cnt}} \quad (1.6)$$

Where  $a = 2.49$  Å is the carbon to carbon atom distance,  $V\pi = 3.033$  eV is the carbon bond energy in the tight binding model,  $e$  is the electron charge unit, and  $D_{cnt}$  is the CNT diameter.

In general, three chiralities can be used in the ternary logic design. The relationship between the chirality, diameter, and threshold voltage are shown in Table 1.1.

Table 1.2 shows some essential parameters of the CNFET model used in all proposed designs for embedded systems with brief descriptions.

TABLE 1.2: CNFET model parameters

	Description	Value
$L_{ch}$	Physical channel length	32 nm
$L_{geff}$	The mean free path in the intrinsic CNT	100 nm
$L_{ss}$ ( $L_{dd}$ )	The length of doped CNT source-side (drain-side) extension region	10 nm
$E_{fi}$	The Fermi level of the doped tube	0.6 eV
$K_{gate}$	The dielectric constant of high-k top gate dielectric material (planer gate)	4
$T_{ox}$	The thickness of the high-k top gate dielectric material (planer gate)	1 nm
$C_{sub}$	The coupling capacitance between the channel region and the substrate	10 pF/m
$C_{csd}$	The coupling capacitance between the channel region and the source/drain region	0 pF/m
$Pitch$	The distance between two adjacent CNTs within the same device	20 nm
$Tubes$	The number of tubes	1

## 1.5 Power Consumption

The power consumption in a transistor is composed of two types: Dynamic and Static.

Dynamic power is the power consumed while charging and discharging the capacitive nodes in the process of switching.

Static power essentially consists of the power used when the transistor is not in the process of switching. If Diode-Connected transistors exist, then the transistors will act as Resistors. Thus, Joule effect power is created and generated heat in the circuit.

$$\text{Total Power consumption : } P = P_s + P_d + P_r$$

$$\text{Static Power : } P_s = N * V_{dd} * I_d$$

$$\text{Dynamic Power : } P_d = N * V_{dd}^2 * f * CL$$

$$\text{Joule effect Power : } P_r = N * R * I_d^2$$

Where,

$N$  : number of transistors in the circuit

$V_{dd}$ : Power Supply

$I_d$  : Current in transistors

$f$  : Frequency of the Vinput

$CL$  : Load Capacitor

$R$  : Resistor value of the Diode-Connected Transistor



## 1.6.2 Binary Logic Gates

Binary digit, called bit, can be represented as (0, 1) corresponding to (0 V, Vdd), (Low, High), or (False, True).

### 1.6.2.1 Inverter Gate

A NOT gate performs a unary function and is often called an inverter or negation. It has a single input  $A$  and a single output  $\bar{A}$ , which is the complement of  $A$ , as shown in Fig. 1.5(a).

In general, the equation of  $\bar{A}$  is equal to  $\bar{A} = (R - 1) - A$ . In binary  $R = 2$ , then  $\bar{A} = 1 - A$ .

When the input is true (Vdd), then the output will be false (0). Similarly, a false input results in a true output.

Table 1.5 shows the truth table of a NOT gate.

TABLE 1.5: Binary NOT truth table

Input $A$	$\bar{A}$
Logic 0 (0V)	1
Logic 1 (Vdd)	0

### 1.6.2.2 AND Gate (Minimum function)

An AND gate has more than one input and one output. The output is equal to the minimum of all its inputs. The output is true only when all of the inputs are true. Whereas, the output is false when at least one of its inputs is false, as shown in Fig. 1.5(b).

Table 1.6 shows the truth table for a two-input AND gate.

### 1.6.2.3 NAND Gate

A NAND gate has more than one input and one output. It is the complement of the AND gate. The output is true when at least one of its inputs is false. Whereas, the output is false only when all inputs are true, as shown in Fig. 1.5(c).

Table 1.6 shows the truth table for a two-input NAND gate.

### 1.6.2.4 OR Gate (Maximum function)

An OR gate has more than one input and one output. The output is equal to the maximum of all its inputs. The output is true when at least one of its inputs is true. Whereas, the output is false only when all of the inputs are false, as shown in Fig. 1.5(d).

Table 1.6 shows the truth table for a two-input OR gate.

### 1.6.2.5 NOR Gate

A NOR gate has more than one input and one output. It is the complement of the OR gate. The output is true only when all of the inputs are false. Whereas, the output is false when at least one of its inputs is true, as shown in Fig. 1.5(e).

Table 1.6 shows the truth table for a two-input NOR gate.

TABLE 1.6: Truth table of some basic binary gates

Input		Output			
<i>A</i>	<i>B</i>	AND	NAND	OR	NOR
0	0	0	1	0	1
0	1	0	1	1	0
1	0	0	1	1	0
1	1	1	0	1	0

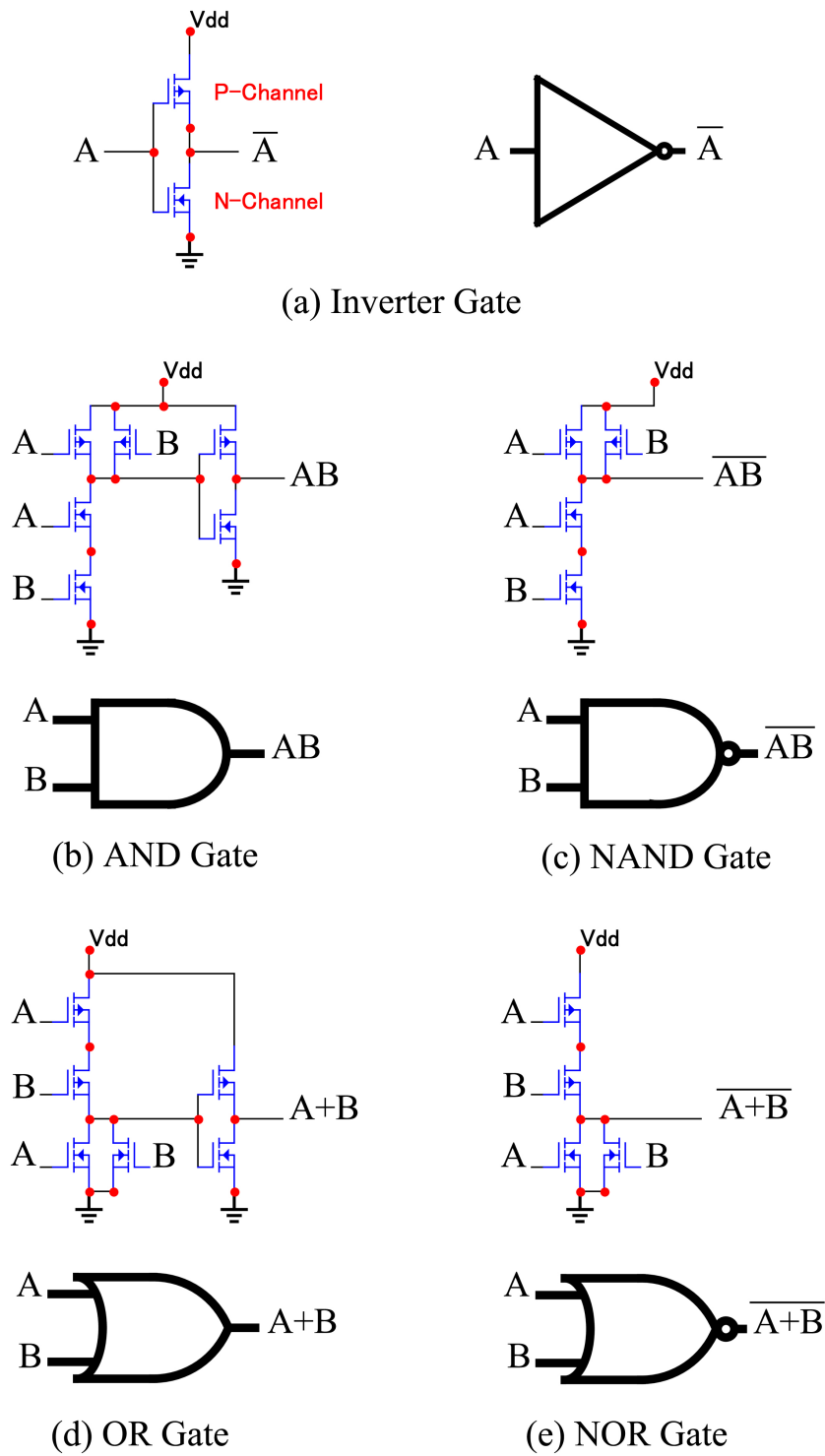


FIGURE 1.5: Basic CMOS Binary Logic Gates.

### 1.6.3 Ternary Logic Gates

Ternary digit, called trit, can be represented in two ways: balanced ternary logic (-1, 0, 1) corresponding to (-Vdd, 0, Vdd), and standard (unbalanced) ternary logic (0, 1, 2) corresponding to (0, Vdd/2, Vdd).

The basic ternary logic gates are TNOT, TAND, TOR, TNAND and TNOR. The ternary equations of the basic ternary logic gates are presented in (1.7):

$$\begin{aligned}
 TNOT(STI) : \quad & \bar{A} = 2 - A, \\
 TAND : \quad & A \bullet B = \min\{A, B\}, \\
 TNAND : \quad & \overline{A \bullet B} = \overline{\min\{A, B\}}, \\
 TOR : \quad & A + B = \max\{A, B\}, \\
 TNOR : \quad & \overline{A + B} = \overline{\max\{A, B\}},
 \end{aligned} \tag{1.7}$$

Where  $A$  and  $B$  are ternary inputs.

#### 1.6.3.1 Ternary Inverter Gates

Ternary Inverter Gates are unary functions (one input one output). There exist three types of ternary inverters, the first is a Positive Ternary Inverter (PTI),  $A_p$ , the second is a Negative Ternary Inverter (NTI),  $A_n$ , and the third one is a standard ternary inverter (STI), which is the complement of  $A$ ,  $\bar{A}$ , as shown in Fig. 1.6(a, b, c).

When the ternary input  $A$  is equal to logic 0 (0V) or 2 (Vdd), then the output of the three ternary inverters is the same as the binary inverter: 0V input becomes Vdd as output and vice versa.

However, when  $A = \text{logic } 1$  (Vdd/2), the PTI output will be logic 2, the NTI output will be logic 0, and the STI output will still logic 1.

Table 1.7 shows the truth table of the three ternary inverters.

TABLE 1.7: Ternary inverters truth table

Ternary Input	PTI	NTI	STI
$A$	$A_p$	$A_n$	$\bar{A}$
Logic 0 (0V)	2	2	2
Logic 1 (0.45V)	2	0	1
Logic 2 (0.9V)	0	0	0

### 1.6.3.2 Other Ternary Logic Gates

The Ternary AND (TAND), Ternary NAND (TNAND), Ternary OR (TOR), and Ternary NOR (TNOR) are described by their truth table in Table 1.8.

The transistor level of basic Ternary Logic Gates are shown in Fig. 1.6.

TABLE 1.8: Truth table of some basic ternary gates

Input		Output			
$A$	$B$	TAND	TNAND	TOR	TNOR
0	0	0	2	0	2
0	1	0	2	1	1
0	2	0	2	2	0
1	0	0	2	1	1
1	1	1	1	1	1
1	2	1	1	2	0
2	0	0	2	2	0
2	1	1	1	2	0
2	2	2	0	2	0

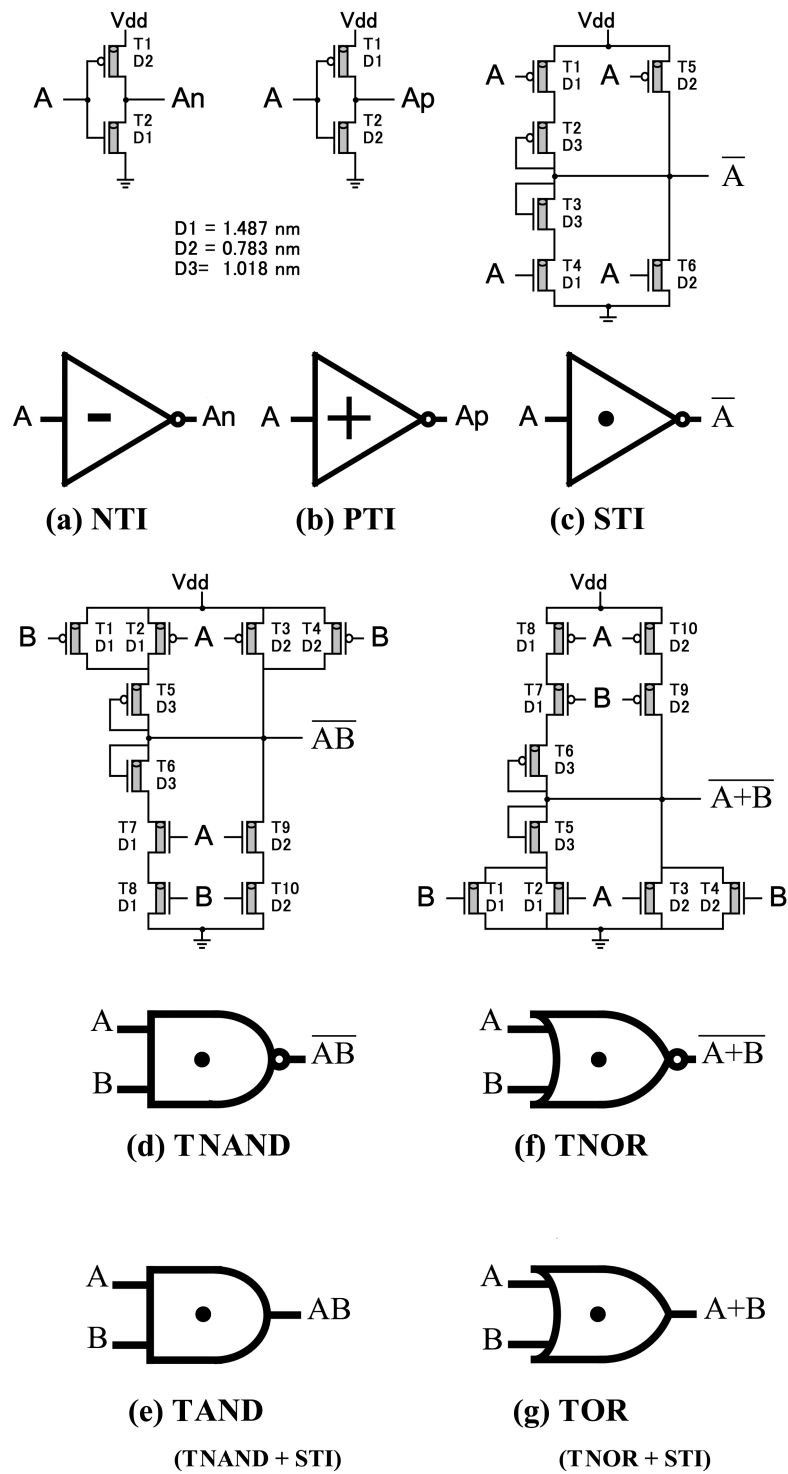


FIGURE 1.6: Basic Ternary Logic Gates [27] using CNFET.

### 1.6.4 Double Pass-transistor Logic (DPL)

Fig.1.7 shows the Double Pass-transistor Logic (DPL) [28], which is a modified version of Complementary Pass-transistor Logic (CPL) by adding P-MOSFET in parallel with the N-MOSFET to eliminate the problems of noise margin and speed degradation at reduced supply voltages associated in CPL circuits. Besides, basic logic gates using DPL ideally have identical propagation delay.

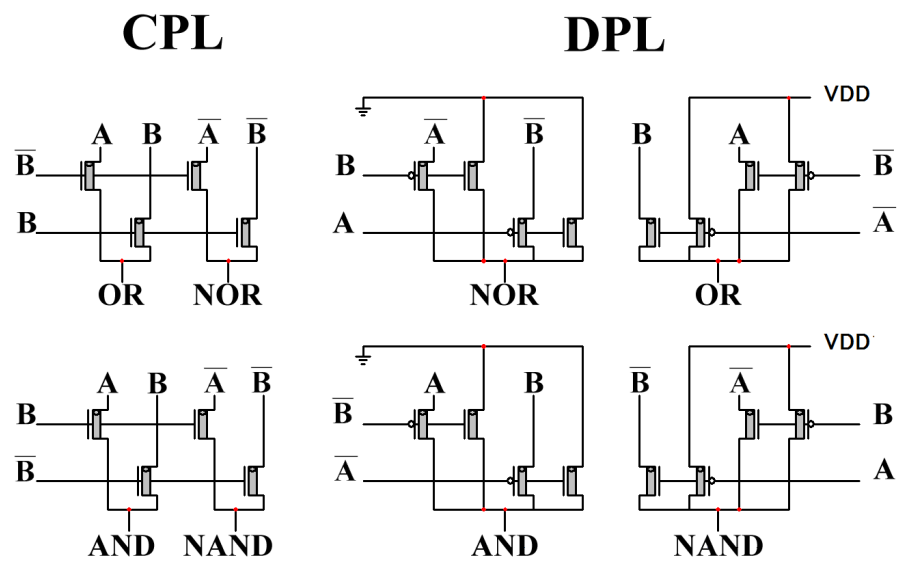


FIGURE 1.7: DPL Gates Design [28]

## **1.7 Objectives**

This thesis has two Objectives to achieve:

### **1.7.1 The First Objective**

The first Objective is to decrease the energy consumption of portable electronics and embedded systems to preserve their battery consumption.

### **1.7.2 The Second Objective**

The second objective is to improve Data Transmission between End devices.

## **1.8 Methodology**

In order to decrease the energy consumption and to improve Data Transmission between End devices, there are five approaches considered for our designs.

### **1.8.1 Choosing the High-Performance Transistor Technology**

Conduct a survey to choose the high-performance transistor technology and we found that Carbon Nanotube Field-Effect Transistor (CNFET) provides the best trade-off in terms of energy efficiency and circuit speed [21] among other transistor technology like CMOS, FinFET, and others.

Therefore, this thesis uses the Stanford CNFET model in [22–24] with  $V_{dd}$  is equal to 0.9 V.

## 1.8.2 Utilizing Ternary Logic System

As described before that the ternary logic system is the most efficient in circuit complexity and cost compared to other bases [16].

Therefore, this thesis uses ternary logic values (0, 1, 2) corresponding to (0,  $V_{dd}/2$ ,  $V_{dd}$ ) = (0 V, 0.45 V, 0.9 V).

## 1.8.3 Applying the Dual Supply Voltages

In general, to get logic 1 (0.45 V) in the ternary circuit from one power supply  $V_{dd}$  (0.9 V), two diode-connected transistors that act like resistors must be added. The use of two transistors is necessary to create a voltage divider in order to produce the ternary logic 1. The results show a notable increase in the static power dissipation due to the direct current from  $V_{dd}$  to the ground [29].

Therefore, this thesis uses dual supply voltages ( $V_{dd}$ ,  $V_{dd}/2$ ) from external power supply to eliminate these two transistors that produce high power consumption and heat.

## 1.8.4 Implementing Energy-Efficient Transistor Arrangement

This thesis uses the best topology transistor arrangement according to paper [30] entitled “Impact of Different Transistor Arrangements on Gate Variability” published in 2018, to increase the robustness of the design regarding the process variability issues.

In general, the best choice is to use the network topology that the transistor in series is as far as possible to the output node. Also, circuit designs with parallel transistors like transmission gates provide better performance.

### 1.8.5 Reducing the number of used transistors

The minimization of transistors count is not the only factor that affects the performance of the proposed circuits, but it is a good factor.

As illustrated before that total Power consumption :  $P = P_s + P_d + P_r$

Static Power :  $P_s = N * Vdd * Id$

Dynamic Power :  $P_d = N * Vdd^2 * f * CL$

Joule effect Power :  $P_r = N * R * Id^2$

Where,

$N$  : number of transistors in the circuit

$Vdd$ : Power Supply

$Id$  : Current in transistors

$f$  : Frequency of the Vinput

$CL$  : Load Capacitor

$R$  : Resistor value of the Diode-Connected Transistor

Therefore, this thesis reduces the number of used transistors, as follows:

- a- Eliminating the diode-connected transistors by using  $Vdd/2$
- b- Applying De Morgan's Law in designing THA1 and TMUL1, to replace for example, (3-AND 1-OR) logic gates with 24 transistors to a 4-NAND logic gate with 16 transistors
- c- Using Transmission Gate (TG) in designing TMUX with 15 transistors instead of using TDecoder, which has 28 transistors
- d- Using unary operators as blocks in our designs

## 1.9 Thesis Outline

This thesis is organized as follow: Chapters 2, 3, and 4 will use CNFET in the designs and HSPICE simulator. Whereas, in chapter 5 will use CMOS DPL gates and Microcap simulator.

Chapter 2 “Ternary Logic Gates”: This chapter represents some of the existing 27 unary operators and TNAND design circuits and proposes seven unary operators and TNAND logic gate.

Chapter 3 “Combinational Logic Circuits”: This chapter represents the existing TDecoders and TMUXs design circuits and proposes two different TDecoders and TMUX.

Chapter 4 “Ternary Arithmetic Logic Units (TALUs)”: This chapter represents the existing THA and TMUL design circuits and proposes three different desings of THAs and three TMULs.

Chapter 5 “Ternary Data Transmission”: This chapter represents the proposed two converters: a Binary-to-Ternary converter and a Ternary-to-Binary converter.

Chapter 6 “Conclusion and Perspectives”.

# Chapter 2

## Ternary Logic Gates

Chapter 1 described the definition and types of ternary logic gates.

This chapter will propose seven unary operators ( $A^1$ ,  $A^2$ ,  $\bar{A}^2$ ,  $A_1$ ,  $1.\bar{A}_n$ ,  $1.\bar{A}_p$ , and STI  $\bar{A}$ ) and TNAND, which are published in ([31], [32]) and can be found in the Appendices (A, B).

### 2.1 Literature Review

In the 1970s, the Unary Operators (one input and one output logic gate) of Ternary Systems were first used to design a universal CMOS circuit for implementation of all 27 unary operators [33–35].

Recently, the researchers utilized the unary operators to design many applications in ternary circuits like TDecoder, TMUX, THA, and TMUL.

In [27], the authors proposed CNFET-based three types of ternary inverters (NTI, PTI, STI) which are three unary operators of the ternary system, TNAND & TNOR logic gates, and TDecoder using the proposed unary operators and TNOR. In [36], the authors presented new unary circuits which are subsequently used to design a “decoder-less” (3:1) TMUX,

a THA, and a TMUL. While in [37, 38], they improved circuit designs for the STI, and TNAND.

In addition, this thesis uses a dual voltage supply. In general, to get logic 1 (0.45V) in the ternary circuit from one power supply Vdd (0.9V), two transistors must be added. The use of two transistors is necessary to create a voltage divider in order to produce the ternary logic 1. The results showed a notable increase in the static power dissipation due to the direct current from Vdd to the ground [29]. *Therefore, this thesis uses Vdd/2 from the same power supply to eliminate these two transistors that produce high power consumption.*

The new designs provide a considerable gain in terms of system performance compared to the designs in [27, 36], as demonstrated in the HSPICE-based simulation results and get the lowest energy consumption (power-delay product (PDP)).

## 2.2 The Proposed Unary Operators of Ternary Systems

This thesis will use nine unary operators to design the ternary circuits, which are shown in Table 2.1 and derived from the equation (2.1).

TABLE 2.1: Truth table of the selected nine unary operators

Ternary Input $A$	PTI $A_p$	NTI $A_n$	STI $\bar{A}$	Decisive Literal $A_1$	Cycle Operators				
					$A^1$	$A^2$	$\bar{A}^2$	$1 \cdot \bar{A}_n$	$1 \cdot \bar{A}_p$
0 (0V)	2	2	2	0	1	2	0	0	0
1 (0.45V)	2	0	1	2	2	0	2	1	0
2 (0.9V)	0	0	0	0	0	1	1	1	1

$$\begin{aligned}
A_p &= \begin{cases} 2, & \text{if } A \neq 0 \\ 0, & \text{if } A = 0 \end{cases} \\
A_n &= \begin{cases} 2, & \text{if } A = 0 \\ 0, & \text{if } A \neq 0 \end{cases} \\
\bar{A} &= 2 - A \\
A_1 &= \begin{cases} 2, & \text{if } A = 1 \\ 0, & \text{if } A \neq 1 \end{cases} \\
A^1 &= (A + 1) \bmod(3) \\
A^2 &= (A + 2) \bmod(3) \\
\bar{A}^2 &= 2 - A^2 \\
1 \cdot \bar{A}_n &= \min\{1, \bar{A}_n\} \\
1 \cdot \bar{A}_p &= \min\{1, \bar{A}_p\}
\end{aligned} \tag{2.1}$$

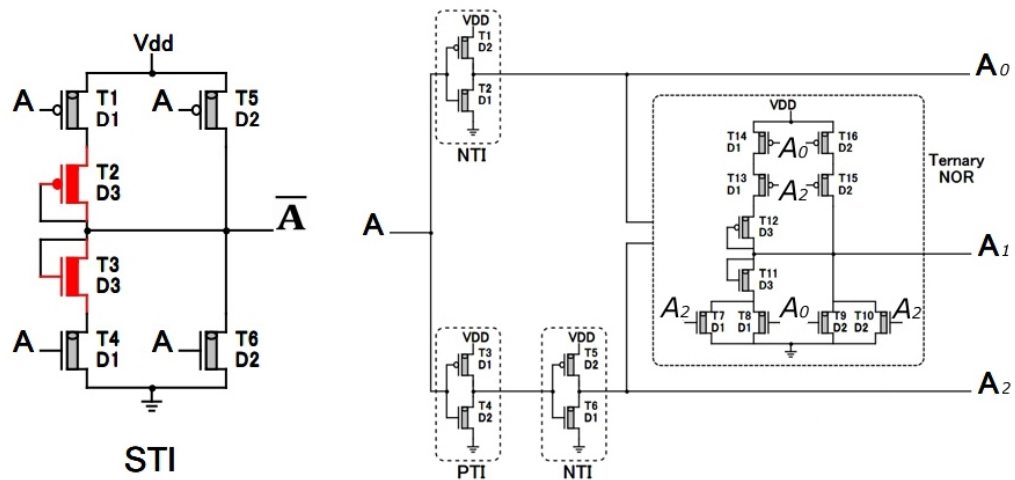
Where  $A \in \{0, 1, 2\}$  is the ternary input.

The first three unary functions are three types of ternary inverters, the first is a positive ternary inverter (PTI),  $A_p$ , the second is a negative ternary inverter (NTI),  $A_n$ , and the third  $\bar{A}$  is a standard ternary inverter (STI), which is the complement of A. The fourth function is the Decisive literal,  $A_1$ . The fifth and the sixth functions are the cycle operators,  $A^1$  and  $A^2$ . The seventh function  $\bar{A}^2$  is the complement of  $A^2$ , and the last two unary functions are the two-inputs ternary AND Gate,  $1 \cdot \bar{A}_n$  and  $1 \cdot \bar{A}_p$ .

The existing Unary Operators' designs in [27], and [36] are shown in Fig. 2.1;

Fig. 2.1 (a) shows three types of ternary inverters ( $A_p$ ,  $A_n$ ,  $\bar{A}$ ) and three Decisive literals ( $A_0$ ,  $A_1$ ,  $A_2$ ) of [27].

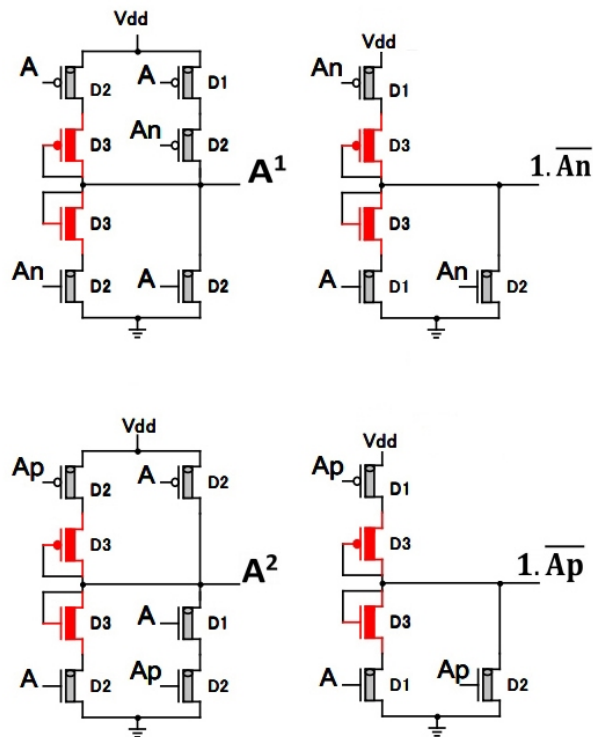
Fig. 2.1 (b) shows the existing four unary operators circuits of [36] ( $A^1$ ,  $A^2$ ,  $1 \cdot \bar{A}_n$ , and  $1 \cdot \bar{A}_p$ ).



The Outputs of Ternary Decoder are Unary Operators

D1 = 1.487 nm  
 D2 = 0.783 nm  
 D3 = 1.018 nm

(a)



(b)

FIGURE 2.1: The Existing unary operators (a) in [27],  $A_p$ ,  $A_n$ ,  $\bar{A}$ ,  $A_0$ ,  $A_1$ , and  $A_2$  (b) in [36],  $A^1$ ,  $A^2$ ,  $1 \cdot \bar{A}_n$ , and  $1 \cdot \bar{A}_p$ .

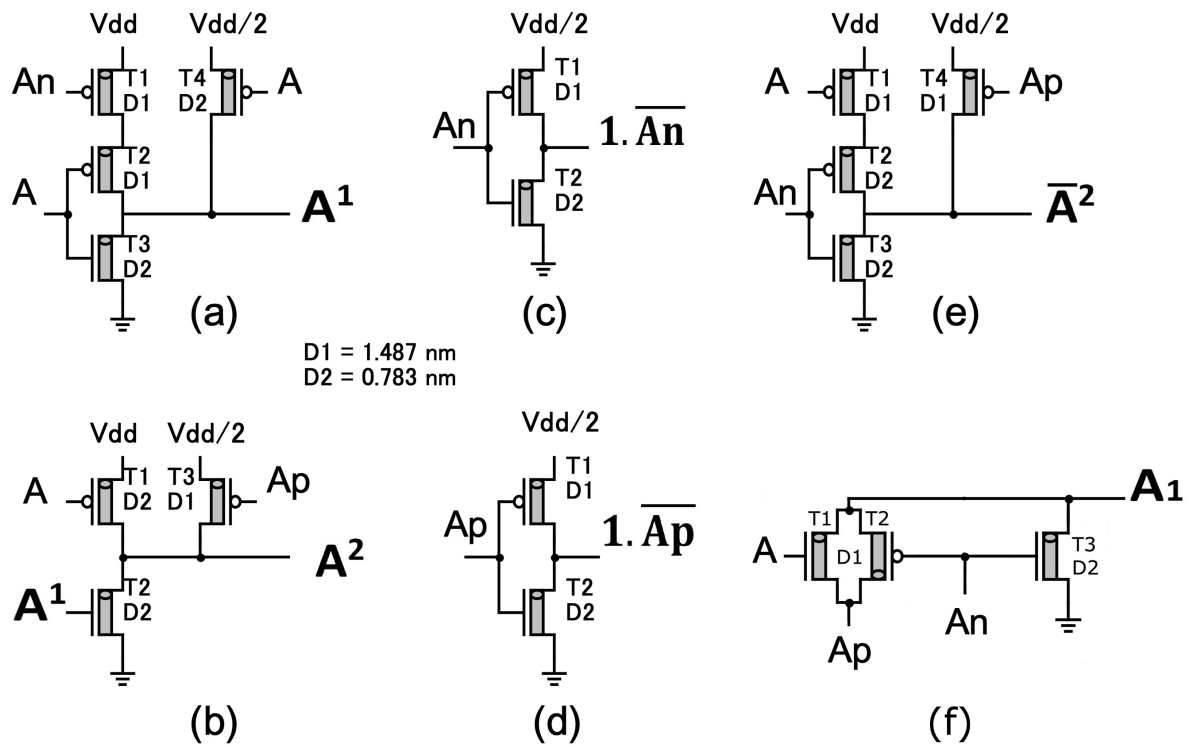


FIGURE 2.2: The transistor level of the proposed six unary operators: (a)  $A^1$ , (b)  $A^2$ , (c)  $1 \cdot \bar{A}_n$ , (d)  $1 \cdot \bar{A}_p$ , (e)  $\bar{A}^2$ , and (f)  $A_1$

This chapter proposes new designs for seven unary operators using CNFET and dual supply voltage ( $V_{dd}$ ,  $V_{dd}/2$ ). This section will explain the six unary operator designs, whereas, the seventh unary operator (STI) will be described in the next section.

Fig. 2.2 shows the transistor level design of the proposed six Unary Operators. (a)  $A^1$ , (b)  $A^2$ , (c)  $1 \cdot \bar{A}_n$ , (d)  $1 \cdot \bar{A}_p$ , (e)  $\bar{A}^2$ , and (f)  $A_1$ .

The chirality, diameter, and threshold voltage ( $V_{th}$ ) of the CNFETs used in Fig. 2.2 are shown in Table 2.2.

### 2.2.1 State of CNFETs with Different Diameters

When the voltage of the gate varies (0 V, 0.45 V, 0.9 V), then the transistor will be turned ON or OFF, which depends on the type and the diameter of CNFET, as described in Table 2.3.

TABLE 2.2: The chirality, diameter, and threshold voltage of the CNTs used in the proposed six unary operators

CNFET Type	Fig.2.2						Chirality	Diameter	Vth
	(a)	(b)	(c)	(d)	(e)	(f)			
P-CNFET	T4	T1	-	-	T2	-	(10, 0)	0.783nm	- 0.559V
P-CNFET	T1, T2	T3	T1	T1	T1, T4	T2	(19, 0)	1.487nm	- 0.289V
N-CNFET	T3	T2	T2	T2	T3	T3	(10, 0)	0.783nm	0.559V
N-CNFET	-	-	-	-	-	T1	(19, 0)	1.487nm	0.289V

TABLE 2.3: The state of CNFETs with D1=1.487 nm and D2=0.783 nm

Type	Diameter	Voltage Gate		
		0V	0.45V	0.9V
P-CNFET	D2	ON	OFF	OFF
	D1	ON	ON	OFF
N-CNFET	D2	OFF	OFF	ON
	D1	OFF	ON	ON

The operations of the proposed unary operators are summarized in Table 2.4.

The advantages of the proposed six Unary Operators are:

1. They provide low power consumption due to eliminating the two transistors that act as resistors (T2, T3 in all circuits [36]) by applying dual supply voltages ( $V_{dd}$ ,  $V_{dd}/2$ )
2. To get logic 1 (0.45 V): one or two transistors must be active (see Table 2.4) whereas, in [36], four transistors in series must be active (T1, T2, T3, T4)
3. Reducing the Transistors Count

TABLE 2.4: The detailed operation of the proposed six unary operators with  $D1=1.487$  nm and  $D2=0.783$  nm

Circuit	$A$ $A_n$ $A_p$	Transistors Turned		Output	
		ON	OFF		
	$0$ $2$ $1$ $0$ $2$ $0$	$T2, T4$ $T1, T2$ $T1, T3$	$T1, T3$ $T3, T4$ $T2, T4$	$1$ $2$ $0$	$A^1$
	$0$ $2$ $1$ $2$ $2$ $0$	$T1$ $T2$ $T3$	$T2, T3$ $T1, T3$ $T1, T2$	$2$ $0$ $1$	$A^2$
	$0$ $2$ $2$ $1$ $0$ $2$ $2$ $0$ $0$	$T1, T3$ $T1, T2$ $T2, T4$	$T2, T4$ $T3, T4$ $T1, T3$	$0$ $2$ $1$	$\overline{A^2}$
	$0$ $2$ $1$ $0$ $2$ $0$	$T2$ $T1$ $T1$	$T1$ $T2$ $T2$	$0$ $1$ $1$	$1 \cdot \overline{A_n}$
	$0$ $2$ $1$ $2$ $2$ $0$	$T2$ $T2$ $T1$	$T1$ $T1$ $T2$	$0$ $0$ $1$	$1 \cdot \overline{A_p}$
	$0$ $2$ $2$ $1$ $0$ $2$ $2$ $0$ $0$	$T3$ $T1, T2$ $T1, T2$	$T1, T2$ $T3$ $T3$	$\text{Ground}$ $A_p = 2$ $A_p = 0$	$A_1$

## 2.3 The Proposed STI & TNAND Logic Gates

The existing STI (TNOT) and TNAND logic gates designs in [27, 37], and [38] are shown in Fig. 2.3 and 2.4.

This chapter proposes new designs of STI and TNAND logic gates, as shown in Fig. 2.5 and Fig. 2.6.

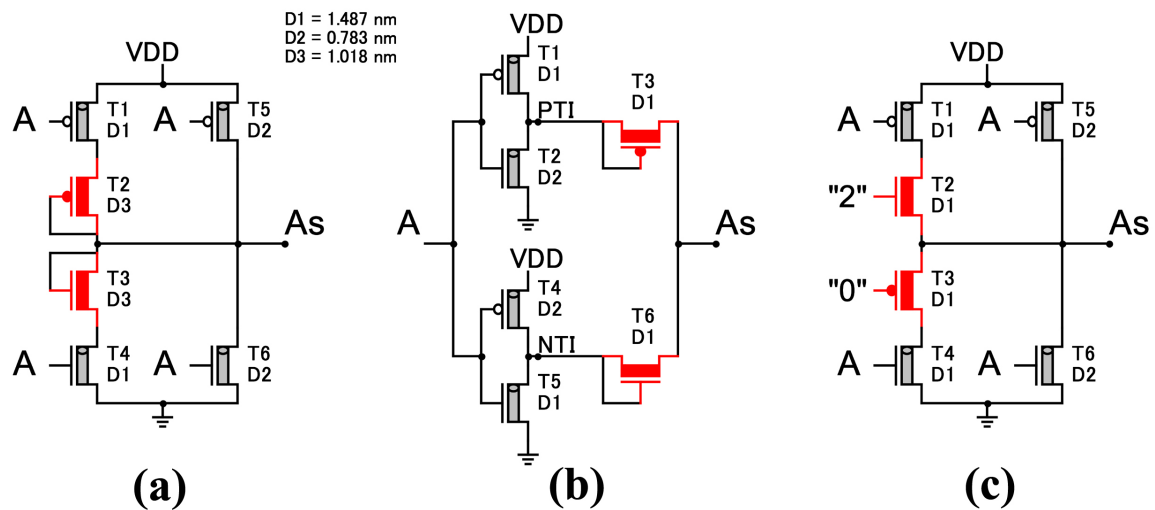


FIGURE 2.3: The Existing STI in (a) [27], (b) [37], and (c) [38].

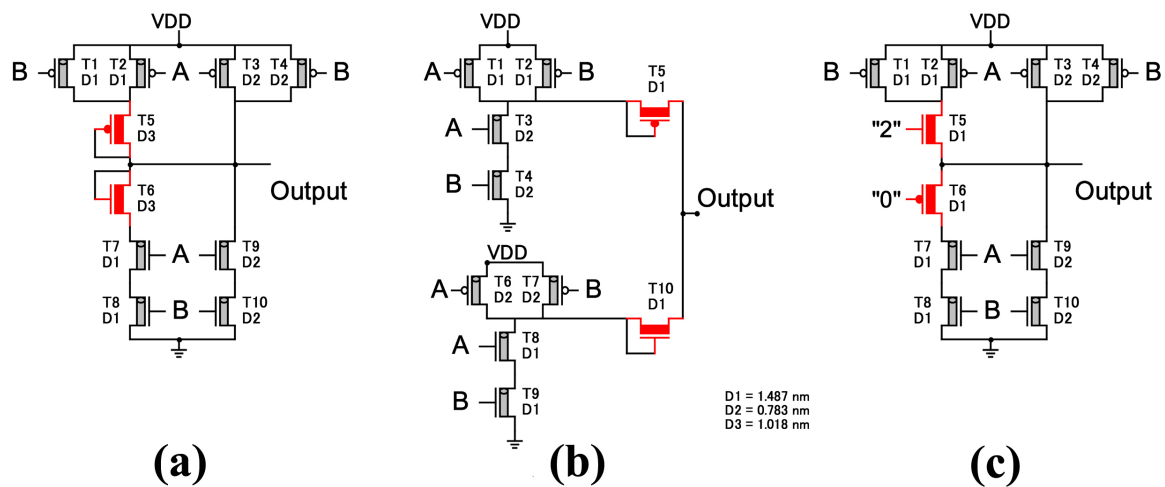


FIGURE 2.4: The Existing TNAND in (a) [27], (b) [37], and (c) [38].

### 2.3.1 The Proposed STI

Fig. 2.5 shows the transistor level design of the proposed STI where the chirality, diameter, and threshold voltage ( $V_{th}$ ) of the CNFETs used are shown in Table 2.5.

Table 2.6 shows the detailed operation of the proposed STI circuit of Fig. 2.5.

When the input  $A$  is logic 0, then transistors (T1, and T4) are turned ON and (T2, and T5) are turned OFF. The output  $A_p$  is equal to logic 2, then transistor (T3) is turned ON. Therefore, the output  $\bar{A}$  is equal to logic 2.

When the input  $A$  is logic 1, then transistor (T1) is turned ON, and (T2, T4, and T5) are turned OFF. The output  $A_p$  is equal to logic 2, then transistor (T3) is turned ON. Therefore,

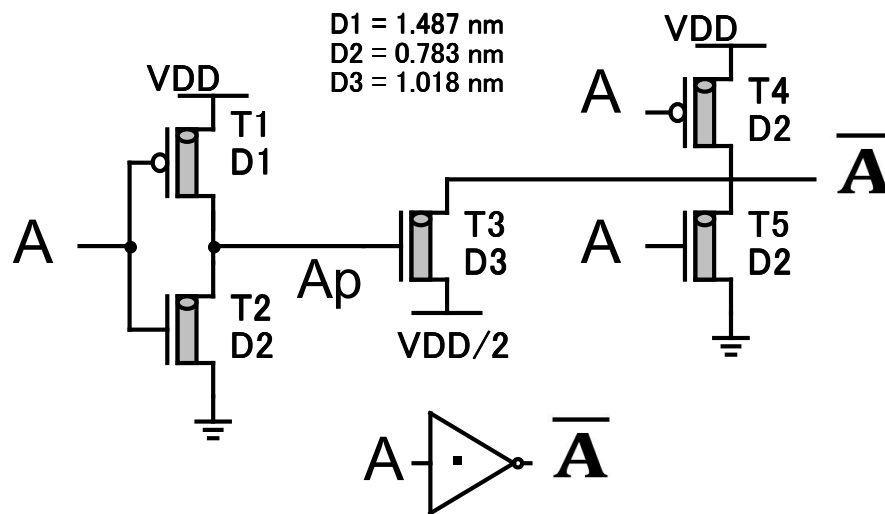


FIGURE 2.5: Transistor level of the proposed STI.

TABLE 2.5: The chirality, diameter, and threshold voltage of the CNTs used in the proposed STI

CNFET Type	Chirality	Diameter	$V_{th}$
P-CNFET (T4)	(10, 0)	0.783nm	- 0.559V
P-CNFET (T1)	(19, 0)	1.487nm	- 0.289V
N-CNFET (T2,T5)	(10, 0)	0.783nm	0.559V
N-CNFET (T3)	(13, 0)	1.018nm	0.428V

TABLE 2.6: The detailed operation of the STI

<b>Ternary Input <math>A</math></b>	<b>0 (0 V)</b>	<b>1 (0.45 V)</b>	<b>2 (0.9 V)</b>
P-CNFET T1	ON	ON	OFF
N-CNFET T2	OFF	OFF	ON
$A_p$	<b>2</b>	<b>2</b>	<b>0</b>
N-CNFET T3	ON	ON	OFF
P-CNFET T4	ON	OFF	OFF
N-CNFET T5	OFF	OFF	ON
<b>Output <math>\bar{A}</math></b>	<b>2</b>	<b>1</b>	<b>0</b>

the output  $\bar{A}$  is equal to logic 1.

Finally, when the input  $A$  is logic 2, then transistors (T2, and T5) are turned ON and (T1, and T4) are turned OFF. The output  $A_p$  is equal to logic 0, then transistor (T3) is turned OFF. Therefore, the output  $\bar{A}$  is equal to logic 0.

### 2.3.2 The Proposed TNAND

Fig. 2.6 shows the transistor level design of the proposed two inputs TNAND where the chirality, diameter, and threshold voltage ( $V_{th}$ ) of the CNFETs used are shown in Table 2.7.

Table 2.8 shows the selected combinations of two ternary inputs  $A$  and  $B$  to describe the operation of the proposed TNAND logic gate circuit of Fig. 2.6.

TABLE 2.7: The chirality, diameter, and threshold voltage of the CNTs used in the proposed TNAND

CNFET Type	Chirality	Diameter	$V_{th}$
P-CNFET (T1,T3,T7,T8)	(10, 0)	0.783nm	- 0.559V
P-CNFET (T5, T6)	(13, 0)	1.018nm	- 0.428V
N-CNFET (T9, T10)	(10, 0)	0.783nm	0.559V
N-CNFET (T2, T4)	(19, 0)	1.487nm	0.289V

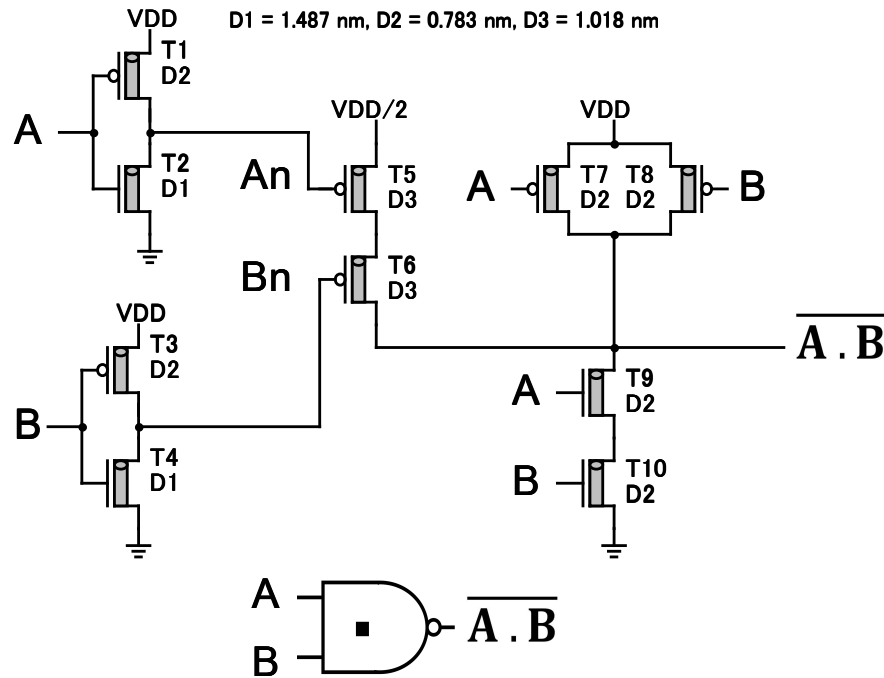


FIGURE 2.6: Transistor level of the proposed TNAND.

TABLE 2.8: The detailed operation of the TNAND with selected inputs

<b>Ternary Inputs (A, B)</b>	<b>(0, 0)</b>	<b>(0, 1)</b>	<b>(1, 1)</b>	<b>(1, 2)</b>
P-CNFET T1	ON	ON	OFF	OFF
N-CNFET T2	OFF	OFF	ON	ON
$A_n$	<b>2</b>	<b>2</b>	<b>0</b>	<b>0</b>
P-CNFET T3	ON	OFF	OFF	OFF
N-CNFET T4	OFF	ON	ON	ON
$B_n$	<b>2</b>	<b>0</b>	<b>0</b>	<b>0</b>
P-CNFET T5	OFF	OFF	ON	ON
P-CNFET T6	OFF	ON	ON	ON
P-CNFET T7	ON	ON	OFF	OFF
P-CNFET T8	ON	OFF	OFF	OFF
N-CNFET T9	OFF	OFF	OFF	OFF
N-CNFET T10	OFF	OFF	OFF	ON
<b>Output TNAND</b>	<b>2</b>	<b>2</b>	<b>1</b>	<b>1</b>

When the inputs ( $A, B$ ) are (0 V, 0 V), then transistors (T1, T3, T7, and T8) are turned ON and (T2, T4, T9, and T10) are turned OFF. The outputs ( $A_n, B_n$ ) are equal to (0.9 V, 0.9 V),

then transistors (T5, and T6) are turned OFF. Therefore, the output is equal to 0.9 V.

When the inputs ( $A$ ,  $B$ ) are (0 V, 0.45 V), then transistors (T1, T4, and T7) are turned ON and (T2, T3, T8, T9, and T10) are turned OFF. The outputs ( $A_n$ ,  $B_n$ ) are equal to (0.9 V, 0 V), then transistor (T6) is turned ON and (T5) is turned OFF. Therefore, the output is equal to 0.9 V.

When the inputs ( $A$ ,  $B$ ) are (0.45 V, 0.45 V), then transistors (T2, and T4) are turned ON and (T1, T3, T7, T8, T9, and T10) are turned OFF. The outputs ( $A_n$ ,  $B_n$ ) are equal to (0 V, 0 V), then transistors (T5, and T6) are turned ON. Therefore, the output is equal to 0.45 V.

Finally, when the inputs ( $A$ ,  $B$ ) are (0.45 V, 0.9 V), then transistors (T2, T4, and T10) are turned ON and (T1, T3, T7, T8, and T9) are turned OFF. The outputs ( $A_n$ ,  $B_n$ ) are equal to (0 V, 0 V), then transistors (T5, and T6) are turned ON. Therefore, the output is equal to 0.45 V.

TABLE 2.9: The advantage of proposed STI &amp; TNAND logic gates

Disadvantage of Existing Logic gates in [27, 37] and [38]	Advantage
<p style="text-align: center;">Shown in Fig. 2.3 and 2.4</p> <p style="text-align: center;">The existing designs suffer from</p> <p style="text-align: center;">High power consumption due to:</p>	<p style="text-align: center;">Shown in Fig. 2.5 and 2.6</p> <p style="text-align: center;">The proposed designs provide</p> <p style="text-align: center;">Low power consumption due to:</p>
<p>1- Two transistors that act as resistors in STI (T2, T3) and in TNAND (T5, T6) [27].</p> <p>2- Two transistors that act as resistors in STI (T3, T6) and in TNAND (T5, T10) [37].</p> <p>3- Two transistors that are always active in STI (T2, T3) and in TNAND (T5, T6) [38].</p>	<p>Eliminating these two transistors by applying dual supply voltages (V<sub>dd</sub> and V<sub>dd</sub>/2).</p>
<p>4- For STI [27, 38]: Four transistors (T1, T2, T3, T4) in series must be active to get logic 1.</p> <p>5- For STI [37]: Four transistors (T1, T3, T6, T5) in series must be active to get logic 1.</p>	<p>For the proposed STI: Only one transistor (T3) must be active to get logic 1.</p>
<p>6- For TNAND [27, 38]: Five or Six transistors [(T1 or T2) or both, T5, T6, T7, T8)] in series must be active to get logic 1.</p> <p>7- For TNAND [37]: Five or Six transistors [(T1 or T2) or both, T5, T10, T8, T9)] in series must be active to get logic 1.</p>	<p>For the proposed TNAND: Two transistors (T5, T6) in series must be active to get logic 1.</p>

Table 2.9 shows the disadvantage of the existing STI and TNAND in [27, 37] and [38].

## 2.4 Simulation Results and Comparisons

The proposed six Unary Operators circuits are simulated, tested, and compared to [27, 36] using the HSPICE simulator and CNFET with 32-nm channel length at a power supply (0.9V), a room temperature (27 °C), and a frequency (1 GHz).

Whereas, the proposed STI and TNAND are simulated, tested, and compared to [27, 37, 38] at different power supplies (0.8V, 0.9V, 1V), different temperatures (10°C, 27°C, 70°C ), and different frequencies (0.5GHz, 1GHz, 2GHz).

All input signals have a fall and rise time equal to 10 ps. The average power consumption, maximum propagation delay, and maximum power delay product (PDP) are obtained for all circuits.

The performance of the proposed circuits will be compared to other designs for the PDP.

Figures from 2.7 to 2.14 illustrate the transient analysis of the proposed six Unary Operators, STI, and TNAND.

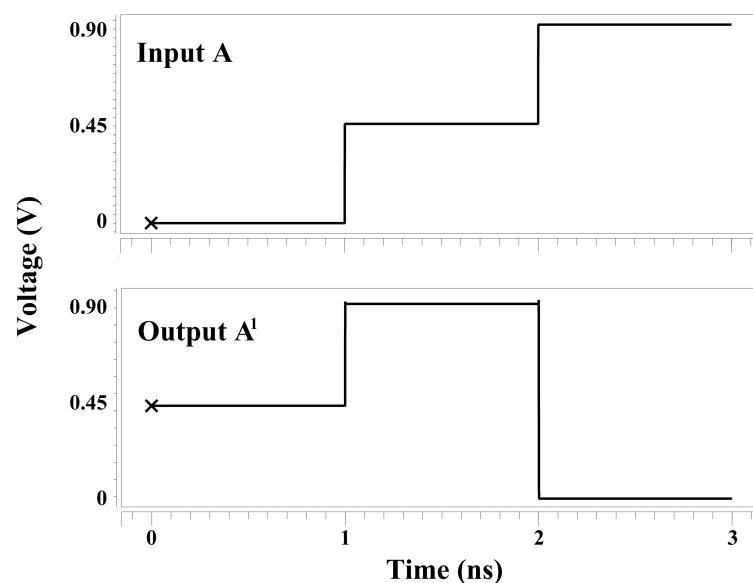
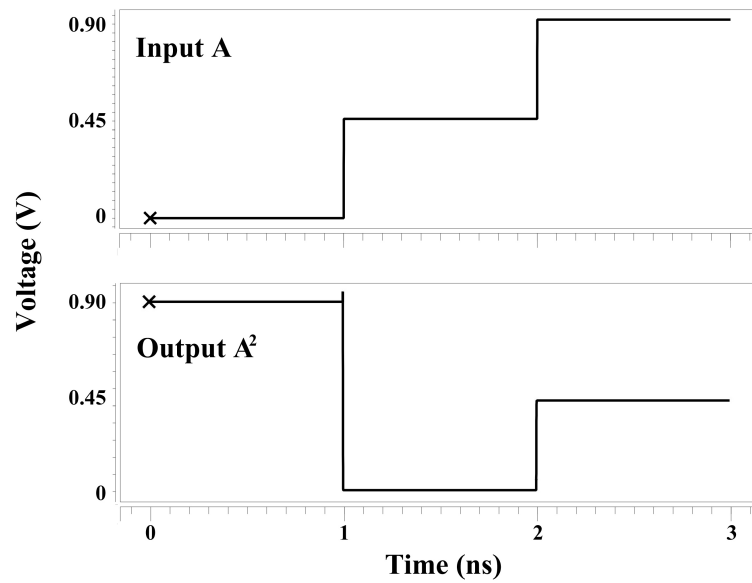
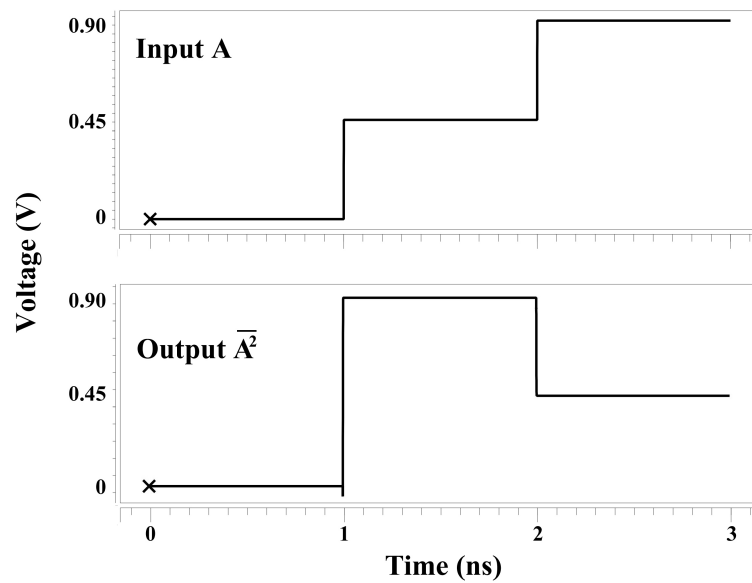
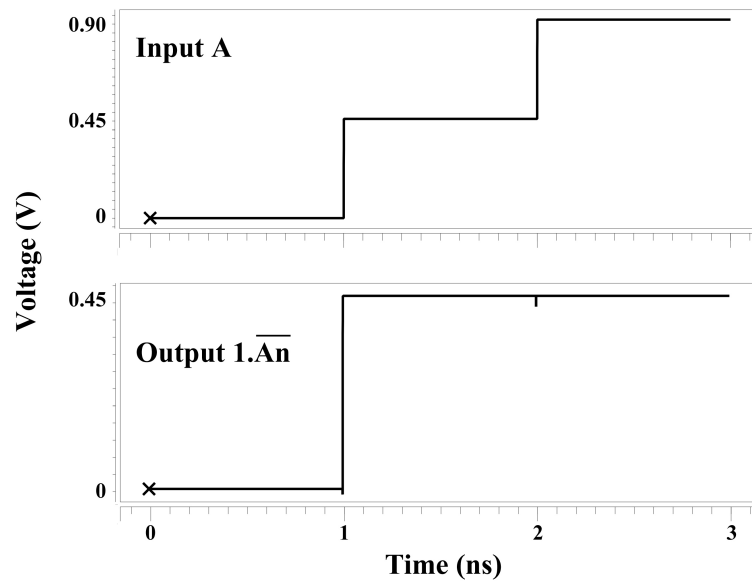
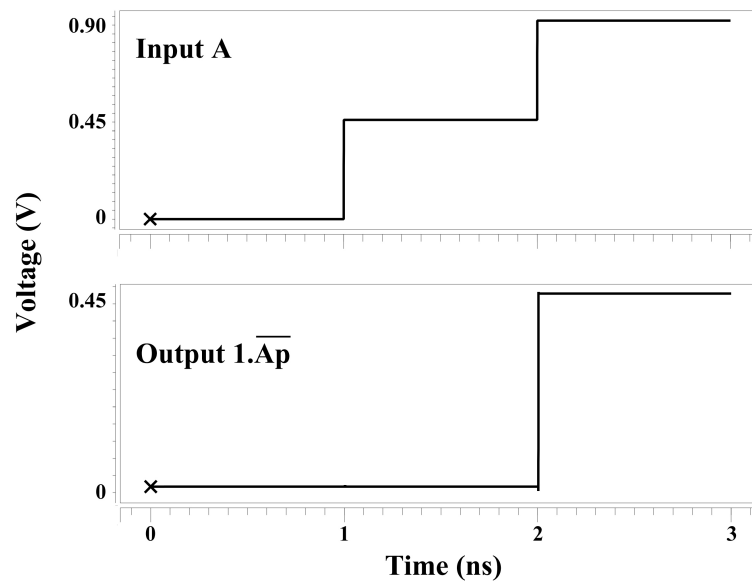


FIGURE 2.7: Transient analysis of the proposed  $A^1$ .

FIGURE 2.8: Transient analysis of the proposed  $A^2$ .FIGURE 2.9: Transient analysis of the proposed  $\bar{A}^2$ .

FIGURE 2.10: Transient analysis of the proposed  $1 \cdot \bar{A}_n$ .FIGURE 2.11: Transient analysis of the proposed  $1 \cdot \bar{A}_p$ .

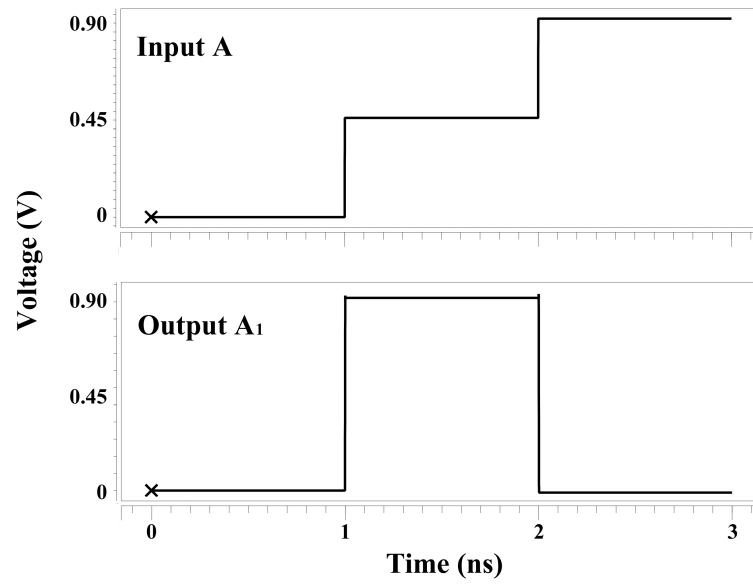
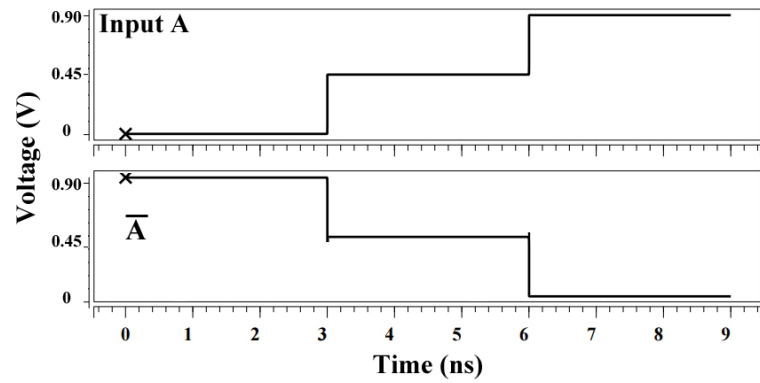
FIGURE 2.12: Transient analysis of the proposed  $A_1$ .

FIGURE 2.13: Transient analysis of the proposed STI.

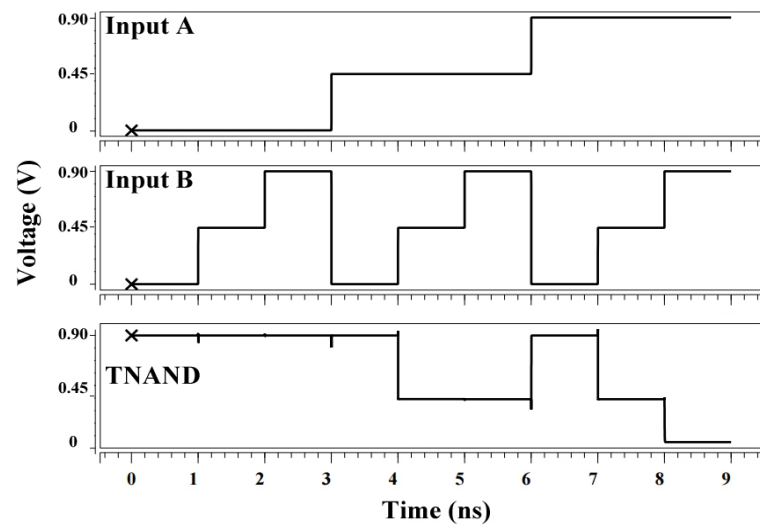


FIGURE 2.14: Transient analysis of the proposed TNAND.

### 2.4.1 Comparison of Transistors Count Of All Circuits

The minimization of Transistors Count is not the only factor that affects the performance of the proposed circuits, but it is a important factor.

Table 2.10 shows the comparison of Transistors Count for the 6 unary operators, STI, and TNAND compared to [27, 36–38]. This comparison of the proposed circuits demonstrates a notable reduction in Transistors Count.

$A^1$ ,  $A^2$ ,  $\bar{A}^2$ ,  $1 \cdot \bar{A}_n$ , and  $1 \cdot \bar{A}_p$  are compared to [36], and the reduction in transistors count are 42.9%, 57.1%, 69.2%, 60%, and 60%, respectively.

For  $A_1$ , 70% compared to  $A_1$  in [27]. For STI, 16.67% compared to STI in [27, 37], and [38]. For TNAND, no reduction in Transistors Count but the results gives better performance.

TABLE 2.10: Comparison of Transistors Count of All Circuits

	[36]	[27]	[37]	[38]	Proposed	Reduction
$A^1$	7	-	-	-	<b>4</b>	42.85 %
$A^2$	7	-	-	-	<b>3</b>	57.14 %
$\bar{A}^2$	13*	-	-	-	<b>4</b>	69.2 %
$1 \cdot \bar{A}_n$	5	-	-	-	<b>2</b>	60 %
$1 \cdot \bar{A}_p$	5	-	-	-	<b>2</b>	60 %
$A_1$	-	10	-	-	<b>3</b>	70 %
<b>STI</b>	-	6	6	6	<b>5</b>	16.66 %
<b>TNAND</b>	-	10	10	10	<b>10</b>	0 %

\* $\bar{A}^2 = A^2$  (7 T) + STI (6 T) = 13 Transistors

## 2.4.2 Comparison of the Unary Operators Circuits

Table 2.11 shows the comparison between the six unary operators to [27, 36] in terms of the average power consumption, maximum propagation delay, and maximum power delay product (PDP).

TABLE 2.11: Comparison between the six unary operators to [27, 36] in terms of the average power consumption, maximum propagation delay, and maximum PDP at Vdd (0.9V), temperature (27 ° C), and frequency (1 GHz)

	Power (nw)	Delay (ps)	PDP (x10 <sup>-20</sup> J)
$A^1$ in [36]	190	4.42	83.98
<b>Proposed <math>A^1</math></b>	50	1.73	8.65
Improvement	73.68%	60.86%	89.7%
<hr/>			
$A^2$ in [36]	180	4.86	87.48
<b>Proposed <math>A^2</math></b>	20	2.10	4.2
Improvement	88.89%	56.79%	95.2%
<hr/>			
$\bar{A}^2$ in [36]	580	7.38	428
<b>Proposed <math>\bar{A}^2</math></b>	4	2.32	0.93
Improvement	99.31%	68.56%	99.78%
<hr/>			
$1 \cdot \bar{A}_n$ in [36]	560	3.72	208.32
<b>Proposed <math>1 \cdot \bar{A}_n</math></b>	6	4.5	2.7
Improvement	98.93%	-21.62%	98.7%
<hr/>			
$1 \cdot \bar{A}_p$ in [36]	200	3.10	62
<b>Proposed <math>1 \cdot \bar{A}_p</math></b>	10	4.14	4.14
Improvement	95%	-33.55%	93.32%
<hr/>			
$A_1$ in [27]	572	6.12	350
<b>Proposed <math>A_1</math></b>	5	1.95	1
Improvement	99.12%	68.13%	99.72%

The comparison of the proposed six unary operators demonstrates a notable reduction in energy consumption (PDP) of 89.7%, 95.2%, 99.78%, 98.7%, and 93.32% compared to  $A^1$ ,  $A^2$ ,  $\bar{A}^2$ ,  $1 \cdot \bar{A}_n$ , and  $1 \cdot \bar{A}_p$  in [36], respectively. And 99.72% compared to  $A_1$  in [27].

### 2.4.3 Comparison of Different STI Circuits

Fig. 2.15 shows the PDP Comparison of the investigated STI at (a) Different Power Supplies, (b) Different Temperatures, and (c) Different Frequencies.

#### 2.4.3.1 Impact of Different Power Supplies

The effect of different power supplies (0.8V, 0.9V, 1V) on the performance metrics of all proposed circuits is studied.

Simulation is done at 1 GHz operating frequency and room temperature at 27°C, as illustrated in Fig. 2.15 (a).

The comparison of the proposed STI demonstrates a notable reduction in PDP, as shown in Fig. 2.15 (a).

At Vdd=0.8V, 28.33%, 88.68%, and 80.37% compared to [27, 37], and [38], respectively.

At Vdd=0.9V, 61.22%, 83.95%, and 86.38% compared to [27, 37], and [38], respectively.

At Vdd=1V, 30.42%, 68.98%, and 74.05% compared to [27, 37], and [38], respectively.

#### 2.4.3.2 Impact of Different Temperatures

Temperature noise is one of the most critical issues which negatively affect the performance of the circuit.

The effect of different temperatures (10°C, 27°C, 70°C) on the performance metrics of all proposed circuits is studied. In simulation, the operating frequency is 1 GHz, and the power supply (Vdd) is 0.9V, as illustrated in Fig. 2.15 (b).

The comparison of the proposed STI demonstrates a notable reduction in PDP, as shown in Fig. 2.15 (b).

At Temperature=10°C, 27.88%, 79.95%, and 78.15% compared to [27, 37], and [38], respectively.

At Temperature=27°C, 61.22%, 83.95%, and 86.38% compared to [27, 37], and [38], respectively.

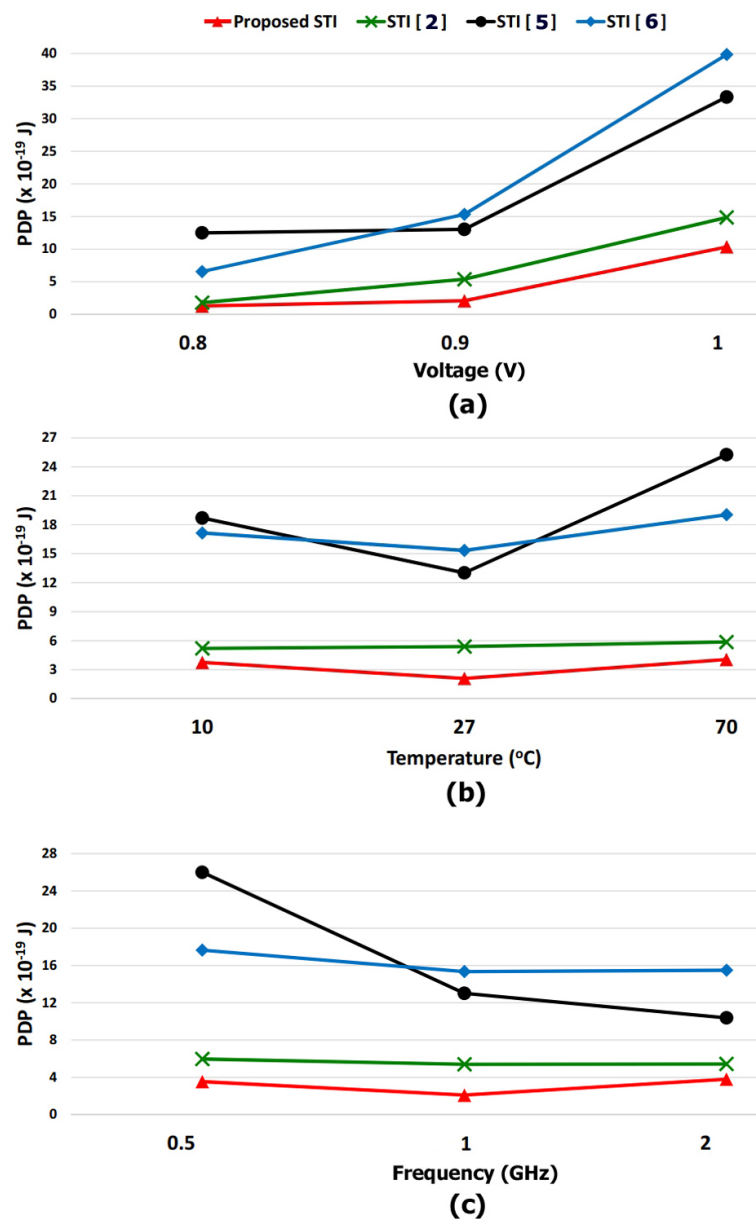


FIGURE 2.15: PDP Comparison of the investigated STI for: (a) Different Power Supplies, (b) Different Temperatures, and (c) Different Frequencies.

At Temperature=70°C, 30.89%, 83.96%, and 78.73% compared to [27, 37], and [38], respectively.

### 2.4.3.3 The Impact of Different Frequencies

Electronic circuits behave very differently at high frequencies due to a change in the behavior of passive components (resistors, inductors, and capacitors) and parasitic effects on active components, PCB tracks.

Recently, high-frequency operation is in demand for electronic devices.

The effect of different frequencies (0.5 GHz, 1 GHz, 2 GHz) on the performance metrics of all proposed circuits is studied. Simulation is done at power supply V<sub>dd</sub> equals 0.9 V, and at 27°C temperature, as illustrated in Fig. 2.15 (c).

The comparison of the proposed STI demonstrates a notable reduction in PDP, as shown in Fig. 2.15 (c).

At frequency=0.5 GHz, 40.60%, 86.38%, and 79.93% compared to [27, 37], and [38], respectively.

At frequency=1 GHz, 61.22%, 83.95%, and 86.38% compared to [27, 37], and [38], respectively.

At frequency=2 GHz, 30.20%, 63.45%, and 75.52% compared to [27, 37], and [38], respectively.

## 2.4.4 Comparison of Different TNAND Circuits

Figure 2.16 shows the PDP Comparison of the investigated TNAND for (a) Different Power Supplies, (b) Different Temperatures, and (c) Different Frequencies.

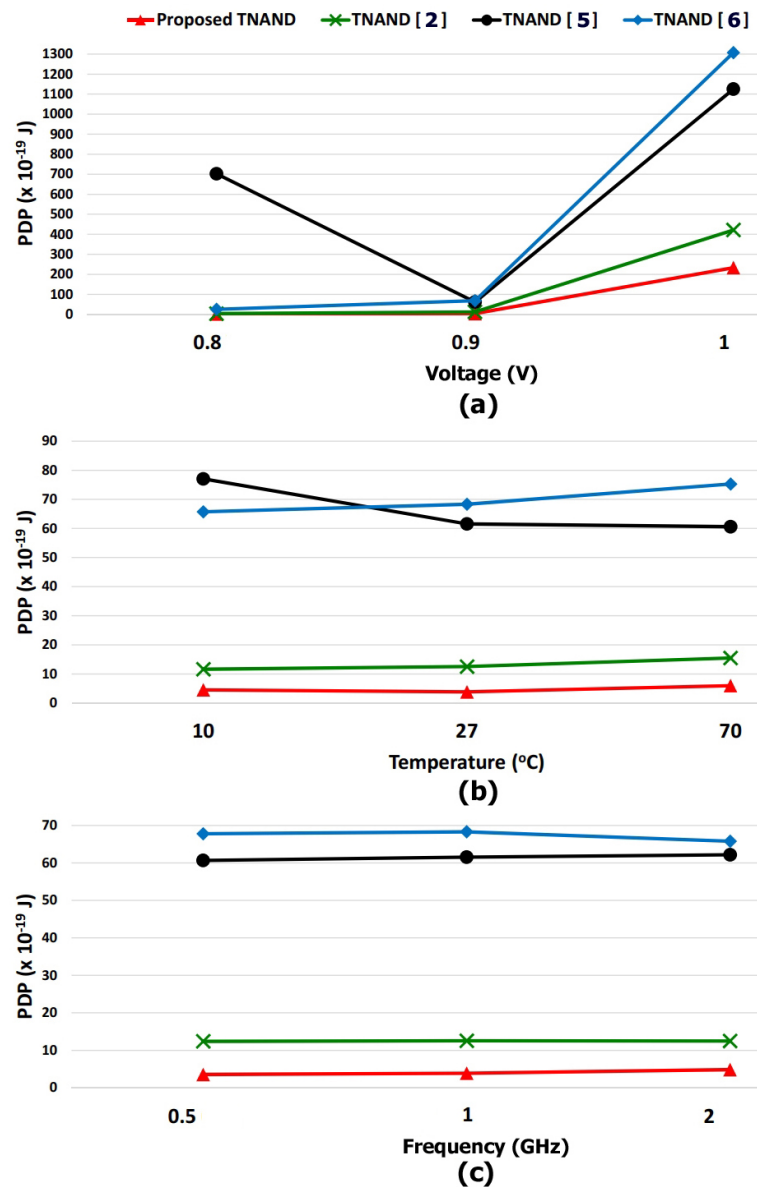


FIGURE 2.16: PDP Comparison of the investigated TNAND at: (a) Different Power Supplies, (b) Different Temperatures, and (c) Different Frequencies.

#### 2.4.4.1 Impact of Different Power Supplies

Simulation is done at 1 GHz operating frequency and room temperature at 27°C, as illustrated in Fig. 2.16 (a).

The comparison of the proposed TNAND demonstrates a notable reduction in PDP, as shown in Fig. 2.16 (a).

At  $V_{dd}=0.8$  V, 32.53%, 99.64%, and 90.07% compared to [27, 37] and [38], respectively.

At  $V_{dd}=0.9$  V, 69.22%, 93.73%, and 94.35% compared to [27, 37] and [38], respectively.

At  $V_{dd}=1$  V, 44.6%, 79.27%, and 98.3% compared to [27, 37], and [38], respectively.

#### 2.4.4.2 Impact of Different Temperatures

The effect of different temperatures (10°C, 27°C, 70°C) on the performance metrics of all proposed circuits is studied.

Simulation is done at 1 GHz operating frequency, and at 0.9V power supply  $V_{dd}$ , as illustrated in Fig. 2.16 (b).

The comparison of the proposed TNAND demonstrates a notable reduction in PDP, as shown in Fig. 2.16 (b).

At Temperature=10°C, 60.88%, 94.09%, and 93.08% compared to [27, 37] and [38], respectively.

At Temperature=27°C, 69.22%, 93.73%, and 94.35% compared to [27, 37] and [38], respectively.

At Temperature=70°C, 61.34%, 90.13%, and 92.06% compared to [27, 37] and [38], respectively.

#### 2.4.4.3 Impact of Different Frequencies

The effect of different frequencies (0.5 GHz, 1 GHz, 2 GHz) on the performance metrics of all proposed circuits is studied.

Simulation is done at at 0.9V power supply  $V_{dd}$ , and at 27°C temperature equals, as illustrated in Fig. 2.16 (c).

The comparison of the proposed TNAND demonstrates a notable reduction in PDP, as shown in Fig. 2.16 (c).

At frequency=0.5 GHz, 71.46%, 94.18%, and 94.79% compared to [27, 37], and [38], respectively.

At frequency=1 GHz, 69.22%, 93.73%, and 94.35% compared to [27, 37], and [38], respectively.

At frequency=2 GHz, 61.27%, 92.23%, and 92.66% compared to [27, 37], and [38], respectively.

## 2.5 Conclusion

This chapter has proposed new designs of seven Unary Operators ( $A^1$ ,  $A^2$ ,  $\bar{A}^2$ ,  $A_1$ ,  $1.\bar{A}_n$ ,  $1.\bar{A}_p$ , and the Standard Ternary Inverter (STI)  $\bar{A}$ ), and TNAND that aims to optimize the trade-off between performance and energy efficiency.

The design process tried to optimize several circuit techniques such as reducing the number of used transistors, utilizing energy-efficient transistor arrangements, and applying the dual supply voltages ( $V_{dd}$  and  $V_{dd}/2$ ).

The proposed ternary circuits are compared to the latest ternary circuits, simulated and tested using HSPICE simulator under various operating conditions with different supply voltages, different temperatures, and different frequencies.

The results prove the merits of the approach in terms of reduced energy consumption (PDP) compared to other existing designs.

Therefore, the proposed circuits can be implemented in low-power portable electronics and embedded systems to save battery consumption.

# Chapter 3

## Ternary Combinational Logic Circuits

### 3.1 Introduction and Literature Review

The combinational logic circuits are time-independent, and they are only determined by the logical function of their current input state, whereas, sequential logic circuits whose outputs depend on both their present inputs and their previous outputs state giving them some form of memory [39].

The combinational logic circuits have two or more inputs and provide two or more outputs. They have no memory or feedback loops like sequential circuits.

In general, combinational logic circuits like Ternary Decoder (TDecoder) or Ternary Multiplexer (TMUX) are made up of basic logic gates like NAND, or NOR gates that are combined or connected.

In [27], the (1:3) TDecoder with 16 CNFETs was proposed, whereas, in [40] and [41], a (1:3) TDecoder with 10 and 11 CNFETs was described in replacing the TNOR of [27] with a binary NOR.

However, in [42], the (3:1) TMUX was designed based on the TDecoder of [27], resulting in a circuit with 28 CNFETs.

In [36], the authors presented new unary circuits which are subsequently used to design a “decoder-less” (3:1) TMUX with 18 CNFETs.

This chapter proposes two different Ternary Decoders (a TDecoder1 using CNFET-based proposed unary operators with 9 CNFETs and a TDecoder2 using DPL binary gates with 12 CMOS transistors), and a (3:1) Ternary multiplexer using CNFET-based proposed unary operators with 15 CNFETs, which are published in ([31], [32], [43]) and can be found in Appendices (A, B, C).

## 3.2 The Proposed Ternary Decoders

The ternary decoder converts *n* trits information inputs to a maximum  $3^n$  unique outputs. It is used in many applications such as the ternary adder, ternary multiplier, ternary memory, and others.

Ternary decoder with one ternary input ( $X$ ) and three binary outputs ( $X_0, X_1, X_2$ ) are described in equation (3.1) and its truth table is shown in Table 3.1.

$$X_{k,k \in \{0,1,2\}} = \begin{cases} 2, & \text{if } x = k \\ 0, & \text{if } x \neq k \end{cases} \quad (3.1)$$

TABLE 3.1: Ternary Decoder truth table

Input	Outputs		
X	$X_2$	$X_1$	$X_0$
0	0	0	2
1	0	2	0
2	2	0	0

TABLE 3.2: The chirality, diameter, and threshold voltage of the CNTs used in the proposed TDecoder1

CNFET Type	Chirality	Diameter	Vth
P-CNFET (T1, T5)	(10, 0)	0.783nm	- 0.559V
P-CNFET (T3, T8)	(19, 0)	1.487nm	- 0.289V
N-CNFET (T4, T6, T9)	(10, 0)	0.783nm	0.559V
N-CNFET (T2, T7)	(19, 0)	1.487nm	0.289V

### 3.2.1 The Proposed TDecoder1 using CNFET

The existing TDecoders in [27, 40], and [41] are shown in Fig. 3.1 with 16, 10, and 11 transistors respectively.

This chapter proposes a new design of TDecoder1 with 9 CNFETs through replacing the TNOR and the second NTI with a novel sub-circuit and a binary inverter respectively, as represented in Fig. 3.2.

Figure 3.2 shows the transistor level design of the proposed TDecoder1. It consists of one negative ternary inverter (NTI), one positive ternary inverter (PTI), one binary inverter, and a novel sub-circuit.

The chirality, diameter, and threshold voltage (Vth) of the CNFETs used are shown in Table 3.2, while the detailed operation of the proposed circuit is described in Table 3.3.

When the input  $X$  is logic 0, then transistors (T1 and T3) are turned ON and (T2, T4, and T7) are turned OFF. The output  $X_0$  and the intermediate  $X_p$  are equal to logic 2. Then (T5 and T8) are turned OFF and (T6 and T9) are turned ON. Therefore, the outputs  $X_1$  and  $X_2$  are equal to logic 0.

When the input  $X$  is logic 1, then transistors (T2, T3, and T7) are turned ON and (T1, and T4) are turned OFF. The output  $X_0$  is equal to logic 0, and the intermediate  $X_p$  is equal to logic 2. Then (T5, and T9) are turned OFF and (T6, and T8) are turned ON. Therefore, the output  $X_1$  is equal to the value of  $X_p$ , which is logic 2, and the output  $X_2$  is equal to logic 0.

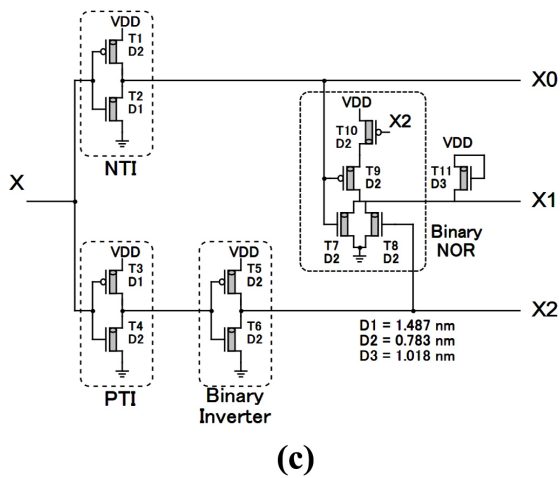
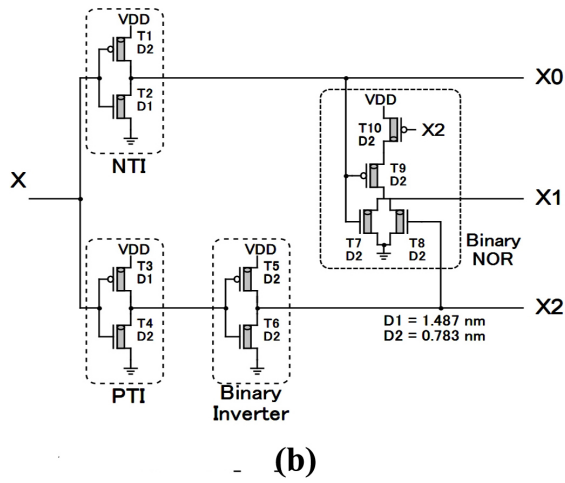
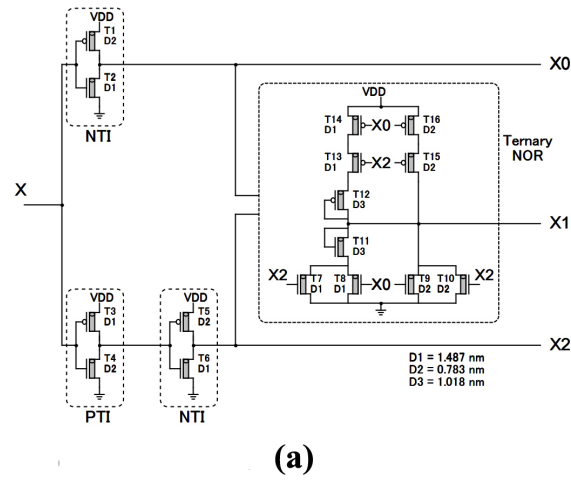


FIGURE 3.1: The Existing TDecoder in (a) [27] with 16 CNFETs, (b) [40] with 10 CNFETs, and (c) [41] with 11 CNFETs.

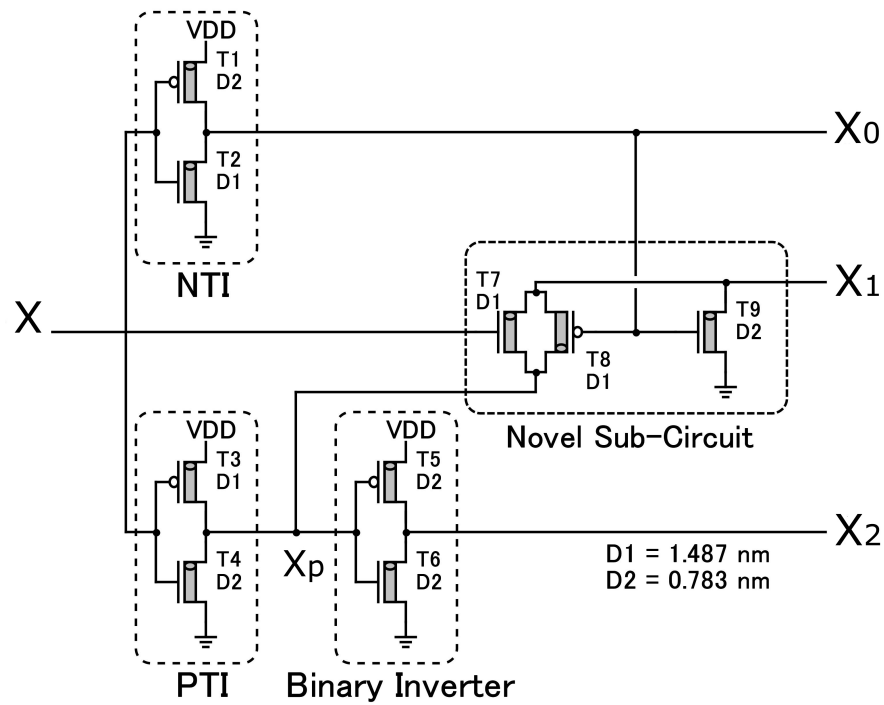


FIGURE 3.2: Transistor level of the proposed TDecoder1 with 9 CNFETs.

TABLE 3.3: The detailed operation of the proposed TDecoder1

<b>Ternary Input <math>X</math></b>	<b>0 (0 V)</b>	<b>1 (0.45 V)</b>	<b>2 (0.9 V)</b>
P-CNFET T1	ON	OFF	OFF
N-CNFET T2	OFF	ON	ON
<b>Output <math>X_0</math></b>	<b>2</b>	<b>0</b>	<b>0</b>
P-CNFET T3	ON	ON	OFF
N-CNFET T4	OFF	OFF	ON
<b>Intermediate <math>X_p</math></b>	<b>2</b>	<b>2</b>	<b>0</b>
P-CNFET T5	OFF	OFF	ON
N-CNFET T6	ON	ON	OFF
<b>Output <math>X_2</math></b>	<b>0</b>	<b>0</b>	<b>2</b>
N-CNFET T7	OFF	ON	ON
P-CNFET T8	OFF	ON	ON
N-CNFET T9	ON	OFF	OFF
<b>Output <math>X_1</math></b>	<b>0</b>	$X_p=2$	$X_p=0$

Finally, when the input  $X$  is logic 2, then transistors (T2, T4, and T7) are turned ON and

(T1 and T3) are turned OFF. The output  $X_0$  and the intermediate  $X_p$  are equal to logic 0. Then (T6 and T9) are turned OFF and (T5 and T8) are turned ON. Therefore, the output  $X_1$  is equal to the value of  $X_p$ , which is logic 0, and the output  $X_2$  is equal to logic 2.

Table 3.4 shows the advantage of the proposed TDecoder using CNFET.

TABLE 3.4: The advantage of the proposed TDecoder1

Disadvantage of the existing TDecoder in [27, 40, 41]	Advantage of the proposed TDecoder1
Shown in in Fig. 3.1 The existing design suffers from High power consumption due to:	Shown in Fig. 3.2 The proposed design provides Low power consumption due to:
1- The Transistors Count of [27, 40, 41] equal to 16, 10, 11 respectively.	Transistors Count = 9.
2- To get $X_1$ , [27] uses the Ternary <i>NOR</i> (10 transistors). 3- To get $X_1$ , [40, 41] use the Binary <i>NOR</i> (4 transistors).	To get $X_1$ , the design uses the novel sub-circuit (3 transistors) including the Transmission Gate (T7, T8) which provides low power consumption and propagation delay.
4- Six transistors (T11, T12, T13, T14, T15, T16) must be active to get $X_1$ equals to logic 2 [27]. 5- Two transistors (T9, T10) in series must be active to get logic $X_1$ equals to logic 2 [40, 41].	Only the Transmission Gate (T7, T8) must be active to get logic $X_1$ equals to logic 2.

### 3.2.2 The Proposed TDecoder2 using DPL Binary Gates

This chapter proposes TDecoder2 using CMOS DPL Binary Logic Gates with 12 transistors and use 0.18  $\mu\text{m}$  CMOS DPL at power  $V_{dd}$  (1.8V), as shown in Fig. 3.3.

Figure 3.3 shows the transistor and gate-level design of the proposed TDecoder2. It consists of two N-channels MOSFET (T1, T2) with threshold voltage equal 0.7V and 1.4V, and three CMOS DPL Binary logic gates, G1 is Inverter, G2 is AND and G3 is NOR logic gate and two resistors (R) 100 K $\Omega$ .

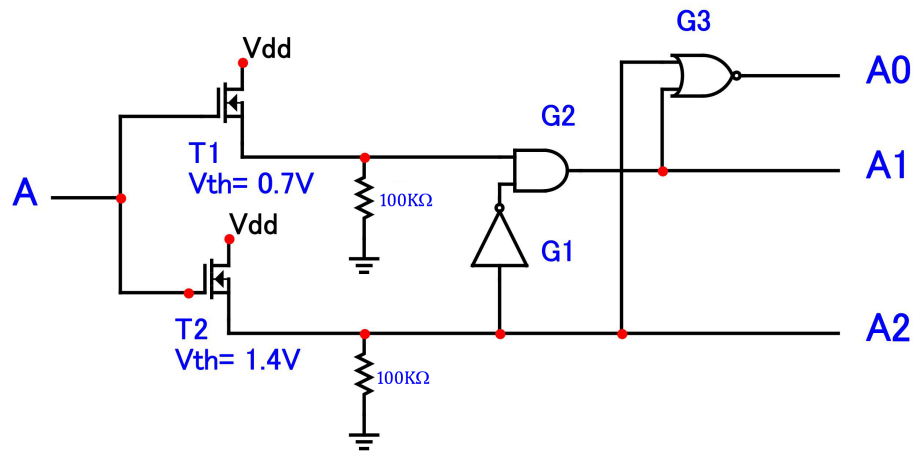


FIGURE 3.3: Transistor and Gate level of the proposed TDecoder2 with 12 transistors.

TABLE 3.5: The detailed operation of the proposed TDecoder2

Ternary Input	T1	T2	Binary Outputs		
	$V_{th} = 0.7V$	$V_{th} = 1.4V$	$A_2$	$A_1$	$A_0$
0 (0V)	OFF	OFF	0	0	2
1 (0.9V)	ON	OFF	0	2	0
2 (1.8V)	ON	ON	2	0	0

The detailed operation of the proposed TDecoder2 is described in Table 3.5.

When the input  $A$  is logic 0, then transistors (T1 and T2) are turned OFF. The output  $A_2$  (from T2 output) is equal to logic 0. The Inputs of the G2 gate are logic 0 (from T1 output) and  $\bar{A}_2$  is equal to logic 2 (from G1 gate output). Then the output of (G2)  $A_1$  is equal to logic 0. The inputs of the G3 gate are  $A_1$  and  $A_2$  equal to (0,0). Therefore, the output  $A_0$  is equal to logic 2.

When the input  $A$  is logic 1, then transistor (T1) is turned ON and (T2) is turned OFF. The output  $A_2$  (from T2 output) is equal to logic 0. The Inputs of the G2 gate are logic 2 (from T1 output) and  $\bar{A}_2$  is equal to logic 2 (from G1 gate output). Then the output of (G2)  $A_1$  is equal to logic 2. The inputs of the G3 gate are  $A_1$  and  $A_2$  equal to (2,0). Therefore, the output  $A_0$  is equal to logic 0.

Finally, when the input  $A$  is logic 2, then transistors (T1 and T2) are turned ON. The output

$A_2$  (from T2 output) is equal to logic 2. The Inputs of the G2 gate are logic 2 (from T1 output) and  $\bar{A}_2$  is equal to logic 0 (from G1 gate output). Then the output of (G2)  $A_1$  is equal to logic 0. The inputs of the G3 gate are  $A_1$  and  $A_2$  equal to (0,2). Therefore, The output  $A_0$  is equal to logic 0.

### 3.3 The Proposed Ternary Multiplexer

A Multiplexer (MUX) can select between several analog or digital input signals and forward it to a single output line.

A 3:1 Ternary Multiplexer (TMUX) is introduced with the general model, as represented in Fig.3.4, it has three inputs ( $I_0, I_1, I_2$ ), one selection ( $S$ ), and one output ( $Z$ ) which depends on ( $S$ ), as described in equation (3.2) and Table 3.7.

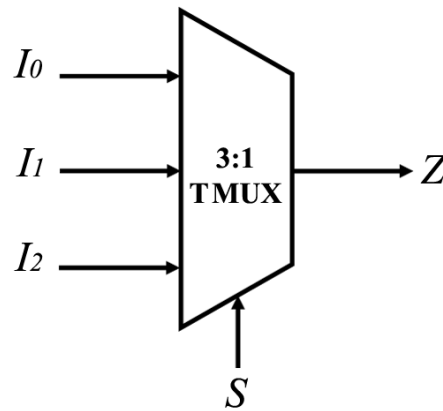


FIGURE 3.4: The model of 3:1 TMUX

$$Z = \begin{cases} I_0, & \text{if } S = 0 \\ I_1, & \text{if } S = 1 \\ I_2, & \text{if } S = 2 \end{cases} \quad (3.2)$$

TABLE 3.6: The diameter, and threshold voltage of the CNTs used in the proposed TMUX

CNFET Type	Diameter	Vth
P-CNFET (T10,T12,T14)	0.783nm	- 0.559V
N-CNFET (T11,T13,T15)	0.783nm	0.559V

The existing (3:1) TMUX in [42] and [36] are shown in Fig. 3.5;

Fig. 3.5 (a) shows the TMUX of [42] with 28 CNFETs using the Ternary Decoder of [27].

Fig. 3.5 (b) shows the TMUX of [36] with 18 transistors without using the Ternary Decoder.

This chapter proposes a “decoder-less” (3:1) TMUX, as shown in Fig.3.6 with 15 transistors using unary operators,  $S_n$ ,  $S_p$ ,  $S_1$ , and the complement of  $S_1$ ,  $\bar{S}_1$ .

The diameter, and threshold voltage of the CNTs used in the proposed (3:1) TMUX are shown in Table 3.6 and the detailed operation of the proposed (3:1) TMUX is shown in Table 3.7.

The first nine transistors are:  $S_n$  (2 transistors),  $S_p$  (2 transistors),  $S_1$  (3 transistors), and  $\bar{S}_1$  (2 transistors) are described in Chapter 2.2.

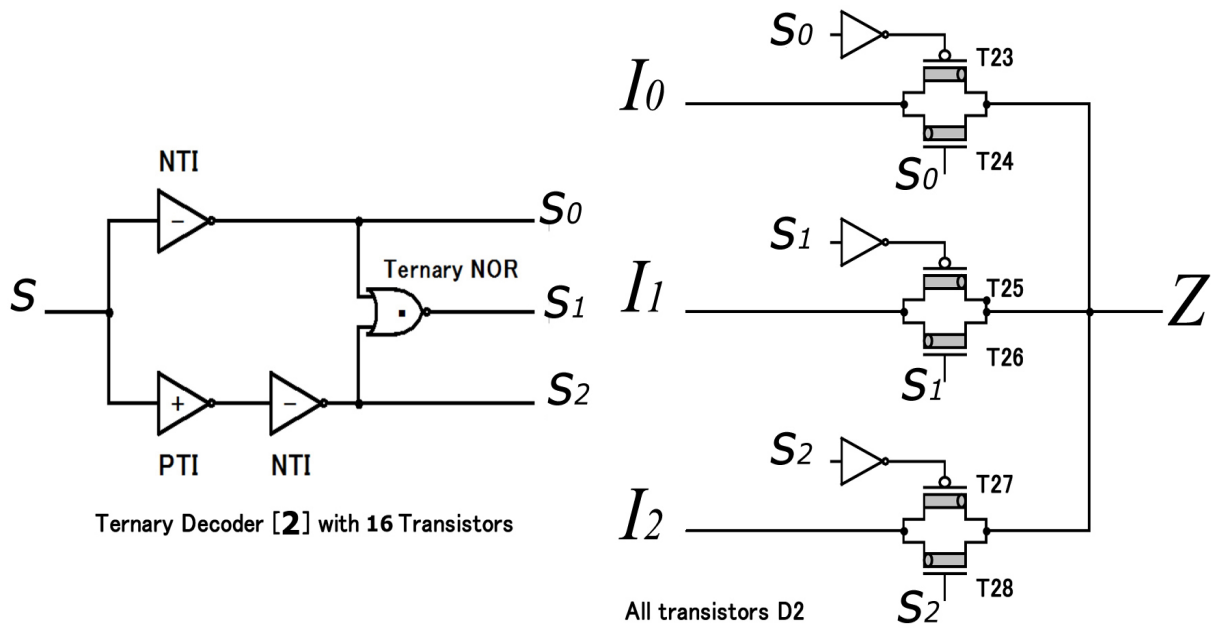
When the selection  $S$  is logic 0 (0 V), then transistors (T10, T11) are turned ON and (T12, T13, T14, T15) are turned OFF. Therefore, the output  $Z$  is equal to the value of the input  $I_0$ .

When the selection  $S$  is logic 1 (0.45 V), then transistors (T12, T13) are turned ON and (T10, T11, T14, T15) are turned OFF. Therefore, the output  $Z$  is equal to the value of the input  $I_1$ .

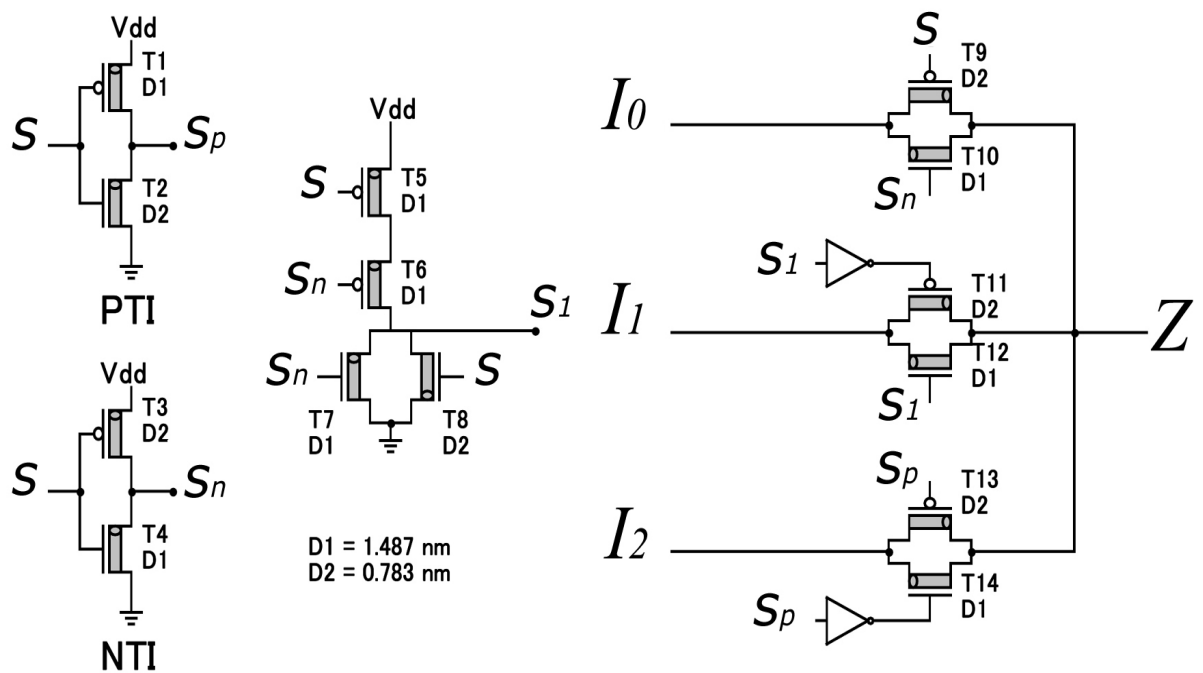
Finally, when the selection  $S$  is logic 2 (0.9 V), then transistors (T14, T15) are turned ON and (T10, T11, T12, T13) are turned OFF. Therefore, the output  $Z$  is equal to the value of the input  $I_2$ .

TABLE 3.7: The operation of the proposed TMUX

<b>Selection (<math>S</math>)</b>	<b>0</b>	<b>1</b>	<b>2</b>
$S_p$	2	2	0
$S_n$ } See Ch 2.2	2	0	0
$S_1$ }	0	2	0
$\bar{S}_1$	2	0	2
P-CNFET T10	ON	OFF	OFF
N-CNFET T11	ON	OFF	OFF
P-CNFET T12	OFF	ON	OFF
N-CNFET T13	OFF	ON	OFF
P-CNFET T14	OFF	OFF	ON
N-CNFET T15	OFF	OFF	ON
<b>Output (<math>Z</math>)</b>	$I_0$	$I_1$	$I_2$



(a)



(b)

FIGURE 3.5: The Existing 3:1 TMUX in (a) [42] with 28 transistors, (b) [36] with 18 transistors.



### 3.4 Simulation Results and Comparisons

The proposed TDecoder1, and TMUX are simulated, tested, and compared to [27, 36, 40–42] using the HSPICE simulator and CNFET with the 32-nm channel length at different power supplies (0.8V, 0.9V, 1V), different temperatures (10°C, 27°C, 70°C), and different frequencies (0.5GHz, 1GHz, 2GHz).

While the proposed TDecoder2 is simulated, tested using MicroCap10 simulator and CMOS DPL Binary gates with 0.18  $\mu\text{m}$  at power supply Vdd (1.8V), a temperature (25°C), and a frequency (0.1 GHz). The simulated circuits utilize an implementation of the AND and NOR DPL gates, as shown in chapter I with the average propagation delay is 42.56 ps, and the average power is 4.08  $\mu\text{w}$  [44].

All input signals have a fall and rise time of 20 ps. The propagation delay of the circuit is measured, for example  $t_1$ , as shown in Fig. 3.7, when the input ( $X$ ) is rising from 0 to 1, and the output ( $X_0$ ) is falling from 2 to 0. A similar procedure is done to get all the possible rising and falling propagation delays for outputs of all studied circuits and find the maximum propagation delay for each circuit.

Then the average power consumption, maximum propagation delay, and maximum PDP are obtained for all circuits.

The performance of the proposed circuits will be compared to other designs for the PDP (energy consumption).

Figures 3.7 and 3.8 illustrate the transient analysis of the proposed TDecoder1 and TDecoder2.

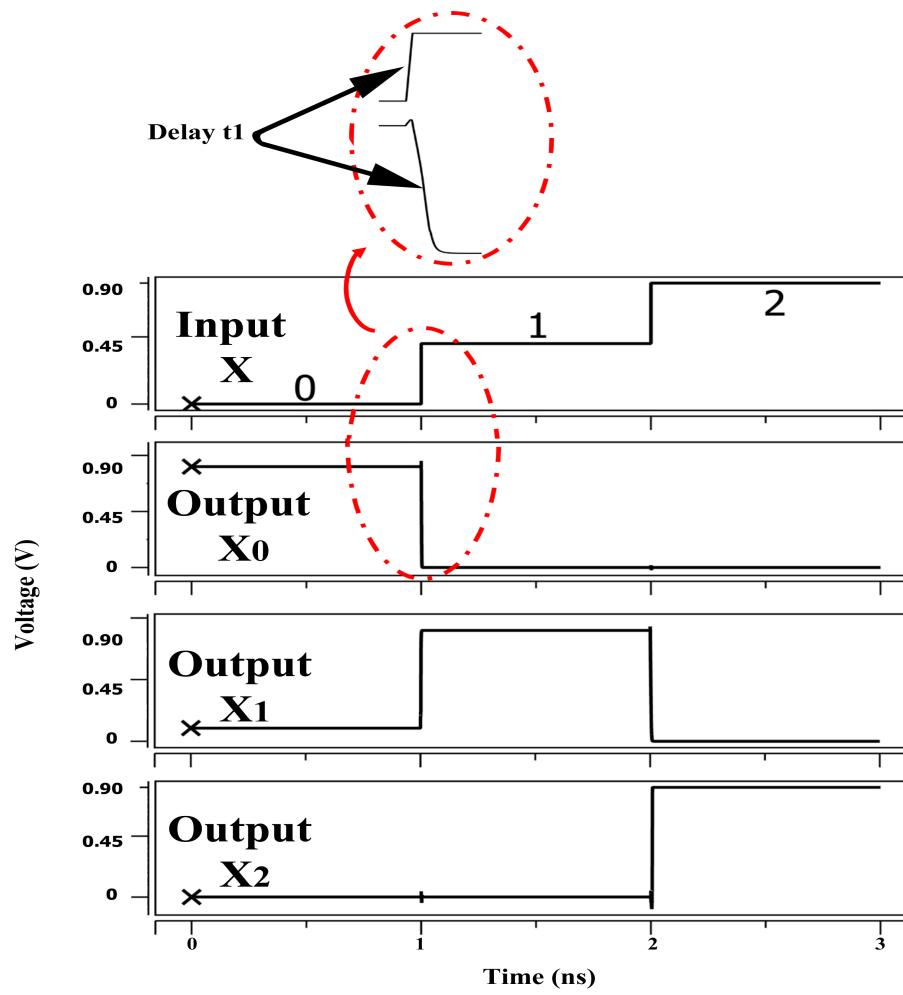


FIGURE 3.7: Transient analysis of the proposed TDecoder1.

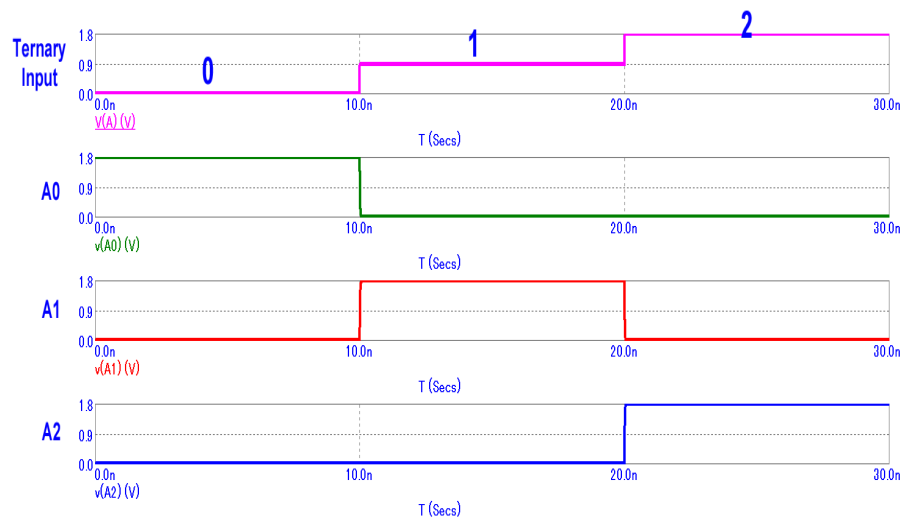


FIGURE 3.8: Transient analysis of the proposed TDecoder2.

TABLE 3.8: Comparison of Transistors Count of All Circuits

	[27]	[40]	[41]	[36]	[42]	<b>Proposed1</b>	<b>Proposed2</b>
TDecoder	16	10	11	-	-	9	12
TMUX	-	-	-	18	28	15	-

### 3.4.1 Comparison of Transistors Count of All Circuits

Table 3.8 shows the comparison of Transistors Count for the TDecoders and TMUXs compared to [27, 36, 40–42].

This comparison of the proposed circuits demonstrates a notable reduction in Transistors Count.

For the TDecoder1, 43.75%, 10%, 18.18%, and 35.71% compared to TDecoder in [27, 40, 41], and proposed TDecoder2, respectively. For the TMUX, 46.43%, and 16.66% compared to TMUX in [36, 42], respectively.

### 3.4.2 Comparison of Different TDecoder Circuits

#### 3.4.2.1 The Impact of Different Power Supplies

Table 3.9 shows the comparison to the existing Ternary Decoder in [27, 40], and [41] with the proposed TDecoder1 using CNFET in terms of the average power consumption, maximum propagation delay, and maximum energy (PDP) at different supply voltages (0.8 V, 0.9 V, 1 V), same temperature (27°C), and same frequency (1 GHz). The boldface values are the best values, among others.

TABLE 3.9: Comparison of average power ( $\mu\text{w}$ ), maximum delay (ps), and maximum PDP ( $\times 10^{-17}$  J) of 4 TDecoders at  $T=27^\circ\text{C}$ ,  $F=1$  GHz, and for different supply voltages

	Vdd=0.8 V			Vdd=0.9 V			Vdd=1 V		
	Power	Delay	PDP	Power	Delay	PDP	Power	Delay	PDP
TDecoder in [27]	2.6	10.4	2.74	3.5	8.91	3.11	11.8	8.24	9.72
TDecoder in [40]	1.9	8.50	1.65	2.7	7.50	2.02	10.4	7.06	7.37
TDecoder in [41]	126	8.67	109.24	185	7.68	142.08	250	7.18	168.73
<b>Prop. TDecoder1</b>	<b>1.9</b>	<b>6.59</b>	<b>1.26</b>	<b>2.6</b>	<b>6.26</b>	<b>1.62</b>	<b>9.1</b>	<b>4.18</b>	<b>3.82</b>

TABLE 3.10: Comparison of average power ( $\mu\text{w}$ ), maximum delay (ps), and maximum PDP ( $\times 10^{-17}$  J) of 4 TDecoders at  $V_{\text{dd}}=0.9$  V,  $F=1$  GHz, and for different Temperatures

	Temp.=10°C			Temp.=27°C			Temp.=70°C		
	Power	Delay	PDP	Power	Delay	PDP	Power	Delay	PDP
TDecoder in [27]	5.1	9.18	4.72	3.5	8.91	3.11	4.4	8.31	3.68
TDecoder in [40]	4.3	7.7	3.33	2.7	7.50	2.02	3.5	7.05	2.50
TDecoder in [41]	184	7.89	145.17	185	7.68	142.08	189	7.20	136.72
<b>Prop. TDecoder1</b>	<b>4</b>	<b>6.4</b>	<b>2.51</b>	<b>2.6</b>	<b>6.26</b>	<b>1.62</b>	<b>3.5</b>	<b>5.85</b>	<b>2.05</b>

TABLE 3.11: Comparison of average power ( $\mu\text{w}$ ), maximum delay (ps), and maximum PDP ( $\times 10^{-17}$  J) of 4 TDecoders at  $T=27^\circ\text{C}$ ,  $V_{\text{dd}}=0.9$  V, and for different frequencies

	f= 2 GHz			f= 1 GHz			f= 0.5 GHz		
	Power	Delay	PDP	Power	Delay	PDP	Power	Delay	PDP
TDecoder in [27]	6.0	8.93	5.17	3.5	8.91	3.11	2.3	8.91	2.11
TDecoder in [40]	4.1	7.54	3.12	2.7	7.50	2.02	2.0	7.5	1.46
TDecoder in [41]	185	7.7	142.24	185	7.68	142.08	184	7.68	142.08
<b>Prop. TDecoder1</b>	<b>4</b>	<b>6.25</b>	<b>2.44</b>	<b>2.6</b>	<b>6.26</b>	<b>1.62</b>	<b>1.8</b>	<b>6.26</b>	<b>1.17</b>

The comparison of the proposed TDecoder1 demonstrates a notable reduction in PDP, as shown in Table 3.9.

At  $V_{dd}=0.8$  V, 54.01%, 23.64%, and 98.85% compared to [27, 40], and [41] respectively.

At  $V_{dd}=0.9$  V, 47.91%, 19.8%, and 98.86% compared to [27, 40], and [41] respectively.

At  $V_{dd}=1$  V, 60.7%, 48.17%, and 97.74% compared to [27, 40], and [41] respectively.

### 3.4.2.2 Impact of Different Temperatures

Table 3.10 shows the comparison to the existing Ternary Decoder in [27, 40], and [41] with the proposed TDecoder1 in terms of the average power consumption, maximum propagation delay, and maximum energy (PDP) at different temperatures (10°C, 27°C, 70°C), same supply voltage  $V_{dd}$  (0.9 V), and same frequency (1 GHz).

The comparison of the proposed TDecoder1 demonstrates a notable reduction in PDP, as shown in Table 3.10.

At Temp.=10°C, 46.82%, 24.62%, and 98.27% compared to [27, 40], and [41] respectively.

At Temp.=27°C, 47.91%, 19.8%, and 98.86% compared to [27, 40], and [41] respectively.

At Temp.=70°C, 44.29%, 18%, and 98.5% compared to [27, 40], and [41] respectively.

### 3.4.2.3 The Impact of Different Frequencies

Table 3.11 shows the comparison to the existing Ternary Decoder in [27, 40], and [41] with the proposed TDecoder1 in terms of the average power consumption, maximum propagation delay, and maximum energy (PDP) at different frequencies (0.5 GHz, 1 GHz, 2 GHz), same temperatures (27°C), and same supply voltage  $V_{dd}$  (0.9 V).

The comparison of the proposed TDecoder1 demonstrates a notable reduction in PDP, as shown in Table 3.11.

At frequency=2 GHz, 52.8%, 21.79%, and 98.28% compared to [27, 40], and [41] respectively.

At frequency=1 GHz, 47.91%, 19.8%, and 98.86% compared to [27, 40], and [41] respectively.

At frequency=0.5 GHz, 44.55%, 19.86%, and 99.18% compared to [27, 40], and [41] respectively.

### 3.4.3 Comparison between the Proposed TDecoders Circuits

As mentioned in chapter I that CNFET provides better energy efficiency compared to CMOS, FinFET, and other transistor technologies [21].

Table 3.12 shows the comparison between the proposed TDecoder1 using CNFET and TDecoder2 using CMOS DPL Binary Gates in terms of the average power consumption, maximum propagation delay, and maximum energy (PDP) at a supply voltage (0.9 V), a room temperature (27°C), and a frequency (1 GHz).

TABLE 3.12: Comparison of average power ( $\mu\text{W}$ ), maximum delay (ps), and maximum PDP ( $\times 10^{-17}$  J) of the two proposed TDecoders

	Power	Delay	PDP
<b>Proposed TDecoder2 using CMOS DPL Binary Gates</b>	13	140	182
<b>Proposed TDecoder1 using CNFET</b>	<b>2.6</b>	<b>6.26</b>	<b>1.62</b>
<b>TDecoder1 Improvement</b>	<b>80%</b>	<b>95.5%</b>	<b>99.1%</b>

The comparison of the proposed TDecoder1 demonstrates a notable reduction in Power (80%), Delay (95.5%), and PDP (99.1%) compared to the proposed TDecoder2, as shown in Table 3.12.

TABLE 3.13: Comparison between three TMUXs at Vdd (0.9 V), temperature (27°C), and frequency (1 GHz)

	Power (nw)	Delay (ps)	PDP ( $\times 10^{-20}$ J)
TMUX in [42]	67.3	14.3	96.3
TMUX in [36]	60.1	9.64	57.9
<b>Proposed TMUX</b>	<b>48.4</b>	<b>8.50</b>	<b>41.1</b>

### 3.4.4 Comparison of Different TMUX Circuits

The proposed TMUX is compared to the TMUX in [36, 42]. The three circuits are simulated and tested using the HSPICE simulator at a frequency of 1 GHz, room temperature (27°C) and a supply voltage Vdd (0.9V).

For a fair comparison, the four circuits are simulated using the same software, implementation techniques, CNFET model parameters, and the same values of  $(I_0, I_1, I_2, S)$ , as follows:

$$I_0 = (210021002)_3, I_1 = (102201001)_3, I_2 = (012012012)_3 \text{ and } S = (000111222)_3.$$

Figure 3.9 illustrates the transient analysis of the proposed (3:1) TMUX. The dotted rectangle for each of the three inputs  $(I_0, I_1, I_2)$  is selected according to the ternary selection  $(S)$  to get the output  $(Z)$ .

Table 3.13 shows the comparison between the three TMUXs in terms of the average power consumption, maximum propagation delay, and maximum PDP.

The comparison of the proposed “decoder-less” TMUX demonstrates a notable reduction in PDP of around 57.32%, and 29.02% compared to [42], and [36], respectively.

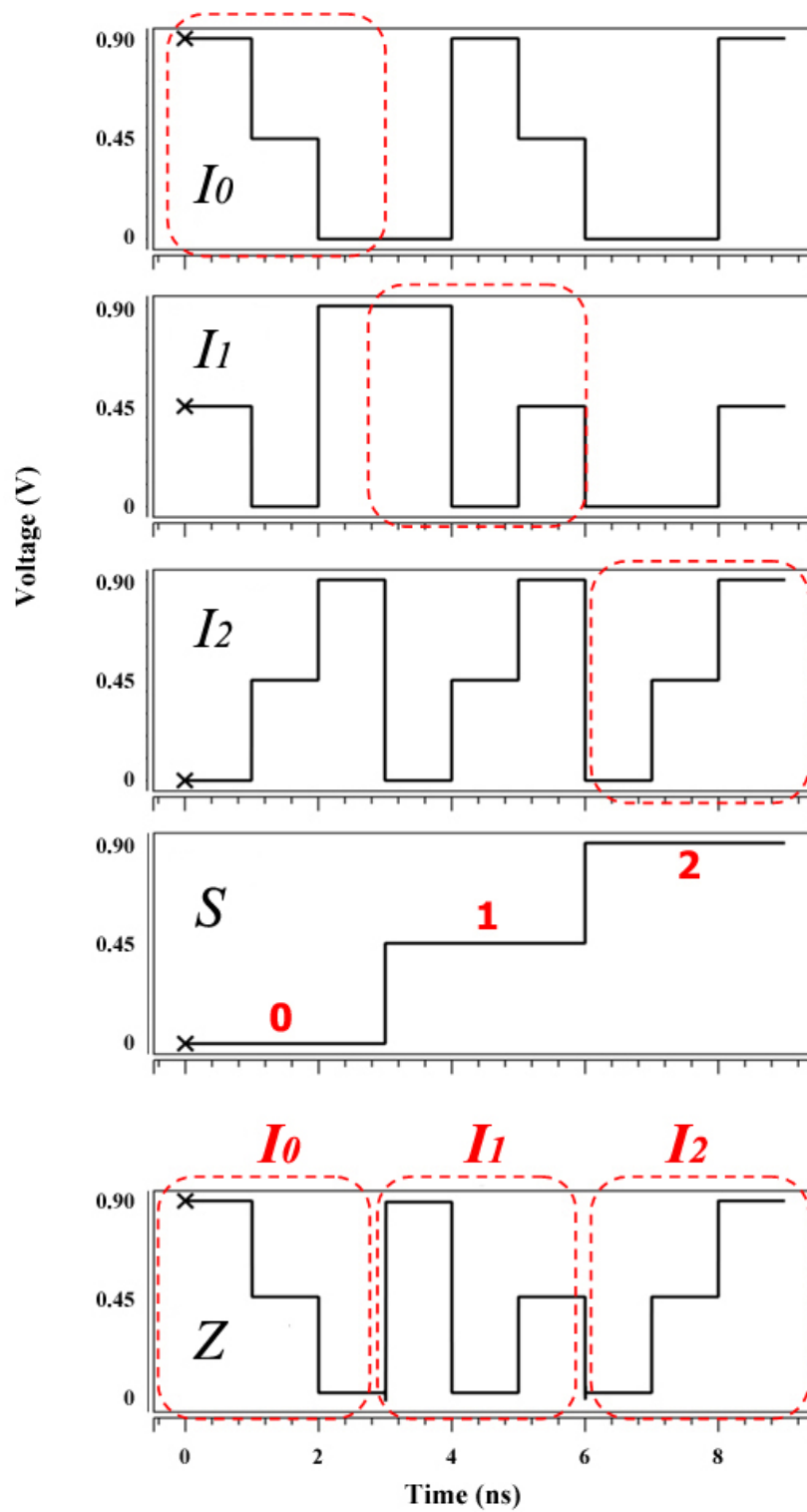


FIGURE 3.9: Transient analysis of the proposed 3:1 TMUX (dotted rectangle corresponds to input selected according to  $S$ ).

### 3.5 Conclusion

This chapter proposed three Ternary Combinational circuits (two different Ternary Decoders (a TDecoder1 using CNFET-based proposed unary operators of the ternary system and a TDecoder2 using DPL binary gates), and a Ternary multiplexer using CNFET-based proposed unary operators of the ternary system).

The design process tried to optimize several circuit techniques such as reducing the number of used transistors, utilizing energy-efficient transistor arrangements, and applying the dual supply voltages ( $V_{dd}$  and  $V_{dd}/2$ ).

The proposed ternary circuits are compared to the latest ternary circuits, simulated and tested using HSPICE simulator under various operating conditions at different supply voltages, different temperatures, and different frequencies.

The results proved the merits of the approach in terms of reduced energy consumption (PDP) compared to other existing designs.

Therefore, the proposed circuits can be implemented in low-power portable electronics and embedded systems to save battery consumption.

# Chapter 4

## Ternary Arithmetic Logic Units (TALU)

### 4.1 Introduction and Literature Review

A Ternary Arithmetic Logic Unit (TALU) is a combinational circuit that performs arithmetic operations like addition and multiplication. A TALU is a fundamental building block of many types of computing circuits like the central processing unit (CPU) of computers, and graphics processing units (GPUs) [45].

In [27], the authors presented a Ternary Half Adder (THA) with 136 CNFETs, and a Ternary Multiplier (TMUL) with 100 CNFETs using their TDecoder (16 CNFETs), binary AND, binary OR, a ternary encoder (level shifter), and a ternary OR. Also, the authors in [46] the proposed a THA with 112 CNFETs, and a TMUL with 86 CNFETs using TDecoders of [27], binary NANDs, binary NORs, a ternary encoder (level shifter), a ternary OR, and a STI. Whereas, in [37] the authors used a TNAND instead of the ternary encoder to design a THA with 112 CNFETs, and a TMUL with 76 CNFETs using their TDecoder (10 transistors), binary NANDs, a binary NOT, a TNAND, and a STI.

However, in [42] the authors the proposed a THA with 168 CNFETs, and a TMUL with 112 CNFETs using cascading their TMUXs (28 CNFETs).

While in [36], Unary Operators and their TMUX (18 CNFETs) were employed in the design of a THA with 64 CNFETs, and a TMUL with 58 CNFETs.

The designs mentioned above either suffer from a large number of transistors in the THA, and TMUL [27, 37, 42, 46] or even in the unary operators circuit [36].

Therefore, this thesis first proposes an efficient circuit implementation of six unary operators, a STI and TNANDs, as shown in Chapter 2, a novel (1:3) TDecoder1 with 9 CNFETs, and a novel “decoder-less” (3:1) TMUX with 15 CNFETs, as shown in Chapter 3, to be used in this Chapter to design three different models of THAs and TMULs, which are published in ([31], [32]) and can be found in Appendices (A, B), as follow:

1. Proposes a THA1 with 85 CNFETs and a TMUL1 with 61 CNFETs using the proposed TDecoder1, a STI, TNANDs, and applying De Morgan’s Law.
2. Proposes a THA2 with 90 CNFETs and a TMUL2 with 60 CNFETs using the proposed cascading TMUX.
3. Proposes a THA3 with 45 CNFETs and a TMUL3 with 40 CNFETs using the proposed Unary Operators combined with TMUX.

## 4.2 The Proposed Ternary Half Adders

THA can add two ternary inputs and provides two outputs: the Sum and the Carry, as shown in Table 4.1.

The basic equations of the Sum and the Carry can be derived in Table 4.1 to lead three designs:

1. Conventional design in [27, 37, 46] which uses equation (4.1).
2. Cascading TMUXs design in [42] which uses equation (4.2).
3. Unary operators-based design in [36] which uses equation (4.3).

$$\begin{aligned}
 Sum &= 2 \bullet (A_0B_2 + A_1B_1 + A_2B_0) + 1 \bullet (A_0B_1 + A_1B_0 + A_2B_2) \\
 Carry &= 1 \bullet (A_1B_2 + A_2B_1 + A_2B_2)
 \end{aligned} \tag{4.1}$$

TABLE 4.1: Truth table of THA

Sum			
A/B	$B_0(0)$	$B_1(1)$	$B_2(2)$
$A_0(0)$	0	1	2
$A_1(1)$	1	2	0
$A_2(2)$	2	0	1

Carry			
A/B	$B_0(0)$	$B_1(1)$	$B_2(2)$
$A_0(0)$	0	0	0
$A_1(1)$	0	0	1
$A_2(2)$	0	1	1

$$\begin{aligned}
 Sum &= A.B_0 + (1.A_0 + 2.A_1 + 0.A_2).B_1 + (2.A_0 + 0.A_1 + 1.A_2).B_2 \\
 Carry &= 0.B_0 + (0.A_0 + 0.A_1 + 1.A_2).B_1 + (0.A_0 + 1.A_1 + 1.A_2).B_2
 \end{aligned} \tag{4.2}$$

$$\begin{aligned}
 Sum &= A.B_0 + A^1.B_1 + A^2.B_2 \\
 Carry &= 0.B_0 + (1 \cdot \bar{A}_p).B_1 + (1 \cdot \bar{A}_n).B_2
 \end{aligned} \tag{4.3}$$

Where  $A_k$  and  $B_k$ ,  $k \in \{0,1,2\}$ , are the outputs of the TDecoder from inputs  $A$  and  $B$ .

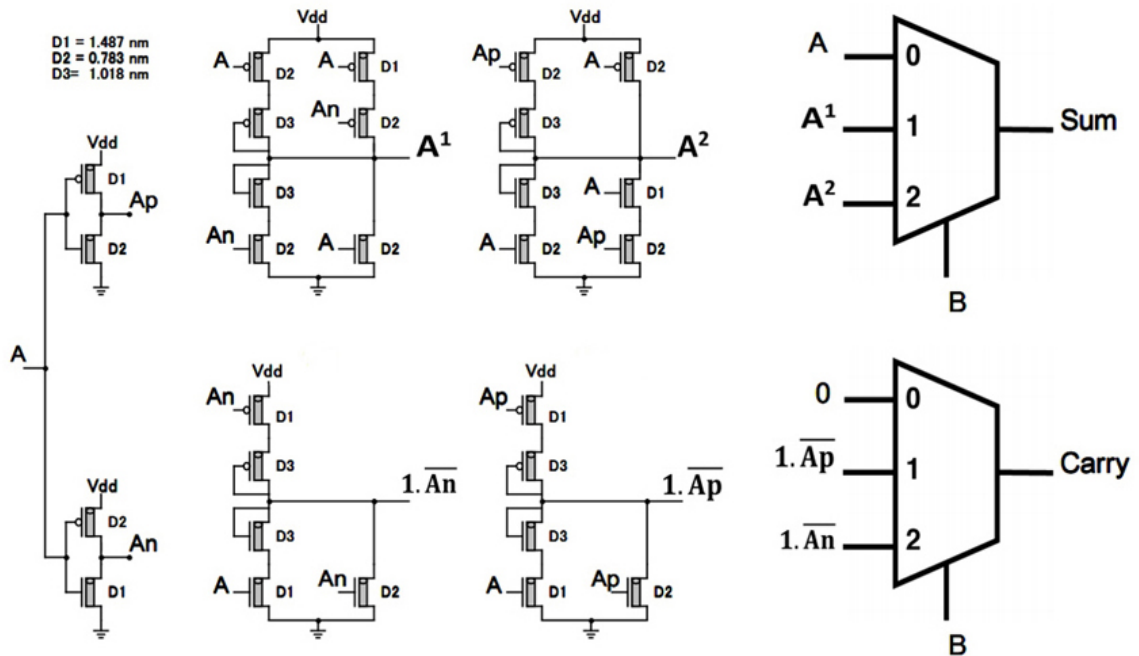


FIGURE 4.1: The Existing THA in [36] with 64 CNFETs.

The existing THA in [27, 37, 46] and [36] are shown in Fig. 4.1 and Fig. ??;

Figure 4.1 shows the THA of [36] with 64 CNFETs that contains (3:1) TMUX (18 transistors) and Unary Operators.

Where Figure 4.2 shows the THA of [27] with 136 CNFETs that contains their sTDecoder (16 transistors), binary ANDs, binary ORs, ternary encoders level shifter, and a ternary OR.

And Figure 4.3 shows the THA of [46] with 112 CNFETs that contains TDecoder of [27], binary NANDs, binary NORs, ternary encoders level shifter, a ternary OR, and a STI.

Finally, Figure 4.4 shows the THA of [37] with 112 CNFETs that contains their TDecoder (10 transistors), binary NANDs, a binary NOT, TNANDs, and a STI.

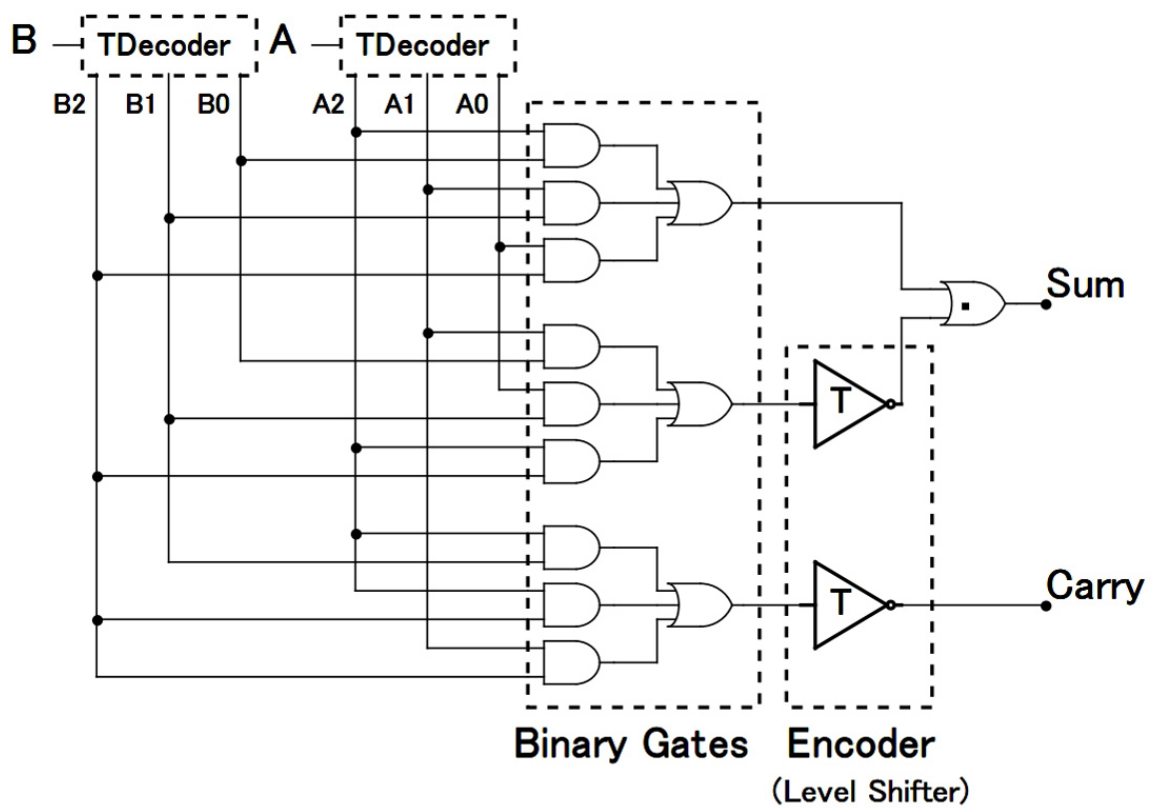


FIGURE 4.2: The Existing THA in [27] with 136 CNFETs.

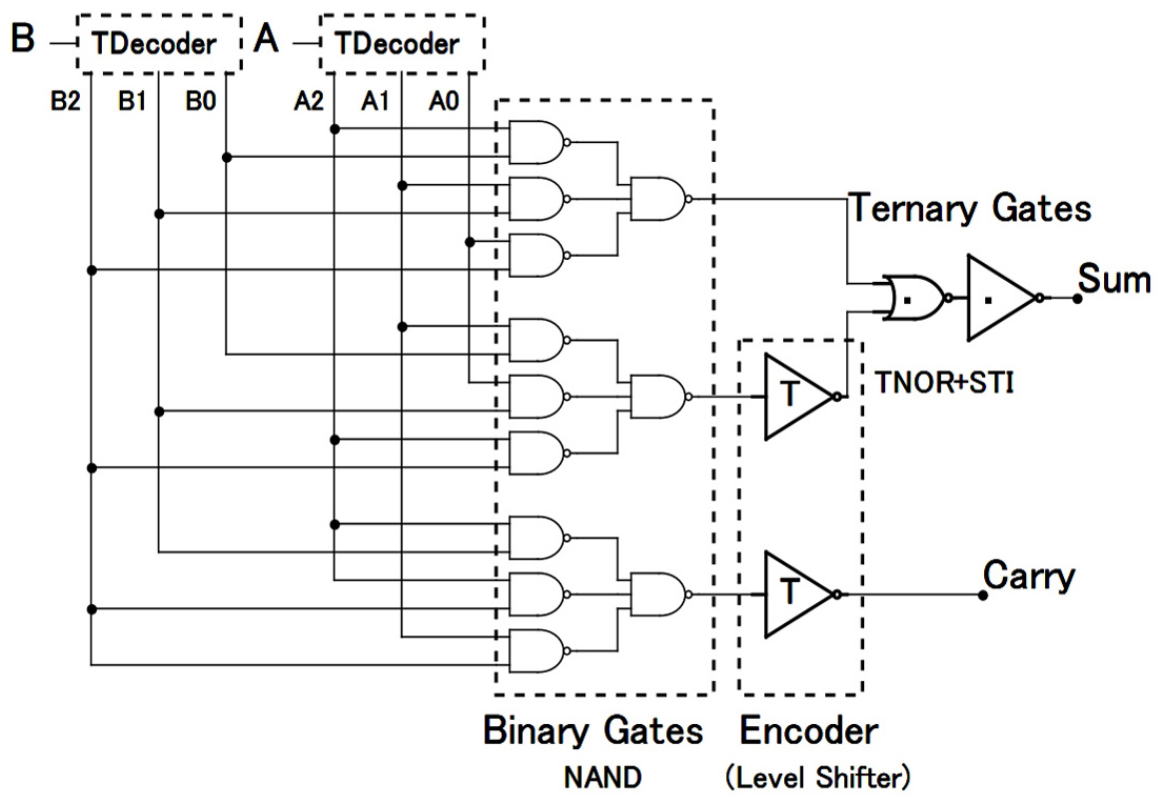


FIGURE 4.3: The Existing THA in [46] with 112 CNFETs.

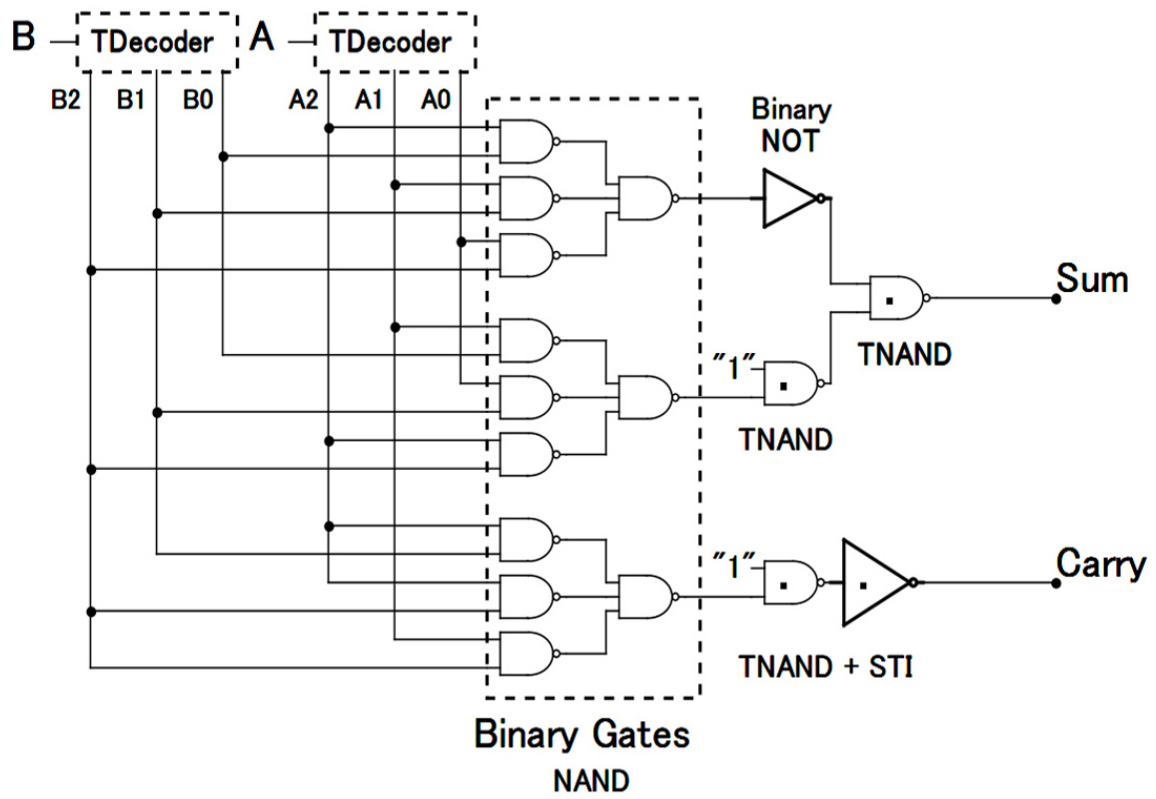


FIGURE 4.4: The Existing THA in [37] with 112 CNFETs.

### 4.2.1 The proposed THA1

This Chapter proposes a new conventional design, which uses equation (4.1), of THA1 with 85 CNFETs using De Morgan's Law and dual power supply ( $V_{dd}$  and  $V_{dd}/2$ ) to eliminate the encoder level shifter in [27, 46].

Figure 4.5 shows the proposed THA1. It consists of two the proposed TDecoder1 (9 CNFETs each), eight 2-inputs binary NAND, three 3-inputs binary NAND, one binary inverter, one the proposed TNAND (10 CNFETs), and one the proposed STI (5 CNFETs).

Table 4.2 shows the total Transistors Count of the proposed THA1.

The operation of the proposed THA1: Two ternary inputs  $A$  and  $B$  fed to the proposed TDecoder1 and produce outputs as  $(A_2, A_1, A_0)$  and  $(B_2, B_1, B_0)$ . These outputs will drive the eight 2-inputs binary NAND, the three 3-inputs binary NAND logic gates, the proposed STI, binary inverter, and the proposed TNAND to get the Sum and the Carry, as final outputs.

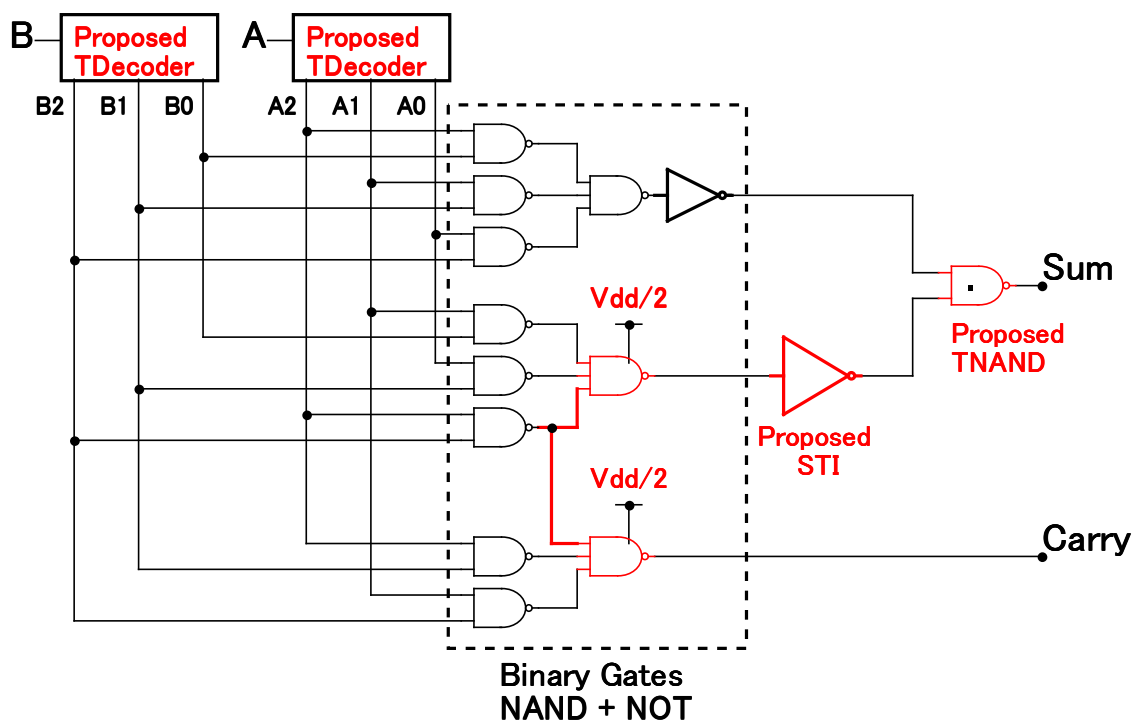


FIGURE 4.5: The proposed THA1 with 85 CNFETs using the proposed TDecoder1, STI, and TNAND.

TABLE 4.2: Total transistors count of the proposed THA1

	No. of Devices	No. of Transistors	Subtotal*
Proposed TDecoder1	2	9	18
Binary 2-NAND	8	4	32
Binary 3-NAND	3	6	18
Binary Inverter	1	2	2
Proposed STI	1	5	5
Proposed TNAND	1	10	10
<b>Total</b>			<b>85</b>

\*Subtotal = No. of Devices x No. of Transistors

### 4.2.2 The proposed THA2

This Chapter proposes another THA design using cascading TMUXs, which uses equation (4.2), of THA2 with 90 CNFETs (6\*15 transistors), as shown in Fig.4.6.

The Existing THA design in [42] with 168 (6\*28 transistors) transistors is the same as Fig.4.6 but with TMUX equals to 28 transistors;

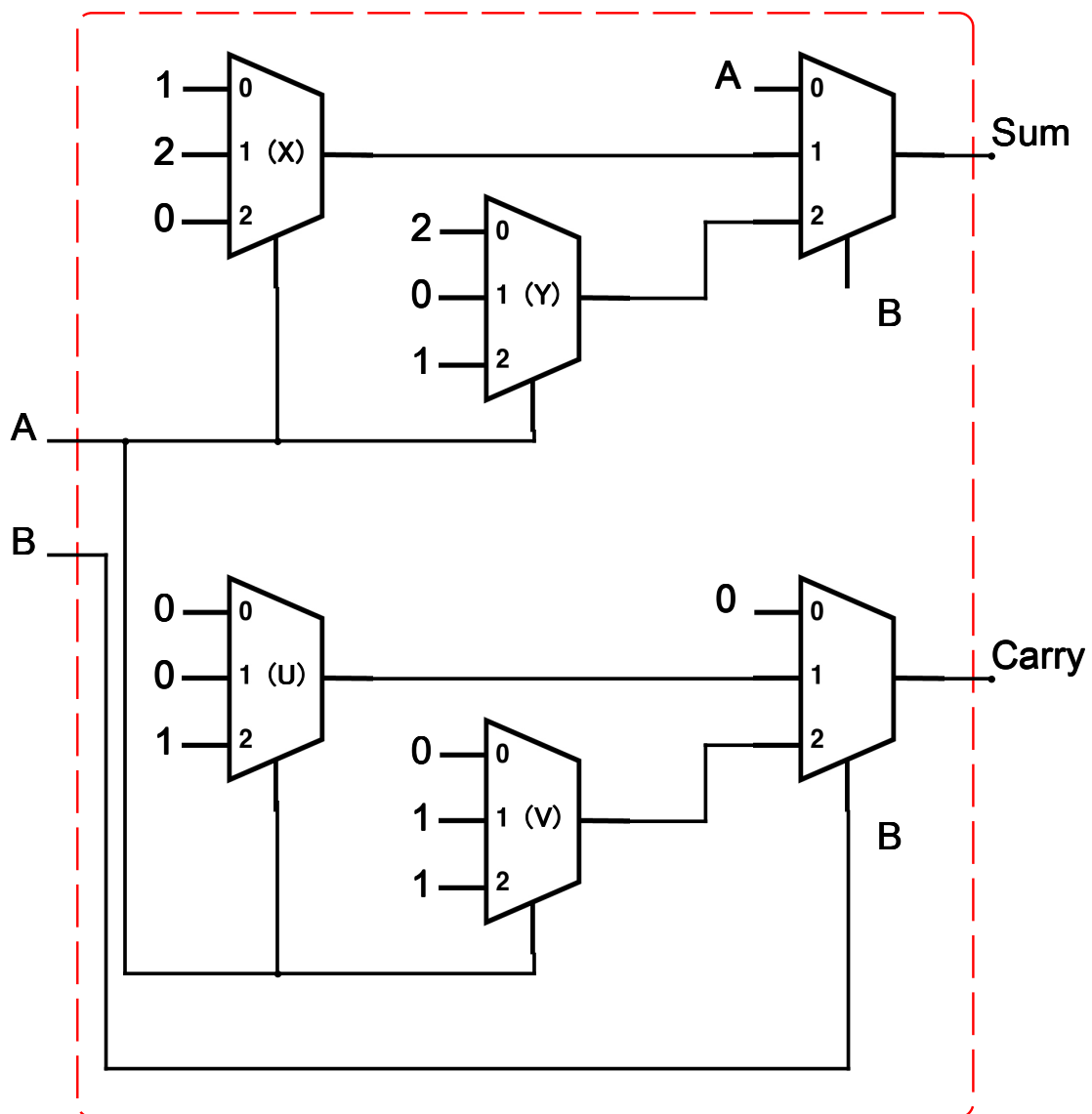


FIGURE 4.6: The proposed THA2 with 90 CNFETs using cascading the proposed TMUX.

The operation of the proposed THA2: Two ternary inputs  $A$  and  $B$  used as selection for the proposed TMUX.

When the selection  $B$  is logic 0, then the Sum-TMUX output will be equal to the values of  $A$  (0, 1, 2) and the Carry-TMUX will be equal to logic 0 for  $A$  (0, 1, 2), respectively.

When the selection  $B$  is logic 1, then the Sum-TMUX output will be equal to the output of X-TMUX (1, 2, 0) for  $A$  (0, 1, 2), respectively.

The Carry-TMUX output will be equal to the output of U-TMUX (0, 0, 1) for  $A$  (0, 1, 2), respectively.

Finally, when the selection  $B$  is logic 2, then the Sum-TMUX output will be equal to the output of Y-TMUX (2, 0, 1) for  $A$  (0, 1, 2), respectively.

The Carry-TMUX output will be equal to the output of V-TMUX (0, 1, 1) for  $A$  (0, 1, 2), respectively.

### 4.2.3 The proposed THA3

This Chapter proposes a third THA design based on new Unary operators combined with the proposed TMUX, which uses equation (4.3), of THA3 with 45 CNFETs, as shown in Fig.4.7.

Table 4.3 shows total transistors count of the proposed THA3 which is equal to 45 transistors, and its operation is described in the following paragraphs where  $A$  and  $B$  are two ternary inputs.

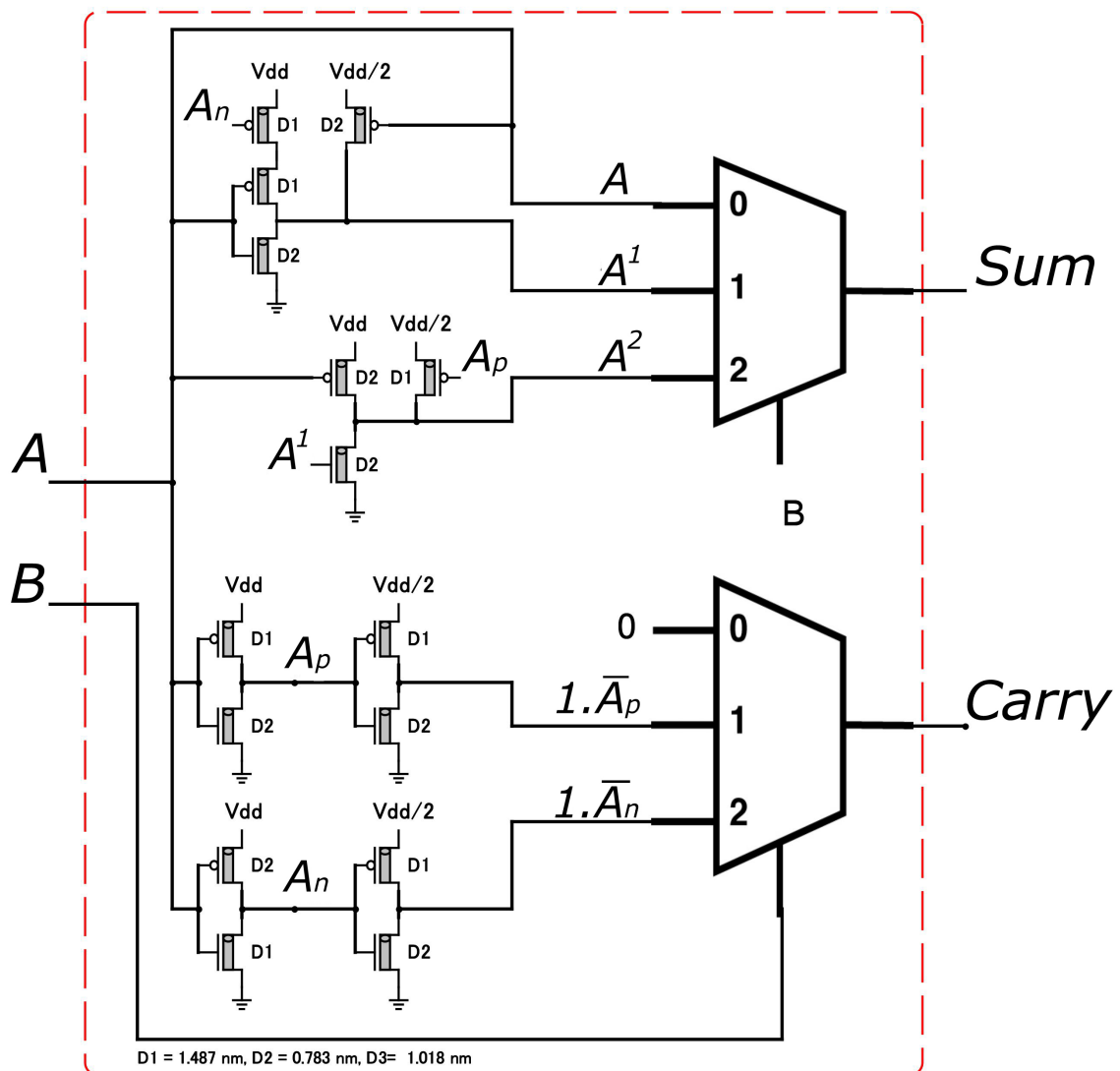


FIGURE 4.7: The proposed THA3 with 45 CNFETs using the proposed TMUX and Unary Operators.

TABLE 4.3: Total transistors count of the proposed THA3

	No. of Devices	No. of Transistors	Subtotal
Proposed TMUX	2	15	30
NTI ( $A_n$ )	1	2	2
PTI ( $A_p$ )	1	2	2
Proposed $A^1$	1	4	4
Proposed $A^2$	1	3	3
Proposed $1 \cdot \bar{A}_p$	1	2	2
Proposed $1 \cdot \bar{A}_n$	1	2	2
Total			45

The input  $A$  fed to NTI, PTI, and the proposed Unary Operators produce the outputs as ( $A^1$ ,  $A^2$ ,  $1 \cdot \bar{A}_p$ ,  $1 \cdot \bar{A}_n$ ).

The outputs ( $A^1$ ,  $A^2$ ) and the input  $A$  are fed to the first the proposed (3:1) TMUX to produce the Sum.

The outputs ( $1 \cdot \bar{A}_p$ ,  $1 \cdot \bar{A}_n$ ) are fed to the second the proposed (3:1) TMUX to produce the Carry.

The input  $B$  is the selection for both the proposed TMUX.

The advantages of the proposed THA3 are:

1. Not using TDecoder compared to [27] and the proposed THA1
2. Not using basic logic gates like “AND”, “OR”, and “NAND” compared to [27] and the proposed THA1
3. Not using the cascading the proposed TMUX compared to [42] and the proposed THA2
4. Using the proposed (3:1) TMUX
5. Using the proposed Unary Operators and the dual power supplies Vdd and Vdd/2

All these advantages can reduce the Transistors Count and energy consumption.

### 4.3 The proposed Ternary Multipliers

A TMUL can multiply two ternary inputs and provides two outputs: the Product and the Carry, as shown in Table 4.4

The basic equations of the Product and the Carry are shown in Table 4.4 to lead three designs:

1. Conventional design in [27, 37, 46] which uses equation (4.4).
2. Cascading TMUXs design in [42] which uses equation (4.5).
3. Unary operators-based design in [36] which uses equation (4.6).

TABLE 4.4: Truth table of TMUL

Product			
A/B	$B_0(0)$	$B_1(1)$	$B_2(2)$
$A_0(0)$	0	0	0
$A_1(1)$	0 } <b>0</b>	1 } <b>A</b>	2 } $\bar{\mathbf{A}}^2$
$A_2(2)$	0 } <b>0</b>	2 } <b>A</b>	1 } $\bar{\mathbf{A}}^2$

Carry			
A/B	$B_0(0)$	$B_1(1)$	$B_2(2)$
$A_0(0)$	0	0	0
$A_1(1)$	0 } <b>0</b>	0 } <b>0</b>	0 } $1 \cdot \bar{\mathbf{A}}_P$
$A_2(2)$	0 } <b>0</b>	0 } <b>0</b>	1 } $1 \cdot \bar{\mathbf{A}}_P$

$$\begin{aligned}
 Product &= 2 \bullet (A_1B_2 + A_2B_1) + 1 \bullet (A_1B_1 + A_2B_2) \\
 Carry &= 1 \bullet A_2B_2
 \end{aligned}
 \tag{4.4}$$

$$\begin{aligned}
 Product &= 0.B_0 + A.B_1 + (0.A_0 + 2.A_1 + 1.A_2).B_2 \\
 Carry &= 0.B_0 + 0.B_1 + (0.A_0 + 0.A_1 + 1.A_2).B_2
 \end{aligned}
 \tag{4.5}$$

$$\begin{aligned}
 Product &= 0 \cdot B_0 + A \cdot B_1 A + \bar{A}^2 B_2 \\
 Carry &= 0 \cdot B_0 + 0 \cdot B_1 + (1 \cdot \bar{A}_p) B_2
 \end{aligned}
 \tag{4.6}$$

Where  $A_k$  and  $B_k$ ,  $k \in \{0,1,2\}$ , are the outputs of the TDecoder from inputs  $A$  and  $B$ .

The existing TMUL in [27] and [36] are shown in Fig. 4.8 and Fig. 4.9;

Figure 4.8 (a) shows the TMUL of [27] with 100 CNFETs that contains TDecoder (16 transistors), binary ANDs, binary ORs, a ternary encoder level shifter, and a ternary OR.

Figure 4.8 (b) shows the TMUL of [46] with 86 CNFETs that contains TDecoder of [27], binary NANDs, binary NORs, a ternary encoder level shifter, a ternary OR, and a STI.

Figure 4.8 (c) shows the TMUL of [37] with 76 CNFETs that contains their TDecoder (10 transistors), binary NANDs, a binary NOT, TNANDs, and a STI.

Figure 4.9 shows the TMUL of [36] with 58 CNFETs that contains (3:1) TMUX (18 transistors) and Unary Operators.

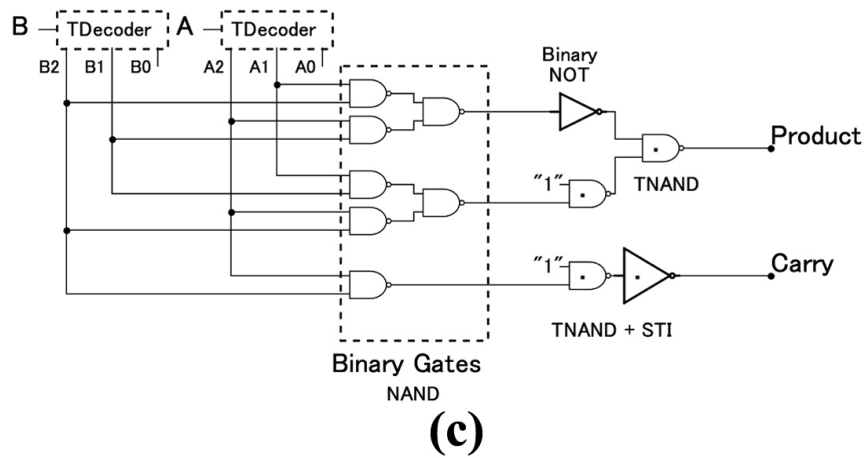
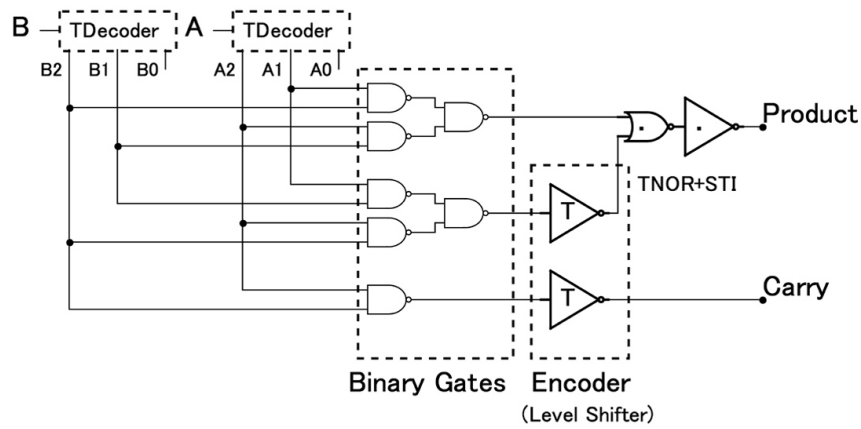
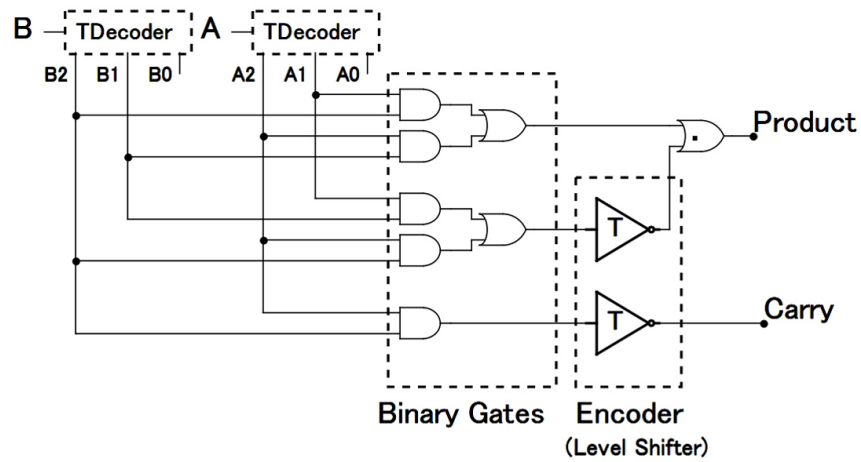


FIGURE 4.8: The Existing TMUL in (a) [27] with 100 CNFETs, (b)[46] with 86 CNFETs, and (b) [37] with 76 CNFETs.

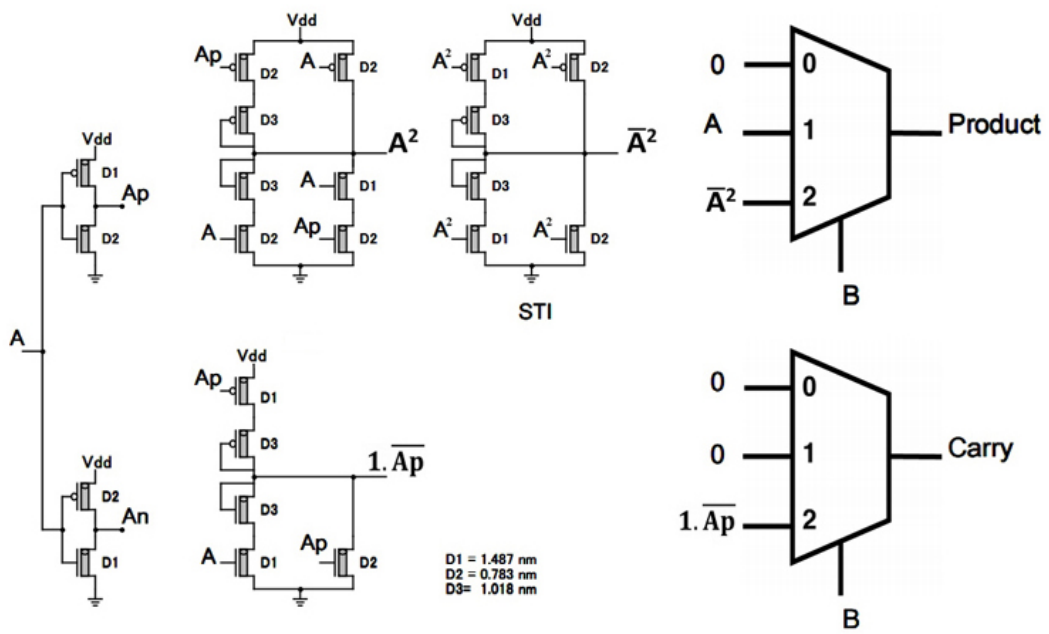


FIGURE 4.9: The Existing TMUL in [36] with 58 CNFETs.

### 4.3.1 The proposed TMUL1

This Chapter proposes a new conventional design of TMUL, which uses equation (4.4), with 61 CNFETs using De Morgan's Law and the dual power supply ( $V_{dd}$  and  $V_{dd}/2$ ) to eliminate the encoder level shifter in [27, 46].

Figure 4.10 shows the proposed TMUL1. It consists of two the proposed TDecoders1 (9 CNFETs each), six binary NANDs, two binary inverters, one the proposed STI (5 CNFETs), and one the proposed TNAND (10 CNFETs).

Table 4.5 shows the total Transistors count of the proposed TMUL1.

The operation of the proposed TMUL1: Two ternary inputs  $A$  and  $B$  are fed to the two the proposed TDecoders1 and produce the outputs as  $(A_2, A_1, A_0)$  and  $(B_2, B_1, B_0)$ , respectively.

These outputs will drive the four 2-inputs binary NAND, the two 2-inputs binary NAND logic gates, the proposed STI, the two binary inverters, and the proposed TNAND to get the Product and the Carry, as final outputs.

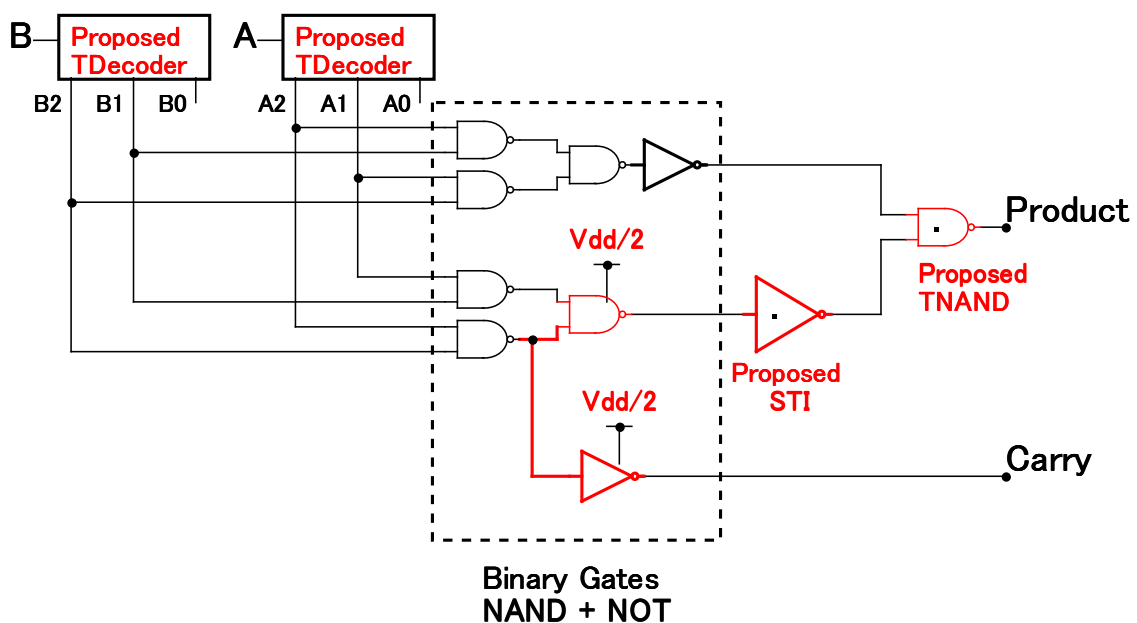


FIGURE 4.10: The proposed TMUL1 with 61 transistors using the proposed TDecoder1, a STI, and TNANDs.

TABLE 4.5: Total transistors count of the proposed TMUL1

	No. of Devices	No. of Transistors	Subtotal
Proposed TDecoder1	2	9	18
Binary NAND	6	4	24
Binary Inverter	2	2	4
Proposed STI	1	5	5
Proposed TNAND	1	10	10
Total			61

### 4.3.2 The proposed TMUL2

This Chapter proposes another design of TMUL based on cascading the proposed TMUXs, which uses equation (4.5), of TMUL2 with 60 CNFETs (4\*15 transistors), as shown in Fig.4.11.

The Existing TMUL design in [42] with 112 CNFETs (4\*28 transistors) is the same as Fig.4.11 but with TMUX equals to 28 transistors.

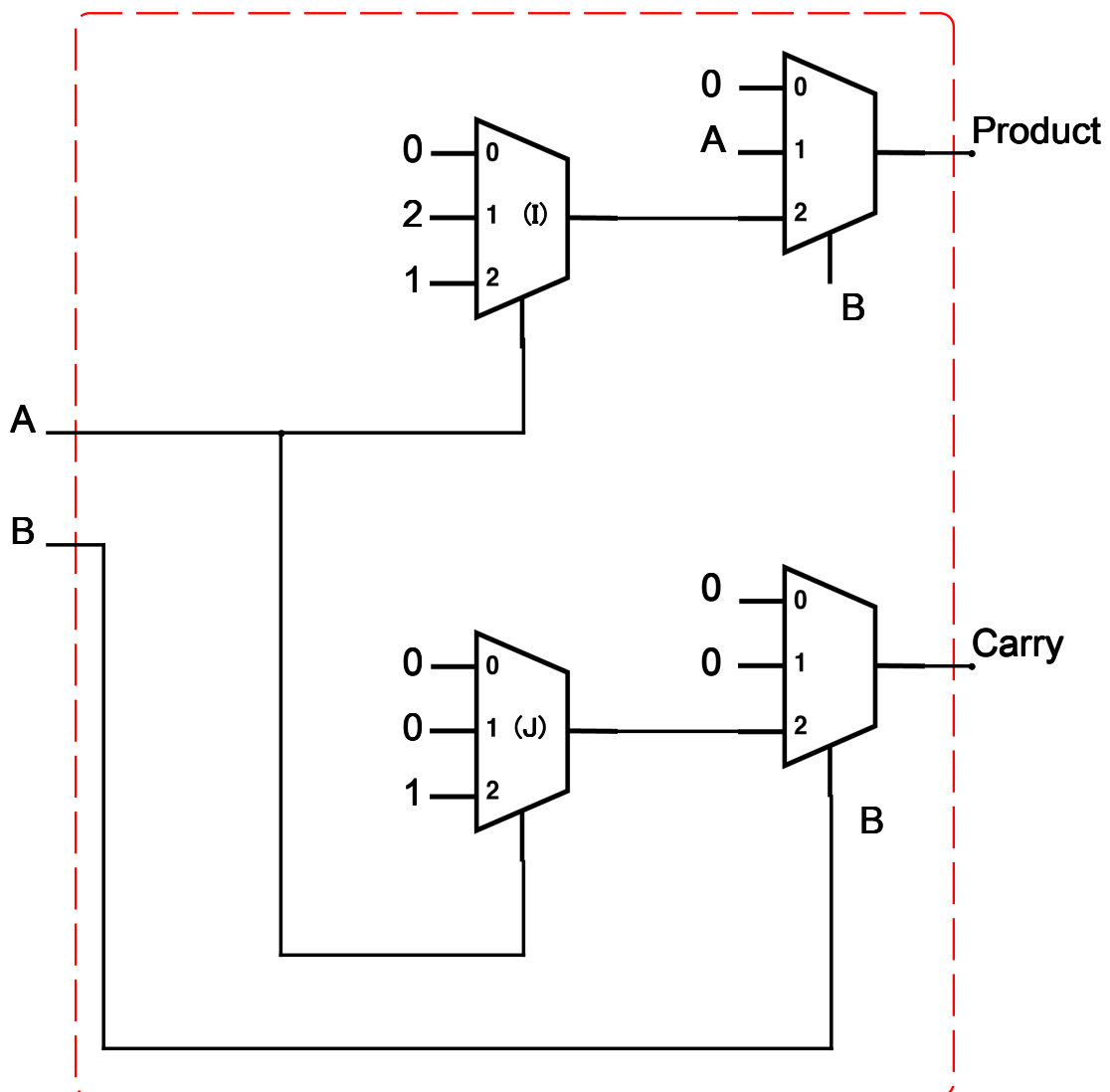


FIGURE 4.11: The proposed TMUL2 with 60 CNFETs using cascading the proposed TMUXs.

The operation of the proposed TMUL2: Two ternary inputs  $A$  and  $B$  are used as selection for the proposed TMUX.

When the selection  $B$  is logic 0, the Product-TMUX output and the Carry-TMUX output will be equal to the logic 0 for  $A$  (0, 1, 2).

When the selection  $B$  is logic 1, the Product-TMUX output will be equal to the values of  $A$  (0, 1, 2) and the Carry-TMUX output will be equal to the logic 0 for  $A$  (0, 1, 2), respectively.

Finally, when the selection  $B$  is logic 2, the Product-TMUX output will be equal to the output of I-TMUX (0, 2, 1) for  $A$  (0, 1, 2), respectively. The Carry-TMUX output will be equal to the output of J-TMUX (0, 0, 1) for  $A$  (0, 1, 2), respectively.

### 4.3.3 The proposed TMUL3

This Chapter proposes a third TMUL design based on Unary operators combined with the proposed TMUX, which uses equation (4.6), with 40 CNFETs, as shown in Fig.4.12.

Table 4.6 shows the total Transistors count of the proposed TMUL3.

The operation of the proposed TMUL3: Two ternary inputs  $A$  and  $B$  are used.

The input  $A$  is fed to NTI ( $A_n$ ), PTI ( $A_p$ ), and to the proposed Unary Operators and produce

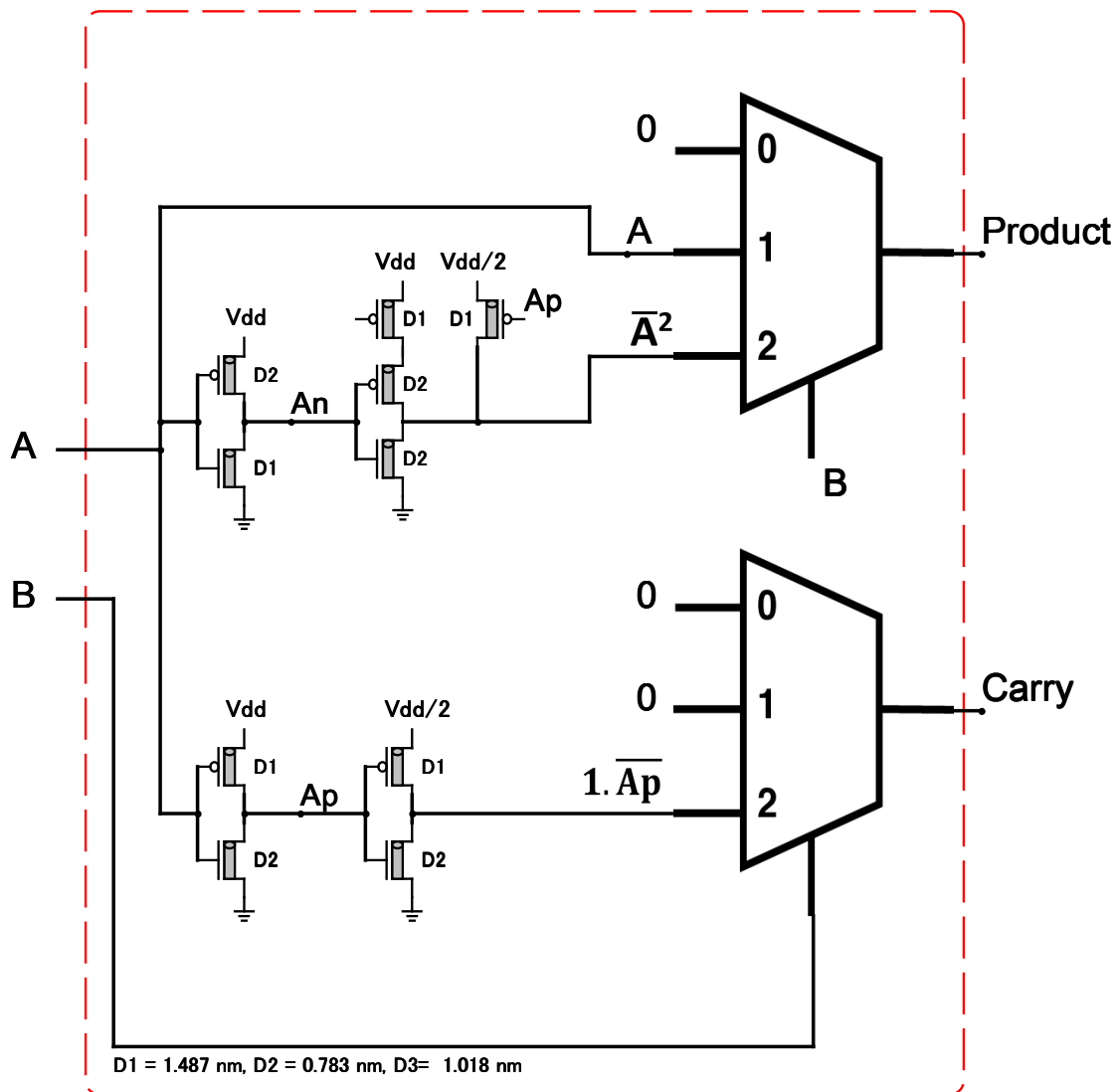


FIGURE 4.12: The proposed TMUL3 with 40 CNFETs using the proposed TMUX and Unary Operators.

TABLE 4.6: Total transistors count of the proposed TMUL3

	No. of Devices	No. of Transistors	Subtotal
Proposed TMUX	2	15	30
NTI ( $A_n$ )	1	2	2
PTI ( $A_p$ )	1	2	2
Proposed $\bar{A}^2$	1	4	4
Proposed $1 \cdot \bar{A}_p$	1	2	2
<b>Total</b>			<b>40</b>

outputs ( $\bar{A}^2, 1 \cdot \bar{A}_p$ ).

The output ( $\bar{A}^2$ ) with the input  $A$  and logic 0 are fed to the first the proposed (3:1) TMUX to get the Product.

The output ( $1 \cdot \bar{A}_p$ ) with two logic 0s are fed to the second the proposed (3:1) TMUX to get the Carry.

Whereas, the input  $B$  is the selection input for both the proposed TMUX.

The advantages of the proposed TMUL3 are:

1. Not using TDecoders compared to [27] and like the proposed TMUL1
2. Not using basic logic gates like “AND”, “OR”, and “NAND” compared to [27] and like the proposed TMUL1
3. Not using the cascading the proposed TMUX compared to [42] and the proposed TMUL2
4. Using the proposed (3:1) TMUX
5. Using the proposed Unary Operators and the dual power supplies Vdd and Vdd/2

All these advantages can reduce the Transistors count and energy consumption.

## 4.4 Simulation Results and Comparisons

The proposed three THAs and three TMULs are simulated, tested, and compared to [27, 36, 37, 42, 46] using the HSPICE simulator and CNFET with the 32-nm channel length at different power supplies (0.8V, 0.9V, 1V), different temperatures (10°C, 27°C, 70°C), and different frequencies (0.5GHz, 1GHz, 2GHz).

All input signals have a fall and rise time of 15 ps. The average power consumption, maximum propagation delay, and maximum PDP are obtained for all circuits.

The performance of the proposed circuits will be compared to other designs for the energy consumption (PDP).

Figures 4.13 and 4.14 illustrate the transient analysis of the proposed THA1 and TMUL1.

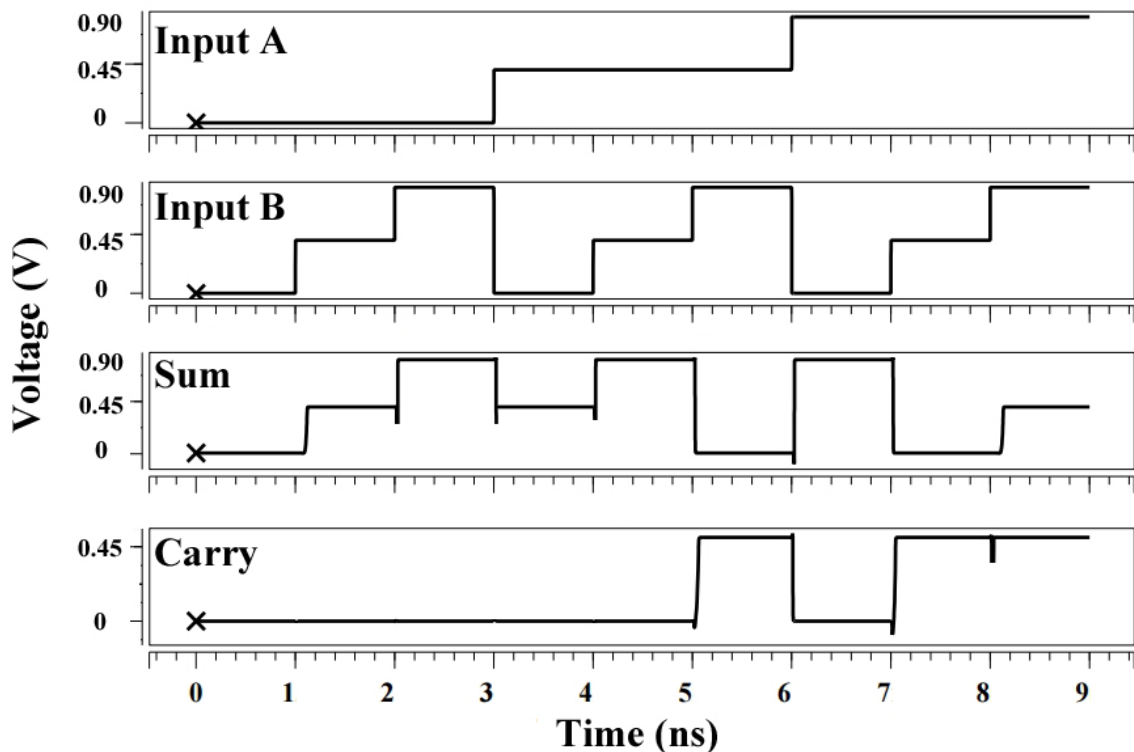


FIGURE 4.13: Transient analysis of the proposed THA1.

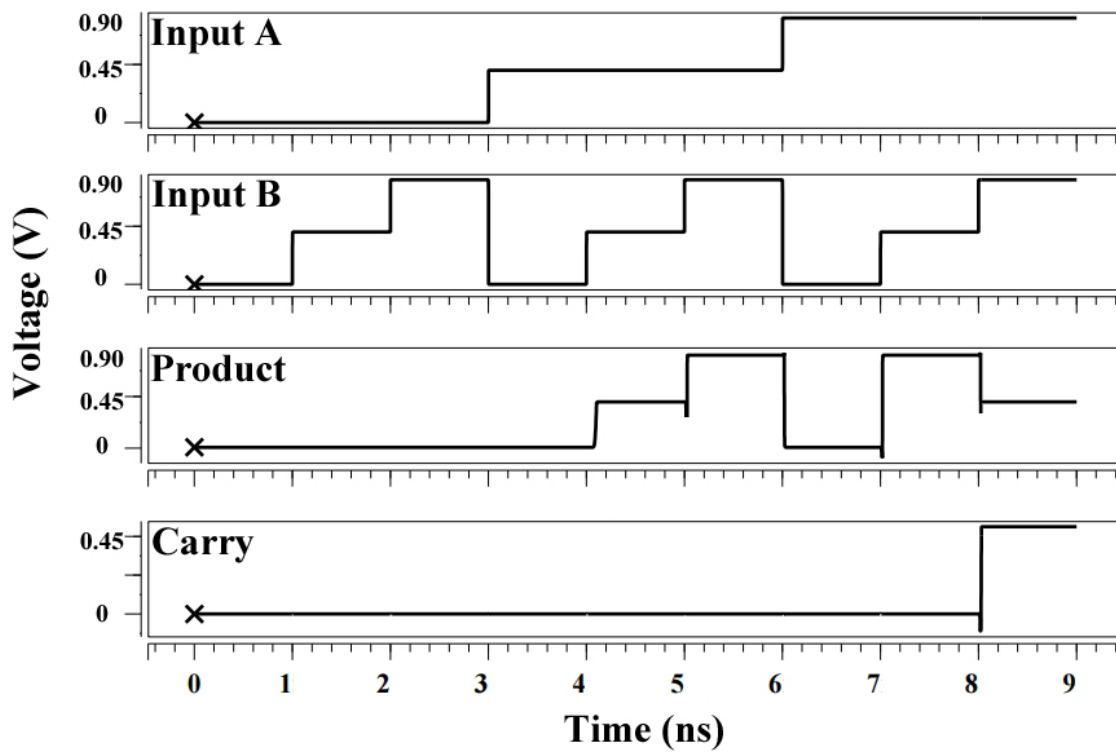


FIGURE 4.14: Transient analysis of the proposed TMUL1.

### 4.4.1 Comparison of Transistors Count

Table 4.7 shows the comparison of Transistors count for the THAs and TMULs of [27, 36, 37, 42, 46] and of the proposed ones.

The proposed THA1 and TMUL1, using conventional design, have a notable reduction in Transistors Count.

Around 37.5%, 24.1%, and 24.1% compared to THA in [27, 46] and [37], respectively.

Around 39%, 29%, and 19.7% compared to TMUL in [27, 46] and [37], respectively.

The proposed THA2 and TMUL2, using cascading TMUXs, have a notable reduction in Transistors count around 46.43% compared to THA, and TMUL in [42].

The proposed THA3 and TMUL3, using TMUX with Unary Operators, have the lowest Transistors count among all the investigated circuits: Around 66.91%, 59.82%, 59.82%, 73.21%, and 29.69% compared to THA in [27, 37, 42, 46] and [36], respectively. Also, around 47.06%, and 50% compared to the proposed THA1, and THA2.

Around 60%, 53.49%, 47.37%, 64.23%, and 31.03% compared to TMUL in [27, 37, 42, 46] and [36], respectively. Also, around 34.43%, and 33.33% compared to the proposed TMUL1, and TMUL2.

TABLE 4.7: Comparison of Transistors Count

	THA	TMUL
[27] Using TDecoder (16T*), AND, OR, TEncoder, and TOR	136	100
[46] Using TDecoder of [27], NAND, NOR, TEncoder, and TNOR	112	86
[37] Using TDecoder (10T), NAND, NOT, and TNAND	112	76
[42] Using cascading TMUXs (28T)	168	112
[36] Using TMUX (18T), and Unary Operators	64	58
<b>Proposed 1:</b> Using the proposed TDecoder1 (9T), STI, and TNAND	85	61
<b>Proposed 2:</b> Using cascading the proposed TMUXs (15T)	<b>90</b>	<b>60</b>
<b>Proposed 3:</b> Using the proposed TMUX, and Unary Operators	<b>45</b>	<b>40</b>

\* T = Transistors

## 4.4.2 Comparison of Different THA Circuits

### 4.4.2.1 Comparison at Different Power Supplies

Table 4.8 shows the comparison to the existing Ternary Half Adder in [27, 36, 37, 42, 46] in terms of the average power consumption, maximum propagation delay, and maximum energy (PDP) at different supply voltages (0.8 V, 0.9 V, 1 V), same temperature (27°C), and same frequency (1 GHz). The boldface values are the best values, among others.

TABLE 4.8: Comparison of average power ( $\mu W$ ), maximum delay (ps), and maximum PDP ( $\times 10^{-18}$  J) for 8 THAs at  $T=27^\circ C$ ,  $F=1$  GHz, and for different supply voltages

	Vdd=0.8 V			Vdd=0.9 V			Vdd=1 V		
	Power	Delay	PDP	Power	Delay	PDP	Power	Delay	PDP
THA in [27]	1.78	112.10	199.53	2.54	56.51	143.53	4.12	55.78	229.81
THA in [46]	1.34	75.42	101.1	1.93	53.14	102.56	3.62	54.36	196.78
THA in [37]	1.11	70.4	78.14	1.84	43.25	79.58	3.32	43.45	144.25
THA in [42]	1.10	27.31	30.04	1.97	21.15	41.66	3.46	19.15	66.26
THA in [36]	0.37	<b>10.35</b>	3.82	0.99	<b>8.52</b>	8.43	2.97	<b>9.10</b>	27.03
<b>Proposed THA1</b>	0.26	105.32	27.38	0.53	74.63	39.55	0.72	73.89	53.2
<b>Proposed THA2</b>	0.08	11.87	0.95	0.14	10.66	1.49	<b>0.4</b>	13.06	5.22
<b>Proposed THA3</b>	<b>0.06</b>	12.65	<b>0.76</b>	<b>0.13</b>	9.50	<b>1.23</b>	<b>0.4</b>	9.67	<b>3.87</b>

As shown in Table 4.8, the comparison of the proposed THA1 demonstrates a notable reduction in PDP.

At Vdd=0.8 V, around 86.28%, 72.92%, and 64.96% compared to [27, 37, 46], respectively.

At Vdd=0.9 V, around 72.44%, 61.44%, and 50.3% compared to [27, 37, 46], respectively.

At Vdd=1 V, around 76.85%, 72.96%, and 63.12% compared to [27, 37, 46], respectively.

The comparison of the proposed THA2 demonstrates a notable reduction in PDP compared to [42], around 96.84%, 96.42%, and 92.12% for Vdd (0.8V, 0.9V, and 1V), respectively.

Whereas, the comparison of the proposed THA3 has the lowest PDP compared to all the investigated models and the proposed THA1 and THA2.

At Vdd=0.8 V, around 99.62%, 99.25%, 99.03%, 97.47%, 80.1%, 97.22%, and 20% compared to [27, 36, 37, 42, 46], the proposed THA1, and the proposed THA2, respectively.

At Vdd=0.9 V, around 99.14%, 98.8%, 98.45%, 97.05%, 85.41%, 96.89%, and 17.45% compared to [27, 36, 37, 42, 46], the proposed THA1, and the proposed THA2, respectively.

At Vdd=1 V, around 98.32%, 98.03%, 97.32%, 94.16%, 85.68%, 92.73%, and 25.86% compared to [27, 36, 37, 42, 46], the proposed THA1, and the proposed THA2, respectively.

#### 4.4.2.2 Comparison at Different Temperatures

Table 4.9 shows the comparison of the proposed THAs to the existing THAs in [27, 36, 37, 42, 46] in terms of the average power consumption, maximum propagation delay, and maximum energy (PDP) at different temperatures (10°C, 27°C, 70°C), same voltage supply Vdd (0.9 V), and same frequency (1 GHz).

TABLE 4.9: Comparison of average power ( $\mu\text{W}$ ), maximum delay (ps), and maximum PDP ( $\times 10^{-18}$  J) for 8 THAs at Vdd=0.9 V, F=1 GHz, and for different temperatures

	Temp.=10°C			Temp.=27°C			Temp.=70°C		
	Power	Delay	PDP	Power	Delay	PDP	Power	Delay	PDP
THA in [27]	2.67	57.68	154	2.54	56.51	143.53	2.79	54.25	151.35
THA in [46]	2.06	55.36	114.04	1.93	53.14	102.56	2.21	51.47	113.75
THA in [37]	1.91	44	84.04	1.84	43.25	79.58	2.15	39.9	85.78
THA in [42]	2.00	21.86	43.72	1.97	21.15	41.66	2.12	19.73	41.83
THA in [36]	0.92	<b>8.69</b>	7.99	0.99	<b>8.52</b>	8.43	1.28	<b>8.11</b>	10.38
<b>Proposed THA1</b>	0.63	76.31	48.07	0.53	74.63	39.55	0.65	71.34	46.37
<b>Proposed THA2</b>	0.15	11.40	1.71	0.14	10.66	1.49	0.20	9.89	1.98
<b>Proposed THA3</b>	<b>0.13</b>	9.96	<b>1.29</b>	<b>0.13</b>	9.50	<b>1.23</b>	<b>0.19</b>	8.68	<b>1.65</b>

As shown in Table 4.9, the comparison of the proposed THA1 demonstrates a notable reduction in PDP.

At Temp.=10°C, around 68.79%, 57.83%, and 42.8% compared to [27, 37, 46], respectively.

At Temp.=27°C, around 72.44%, 61.44%, and 50.3% compared to [27, 37, 46], respectively.

At Temp.=70°C, around 69.36%, 59.24%, and 45.94% compared to [27, 37, 46], respectively.

The comparison of the proposed THA2 demonstrates a notable reduction in PDP compared to [42], around 96.09%, 96.42%, and 95.27% at temperature (10°C, 27°C, and 70°C), respectively.

Whereas, the comparison of the proposed THA3 has the lowest PDP compared to all the investigated models and the proposed THA1, and THA2.

At Temp.=10°C, around 99.16%, 98.87%, 98.47%, 97.05%, 83.85%, 97.32%, and 24.56% compared to [27, 36, 37, 42, 46], the proposed THA1, and the proposed THA2, respectively.

At Temp.=27°C, around 99.14%, 98.8%, 98.45%, 97.05%, 85.41%, 96.89%, and 17.45% compared to [27, 36, 37, 42, 46], the proposed THA1, and the proposed THA2, respectively.

At Temp.=70°C, around 98.91%, 98.55%, 98.08%, 96.06%, 84.1%, 96.44%, and 16.67% compared to [27, 36, 37, 42, 46], the proposed THA1, and the proposed THA2, respectively.

#### 4.4.2.3 Comparison at Different Frequencies

Table 4.10 shows the comparison of the proposed THAs to the existing THAs in [27, 36, 37, 42, 46] in terms of the average power consumption, maximum propagation delay, and maximum energy (PDP) at different frequencies (2 GHz, 1 GHz, 0.5 GHz), same temperatures (27°C), and same voltage supply V<sub>dd</sub> (0.9 V).

As shown in Table 4.10, the comparison of the proposed THA1 demonstrates a considerable reduction in PDP.

At freq.=2 GHz, around 72.18%, 60.4%, and 48.76% compared to [27, 37, 46], respectively.

At freq.=1 GHz, around 72.44%, 61.44%, and 50.3% compared to [27, 37, 46], respectively.

At freq.=0.5 GHz, around 74.37%, 66.04%, and 55.85% compared to [27, 37, 46], respectively.

TABLE 4.10: Comparison of average power ( $\mu\text{W}$ ), maximum delay (ps), and maximum PDP ( $\times 10^{-18}$  J) for 8 THAs at  $T=27^\circ\text{C}$ ,  $V_{dd}=0.9$  V, and for different frequencies

	f= 2 GHz			f= 1 GHz			f= 0.5 GHz		
	Power	Delay	PDP	Power	Delay	PDP	Power	Delay	PDP
THA in [27]	2.73	55.9	152.6	2.54	56.51	143.53	2.35	56.81	133.5
THA in [46]	2.05	52.3	107.21	1.93	53.14	102.56	1.88	53.61	100.78
THA in [37]	1.94	42.7	82.84	1.84	43.25	79.58	1.79	43.3	77.5
THA in [42]	2.14	21.20	45.37	1.97	21.15	41.66	1.89	21.20	40.07
THA in [36]	1.25	<b>8.46</b>	10.58	0.99	<b>8.52</b>	8.43	1.17	<b>8.56</b>	10.02
<b>Proposed THA1</b>	0.58	73.2	42.45	0.53	74.63	39.55	0.48	71.3	34.22
<b>Proposed THA2</b>	0.21	10.90	2.29	0.14	10.66	1.49	<b>0.11</b>	10.89	1.19
<b>Proposed THA3</b>	<b>0.17</b>	9.54	<b>1.62</b>	<b>0.13</b>	9.50	<b>1.23</b>	<b>0.11</b>	9.47	<b>1.04</b>

The comparison of the proposed THA2 demonstrates a notable reduction in PDP compared to [42], around 94.95%, 96.42%, and 97.03% for frequency (2 GHz, 1 GHz, and 0.5 GHz), respectively.

Whereas, the comparison of the proposed THA3 has the lowest PDP compared to all the investigate models and the proposed THA1, and THA2.

At frequency=2 GHz, around 98.94%, 98.49%, 98.04%, 96.43%, 84.69%, 96.18%, and 29.26% compared to [27, 36, 37, 42, 46], the proposed THA1, and the proposed THA2, respectively.

At frequency=1 GHz, around 99.14%, 98.8%, 98.45%, 97.05%, 85.41%, 96.89%, and 17.45% compared to [27, 36, 37, 42, 46], the proposed THA1, and the proposed THA2, respectively.

At frequency=0.5 GHz, around 99.22%, 98.97%, 98.66%, 97.4%, 89.62%, 96.96%, and 12.61% compared to [27, 36, 37, 42, 46], the proposed THA1, and the proposed THA2, respectively.

### 4.4.3 Comparison at Different TMUL Circuits

#### 4.4.3.1 Comparison to Different Power Supplies

Table 4.11 shows the comparison of the proposed TMULs to the existing Ternary Multipliers in [27, 36, 37, 42, 46] in terms of the average power consumption, maximum propagation delay, and maximum energy (PDP) at different supply voltages (0.8 V, 0.9 V, 1 V), same temperature (27°C), and same frequency (1 GHz). The boldface values are the best values, among others.

TABLE 4.11: Comparison of average power ( $\mu\text{W}$ ), maximum delay (ps), and maximum PDP ( $\times 10^{-18}$  J) for 8 TMULs at  $T=27^\circ\text{C}$ ,  $F=1$  GHz, and for different supply voltages

	Vdd=0.8 V			Vdd=0.9 V			Vdd=1 V		
	Power	Delay	PDP	Power	Delay	PDP	Power	Delay	PDP
TMUL in [27]	1.32	68.72	90.71	1.88	46.32	87.08	3.07	48.46	148.77
TMUL in [46]	1	57.32	57.32	1.45	43.05	62.42	2.48	45.25	112.22
TMUL in [37]	0.8	48.75	39	1.32	31.26	41.26	2.24	32.9	73.69
TMUL in [42]	1.07	23.75	25.41	1.93	18.21	35.15	3.37	16.32	54.99
TMUL in [36]	0.27	18.09	4.88	0.64	16.63	10.64	1.40	16.82	23.55
<b>Proposed TMUL1</b>	0.30	67.80	20.34	0.42	54.82	23.02	0.72	56.34	40.56
<b>Proposed TMUL2</b>	0.08	<b>13.83</b>	1.10	0.17	<b>9.65</b>	1.64	0.53	<b>9.18</b>	4.86
<b>Proposed TMUL3</b>	<b>0.06</b>	16.96	<b>1.02</b>	<b>0.07</b>	11.61	<b>0.81</b>	<b>0.15</b>	10.02	<b>1.50</b>

As shown in Table 4.11, the comparison of the proposed TMUL1 demonstrates a notable reduction in PDP.

At Vdd=0.8 V, around 77.58%, 64.52%, and 47.85% compared to [27, 37, 46], respectively. At Vdd=0.9 V, around 73.56%, 63.12%, and 44.21% compared to [27, 37, 46], respectively. At Vdd=1 V, around 72.74%, 63.86%, and 44.96% compared to [27, 37, 46], respectively.

The comparison of the proposed TMUL2 demonstrates a notable reduction in PDP compared to [42]: around 95.67%, 95.33%, and 91.16% at Vdd (0.8V, 0.9V, and 1V), respectively.

Whereas, the comparison of the proposed TMUL3 has the lowest PDP compared to all the investigated models and the proposed TMUL1, and TMUL2.

At Vdd=0.8 V, around 98.88%, 98.22%, 97.38%, 95.99%, 79.1%, 94.99%, and 7.27% compared to [27, 36, 37, 42, 46], the proposed TMUL1, and the proposed TMUL2, respectively.

At Vdd=0.9 V, around 99.07%, 98.7%, 98.04%, 97.7%, 92.39%, 96.48%, and 50.61% compared to [27, 36, 37, 42, 46], the proposed TMUL1, and the proposed TMUL2, respectively.

At Vdd=1 V, around 98.99%, 98.66%, 97.96%, 97.27%, 93.63%, 96.3%, and 69.14% compared to [27, 36, 37, 42, 46], the proposed TMUL1, and the proposed TMUL2, respectively.

#### 4.4.3.2 Comparison at Different Temperatures

Table 4.12 shows the comparison to the existing TMULs in [27, 36, 37, 42, 46] in terms of the average power consumption, maximum propagation delay, and maximum energy (PDP) at different temperatures (10°C, 27°C, 70°C), same voltage supply Vdd (0.9 V), and same frequency (1 GHz).

TABLE 4.12: Comparison of average power ( $\mu\text{W}$ ), maximum delay (ps), and maximum PDP ( $\times 10^{-18}$  J) for 8 TMULs at Vdd=0.9 V, F=1 GHz, and at different temperatures

	Temp.=10°C			Temp.=27°C			Temp.=70°C		
	Power	Delay	PDP	Power	Delay	PDP	Power	Delay	PDP
TMUL in [27]	1.98	48.23	95.49	1.88	46.32	87.08	2.06	44.9	92.50
TMUL in [46]	1.58	45.92	72.55	1.45	43.05	62.42	1.65	42.12	69.49
TMUL in [37]	1.37	33.45	45.82	1.32	31.26	41.26	1.57	29.83	46.83
TMUL in [42]	1.95	18.74	36.54	1.93	18.21	35.15	2.08	17.05	35.46
TMUL in [36]	0.60	17.25	10.35	0.64	16.63	10.64	0.83	15.34	12.73
<b>Proposed TMUL1</b>	0.50	56.15	28.07	0.42	54.82	23.02	0.52	52.89	27.50
<b>Proposed TMUL2</b>	0.16	<b>10.03</b>	1.60	0.17	<b>9.65</b>	1.64	0.23	<b>8.82</b>	2.03
<b>Proposed TMUL3</b>	<b>0.09</b>	11.97	<b>1.07</b>	<b>0.07</b>	11.61	<b>0.81</b>	<b>0.10</b>	10.75	<b>1.07</b>

As shown in Table 4.12, the comparison of the proposed TMUL1 demonstrates a notable reduction in PDP.

At Temp.=10°C, around 70.6%, 61.31%, and 38.74% compared to [27, 37, 46], respectively.

At Temp.=27°C, around 73.56%, 63.12%, and 44.21% compared to [27, 37, 46], respectively.

At Temp.=70°C, around 70.27%, 60.43%, and 41.28% compared to [27, 37, 46], respectively.

The comparison of the proposed TMUL2 demonstrates a notable reduction in PDP compared to [42]: around 95.62%, 95.33%, and 94.28% at Temperature (10°C, 27°C, and 70°C), respectively.

Whereas, the comparison of the proposed TMUL3 has the lowest PDP compared to all the investigated models and the proposed TMUL1, and TMUL2.

At Temperature=10°C, around 98.88%, 98.53%, 97.66%, 97.07%, 89.66%, 96.19%, and 33.13% compared to [27, 36, 37, 42, 46], the proposed TMUL1, and the proposed TMUL2, respectively.

At Temperature=27°C, around 99.07%, 98.7%, 98.04%, 97.7%, 92.39%, 96.48%, and 50.61% compared to [27, 36, 37, 42, 46], the proposed TMUL1, and the proposed TMUL2, respectively.

At Temperature=70°C, around 98.84%, 98.46%, 97.72%, 96.98%, 91.59%, 96.11%, and 47.29% compared to [27, 36, 37, 42, 46], the proposed TMUL1, and the proposed TMUL2, respectively.

#### 4.4.3.3 Comparison at Different Frequencies

Table 4.13 shows the comparison to the existing TMUL in [27, 36, 37, 42, 46] in terms of the average power consumption, maximum propagation delay, and maximum energy (PDP) at different frequencies (2 GHz, 1 GHz, 0.5 GHz), same temperatures (27°C), and same voltage supply Vdd (0.9 V).

As shown in Table 4.13, the comparison of the proposed TMUL1 demonstrates a considerable reduction in PDP.

TABLE 4.13: Comparison of average power ( $\mu\text{W}$ ), maximum delay (ps), and maximum PDP ( $\times 10^{-18}$  J) for 8 TMULs at  $T=27^\circ\text{C}$ ,  $V_{\text{dd}}=0.9$  V, and at different frequencies

	f= 0.5 GHz			f= 1 GHz			f= 2 GHz		
	Power	Delay	PDP	Power	Delay	PDP	Power	Delay	PDP
TMUL in [27]	1.74	46.11	80.23	1.88	46.32	87.08	2.03	45.85	93.08
TMUL in [46]	1.41	43.15	60.84	1.45	43.05	62.42	1.54	42.21	65
TMUL in [37]	1.28	31.42	40.21	1.32	31.26	41.26	1.39	30.11	41.85
TMUL in [42]	1.87	18.18	33.99	1.93	18.21	35.15	2.05	18.20	37.31
TMUL in [36]	0.62	16.67	10.34	0.64	16.63	10.64	0.89	6.55	5.83
<b>Proposed TMUL1</b>	0.38	51.89	19.72	0.42	54.82	23.02	0.46	53.15	24.45
<b>Proposed TMUL2</b>	0.15	<b>9.63</b>	1.44	0.17	<b>9.65</b>	1.64	0.20	<b>9.64</b>	1.93
<b>Proposed TMUL3</b>	<b>0.06</b>	11.60	<b>0.69</b>	<b>0.07</b>	11.61	<b>0.81</b>	<b>0.09</b>	11.62	<b>1.05</b>

At freq.=2 GHz, around 73.73%, 62.38%, and 41.58% compared to [27, 37, 46], respectively.

At freq.=1 GHz, around 73.56%, 63.12%, and 44.21% compared to [27, 37, 46], respectively.

At freq.=0.5 GHz, around 75.42%, 67.59%, and 50.96% compared to [27, 37, 46], respectively.

The comparison of the proposed TMUL2 demonstrates a notable reduction in PDP compared to [42]: around 94.83%, 95.33%, and 95.76% at frequency (2 GHz, 1 GHz, and 0.5 GHz), respectively.

Whereas, the comparison of the proposed TMUL3 has the lowest PDP compared to all the investigated models and the proposed TMUL1, and TMUL2.

At frequency=2 GHz, around 98.87%, 98.38%, 97.49%, 97.19%, 81.99%, 95.71%, and 45.6% compared to [27, 36, 37, 42, 46], the proposed TMUL1, and the proposed TMUL2, respectively.

At frequency=1 GHz, around 99.07%, 98.7%, 98.04%, 97.7%, 92.39%, 96.48%, and 50.61% compared to [27, 36, 37, 42, 46], the proposed TMUL1, and the proposed TMUL2, respectively.

At frequency=0.5 GHz, around 99.14%, 98.87%, 98.28%, 97.97%, 93.33%, 96.5%, and

52.08% compared to [27, 36, 37, 42, 46], the proposed TMUL1, and the proposed TMUL2, respectively.

#### 4.4.4 Process Variations

Process variations have a great impact on the performance and robustness of nanoscale devices and circuits. Hence, all circuits are tested in the presence of major process variations: TOX, CNT diameter, CNT's count, and channel length [47].

##### TOX

In the Stanford CNFET model, TOX is the oxide thickness of the Gate Dielectric  $k_1$  material ( $HfO_2$ ), as shown in 4.15. The variation in TOX will lead to leakage current. By decreasing TOX, the leakage current will increase, then the PDP will also increase and Vice Versa.

##### CNT Diameter

The CNT diameter variation is one of the multiple problems of CNFET imperfections caused due to nonidealities in the CNT synthesis process, which negatively affects the performance of CNFET circuits because this variation will lead to variation in threshold voltage. This problem has more impact on MVL designs where transistors with different threshold voltages are applied.

##### CNT's Count

Variation in the count of CNTs leads to a change in circuit parameters because it changes the output current of the transistor, which may cause a problem in the circuit functionality.

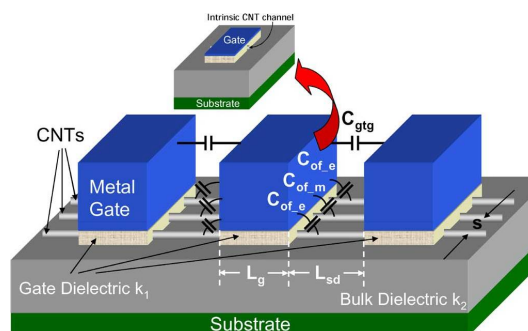


FIGURE 4.15: Stanford CNFET Model.

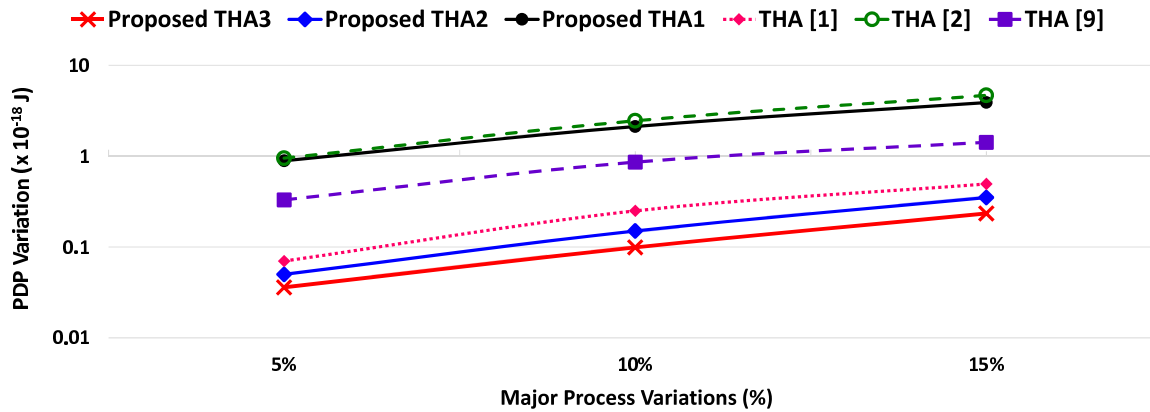


FIGURE 4.16: THAs Major Process Variations: TOX, CNT Diameter, CNT's Count, and Channel length.

### Channel Length

Variation in channel length will lead to the variation of the channel between drain and source, which negatively affects the performance of CNFET circuits.

Therefore, this paper uses Monte Carlo analysis based on the Gaussian distributions with 5%, 10%, and 15% variations at the  $\pm 3\sigma$  level with the number of simulation running is equal to 1000.

Monte Carlo analysis is based on statistical distributions. It simulates mismatching and process variations. In each simulation run, it calculates every parameter randomly according to a statistical distribution model.

The energy variations of all THA and TMUL circuits in the presence of the major process variations are shown in Fig. 4.16 and 4.17.

As shown in Fig. 4.16 and 4.17, The proposed THA3 and TMUL3 have a lower sensitivity to process variations and are more robustness compared to the other designs because their PDP variations are the smallest among all the investigated circuits.

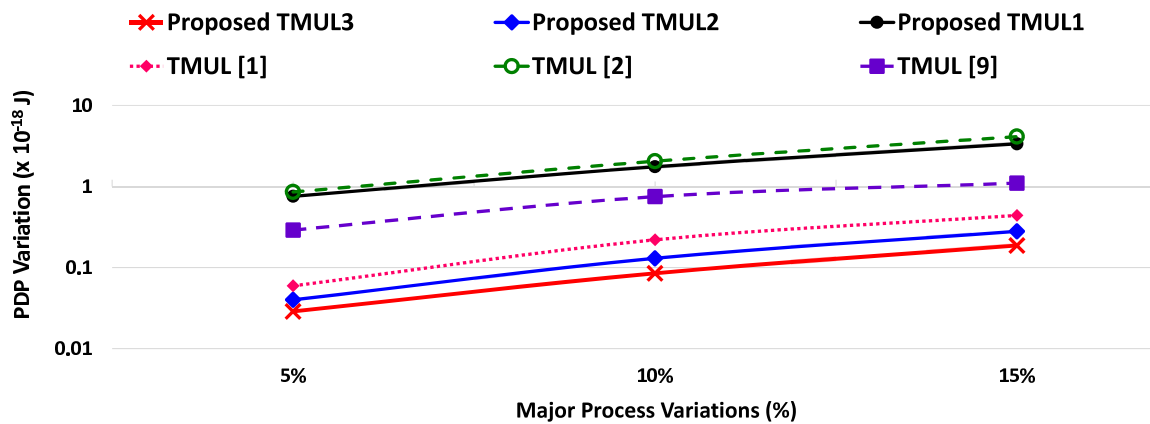


FIGURE 4.17: TMULs Major Process Variations: TOX, CNT Diameter, CNT's Count, and Channel length.

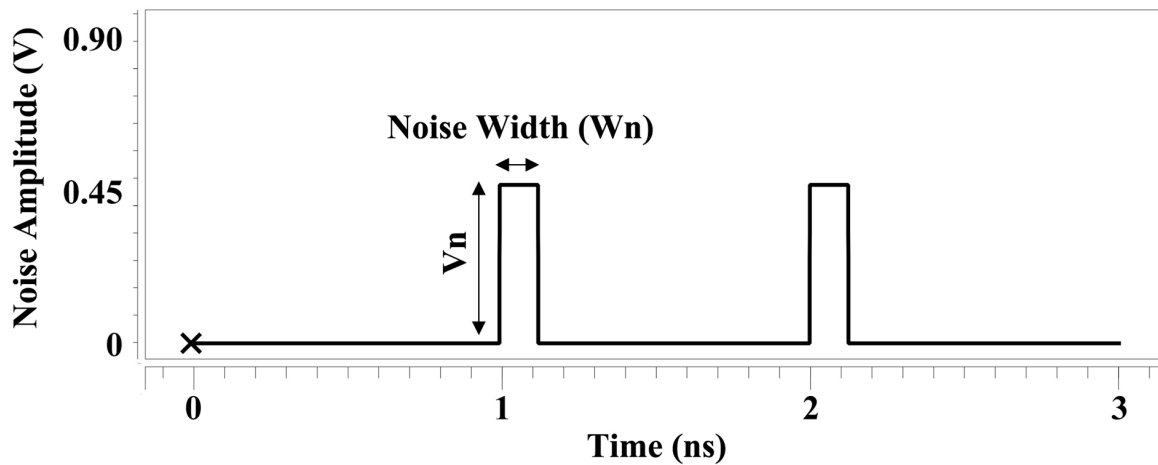


FIGURE 4.18: Noise Signal.

#### 4.4.5 Noise Effect

Digital circuits are inherently noise-tolerant, and they are only affected by noises with high amplitude and wide width.

The Noise Immunity Curve (NIC) is used to determine the impact of noisy inputs on all THA and TMUL circuits.

The noise signal, shown in Fig.4.18, is injected into inputs of all THAs and TMULs.

As shown in Fig.4.18, the noise signal has pulse width ( $W_n$ ) and pulse amplitude ( $V_n$ ).

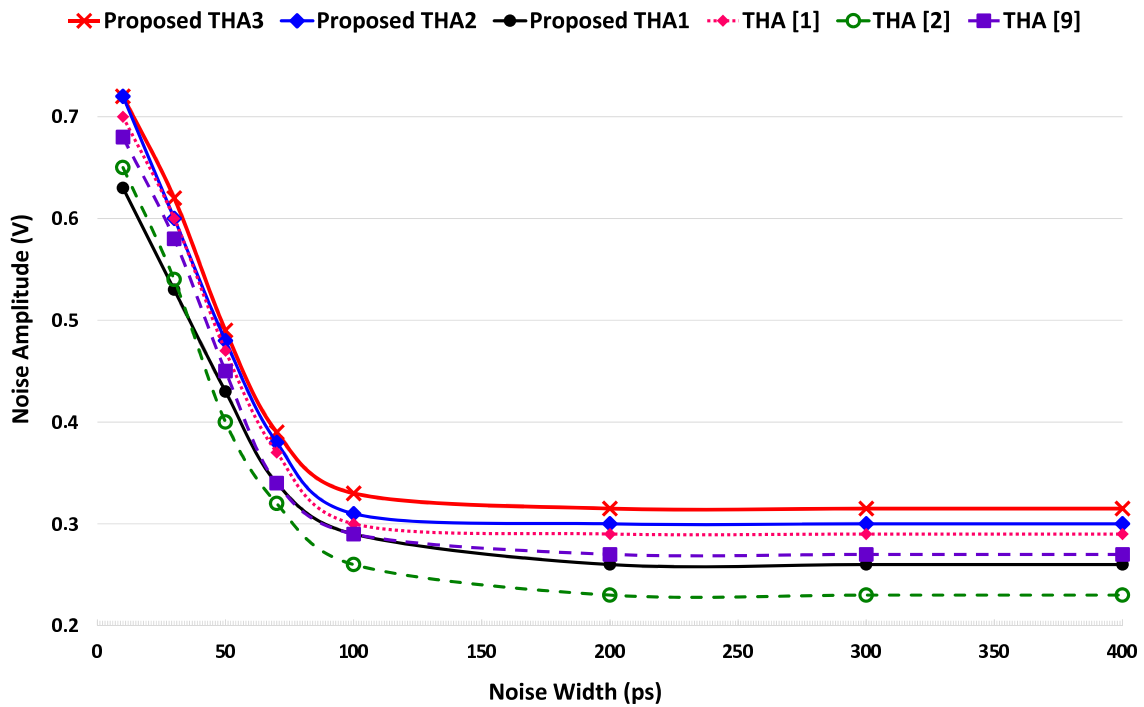


FIGURE 4.19: THAs Noise Immunity Curve (NIC).

Each point on the NIC curve is a pair of  $(W_n, V_n)$ . Above that point, the circuit will produce an error on the output. The region above the NIC curve is an unsafe zone, whereas the region below the NIC curve is a safe zone against noise pulses.

Therefore, any circuit with higher NIC demonstrates a more noise-tolerant circuit [48].

The proposed THA3 and TMUL3 show higher noise immunity compared to all the investigated circuits, as shown in Fig. 4.19 and 4.20.

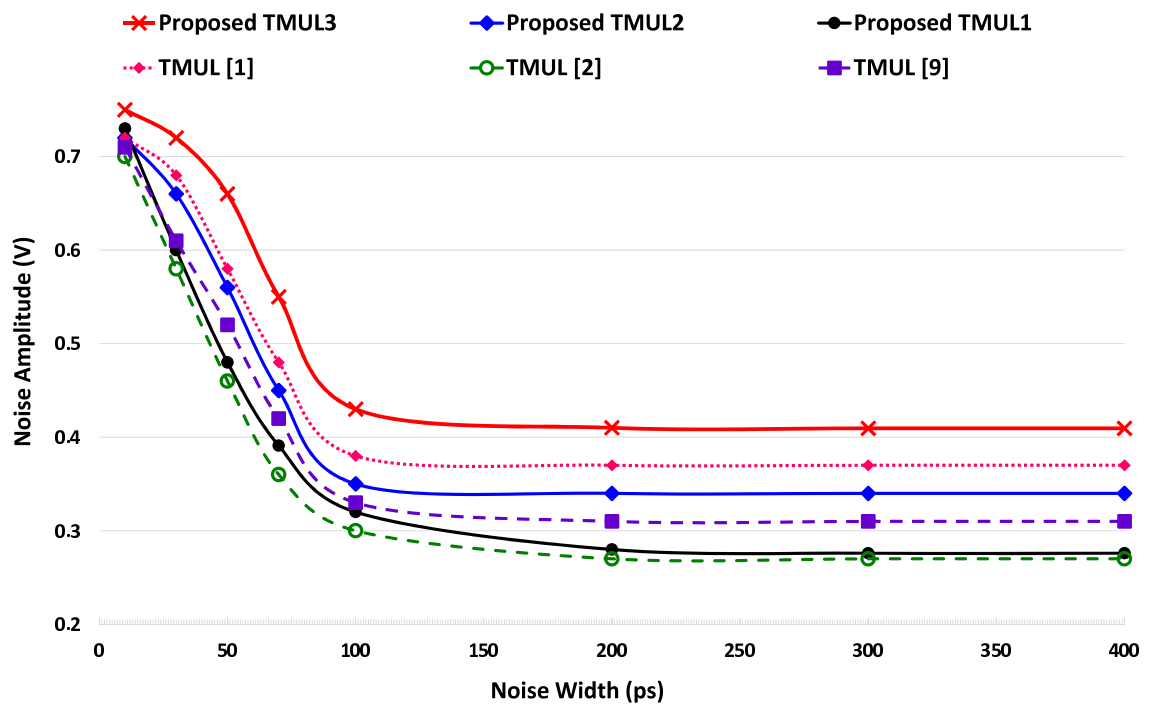


FIGURE 4.20: TMULs Noise Immunity Curve (NIC).

## 4.5 Conclusion

This Chapter has proposed three different designs of THA and TMUL. The first design uses the proposed TDecoder1, binary NANDs, the proposed STI, and the proposed TNAND. The second design uses the proposed cascading TMUX. The third design uses the proposed unary operators and the proposed TMUX.

The design process tried to optimize several circuit techniques such as reducing the number of the used transistors, utilizing energy-efficient transistor arrangements, and applying the dual supply voltages ( $V_{dd}$  and  $V_{dd}/2$ ).

The proposed ternary circuits are compared to the latest existing ternary circuits, simulated and tested using HSPICE simulator under various operating conditions at different supply voltages, different temperatures, and different frequencies.

The results prove the merits of the approach in terms of reduced energy consumption (PDP) compared to other existing designs.

Moreover, the noise immunity curve (NIC) and Monte Carlo analysis for major process variations (TOX, CNT Diameter, CNT's Count, and Channel length) were studied. The results confirmed that the third proposed THA3 and TMUL3 had higher robustness and higher noise tolerance, among other designs.

Therefore, the proposed circuits can be implemented in low-power portable electronics and embedded systems to save battery consumption.

# Chapter 5

## Ternary Data Transmission

### 5.1 Introduction and Literature Review

In general, data transmission transfer data over a communication medium to one or more computers, smartphones, embedded systems, or any electronic devices [49, 50].

Besides external communication, data transmission also may be internal between the computer components, for example, between the CPU and the RAM or HDD [51].

Transmission media usually used in communication channels are a copper wire (coaxial cable, twisted pair), glass fiber, microwave, radio, or infrared [52].

There are limitations on binary data transmission at the physical layer in cable connections between hosts (computers, hubs, switches, and routers), such as bandwidth, delay, and size of data.

Therefore, this chapter will propose a novel bi-directional circuit that contains two converters (Binary-to-Ternary and Ternary-to-Binary). When sending data, the circuit will convert from the binary system to the ternary system, whereas, when receiving data, the circuit will convert from the ternary system to the binary system.

The proposed Data Transmission model between routers is introduced with the general model, as represented in Fig.5.1. It has two bi-directional converters between the routers.

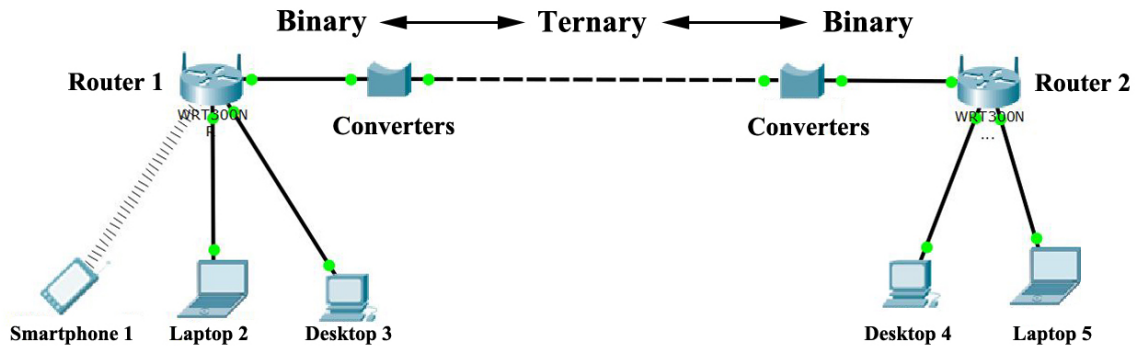


FIGURE 5.1: The proposed Data Transmission model between routers.

The design of binary-to-ternary converters and ternary-to-binary converters has recently constituted an active area of research, and valued papers are selected.

In [53, 54], a circuit that converts two binary bits to one ternary digit (trit) was proposed. In [55], the authors proposed a binary-to-ternary converter based on the Josephson junction (JJ). In [56], the designed converter circuit is characterized by a dual supply operation. Finally, in [57], the authors proposed a novel binary-to-ternary converter based on DPL, which gives the best performance than all mentioned papers above.

In [58], CMOS circuit is proposed to convert one trit into two bits, while the circuits in [59–63] represent ternary, quaternary, quinary, octal and hexadecimal to binary converters that use multiple input floating gate MOSFETs. Also, in [64], a novel Ternary-to-Binary Converter used in Quantum-dot Cellular Automata proposed, while in [65], three circuits are used to convert ternary data to bits.

The above mentioned converters suffer from high power consumption [55, 56, 58–60], large propagation delay [56, 57], complex circuit [56, 64, 65] or even errors in the output when two binary inputs are set as high level voltage [53, 54].

Therefore, this chapter proposes novel bi-directional converters, which are published in ([66], [67]) and can be found in Appendices (D, E).

Binary-to-ternary converter using CMOS DPL Gates and ternary-to-binary converter using CNFETs, which provide a drastic reduction in power consumption, lower the propagation delay, and provide a small, simple and error-free circuit implementation (for all possible inputs) compared to others circuits.

## 5.2 The Proposed Binary-to-Ternary Converter using CMOS DPL Gates

The proposed circuit converts four binary bits to three ternary trits using Double Pass-Transistor Logic (DPL) CMOS binary logic gates. It is simulated using Micro-Cap V10 PSPICE simulator and it demonstrates a notable reduction in devices count, propagation delay, and energy consumption.

A novel four to three binary-to-ternary converter model is shown in Fig.5.2.

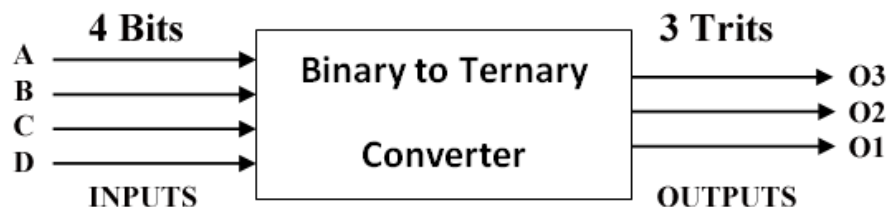


FIGURE 5.2: Binary-to-Ternary model

As shown in Fig.5.2, four binary bits are provided as input (A, B, C, D). The input “A” is the most significant bit (MSB), and the input “D” is the least significant bit (LSB). Three trits are provided as output (O3, O2, O1). The output “O3” is the most significant trit (MST), and “O1” is the least significant trit (LST), using simple ternary logic (0, 1, 2).

Among the 27 trits combinations, only 16 are used to represent all the four-bit combinations while the remaining 11 could be used for additional features such as error detection.

The 16 combinations that are produced in the converter circuit are shown in Table 5.1. The voltage supply used in the proposed circuit is 1.8V to decrease power consumption. Therefore, DPL is used to eliminate noise, as described in chapter 1.

Binary digits are (0: Low, and 1: High) and Ternary trits are (0: Low, 1: Medium, and 2: High). This chapter will use, “0” to represents low-level voltage (0V), “1” to represents medium-level voltage (0.9V), and “2” to represents high-level voltage (1.8V) for the both binary and ternary system.

TABLE 5.1: Binary-to-Ternary truth table

Decimal	Binary Inputs				Ternary Outputs		
	A	B	C	D	O3	O2	O1
0	0	0	0	0	0	0	0
1	0	0	0	2	0	0	1
2	0	0	2	0	0	0	2
3	0	0	2	2	0	1	0
4	0	2	0	0	0	1	1
5	0	2	0	2	0	1	2
6	0	2	2	0	0	2	0
7	0	2	2	2	0	2	1
8	2	0	0	0	0	2	2
9	2	0	0	2	1	0	0
10	2	0	2	0	1	0	1
11	2	0	2	2	1	0	2
12	2	2	0	0	1	1	0
13	2	2	0	2	1	1	1
14	2	2	2	0	1	1	2
15	2	2	2	2	1	2	0

The procedure to build the proposed circuit starts with a novel technique by decomposing each ternary output in Table 5.1 to two intermediate binary outputs, as shown in Table 5.2 and Table 5.3.

TABLE 5.2: Decomposition of O1 to two intermediate Binary Outputs

<b>Ternary Output</b>	<b>Intermediate Binary Outputs</b>	
<b>O1</b>	<b>O1a</b>	<b>O1b</b>
Logic 0 (0V)	0	0
Logic 1 (0.9V)	0	2
Logic 2 (1.8V)	2	0

TABLE 5.3: Decomposition of the three ternary outputs

<b>Binary Inputs</b>				<b>Ternary Outputs as Intermediate Binary</b>				
				<b>O3</b>	<b>O2</b>		<b>O1</b>	
<b>A</b>	<b>B</b>	<b>C</b>	<b>D</b>	<b>O3b</b>	<b>O2a</b>	<b>O2b</b>	<b>O1a</b>	<b>O1b</b>
0	0	0	0	0	0	0	0	0
0	0	0	2	0	0	0	0	2
0	0	2	0	0	0	0	2	0
0	0	2	2	0	0	2	0	0
0	2	0	0	0	0	2	0	2
0	2	0	2	0	0	2	2	0
0	2	2	0	0	2	0	0	0
0	2	2	2	0	2	0	0	2
2	0	0	0	0	2	0	2	0
2	0	0	2	2	0	0	0	0
2	0	2	0	2	0	0	0	2
2	0	2	2	2	0	0	2	0
2	2	0	0	2	0	2	0	0
2	2	0	2	2	0	2	0	2
2	2	2	0	2	0	2	2	0
2	2	2	2	2	2	0	0	0

The second step involves using Karnaugh maps to get an optimized circuit for each intermediate output in Table 5.3. The minimization process results in equations 5.1- 5.5.

$$O1a = \overline{A}\overline{B}C\overline{D} + \overline{A}B\overline{C}D + A\overline{B}\overline{C}\overline{D} + A\overline{B}C\overline{D} + ABC\overline{D} \quad (5.1)$$

$$O1b = \overline{A}\overline{B}\overline{C}D + \overline{A}B\overline{C}\overline{D} + \overline{A}BC\overline{D} + A\overline{B}C\overline{D} + ABC\overline{D} \quad (5.2)$$

$$O2a = \overline{A}BC + \overline{A}B\overline{C}D + BCD + A\overline{B}\overline{C}\overline{D} \quad (5.3)$$

$$O2b = B\overline{C} + AB\overline{D} + \overline{A}\overline{B}CD \quad (5.4)$$

$$O3b = AB + AC + AD \quad (5.5)$$

The resulting equations are implemented in the binary-to-ternary converter circuit shown in Fig. 5.3.

Figure 5.3 represents the binary-to-ternary converter with four binary inputs (A, B, C, D) and three ternary outputs (O1, O2, O3). The intermediate binary outputs labeled as O1a, O1b, O2a, O2b, and O3b.

An enhancement MOSFET (M) is used as a switch after each of the intermediate outputs O1a and O2a. When O1a or O2a is at high-level voltage, then the transistor M will be turned “ON” to pass the 1.8 volts to the final output O1, and it will be “OFF” when the O1a or O2a is at low-level voltage.

Similarity, two diode-connected transistors (R) that act like resistors are added after the intermediate outputs (O1b, O2b, O3b), these transistors act as a voltage divider. For example, when O1b is equal to 1.8V, then the output O1 is equal to 0.9V. When O1b is equal to 0V and O1a is equal to 1.8V, then the two transistors (Rs) will become two parallel resistors with equivalent resistance (Req) which will drop the output voltage O1 to 1.7V, as described in Table 5.4.

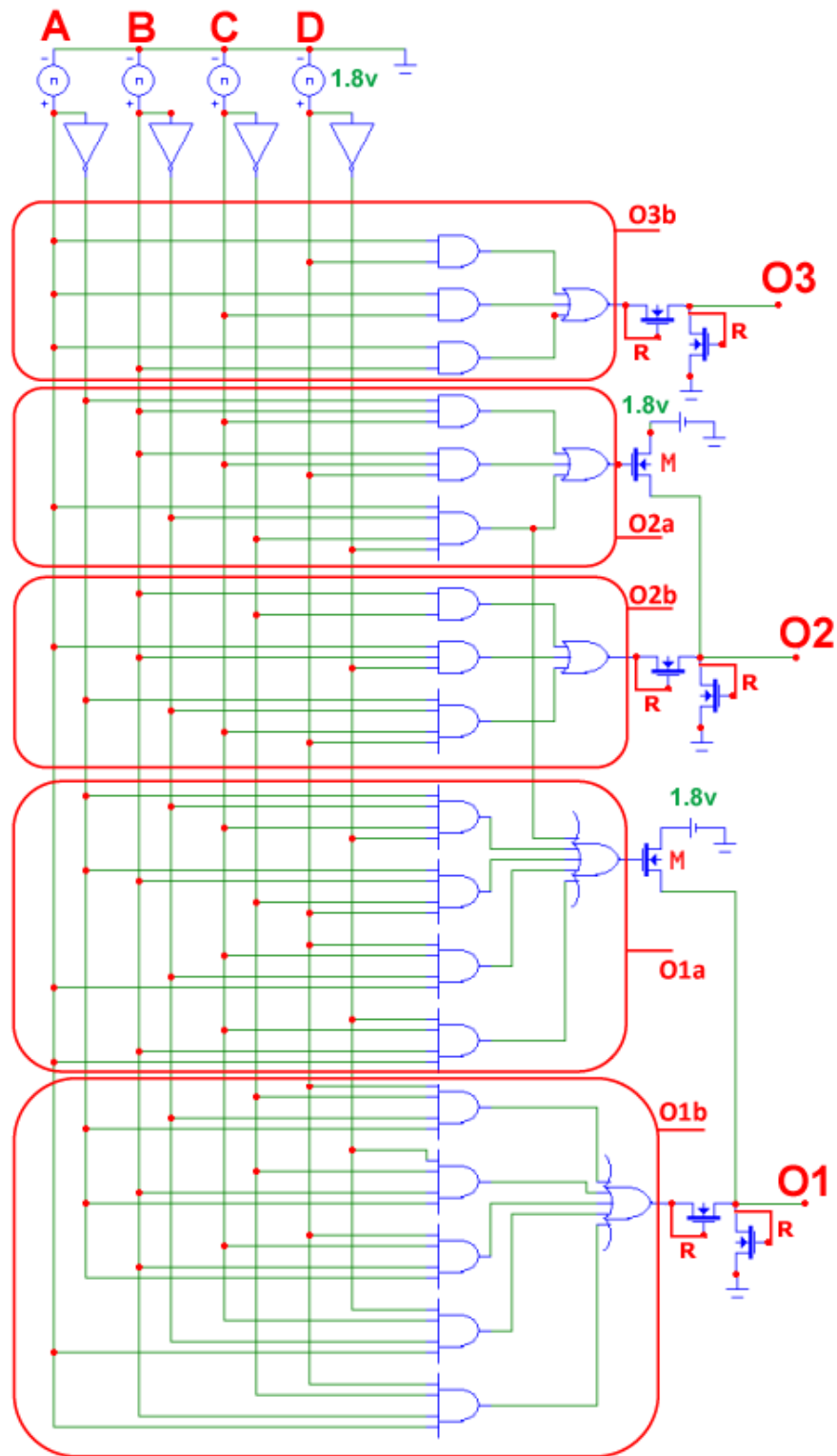


FIGURE 5.3: The Proposed binary-to-ternary Converter Circuit

TABLE 5.4: Combination of Ternary Output O1

O1a	O1b	Transistor (M)	(2 Rs)	O1
0V	0V	OFF	Req	0V (Logic 0)
0V	1.8V	OFF	Divider	0.9V (Logic 1)
1.8V	0V	ON	Req	1.7V (Logic 2)
1.8V	1.8V	<b>This Case Does Not Exist Whereas, in [53] and [54] have errors</b>		

The same procedure will be done for the outputs O2 and O3.

The proposed design has a notable advantage over previous converter designs in [53] and [54] since no error occurs for any input combination. As demonstrated in Tables 5.3 and 5.4, the intermediate binary outputs O<sub>ia</sub>, and O<sub>ib</sub> (i=1, 2) cannot be high at the same time, which offers a significant advantage in simplifying the circuit.

The device count in the proposed circuit is calculated in Table 5.5.

TABLE 5.5: Device count in the proposed circuit (Fig.5.3)

Device Name	No. of devices	No. of Transistors	Subtotal
Inverter Gate	4	1 input *2 =2	8
2 inputs AND Gate	2	2 inputs *2 = 4	8
3 inputs AND Gate	3	3 inputs *2 = 6	18
4 inputs AND Gate	11	4 inputs *2 = 8	88
3 inputs OR Gate	3	3 inputs *2 = 6	18
5 inputs OR Gate	2	5 inputs *2 = 10	20
MOSFET	8	1	8
Internal Resistor (one per each gate)			25
Internal Capacitor (one per each gate)			25
<b>Total No. of Devices</b>			<b>218</b>

## 5.2.1 Simulation Results and Comparisons

In [57], the authors proposed a novel binary-to-ternary converter based on DPL, which gives the best performance than binary-to-ternary converters in [53–56, 64].

Therefore, the proposed converter will be compared to the latest converter circuit designs described in [57].

For fair comparisons, both circuits are implemented, simulated, and analyzed using the same software Micro-Cap V10 PSPICE Simulator with CMOS technology 0.18  $\mu\text{m}$ .

The simulated circuits utilize an implementation of the AND and OR DPL gates as previously described in [28]. At a temperature of 25  $^{\circ}\text{C}$ , average propagation delay (42.56 ps), and average power (4.08  $\mu\text{W}$ ), as stated in [68].

Figure 5.4 shows the transient simulation analysis of the proposed circuit at a temperature of 25  $^{\circ}\text{C}$ , power supply (1.8V), and frequency (0.33 GHz).

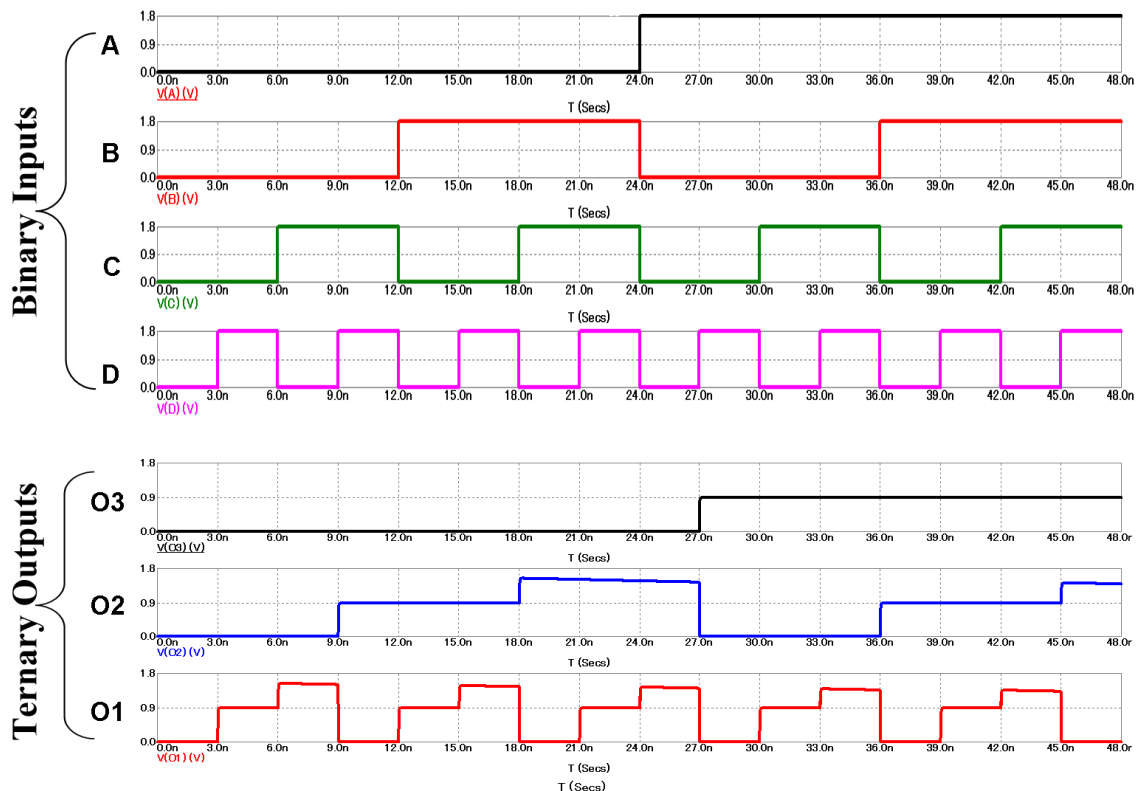


FIGURE 5.4: The simulation transient analysis of the proposed circuit

TABLE 5.6: Comparison to the latest novel converter in [57]

	<b>Converter [57]</b>	<b>Proposed</b>	<b>Improvement</b>
Frequency	0.33 GHz	0.33 GHz	
Device Count	426	218	48.83%
MAX. Delay	0.91 ns	0.09 ns	90.1%
Avg. Power	270.42 $\mu$ w	263.5 $\mu$ w	2.56%
MAX. Energy	246 $10^{-18}$ J	23.7 $10^{-18}$ J	90.36%
Type of used gates	Ternary & binary gates	Binary gates	Faster [69]

The following performance metrics will be used to compare to [57]: the frequency, the device count inside the circuit, the maximum propagation delay, the average power consumption, the maximum energy consumption, and the type of used logic gates.

The propagation delays in the proposed circuit are: From ternary “0” to “1” is 0.07 ns, from “1” to “2” is 0.09 ns and from “2” to “0” is 0.06 ns.

The simulation of the proposed converter shows that the average power consumption is 349.9  $\mu$ w.

Table 5.6 summarizes the comparison to the latest novel converter in [57].

The proposed (4:3) converter is bigger than the latest (3:2) converter in [57]. Despite that, the proposed converter gets better results compared to [57], as shown in Table 5.6.

### 5.3 The Proposed Ternary-to-Binary Converter using CN-FET

This chapter proposes two to three CNFET-Based Ternary-to-Binary converter model, as shown in Fig.5.5.

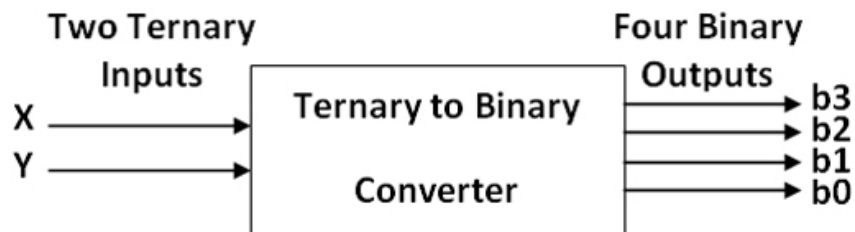


FIGURE 5.5: Ternary-to-Binary model

Figure 5.5 shows two ternary inputs (X, Y): Where the input “X” is the most significant trit (MST), and the input “Y” is the least significant trit (LST). Four binary outputs (b3, b2, b1, b0): Where the output “b3” is the most significant bit (MSB), and “b0” is the least significant bit (LSB). Among the 16 ( $2^4$ ) binary combinations, it will cover the 9 ( $3^2$ ) ternary combinations while the remaining 7 combinations could use for additional features such as error detection.

The “decoder-less” circuit of Fig. 5.6 converts 2-trits to 4-bits via 2-subcircuits.

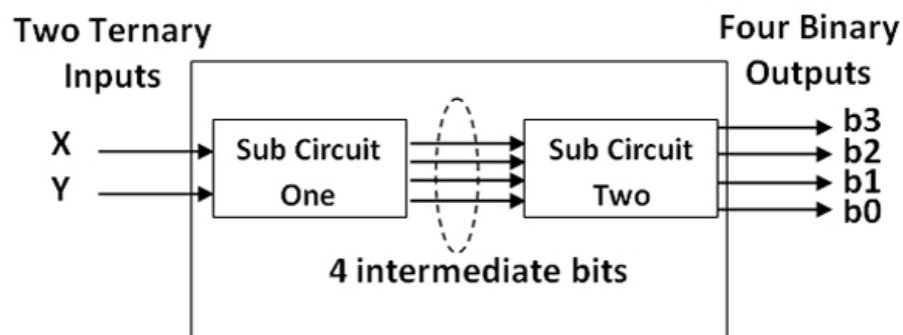


FIGURE 5.6: Ternary-to-Binary model

The novel sub-circuit-one converts 2-trits to 4 intermediate bits while the sub-circuit-two converts the intermediate bits to four final bit outputs, as described in Table 5.7. A novel

technique used: each trit transformed into the corresponding two bits, i.e., ternary logic “0” transformed into two bits ”00”, ternary logic “1” into binary ”02” and ternary logic “2” into ”20”.

TABLE 5.7: Convert 2 trits to 4 intermediate bits then final 4 bits

Ternary Inputs		Intermediate bits				Binary Outputs			
$X$	$Y$	$X_2$	$X_1$	$Y_2$	$Y_1$	<b>b3</b>	<b>b2</b>	<b>b1</b>	<b>b0</b>
0	0	0	0	0	0	0	0	0	0
0	1	0	0	0	2	0	0	0	2
0	2	0	0	2	0	0	0	2	0
1	0	0	2	0	0	0	0	2	2
1	1	0	2	0	2	0	2	0	0
1	2	0	2	2	0	0	2	0	2
2	0	2	0	0	0	0	2	2	0
2	1	2	0	0	2	0	2	2	2
2	2	2	0	2	0	2	0	0	0

### 5.3.1 The Novel Sub-Circuit-One Design

This novel sub-circuit-one made of two similar circuits, each one will convert 1-trit ( $X$ ) to 2-intermediate bits ( $X_1$  and  $X_2$ ), as shown in Fig. 5.7. It is containing a PTI inverter, an NTI inverter, and a key component “black box”, as described in Table 5.8.

The ternary input  $X$  is fed to the inverter (PTI) which has two transistors (T1, T2) to get  $X_p$  as output which is fed to the inverter (NTI) which has two transistors (T3, T4) to get the binary intermediate target  $X_2$ . Also,  $X$  and  $X_p$  are fed to the black box which has 6 transistors (T5-T10) to get the binary intermediate target  $X_1$ , as shown in Fig. 5.7.

Two CNFET-diameters are used in the novel design: D1= 1.487nm which corresponds to the voltage thresholds  $V_{th}=0.289V$  for N-CNFET and  $-0.289V$  for P-CNFET, and D2=0.783 nm which corresponds to  $V_{th}=0.559V$  for N-CNFET and  $-0.559V$  for P-CNFET.

Table 5.8 summarizes all the detailed operations of the sub-circuit-one functionality of Fig. 5.7.

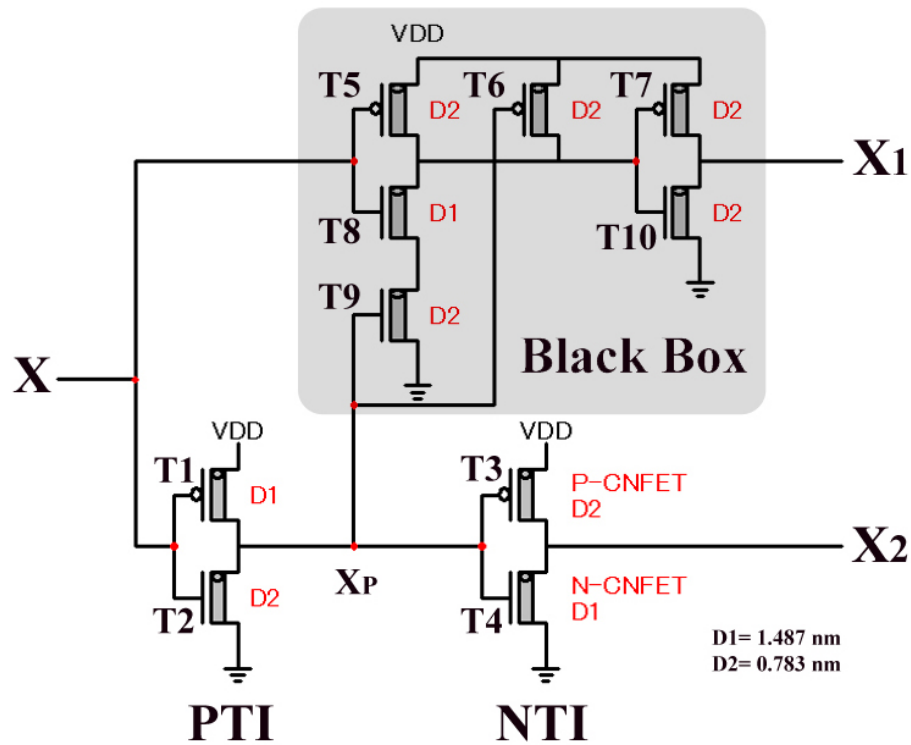


FIGURE 5.7: Novel transistor level for 1-trit input to 2-intermediate bits outputs

TABLE 5.8: The Sub-Circuit-One detailed truth table

$X$	0	1	2
$X_p$	2	2	0
P-CNFET T3 (-0.559V)	OFF	OFF	ON
N-CNFET T4 (0.289V)	ON	ON	OFF
Output $X_2$	0	0	2
P-CNFET T5 (-0.559V)	ON	OFF	OFF
P-CNFET T6 (-0.559V)	OFF	OFF	ON
P-CNFET T7 (-0.559V)	OFF	ON	OFF
N-CNFET T8 (0.289V)	OFF	ON	ON
N-CNFET T9 (0.559V)	ON	ON	OFF
N-CNFET T10 (0.559V)	ON	OFF	ON
Output $X_1$	0	2	0

### 5.3.2 The Sub-Circuit-Two Design

All the 4-bit intermediate output combinations, detailed in Table 5.7, are now processed using the sub-circuit-two of the ternary to binary converter. It will be optimized using a

Karnaugh map to get the following Boolean equations:

$$b_0 = \overline{X_1} Y_1 + X_1 \overline{Y_1} \quad (5.6)$$

$$b_1 = X_2 \overline{Y_2} + \overline{X_2} \overline{X_1} Y_2 + X_1 \overline{Y_2} \overline{Y_1} \quad (5.7)$$

$$b_2 = X_1 Y_1 + X_1 Y_2 + X_2 \overline{Y_2} \quad (5.8)$$

$$b_3 = X_2 Y_2 \quad (5.9)$$

Figure 5.8 shows the complete schematic Ternary-to-Binary circuit based on the previous four equations (5.6) till (5.9). As a result, the Ternary-to-Binary converter has 102 transistors, as detailed in Table 5.9.

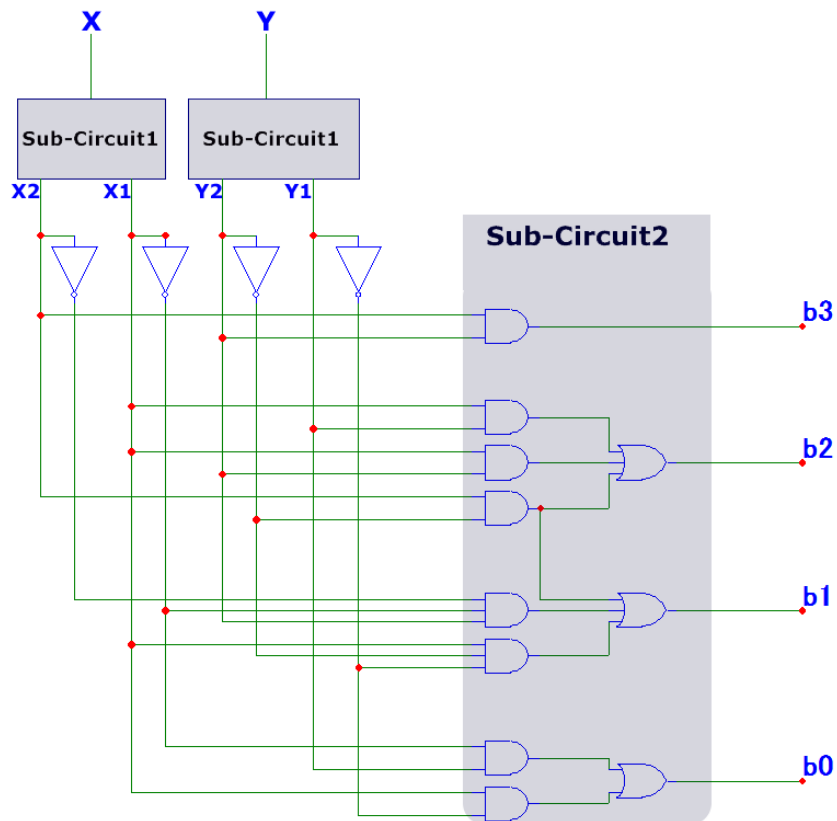


FIGURE 5.8: The proposed schematic Ternary-to-Binary Converter.

Two ternary inputs X and Y are fed to the novel two sub-circuit-one and output the intermediate binary (X2, X1) and (Y2, Y1). After that, the outputs are passed to eight binary “AND” logic gates followed by three binary “OR” logic gates to get the 4 binary outputs (b3, b2, b1, b0), as shown in Fig. 5.8.

TABLE 5.9: Total transistors count in the Ternary-to-Binary converter circuit

	No. of devices	No. Transistors	Subtotal
1-trit to 2 bits circuit	2	10	20
Inverter	4	2	8
2 inputs AND	6	6	36
3 inputs AND	2	8	16
2 inputs OR	1	6	6
3 inputs OR	2	8	16
<b>Total</b>			<b>102</b>

TABLE 5.10: Comparison between the three converter circuits

	CNFETs No.	Power $\mu\text{W}$	Delay ps	PDP $\times 10^{-17} \text{J}$
[58] Using CMOS	127	$8.7 \times 10^6$	8000	$69.6 \times 10^9$
[27] Using CNFET and TDecoder	110	0.425	16.55	0.703
The Proposed converter using CNFET and “Decoder-less”	102	0.143	16.19	0.232

### 5.3.3 Simulation Results and Comparisons

The proposed Ternary-to-Binary converter is simulated and tested using HSPICE simulator with a power supply of 0.9V as Vdd. Fig. 5.9 illustrates the transient analysis of the proposed converter: the X-axis represents the time with a step of 1 ns, and the Y-axis represents the voltage with a step of 0.2 volts.

Table 5.10 shows the comparisons between the CNFET and CMOS converters concerning the number of CNFET, the average power consumption, the maximum propagation delay, and the maximum Power Delay Product (PDP).

The performance of the CNFET-based circuit design is better than the CMOS-based design, as shown in Table 5.10.

The comparison of the proposed Ternary-to-Binary converter demonstrates a notable reduction in Transistors count of around 19.68%, and 72.72% compared to [58] and [27], respectively.

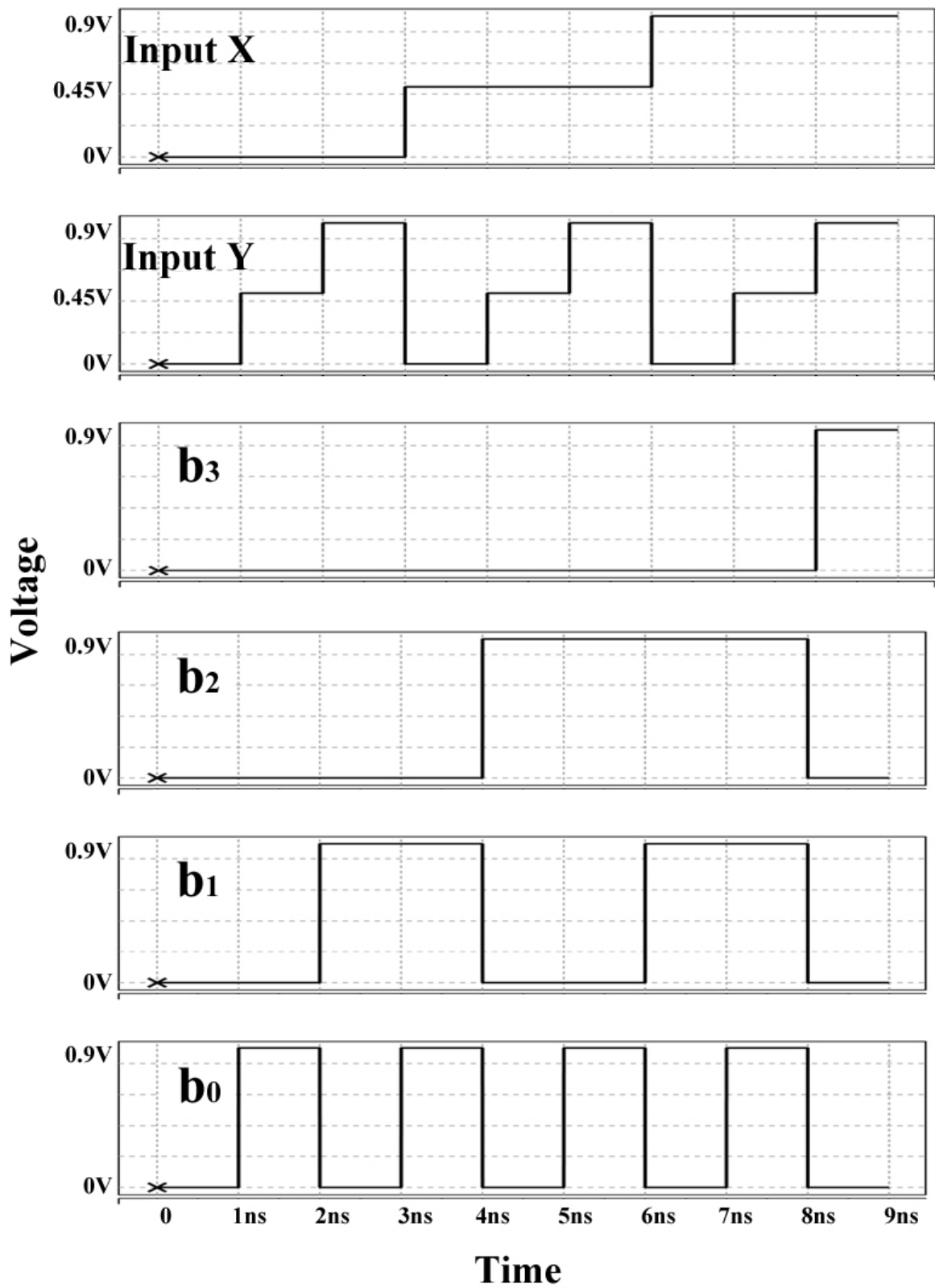


FIGURE 5.9: Transient analysis of the proposed Ternary-to-Binary converter.

Also, a notable reduction in PDP of around 99.99%, and 66.99% compared to [58] and [27], respectively.

## 5.4 Conclusion

This chapter proposed a bi-directional circuit that contains two converters. A binary-to-ternary converter and ternary-to-binary converter.

The first part proposed a binary-to-ternary converter with novel techniques that takes four bits and produces three trits using Double Pass-Transistor Logic (DPL).

The proposed binary-to-ternary converter is designed and simulated using Micro-Cap V10 PSPICE simulator. Finally, logical analysis and simulation results demonstrate the merits of the approach in terms of reduced latency and energy consumption compared to other converters.

The second part has proposed a novel ternary-to-binary converter "decoder-less" using CN-FET that takes two trits as input and provides four bits as output.

The proposed ternary-to-binary converter is then simulated and tested by the HSPICE simulator. Logical analysis and simulation results prove the merits of the implementation compared to the existing designs in terms of transistor count, reduced latency, and energy efficiency.

# Chapter 6

## Conclusion and Perspectives

### 6.1 Conclusion

This thesis proposes new designs include eight ternary logic gates, three ternary combinational circuits, and six Ternary Arithmetic Logic Units (TALU). The ternary logic gates are seven unary operators of the ternary system ( $A^1$ ,  $A^2$ ,  $\bar{A}^2$ ,  $A_1$ ,  $1.\bar{A}_n$ ,  $1.\bar{A}_p$ , and the Standard Ternary Inverter (STI)  $\bar{A}$ ), and Ternary NAND based on Carbon Nanotube Field-Effect Transistor (CNFET). Ternary combinational circuits, two different designs for Ternary Decoders (TDecoder) and Ternary Multiplexer (TMUX). TDecoder1 using CNFET-based proposed unary operators and TDecoder2 using Double-Pass Logic (DPL) binary gates. TMUX using CNFET-based proposed unary operators. And Ternary Arithmetic Logic Units are three different designs for Ternary Half-Adders (THA) and Ternary Multipliers (TMUL): (1) The first design uses the proposed TDecoder1, STI, and TNAND. (2) While the second design uses the cascading proposed TMUX. (3) As for the third design, it uses the proposed unary operators and TMUX.

All proposed circuits aim to optimize the trade-off between high-performance and energy-efficiency in order to implement them in low-power portable electronics and embedded systems to preserve battery consumption.

The design process tried to optimize several circuit techniques such as reducing the number

of the used transistors, utilizing energy-efficient transistor arrangements, and applying the dual supply voltages ( $V_{dd}$  and  $V_{dd}/2$ ) to achieve its aim.

The proposed ternary circuits are then compared to the latest ternary circuits, simulated and tested using HSPICE simulator under various operating conditions at different supply voltages, different temperatures, and different frequencies.

The results prove the merits of the approach in terms of reduced energy consumption (PDP) compared to other existing designs.

Moreover, the noise immunity curve (NIC) and Monte Carlo analysis for major process variations (TOX, CNT Diameter, CNT's Count, and Channel length) were studied. The results confirmed that the proposed THA had higher robustness and higher noise tolerance, among other designs.

In addition, the second aim is using ternary data transmission to improve data communications between hosts. Also, this thesis proposes a bi-directional circuit that contains two converters: (1) a binary-to-ternary converter and (2) a ternary-to-binary converter.

The proposed binary-to-ternary converter with novel techniques takes four bits as inputs and produces three trits as outputs using Double Pass-Transistor (DPL). The proposed circuit is then simulated and tested using the Micro-Cap V10 PSPICE simulator.

While the proposed ternary-to-binary converter "decoder-less" using CNFET takes two trits as inputs and provide four bits as outputs. The proposed circuit is then simulated and tested using the HSPICE simulator.

Finally, logical analysis and simulation results prove the merits of the approaches compared to existing designs in terms of transistor count, reduced latency, and energy efficiency.

## 6.2 Perspectives

Our methodology can be used to design Ternary Sequential Circuits like:

1. Ternary Flip Flops
2. Ternary Memory
3. Ternary CPU

Moreover, Application to different Engineering areas, as follow:

1. Biomedical & healthcare like:
  - ElectroCardioGram (ECG)
  - ElectroEncephaloGram (EEG)
  - Implantable Medical Devices (IMD)
  - Magnetic Resonance Imaging (MRI)
  - Sensors
2. Mechanical Engineering like:
  - Computer box or Electronic Control Unit (ECU)
  - Cloud Vehicular Networks (CVN)
  - Electronic Fuel Injection (EFI)
3. Almost in all digital and control circuits

## **Appendix A**

# **High-Performance and Energy-Efficient CNFET-Based Designs for Ternary Logic Circuits**

Received May 14, 2019, accepted July 2, 2019, date of publication July 11, 2019, date of current version July 30, 2019.

Digital Object Identifier 10.1109/ACCESS.2019.2928251

# High-Performance and Energy-Efficient CNFET-Based Designs for Ternary Logic Circuits

RAMZI A. JABER<sup>1</sup>, (Student Member, IEEE), ABDALLAH KASSEM<sup>2</sup>, (Senior Member, IEEE), AHMAD M. EL-HAJJ<sup>1</sup>, (Member, IEEE), LINA A. EL-NIMRI<sup>3</sup>, AND ALI MASSOUD HAIDAR<sup>1</sup>

<sup>1</sup>Department of Computer and Electrical Engineering, Beirut Arab University, Beirut 11072809, Lebanon

<sup>2</sup>Department of Electrical and Computer Engineering, Notre Dame University-Louaize, Zouk Mikael, Lebanon

<sup>3</sup>Department of Business Computer, Lebanese University, Beirut, Lebanon

Corresponding author: Ramzi A. Jaber (r.jaber@bau.edu.lb)

**ABSTRACT** Recently, the demand for portable electronics and embedded systems has increased. These devices need low-power circuit designs because they depend on batteries as an energy resource. Moreover, multi-valued logic (MVL) circuits provide notable improvements over binary circuits in terms of interconnect complexity, chip area, propagation delay, and energy consumption. Therefore, this paper proposes new ternary circuits aiming to lower the power delay product (PDP) to save battery consumption. The proposed designs include new ternary gates [standard ternary inverter (STI) and ternary nand (TNAND)] and combinational circuits [ternary decoder (TDecoder), ternary half-adder (THA), and ternary multiplier (TMUL)] using carbon nano-tube field-effect transistors (CNFETs). This paper employs the best trade-off between reducing the number of used transistors, utilizing energy-efficient transistor arrangement such as transmission gate, and applying the dual supply voltages ( $V_{dd}$  and  $V_{dd}/2$ ). The five proposed designs are compared with the latest 15 ternary circuits using the HSPICE simulator for different supply voltages, different temperatures, and different frequencies; 180 simulations are performed to prove the efficiency of the proposed designs. The results show the advantage of the proposed designs in reduction over 43% in terms of transistors' count for the ternary decoder and over 88%, 99%, 98%, 86%, and 78% in energy consumption (PDP) for the STI, TNAND, TDecoder, THA, and TMUL, respectively.

**INDEX TERMS** Carbon nano-tube field effect transistors (CNFET), ternary combinational circuits, ternary logic gates, multi-valued logic (MVL), power delay product.

## I. INTRODUCTION

The limitation in the binary circuit is due to a large number of connections thus requiring a big chip area and a notable increase in energy consumption. Whereas, Multi-Valued Logic (MVL) system has more than two-valued logic to lower interconnections, chip area of up to 70% [1], and energy consumption by more than 50% [2]. Moreover, the authors of [3] has proved mathematically that ternary logic is the most efficient in circuit complexity and cost compared to other bases. Ternary logic systems can be represented in two ways: balanced ternary logic  $(-1, 0, 1)$  corresponding to

$(-V_{dd}, 0, V_{dd})$ , and standard (unbalanced) ternary logic  $(0, 1, 2)$  corresponding to  $(0, V_{dd}/2, V_{dd})$ .

For the past decade, MVL has attracted researchers' attention over binary logic. MVL can be implemented in software (algorithm) and circuit design such as logic gates, combinational circuits, memory circuits, programmable logic arrays (PLAs), MV-Quantum Logic, and wireless sensor networks [4]–[10].

Different transistor technologies have been used such as CMOS [11], FinFet [12], and CNFET [13]–[18]. Among the mentioned techniques, CNFET provides the best trade-off in terms of energy efficiency and circuit speed [19].

Therefore, this paper uses CNFET technology in the design of the ternary circuits. The proposed designs will compare to the latest CNFET-based designs in [13]–[18], which are

The associate editor coordinating the review of this manuscript and approving it for publication was Bora Onat.

known to provide efficient circuit designs in terms of transistor count, power and PDP. In particular, [13] presents the *STI*, *TNAND*, *TNOR*, *TDecoder*, *THA*, and *TMUL* using CNFET. In [14] and [17], a ternary decoder design described in replacing the *TNOR* with a binary *NOR*. In [15], [16], [18], improved circuit designs for the *STI*, *TNAND*, *THA*, and *TMUL*, are presented.

This paper proposes new designs for the *STI*, *TNAND*, *TDecoder*, *THA*, and *TMUL* by reducing the number of used transistors, utilizing energy-efficient transistor arrangement such as transmission gate and applying the dual supply voltages  $V_{dd}$  (0.9 V), and  $V_{dd}/2$  (0.45 V) from the same power supply [18].

The new designs provide a considerable gain in terms of system performance which they have the lowest PDP compared to the designs in [13]–[18] as demonstrated in the HSPICE-based simulation results. Therefore, the proposed circuits can be implemented in low-power portable electronics and embedded systems to save battery consumption.

The rest of the paper is organized as follows: Section II provides a background of CNFETs and existing ternary logic gates, while the proposed new ternary logic gates are described in section III, and the proposed combinational circuits in section IV. Simulation results and comparisons are discussed in section V followed by the Conclusion.

## II. BACKGROUND

### A. CNFET DESIGN

Full details about the Stanford CNFET model found at [20]–[22], but it is worth mentioning that the CNFETs use a semiconducting single-walled CNT as a channel for conduction with high drive current  $35 \mu A$  when the supply voltage  $V_{dd}$  is equal to 0.9 V. The improvement of intrinsic CNFET over bulk MOSFET device is about 13 times better. The angle of atom arrangement along the tube in a single-walled CNT (SWCNT) is chirality vector which is represented by the integer pair  $(n, m)$ . This chirality vector determines if the CNT is metallic or semiconducting; if  $n = m$  or  $n - m = 3j$ , where  $j$  is an integer, then the nanotube is metallic else it is semiconducting. The CNFET diameter can be calculated from the equation in (1):

$$D_{cnt} = \frac{\sqrt{3} \cdot a_0}{\pi} \sqrt{n^2 + m^2 + nm} \quad (1)$$

where  $a_0 = 0.142 \text{ nm}$  is the inter-atomic distance between each carbon atom and its neighbor, and the integer pair  $(n, m)$  represents the chirality vector. The characteristics of the CNFET model are similar to traditional MOSFETs. Except for the threshold voltage which is calculated by the following equation (2):

$$V_{th} = \frac{E_g}{2 \cdot e} = \frac{\sqrt{3}}{3} \frac{a \cdot V\pi}{e \cdot D_{cnt}} \quad (2)$$

where  $a = 2.49 \text{ \AA}$  is the carbon to carbon atom distance,  $V\pi = 3.033 \text{ eV}$  is the carbon bond energy in the tight binding

**TABLE 1.** The relation between the chirality, diameter, and threshold voltage.

Chirality	CNT diameter	Threshold voltage	
		N-CNFET	P-CNFET
(19,0)	1.487nm	0.289V	- 0.289V
(13,0)	1.018nm	0.428V	- 0.428V
(10,0)	0.783nm	0.559V	- 0.559V

**TABLE 2.** The truth table for the three ternary inverters.

Ternary Input	STI	NTI	PTI
Logic 0 (0 V)	2	2	2
Logic 1 (0.45 V)	1	0	2
Logic 2 (0.9 V)	0	0	0

**TABLE 3.** The truth table for Two-inputs *TNAND* and *TNOR* logic gates.

Input		Output	
A	B	TNAND	TNOR
0	0	2	2
0	1	2	1
0	2	2	0
1	0	2	1
1	1	1	1
1	2	1	0
2	0	2	0
2	1	1	0
2	2	0	0

model,  $e$  is the electron charge unit, and  $D_{cnt}$  is the CNT diameter.

In general, three chiralities can be used in the ternary logic design. Table 1 shows the relationship between the chirality, diameter, and threshold voltage.

### B. EXISTING TERNARY LOGIC GATES

The basic ternary logic gates are *NOT*, *AND*, *OR*, *NAND* and *NOR*.  $A_i$  and  $B_j$  are the ternary inputs where  $i$  and  $j \in \{0, 1, 2\}$ . The ternary equations of the basic ternary logic gates are presented in (3):

$$\begin{aligned} NOT: \quad \overline{A_i} &= 2 - A_i, \\ AND: \quad A_i \cdot B_j &= \min\{A_i, B_j\}, \\ OR: \quad A_i + B_j &= \max\{A_i, B_j\}, \\ NAND: \quad \overline{A_i \cdot B_j} &= \min\{A_i, B_j\}, \\ NOR: \quad \overline{A_i + B_j} &= \max\{A_i, B_j\}, \end{aligned} \quad (3)$$

In [13], the authors present three types of ternary inverters, *TNAND*, and *TNOR* logic gate using CNFET.

**TABLE 4.** The disadvantage of existing logic gates in [13], [16], and [18] and the advantage of proposed logic gates.

Disadvantage	Advantage
Shown in Fig. 15 and 16 in the appendix The existing designs suffer from High power consumption due to:	Shown in Fig. 1 and 2 The proposed designs provide Low power consumption due to:
1- Two transistors that act as resistors in <i>STI</i> (T2, T3) and in <i>TNAND</i> (T5, T6) [13].	Eliminating these two transistors by applying dual supply voltages (V <sub>dd</sub> and V <sub>dd</sub> /2).
2- Two transistors that act as resistors in <i>STI</i> (T3, T6) and in <i>TNAND</i> (T5, T10) [16].	
3- Two transistors that are always active in <i>STI</i> (T2, T3) and in <i>TNAND</i> (T5, T6) [18].	
4- For <i>STI</i> [13], [18]: Four transistors (T1, T2, T3, T4) in series must be active to get logic 1.	For the proposed <i>STI</i> : Only one transistor (T3) must be active to get logic 1.
5- For <i>STI</i> [16]: Four transistors (T1, T3, T6, T5) in series must be active to get logic 1.	
6- For <i>TNAND</i> [13], [18]: Five or Six transistors [(T1 or T2) or both, T5, T6, T7, T8]) in series must be active to get logic 1.	For the proposed <i>TNAND</i> : Two transistors (T5, T6) in series must be active to get logic 1.
7- For <i>TNAND</i> [16]: Five or Six transistors [(T1 or T2) or both, T5, T10, T8, T9]) in series must be active to get logic 1.	

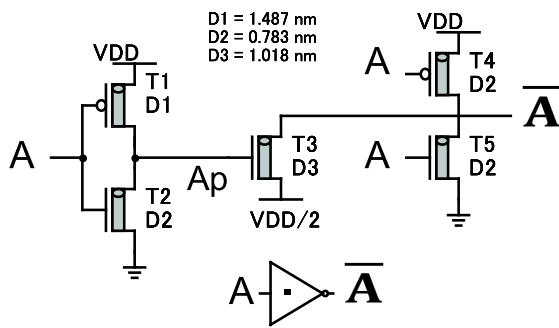
The first inverter is a standard ternary inverter (*STI*), the second is a negative ternary inverter (*NTI*), and the third one is a positive ternary inverter (*PTI*). Table 2 shows the truth table for the three ternary inverters.

Table 3 shows the truth table for Two-inputs *TNAND* and *TNOR* logic gates.

**III. PROPOSED TERNARY LOGIC GATES**

The existing *STI* and *TNAND* logic gates designs in [13], [16], and [18] are shown in Fig. 15 and 16 in the appendix.

This section proposes new designs of *STI* and *TNAND* logic gates as shown in Fig. 1 and Fig. 2.



**FIGURE 1.** Transistor level of the proposed *STI*.

Table 4 shows the disadvantage of the existing *STI* and *TNAND* in [13], [16], and [18] and the advantage of the proposed ternary logic gates.

**A. PROPOSED STANDARD TERNARY INVERTER**

Fig. 1 shows the transistor level design of the proposed *STI* where the chirality, diameter, and threshold voltage (V<sub>th</sub>) of the CNFETs used are shown in Table 5.

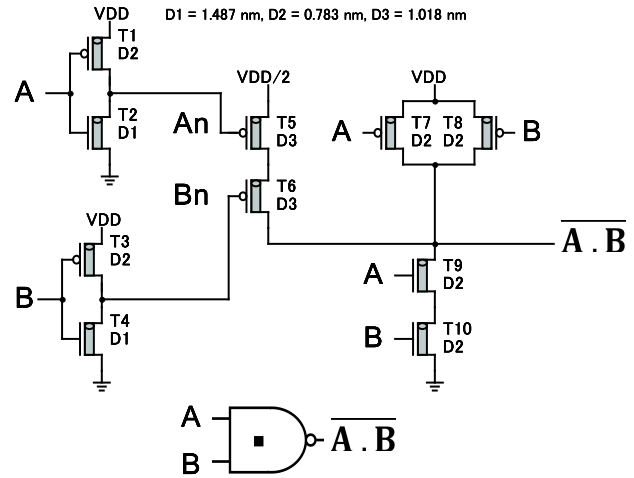


**FIGURE 2.** Transistor level of the proposed *TNAND*.

**TABLE 5.** The chirality, diameter, and threshold voltage of the CNTs used in the proposed *STI*.

CNFET Type	Chirality	Diameter	V <sub>th</sub>
P-CNFET (T4)	(10, 0)	0.783nm	- 0.559V
P-CNFET (T1)	(19, 0)	1.487nm	- 0.289V
N-CNFET (T2,T5)	(10, 0)	0.783nm	0.559V
N-CNFET (T3)	(13, 0)	1.018nm	0.428V

Table 6 shows the detailed operation of the proposed *STI* circuit of Fig. 1.

When the input A is logic 0, then transistors (T1, and T4) are turned ON and (T2, and T5) are turned OFF. The output A<sub>p</sub> is equal to logic 2, then transistor (T3) is turned ON. Therefore, the output A-bar is equal to logic 2.

**TABLE 6.** The detailed operation of *STI* of Fig. 1.

Ternary Input <i>A</i>	0 (0 V)	1 (0.45 V)	2 (0.9 V)
P-CNFET T1	ON	ON	OFF
N-CNFET T2	OFF	OFF	ON
<i>A<sub>p</sub></i>	2	2	0
N-CNFET T3	ON	ON	OFF
P-CNFET T4	ON	OFF	OFF
N-CNFET T5	OFF	OFF	ON
<b>Output <math>\bar{A}</math></b>	<b>2</b>	<b>1</b>	<b>0</b>

When the input *A* is logic 1, then transistor (T1) is turned ON, and (T2, T4, and T5) are turned OFF. The output *A<sub>p</sub>* is equal to logic 2, then transistor (T3) is turned ON. Therefore, the output  $\bar{A}$  is equal to logic 1.

Finally, when the input *A* is logic 2, then transistors (T2, and T5) are turned ON and (T1, and T4) are turned OFF. The output *A<sub>p</sub>* is equal to logic 0, then transistor (T3) is turned OFF. Therefore, the output  $\bar{A}$  is equal to logic 0.

**B. PROPOSED TERNARY NAND**

Fig. 2 shows the transistor level design of the proposed two inputs *TNAND* where the chirality, diameter, and threshold voltage (*V<sub>th</sub>*) of the CNFETs used are shown in Table 7.

**TABLE 7.** The chirality, diameter, and threshold voltage of the CNTs used in the proposed *TNAND*.

CNFET Type	Chirality	Diameter	<i>V<sub>th</sub></i>
P-CNFET (T1,T3,T7,T8)	(10, 0)	0.783nm	- 0.559V
P-CNFET (T5, T6)	(13, 0)	1.018nm	- 0.428V
N-CNFET (T9, T10)	(10, 0)	0.783nm	0.559V
N-CNFET (T2, T4)	(19, 0)	1.487nm	0.289V

Table 8 shows the selected combinations of two ternary inputs *A* and *B* to describe the operation of the proposed *TNAND* logic gate circuit of Fig. 2.

When the inputs (*A, B*) are (0 V, 0 V), then transistors (T1, T3, T7, and T8) are turned ON and (T2, T4, T9, and T10) are turned OFF. The outputs (*A<sub>n</sub>, B<sub>n</sub>*) are equal to (0.9 V, 0.9 V), then transistors (T5, and T6) are turned OFF. Therefore, the output is equal to 0.9 V.

When the inputs (*A, B*) are (0 V, 0.45 V), then transistors (T1, T4, and T7) are turned ON and (T2, T3, T8, T9, and T10) are turned OFF. The outputs (*A<sub>n</sub>, B<sub>n</sub>*) are equal to (0.9 V, 0 V), then transistor (T6) is turned ON and (T5) is turned OFF. Therefore, the output is equal to 0.9 V.

When the inputs (*A, B*) are (0.45 V, 0.45 V), then transistors (T2, and T4) are turned ON and (T1, T3, T7, T8, T9, and T10) are turned OFF. The outputs (*A<sub>n</sub>, B<sub>n</sub>*) are equal to (0 V, 0 V), then transistors (T5, and T6) are turned ON. Therefore, the output is equal to 0.45 V.

**TABLE 8.** The detailed operation of *TNAND* with selected inputs of Fig. 2.

Ternary Inputs ( <i>A, B</i> )	(0, 0)	(0, 1)	(1, 1)	(1, 2)
P-CNFET T1	ON	ON	OFF	OFF
N-CNFET T2	OFF	OFF	ON	ON
<i>A<sub>n</sub></i>	2	2	0	0
P-CNFET T3	ON	OFF	OFF	OFF
N-CNFET T4	OFF	ON	ON	ON
<i>B<sub>n</sub></i>	2	0	0	0
P-CNFET T5	OFF	OFF	ON	ON
P-CNFET T6	OFF	ON	ON	ON
P-CNFET T7	ON	ON	OFF	OFF
P-CNFET T8	ON	OFF	OFF	OFF
N-CNFET T9	OFF	OFF	OFF	OFF
N-CNFET T10	OFF	OFF	OFF	ON
<b>Output <i>TNAND</i></b>	<b>2</b>	<b>2</b>	<b>1</b>	<b>1</b>

Finally, when the inputs (*A, B*) are (0.45 V, 0.9 V), then transistors (T2, T4, and T10) are turned ON and (T1, T3, T7, T8, and T9) are turned OFF. The outputs (*A<sub>n</sub>, B<sub>n</sub>*) are equal to (0 V, 0 V), then transistors (T5, and T6) are turned ON. Therefore, the output is equal to 0.45 V.

**IV. PROPOSED COMBINATIONAL CIRCUITS**

This section proposes some of the combinational circuits such as *TDecoder*, *THA*, and *TMUL*.

**A. PROPOSED TERNARY DECODER**

The ternary decoder converts *n* trits information inputs to a maximum 3<sup>*n*</sup> unique outputs. It is used in many applications such as the ternary adder, ternary multiplier, ternary memory, and others.

Ternary decoder with one ternary input (*X*), and three binary outputs (*X<sub>0</sub>, X<sub>1</sub>, X<sub>2</sub>*) are described mathematically in equation (4) and its truth table is shown in Table 10.

$$X_{k,k \in \{0,1,2\}} = \begin{cases} 2, & \text{if } x = k \\ 0, & \text{if } x \neq k \end{cases} \quad (4)$$

The existing *TDecoders* in [13], [14], and [17] are shown in Fig. 17 in the appendix with 16, 10, and 11 transistors respectively.

This section proposes a new design of *TDecoder* with 9 transistors through replacing the *TNOR* and the second *NTI* with a novel sub-circuit and a binary inverter respectively as represented in Fig. 3.

Fig. 3 shows the transistor level design of the proposed *TDecoder*. It consists of one negative ternary inverter (NTI), one positive ternary inverter (PTI), one binary inverter, and a novel sub-circuit.

Table 9 shows the disadvantage of the existing *TDecoder* in [13], [14], and [17] and the advantage of the proposed *TDecoder*.

**TABLE 9.** The disadvantage of existing *TDecoder* in [13], [14], and [17] and the advantage of proposed *TDecoder*.

Disadvantage	Advantage
Shown in in Fig. 17 in the appendix The existing design suffers from High power consumption due to:	Shown in Fig. 3 The proposed design provides Low power consumption due to:
1- The Transistors' count of [13], [14], [17] equal to 16, 10, 11 respectively.	Transistors' count = 9.
2- To get $X_1$ , [13] uses the Ternary <i>NOR</i> (10 transistors).	To get $X_1$ , the design uses the novel sub-circuit (3 transistors) including the Transmission Gate (T7, T8) which provides low power consumption and propagation delay.
3- To get $X_1$ , [14], [17] use the Binary <i>NOR</i> (4 transistors).	
4- Six transistors (T11, T12, T13, T14, T15, T16) must be active to get $X_1$ equals to logic 2 [13].	Only the Transmission Gate (T7, T8) must be active to get logic $X_1$ equals to logic 2.
5- Two transistors (T9, T10) in series must be active to get logic $X_1$ equals to logic 2 [14], [17].	

**TABLE 10.** Ternary decoder truth table.

Input X	Outputs		
	$X_2$	$X_1$	$X_0$
0	0	0	2
1	0	2	0
2	2	0	0

**TABLE 11.** The chirality, diameter, and threshold voltage of the CNTs used in the proposed *TDecoder*.

CNFET Type	Chirality	Diameter	Vth
P-CNFET (T1, T5)	(10, 0)	0.783nm	- 0.559V
P-CNFET (T3, T8)	(19, 0)	1.487nm	- 0.289V
N-CNFET (T4, T6, T9)	(10, 0)	0.783nm	0.559V
N-CNFET (T2, T7)	(19, 0)	1.487nm	0.289V

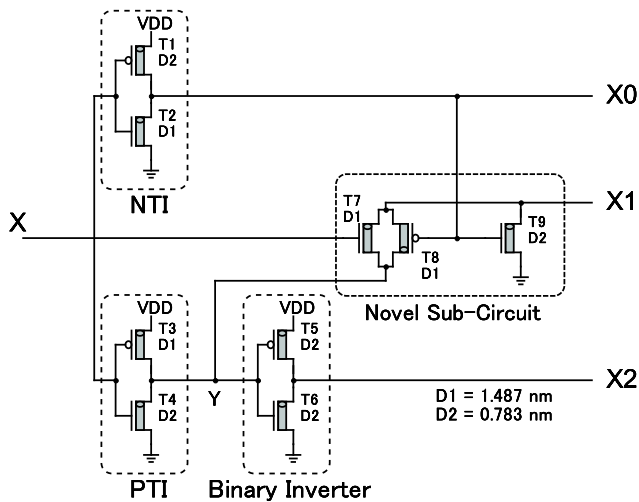


**FIGURE 3.** Transistor level of the proposed *TDecoder* with 9 CNFETs.

**TABLE 12.** The detailed operation of the proposed *TDecoder* of Fig. 3.

Ternary Input X	0 (0 V)	1 (0.45 V)	2 (0.9 V)
P-CNFET T1	ON	OFF	OFF
N-CNFET T2	OFF	ON	ON
<b>Output <math>X_0</math></b>	<b>2</b>	<b>0</b>	<b>0</b>
P-CNFET T3	ON	ON	OFF
N-CNFET T4	OFF	OFF	ON
<b>Intermediate Y</b>	<b>2</b>	<b>2</b>	<b>0</b>
P-CNFET T5	OFF	OFF	ON
N-CNFET T6	ON	ON	OFF
<b>Output <math>X_2</math></b>	<b>0</b>	<b>0</b>	<b>2</b>
N-CNFET T7	OFF	ON	ON
P-CNFET T8	OFF	ON	ON
N-CNFET T9	ON	OFF	OFF
<b>Output <math>X_1</math></b>	<b>0</b>	<b>Y=2</b>	<b>Y=0</b>

The chirality, diameter, and threshold voltage ( $V_{th}$ ) of the CNFETs used are shown in Table 11, and the detailed operation of the proposed circuit described in Table 12.

When the input  $X$  is logic 0, then transistors (T1, and T3) are turned ON and (T2, T4, and T7) are turned OFF. The output  $X_0$  and the intermediate  $Y$  are equal to logic 2. Then (T5, and T8) are turned OFF and (T6, and T9) are turned ON. Therefore, the outputs  $X_1$  and  $X_2$  are equal to logic 0.

When the input  $X$  is logic 1, then transistors (T2, T3, and T7) are turned ON and (T1, and T4) are turned OFF.

The output  $X_0$  is equal to logic 0, and the intermediate  $Y$  is equal to logic 2. Then (T5, and T9) are turned OFF and (T6, and T8) are turned ON. Therefore, the output  $X_1$  is equal to the value of  $Y$  which is logic 2 and the output  $X_2$  is equal to logic 0.

Finally, when the input  $X$  is logic 2, then transistors (T2, T4, and T7) are turned ON and (T1, and T3) are turned OFF. The output  $X_0$  and the intermediate  $Y$  are equal to logic 0. Then (T6, and T9) are turned OFF and (T5, and T8)

TABLE 13. Karnaugh Map of *THA*.

Sum			
<i>A/B</i>	$B_0(0)$	$B_1(1)$	$B_2(2)$
$A_0(0)$	0	1	2
$A_1(1)$	1	2	0
$A_2(2)$	2	0	1

Carry			
<i>A/B</i>	$B_0(0)$	$B_1(1)$	$B_2(2)$
$A_0(0)$	0	0	0
$A_1(1)$	0	0	1
$A_2(2)$	0	1	1

are turned ON. Therefore, the output  $X_1$  is equal to the value of  $Y$  which is logic 0, and the output  $X_2$  is equal to logic 2.

**B. PROPOSED TERNARY HALF ADDER**

Ternary half adder (*THA*) is able to add two ternary inputs and provides two outputs: the Sum and the Carry. Table 13 shows the Karnaugh map of *THA*. The equations of sum and carry derived from Table 13 are (5) and (6) as follow:

$$Sum = 2 \cdot (A_0B_2 + A_1B_1 + A_2B_0) + 1 \cdot (A_0B_1 + A_1B_0 + A_2B_2) \quad (5)$$

$$Carry = 1 \cdot (A_1B_2 + A_2B_1 + A_2B_2) \quad (6)$$

where  $A_k$  and  $B_k$ , are the outputs of the *TDecoder* from inputs A and B respectively.

The existing *THA* in [13], [15], and [16] are shown in Fig. 18 in the appendix with 136, 112, and 112 transistors respectively.

This section proposes a new design of *THA* with 85 transistors using De Morgan’s Law and dual power supply (Vdd and Vdd/2) to eliminate the encoder level shifter in [13], [15]. Also, it uses the proposed *TDecoder* of Fig. 3, the proposed *STI* of Fig. 1 and the proposed *TNAND* of Fig. 2, and removes one common *NAND* as illustrate in Fig. 4.

Fig. 4 shows the proposed *THA*. It consists of two proposed *TDecoders*, eight 2-inputs binary *NAND*, three 3-inputs binary *NAND*, one binary inverter, one proposed *TNAND*, and one proposed *STI*.

Table 14 shows the total transistors’ count of the proposed *THA*.

The operation of the proposed *THA*: Two ternary inputs A and B fed to the proposed *TDecoder* and produce outputs as ( $A_2, A_1, A_0$ ) and ( $B_2, B_1, B_0$ ). These outputs will drive the eight 2-inputs binary *NAND*, the three 3-inputs binary *NAND* logic gates, the proposed *STI*, binary inverter, and the proposed *TNAND* to get the Sum and the Carry as final outputs.

**C. PROPOSED TERNARY MULTIPLIER**

Ternary multiplier (*TMUL*) is able to multiply two ternary inputs and provides two outputs: the Product and the Carry. Table 15 shows the Karnaugh map of *TMUL*. The equations

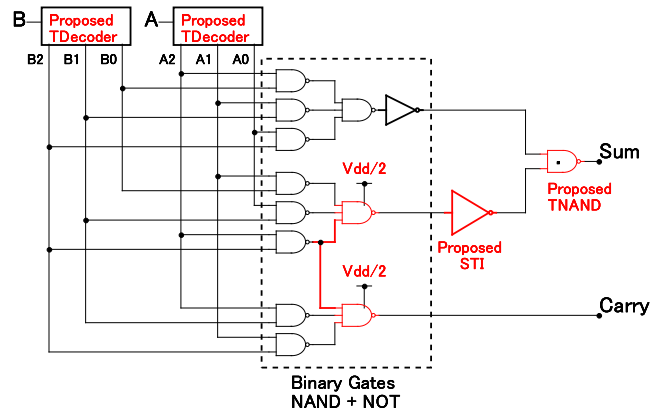


FIGURE 4. Proposed *THA* with 85 transistors.

TABLE 14. Total transistors’ count of the proposed *THA*.

	No. of Devices	No. of Transistors	Subtotal*
Proposed <i>TDecoder</i>	2	9	18
Binary 2- <i>NAND</i>	8	4	32
Binary 3- <i>NAND</i>	3	6	18
Binary Inverter	1	2	2
Proposed <i>STI</i>	1	5	5
Proposed <i>TNAND</i>	1	10	10
Total			85

\*Subtotal = No. of Devices x No. of Transistors

TABLE 15. Karnaugh Map of *TMUL*.

Product			
<i>A/B</i>	$B_0(0)$	$B_1(1)$	$B_2(2)$
$A_0(0)$	0	0	0
$A_1(1)$	0	1	2
$A_2(2)$	0	2	1

Carry			
<i>A/B</i>	$B_0(0)$	$B_1(1)$	$B_2(2)$
$A_0(0)$	0	0	0
$A_1(1)$	0	0	0
$A_2(2)$	0	0	1

of Product and Carry derived from Table 15 are (7) and (8) as follow:

$$Product = 2 \cdot (A_1B_2 + A_2B_1) + 1 \cdot (A_1B_1 + A_2B_2) \quad (7)$$

$$Carry = 1 \cdot A_2B_2 \quad (8)$$

where  $A_k$  and  $B_k$ , are the outputs of the *TDecoder* from inputs A and B respectively.

The existing *TMUL* in [13], [15], and [16] are shown in Fig. 19 in the appendix with 100, 86, and 76 transistors respectively.

This section proposes a new design of *TMUL* with 61 transistors using De Morgan’s Law and the dual power supply (Vdd and Vdd/2) to eliminate the encoder level shifter in

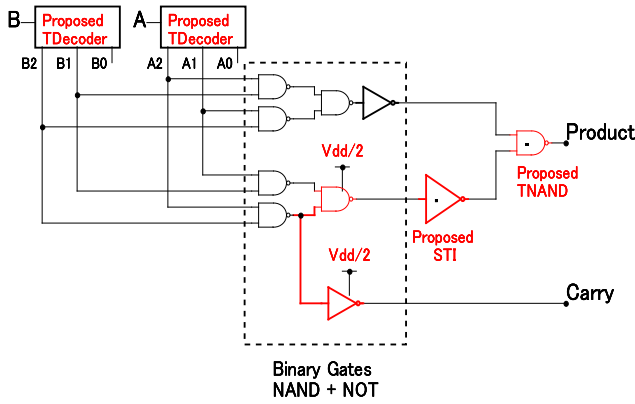


FIGURE 5. Proposed *TMUL* with 61 transistors.

[13], [15]. Also, it uses the proposed *TDecoder* of Fig. 3, the proposed *STI* of Fig. 1 and the proposed *NAND* of Fig. 2, and removes one common *NAND* as illustrate in Fig. 5.

Fig. 5 shows the proposed *TMUL*. It consists of two proposed *TDecoders*, six binary *NAND*, two binary inverters, one proposed *STI*, and one proposed *TNAND*.

TABLE 16. Total transistors' count of the proposed *TMUL*.

	No. of Devices	No. of Transistors	Subtotal*
Proposed <i>TDecoder</i>	2	9	18
Binary <i>NAND</i>	6	4	24
Binary Inverter	2	2	4
Proposed <i>STI</i>	1	5	5
Proposed <i>TNAND</i>	1	10	10
<b>Total</b>			<b>61</b>

\*Subtotal = No. of Devices x No. of Transistors

Table 16 shows the total transistors' count of the proposed *TMUL*.

The operation of the proposed *TMUL*: Two ternary inputs *A* and *B* fed to the proposed *TDecoders* and produce outputs as ( $A_2, A_1, A_0$ ) and ( $B_2, B_1, B_0$ ). These outputs will drive the four 2-inputs binary *NAND*, the two 2-inputs binary *NAND* logic gates, the proposed *STI*, the two binary inverters, and the proposed *TNAND* to get the Product and the Carry as final outputs.

### V. SIMULATION RESULTS AND COMPARISONS

As mentioned in the Introduction that CNFET provides better energy efficiency compared to CMOS, FinFET, and other transistor technologies [19].

Therefore, the proposed *STI*, *TNAND*, *TDecoder*, *THA*, and *TMUL* are simulated and compared to CNFET-Based ternary circuits in [13]–[18].

All the twenty circuits are extensively simulated and tested using the HSPICE simulator with 32-nm channel length for different power supplies (0.8 V, 0.9 V, 1 V), different temperatures (10°C, 27°C, 70°C), and different frequencies (0.5 GHz, 1 GHz, 2 GHz).

One hundred eighty simulations are performed to study the performance and efficiency of the proposed five circuits in the separate sections below.

Although CNFET-based circuit may suffer performance changes due to device variability, this effect has not been considered in this work.

Table 17 shows some essential parameters of the CNFET model used in all the circuits with brief descriptions.

TABLE 17. Some of CNFET model parameters.

	Description	Value
$L_{ch}$	Physical channel length	32 nm
$L_{geff}$	The mean free path in the intrinsic CNT	100 nm
$L_{ss} (L_{dd})$	The length of doped CNT source-side (drain-side) extension region	10 nm
$E_{fi}$	The Fermi level of the doped S/D tube	0.6 eV
$K_{gate}$	The dielectric constant of high-k top gate dielectric material (planer gate)	4
$T_{ox}$	The thickness of the high-k top gate dielectric material (planer gate)	1 nm
$C_{sub}$	The coupling capacitance between the channel region and the substrate	10 pF/m
$C_{csd}$	The coupling capacitance between the channel region and the source/drain region	0 pF/m
$Pitch$	The distance between two adjacent CNTs within the same device	20 nm
$Tubes$	The number of tubes in the device	1

All input signals have a rise and fall time of 20 ps. The propagation delay of the circuit is measured, for example, for  $t_1$  as shown in Fig. 8, when the input ( $X$ ) is rising from 0 to 1, and the output ( $X_0$ ) is falling from 2 to 0. A similar procedure is done to get all possible rising and falling propagation delays for outputs of all studied circuits and find the maximum propagation delay for each circuit.

Then the average power consumption, maximum propagation delay, and maximum power delay product (PDP) are obtained for all circuits.

The performance of the five proposed circuits will be compared to other designs for the Power-Delay Product PDP (energy consumption).

#### A. TRANSIENT ANALYSIS OF PROPOSED CIRCUITS

Fig. 6 – 10 illustrate the transient analysis of the proposed *STI*, *TNAND*, *TDecoder*, *THA*, and *TMUL* respectively.

#### B. COMPARISON OF TRANSISTORS' COUNT

The minimization of transistors' count is not the only factor that affects the performance of the proposed circuits, but it is

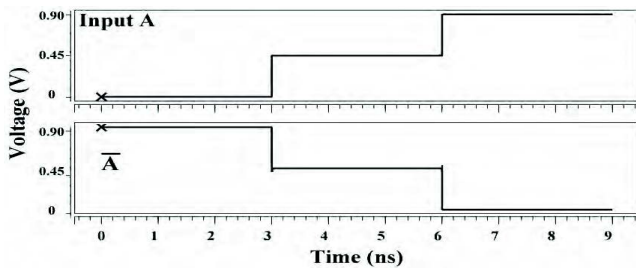


FIGURE 6. Transient analysis of the proposed *STI*.

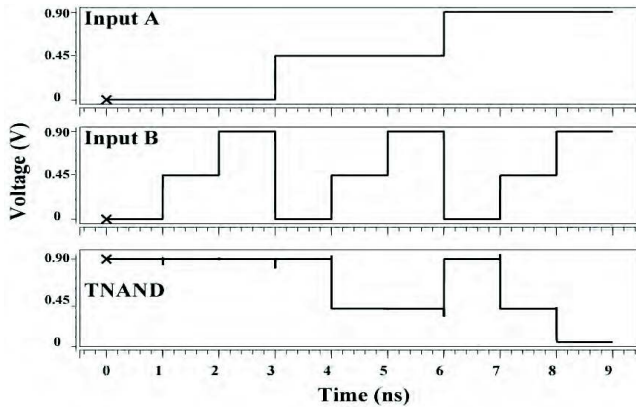


FIGURE 7. Transient analysis of the proposed *TNAND*.

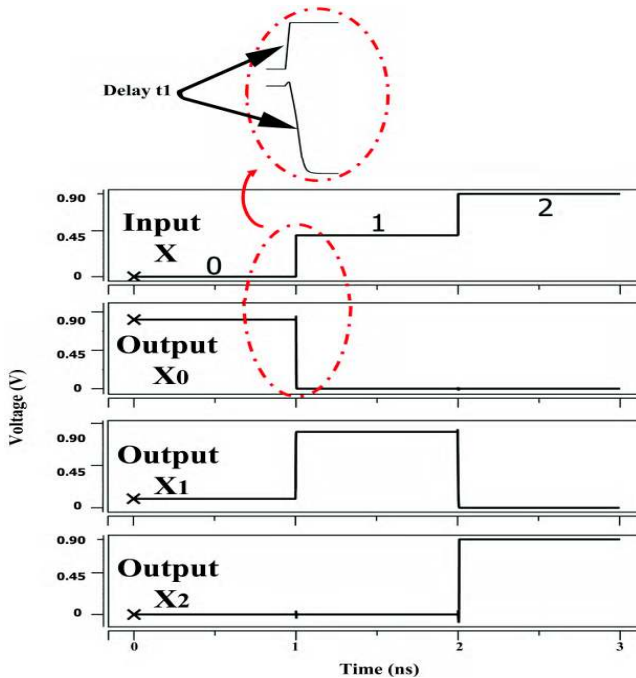


FIGURE 8. Transient analysis of the proposed *TDecoder*.

a good factor. The other factors are described in the following subsections.

Table 18 shows the comparison of transistors' count for *STI*, *TNAND*, *TDecoder*, *THA*, and *TMUL* compared to [13]–[18].

This comparison of the proposed circuits demonstrates a notable reduction in transistors' count. For *STI*, around 16.67% compared to *STI* in [13], [16], and [18]. For *TNAND*,

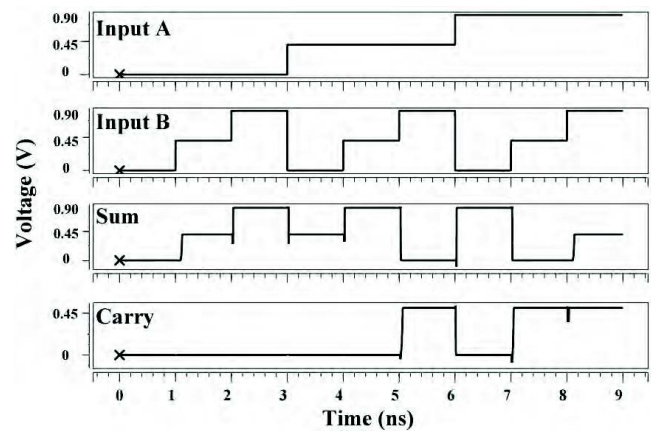


FIGURE 9. Transient analysis of the proposed *THA*.

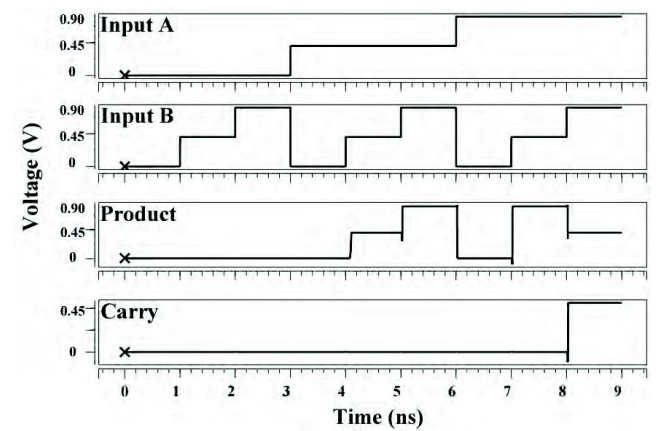


FIGURE 10. Transient analysis of the proposed *TMUL*.

TABLE 18. Comparison of transistors' count of all circuits.

	[13]	[16]	[15]	[18]	[17]	[14]	Proposed
<i>STI</i>	6	6	–	6	–	–	<b>5</b>
<i>TNAND</i>	10	10	–	10	–	–	<b>10</b>
<i>TDecoder</i>	16	–	–	–	11	10	<b>9</b>
<i>THA</i>	136	112	112	–	–	–	<b>85</b>
<i>TMUL</i>	100	76	86	–	–	–	<b>61</b>

around 0% compared to *TNAND* in [13], [16], and [18]. For *TDecoder*, around 43.75%, 10%, and 18.18% compared to *TDecoder* in [13], [14], and [17] respectively. For *THA*, around 37.5%, 24.11%, and 24.11% compared to *THA* in [13], [15], and [16] respectively. For *TMUL*, around 39%, 29.07%, and 19.74% compared to *TMUL* in [13], [15], and [16] respectively.

### C. COMPARISON OF DIFFERENT *STI* CIRCUITS

Fig. 11 shows the PDP Comparison of the investigated *STI* for (a) Different Power Supplies, (b) Different Temperatures, and (c) Different Frequencies.

#### 1) IMPACT OF DIFFERENT POWER SUPPLIES

The effect of different power supplies (0.8 V, 0.9 V, 1 V) on the performance metrics of all proposed circuits is studied.

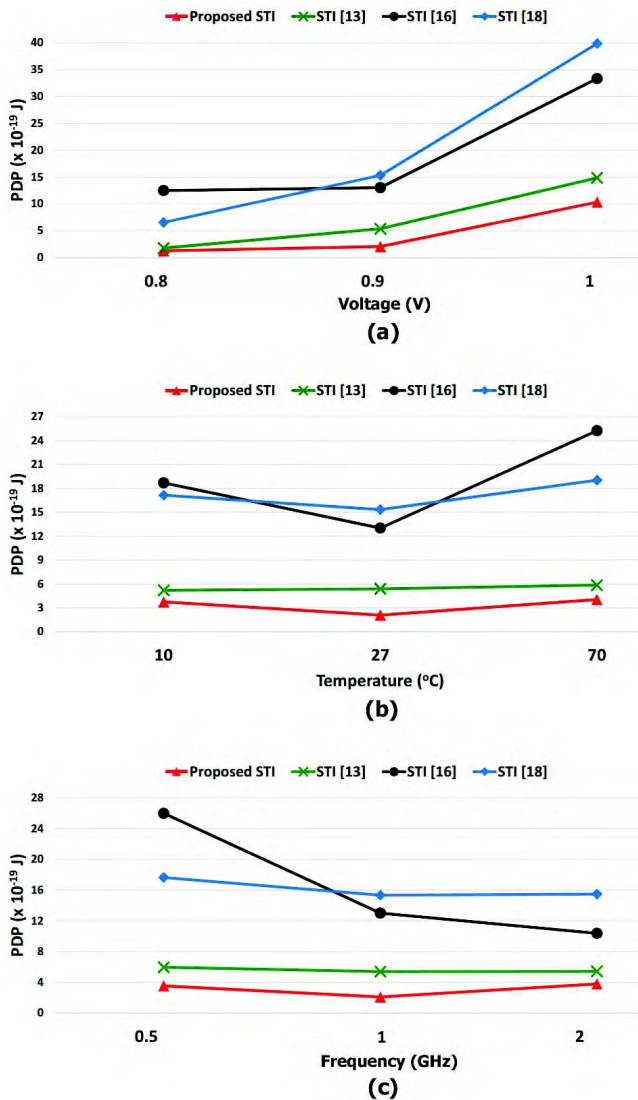


FIGURE 11. PDP Comparison of the investigated *STI* for: (a) different power supplies, (b) different temperatures, and (c) different frequencies.

Simulation is done at 1 GHz operating frequency and room temperature at 27°C as illustrated in Fig. 11 (a).

The comparison of the proposed *STI* demonstrates a notable reduction in PDP as shown in Fig. 11 (a). For V<sub>dd</sub>=0.8 V, around 28.33%, 88.68%, and 80.37% compared to [13], [16], and [18] respectively. For V<sub>dd</sub>=0.9 V, around 61.22%, 83.95%, and 86.38% compared to [13], [16], and [18] respectively. For V<sub>dd</sub>=1 V, around 30.42%, 68.98%, and 74.05% compared to [13], [16], and [18] respectively.

## 2) IMPACT OF DIFFERENT TEMPERATURES

Temperature noise is one of the most critical issues which negatively affect the performance of the circuit.

The effect of different temperatures (10°C, 27°C, 70°C) on the performance metrics of all proposed circuits is studied. Simulation is done at 1 GHz operating frequency, and power supply V<sub>dd</sub> equals 0.9 V as illustrated in Fig. 11 (b).

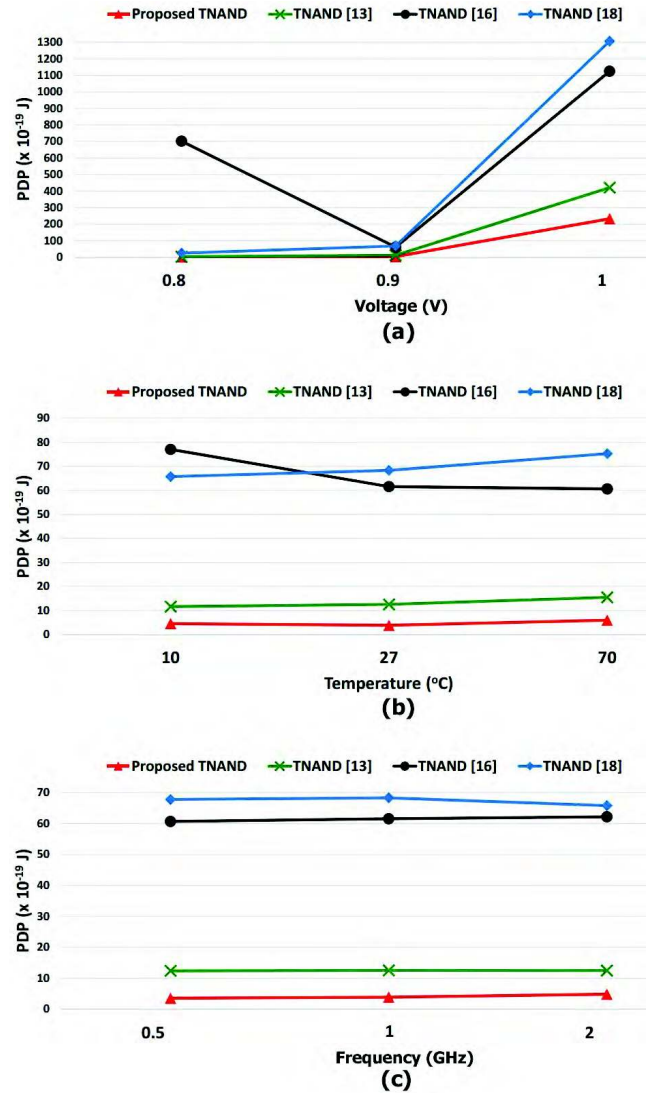


FIGURE 12. PDP Comparison of the investigated *TNAND* for: (a) different power supplies, (b) different temperatures, and (c) different frequencies.

The comparison of the proposed *STI* demonstrates a notable reduction in PDP as shown in Fig. 11 (b). For Temperature = 10°C, around 27.88%, 79.95%, and 78.15% compared to [13], [16], and [18] respectively. For Temperature = 27°C, around 61.22%, 83.95%, and 86.38% compared to [13], [16], and [18] respectively. For Temperature = 70°C, around 30.89%, 83.96%, and 78.73% compared to [13], [16], and [18] respectively.

## 3) IMPACT OF DIFFERENT FREQUENCIES

Electronic circuits behave very differently at high frequencies because due to a change in the behavior of passive components (resistors, inductors, and capacitors) and parasitic effects on active components, PCB tracks and grounding patterns at high frequencies.

Recently, High-frequency operation is a demand for electronic devices.

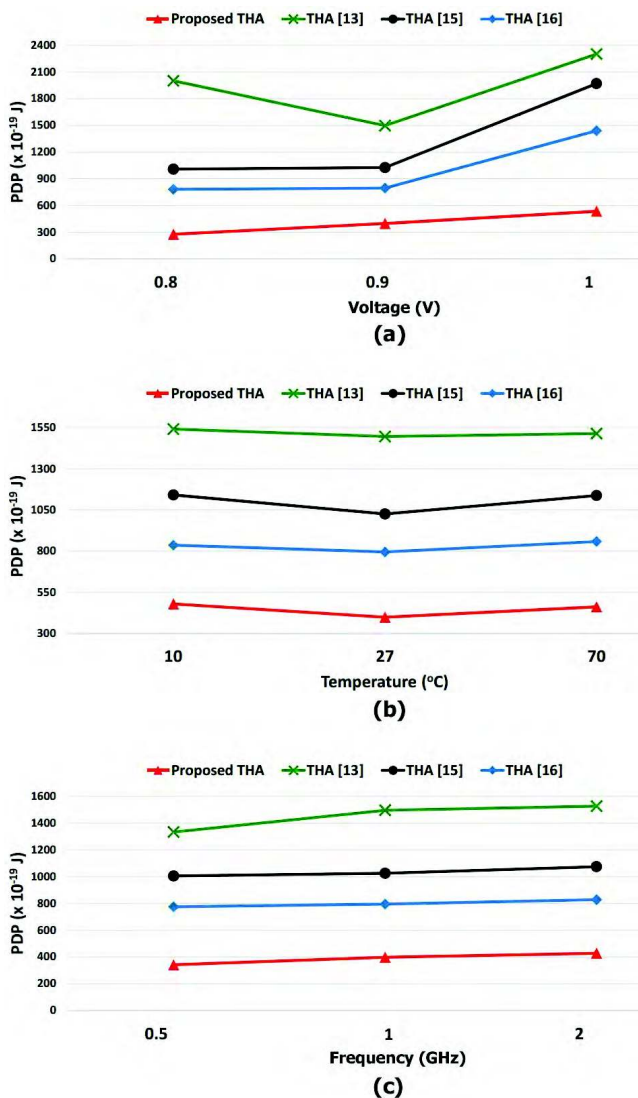


FIGURE 13. PDP Comparison of the investigated THA for: (a) different power supplies, (b) different temperatures, and (c) different frequencies.

The effect of different frequencies (0.5 GHz, 1 GHz, 2 GHz) on the performance metrics of all proposed circuits is studied. Simulation is done at power supply V<sub>dd</sub> equals 0.9 V, and temperature equals 27°C as illustrated in Fig. 11(c).

The comparison of the proposed STI demonstrates a notable reduction in PDP as shown in Fig. 11 (c). For frequency = 0.5 GHz, around 40.60%, 86.38%, and 79.93% compared to [13], [16], and [18] respectively. For frequency = 1 GHz, around 61.22%, 83.95%, and 86.38% compared to [13], [16], and [18] respectively. For frequency = 2 GHz, around 30.20%, 63.45%, and 75.52% compared to [13], [16], and [18] respectively.

**D. COMPARISON OF DIFFERENT TNAND CIRCUITS**

Fig. 12 shows the PDP Comparison of the investigated TNAND for (a) Different Power Supplies, (b) Different Temperatures, and (c) Different Frequencies.

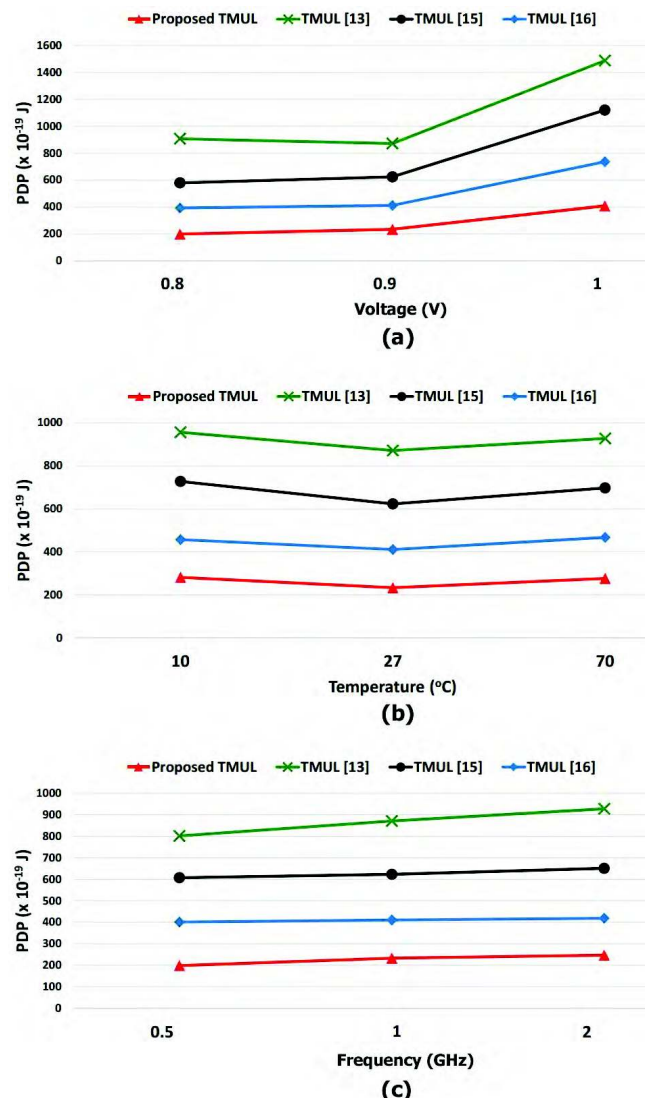


FIGURE 14. PDP Comparison of the investigated TMUL for: (a) different power supplies, (b) different temperatures, and (c) different frequencies.

**1) IMPACT OF DIFFERENT POWER SUPPLIES**

Simulation is done at 1 GHz operating frequency and room temperature at 27°C as illustrated in Fig. 12 (a).

The comparison of the proposed TNAND demonstrates a notable reduction in PDP as shown in Fig. 12 (a). For V<sub>dd</sub>=0.8 V, around 32.53%, 99.64%, and 90.07% compared to [13], [16], and [18] respectively. For V<sub>dd</sub>=0.9 V, around 69.22%, 93.73%, and 94.35% compared to [13], [16], and [18] respectively. For V<sub>dd</sub>=1 V, around 44.6%, 79.27%, and 98.3% compared to [13], [16], and [18] respectively.

**2) IMPACT OF DIFFERENT TEMPERATURES**

The effect of different temperatures (10°C, 27°C, 70°C) on the performance metrics of all proposed circuits is studied.

Simulation is done at 1 GHz operating frequency, and power supply V<sub>dd</sub> equals 0.9 V as illustrated in Fig. 12 (b).

The comparison of the proposed TNAND demonstrates a notable reduction in PDP as shown in Fig. 12 (b).

**TABLE 19.** Comparison of average power ( $\mu\text{W}$ ), maximum delay (ps), and maximum PDP ( $\times 10^{-19}$  J) of 4 TDecoders with  $T = 27^\circ\text{C}$ ,  $F=1$  GHz, and for different supply voltages.

	Vdd=0.8 V			Vdd=0.9 V			Vdd=1 V		
	Power	Delay	PDP	Power	Delay	PDP	Power	Delay	PDP
TDecoder [13]	2.6	10.4	2.74	3.5	8.91	3.11	11.8	8.24	9.72
TDecoder [14]	1.9	8.50	1.65	2.7	7.50	2.02	10.4	7.06	7.37
TDecoder [17]	126	8.67	109.24	185	7.68	142.08	250	7.18	168.73
<b>Proposed TDecoder</b>	<b>1.9</b>	<b>6.59</b>	<b>1.26</b>	<b>2.6</b>	<b>6.26</b>	<b>1.62</b>	<b>9.1</b>	<b>4.18</b>	<b>3.82</b>

**TABLE 20.** Comparison of average power ( $\mu\text{W}$ ), maximum delay (ps), and maximum PDP ( $\times 10^{-19}$  J) of 4 TDecoders with Vdd=0.9 V,  $F=1$  GHz, and for different temperatures.

	Temp.=10°C			Temp.=27°C			Temp.=70°C		
	Power	Delay	PDP	Power	Delay	PDP	Power	Delay	PDP
TDecoder [13]	5.1	9.18	4.72	3.5	8.91	3.11	4.4	8.31	3.68
TDecoder [14]	4.3	7.7	3.33	2.7	7.50	2.02	3.5	7.05	2.50
TDecoder [17]	184	7.89	145.17	185	7.68	142.08	189	7.20	136.72
<b>Proposed TDecoder</b>	<b>4</b>	<b>6.4</b>	<b>2.51</b>	<b>2.6</b>	<b>6.26</b>	<b>1.62</b>	<b>3.5</b>	<b>5.85</b>	<b>2.05</b>

**TABLE 21.** Comparison of average power ( $\mu\text{W}$ ), maximum delay (ps), and maximum PDP ( $\times 10^{-19}$  J) of 4 TDecoders with  $T = 27^\circ\text{C}$ , Vdd=0.9 V, and for different frequencies.

	f= 2 GHz			f= 1 GHz			f= 0.5 GHz		
	Power	Delay	PDP	Power	Delay	PDP	Power	Delay	PDP
TDecoder [13]	6.0	8.93	5.17	3.5	8.91	3.11	2.3	8.91	2.11
TDecoder [14]	4.1	7.54	3.12	2.7	7.50	2.02	2.0	7.5	1.46
TDecoder [17]	185	7.7	142.24	185	7.68	142.08	184	7.68	142.08
<b>Proposed TDecoder</b>	<b>4</b>	<b>6.25</b>	<b>2.44</b>	<b>2.6</b>	<b>6.26</b>	<b>1.62</b>	<b>1.8</b>	<b>6.26</b>	<b>1.17</b>

For Temperature =  $10^\circ\text{C}$ , around 60.88%, 94.09%, and 93.08% compared to [13], [16], and [18] respectively. For Temperature =  $27^\circ\text{C}$ , around 69.22%, 93.73%, and 94.35% compared to [13], [16], and [18] respectively. For Temperature =  $70^\circ\text{C}$ , around 61.34%, 90.13%, and 92.06% compared to [13], [16], and [18] respectively.

### 3) IMPACT OF DIFFERENT FREQUENCIES

The effect of different frequencies (0.5 GHz, 1 GHz, 2 GHz) on the performance metrics of all proposed circuits is studied.

Simulation is done at power supply Vdd equals 0.9 V, and temperature equals  $27^\circ\text{C}$  as illustrated in Fig. 12 (c).

The comparison of the proposed *TNAND* demonstrates a notable reduction in PDP as shown in Fig. 12 (c). For frequency = 0.5 GHz, around 71.46%, 94.18%, and 94.79% compared to [13], [16], and [18] respectively. For frequency = 1 GHz, around 69.22%, 93.73%, and 94.35% compared to [13], [16], and [18] respectively. For frequency = 2 GHz, around 61.27%, 92.23%, and 92.66% compared to [13], [16], and [18] respectively.

## E. COMPARISON OF DIFFERENT TDECODER CIRCUITS

### 1) IMPACT OF DIFFERENT POWER SUPPLIES

Table 19 shows the comparison to the existing Ternary Decoder in [13], [14], and [17] in terms of the average power consumption, maximum propagation delay, and maximum energy (PDP) for different supply voltages (0.8 V, 0.9 V, 1 V), same temperature ( $27^\circ\text{C}$ ), and same frequency (1 GHz). The boldface values are the best values among others.

The comparison of the proposed Ternary Decoder demonstrates a notable reduction in PDP as shown in Table 19. For Vdd=0.8 V, around 54.01%, 23.64%, and 98.85% compared to [13], [14], and [17] respectively. For Vdd=0.9 V, around 47.91%, 19.8%, and 98.86% compared to [13], [14], and [17] respectively. For Vdd=1 V, around 60.7%, 48.17%, and 97.74% compared to [13], [14], and [17] respectively.

### 2) IMPACT OF DIFFERENT TEMPERATURES

Table 20 shows the comparison to the existing Ternary Decoder in [13], [14], and [17] in terms of the average power consumption, maximum propagation delay, and maximum energy (PDP) for different temperatures ( $10^\circ\text{C}$ ,  $27^\circ\text{C}$ ,  $70^\circ\text{C}$ ), same supply voltage Vdd (0.9 V), and same frequency (1 GHz).

The comparison of the proposed Ternary Decoder demonstrates a notable reduction in PDP as shown in Table 20. For Temperature =  $10^\circ\text{C}$ , around 46.82%, 24.62%, and 98.27% compared to [13], [14], and [17] respectively. For Temperature =  $27^\circ\text{C}$ , around 47.91%, 19.8%, and 98.86% compared to [13], [14], and [17] respectively. For Temperature =  $70^\circ\text{C}$ , around 44.29%, 18%, and 98.5% compared to [13], [14], and [17] respectively.

### 3) IMPACT OF DIFFERENT FREQUENCIES

Table 21 shows the comparison to the existing Ternary Decoder in [13], [14], and [17] in terms of the average power consumption, maximum propagation delay, and maximum energy (PDP) for different frequencies (0.5 GHz, 1 GHz,

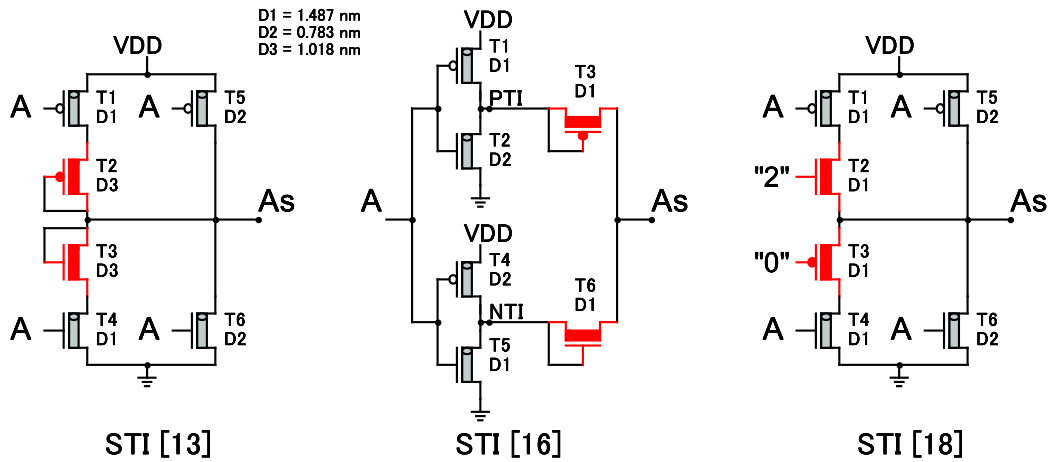


FIGURE 15. Existing STI in (a) [13], (b) [16], and (c) [18].

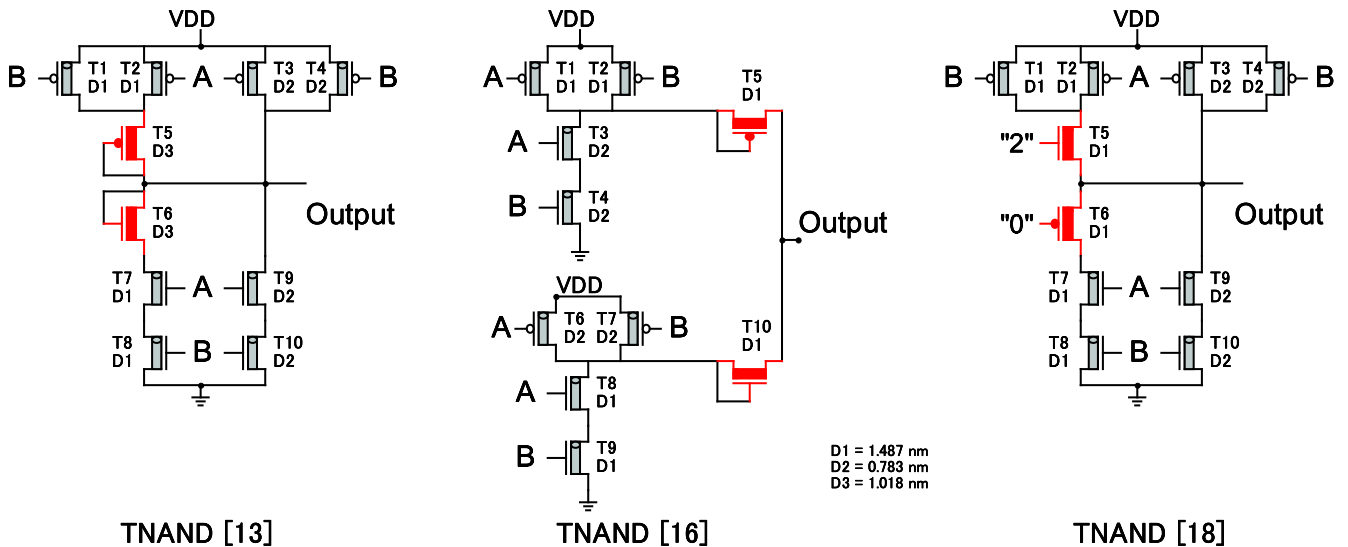


FIGURE 16. Existing TNAND in (a) [13], (b) [16], and (c) [18].

2 GHz), same temperatures (27°C), and same supply voltage Vdd (0.9 V).

The comparison of the proposed Ternary Decoder demonstrates a notable reduction in PDP as shown in Table 21. For frequency = 2 GHz, around 52.8%, 21.79%, and 98.28% compared to [13], [14], and [17] respectively. For frequency = 1 GHz, around 47.91%, 19.8%, and 98.86% compared to [13], [14], and [17] respectively. For frequency = 0.5 GHz, around 44.55%, 19.86%, and 99.18% compared to [13], [14], and [17] respectively.

**F. COMPARISON OF DIFFERENT THA CIRCUITS**

Fig. 13 shows the PDP Comparison of the investigated THA for (a) Different Power Supplies, (b) Different Temperatures, and (c) Different Frequencies.

**1) IMPACT OF DIFFERENT POWER SUPPLIES**

Simulation is done at 1 GHz operating frequency and room temperature at 27°C as illustrated in Fig. 13 (a).

The comparison of the proposed THA demonstrates a notable reduction in PDP as shown in Fig. 13 (a). For Vdd=0.8 V, around 86.16%, 72.53%, and 64.55% compared to [13], [15], and [16] respectively. For Vdd=0.9 V, around 73.43%, 61.24%, and 49.97% compared to [13], [15], and [16] respectively. For Vdd=1 V, around 76.75%, 72.82%, and 62.85% compared to [13], [15], and [16] respectively.

**2) IMPACT OF DIFFERENT TEMPERATURES**

The effect of different temperatures (10°C, 27°C, 70°C) on the performance metrics of all proposed circuits is studied.

Simulation is done at 1 GHz operating frequency, and power supply Vdd equals 0.9 V as illustrated in Fig. 13 (b).

The comparison of the proposed THA demonstrates a notable reduction in PDP as shown in Fig. 13 (b). For Temperature = 10°C, around 68.97%, 58.08%, and 42.78% compared to [13], [15], and [16] respectively. For Temperature = 27°C, around 73.43%, 61.24%, and 49.97% compared

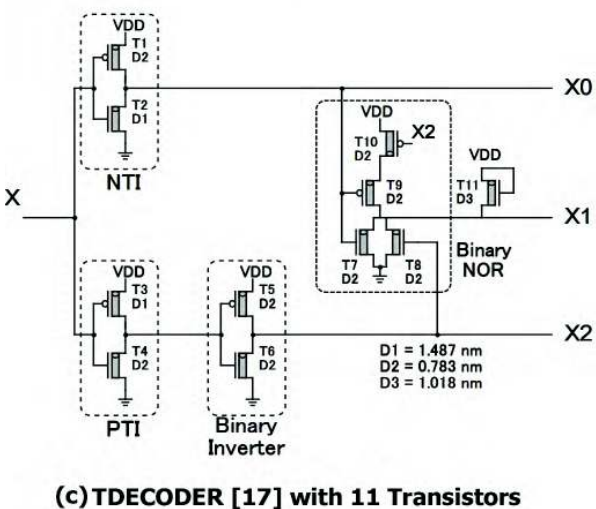
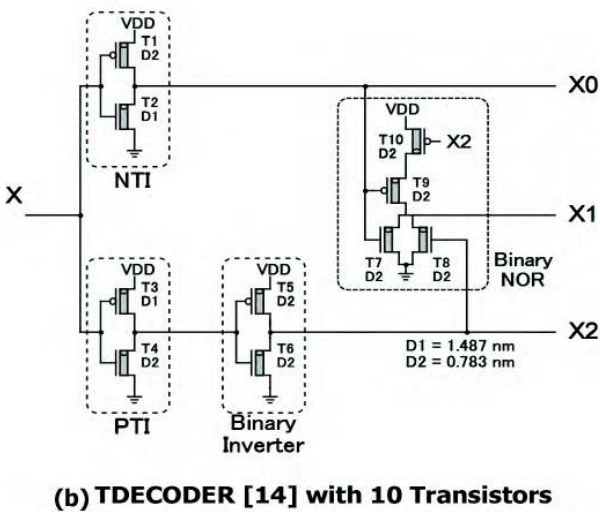
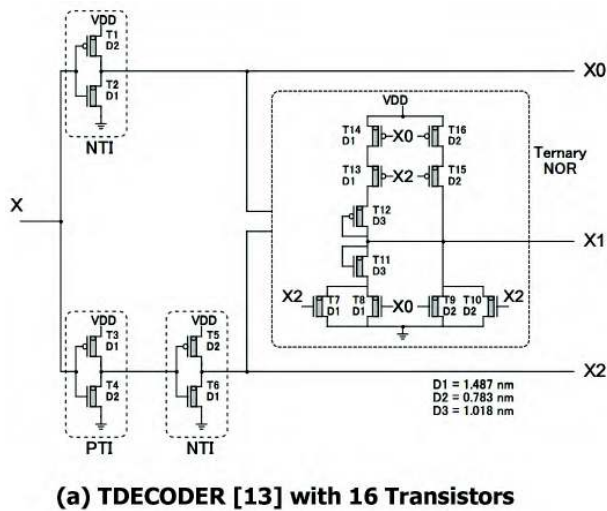


FIGURE 17. Existing TDecoder in (a) [13], (b) [14], and (c) [17].

to [13], [15], and [16] respectively. For Temperature = 70°C, around 69.58%, 59.51%, and 46.28% compared to [13], [15], and [16] respectively.

### 3) IMPACT OF DIFFERENT FREQUENCIES

The effect of different frequencies (0.5 GHz, 1 GHz, 2 GHz) on the performance metrics of all proposed circuits is studied.

Simulation is done at power supply Vdd equals 0.9 V, and temperature equals 27°C as illustrated in Fig. 13 (c).

The comparison of the proposed THA demonstrates a notable reduction in PDP as shown in Fig. 13 (c). For frequency = 0.5 GHz, around 74.4%, 66.04%, and 55.94% compared to [13], [15], and [16] respectively. For frequency = 1 GHz, around 73.43%, 61.24%, and 49.97% compared to [13], [15], and [16] respectively. For frequency = 2 GHz, around 72.01%, 60.22%, and 48.4% compared to [13], [15], and [16] respectively.

### G. COMPARISON OF DIFFERENT TMUL CIRCUITS

Fig. 14 shows the PDP Comparison of the investigated TMUL for (a) Different Power Supplies, (b) Different Temperatures, and (c) Different Frequencies.

#### 1) IMPACT OF DIFFERENT POWER SUPPLIES

Simulation is done at 1 GHz operating frequency and room temperature at 27°C as illustrated in Fig. 14 (a).

The comparison of the proposed TMUL demonstrates a notable reduction in PDP as shown in Fig. 14 (a). For Vdd=0.8 V, around 78.16%, 65.77%, and 49.49% compared to [13], [15], and [16] respectively. For Vdd=0.9 V, around 73.19%, 62.52%, and 43.19% compared to [13], [15], and [16] respectively. For Vdd=1 V, around 72.58%, 63.58%, and 44.55% compared to [13], [15], and [16] respectively.

#### 2) IMPACT OF DIFFERENT TEMPERATURES

The effect of different temperatures (10°C, 27°C, 70°C) on the performance metrics of all proposed circuits is studied.

Simulation is done at 1 GHz operating frequency, and power supply Vdd equals 0.9 V as illustrated in Fig. 14 (b).

The comparison of the proposed TMUL demonstrates a notable reduction in PDP as shown in Fig. 14 (b). For Temperature = 10°C, around 70.51%, 61.25%, and 38.36% compared to [13], [15], and [16] respectively. For Temperature = 27°C, around 73.19%, 62.52%, and 43.19% compared to [13], [15], and [16] respectively. For Temperature = 70°C, around 70.17%, 60.32%, and 40.82% compared to [13], [15], and [16] respectively.

#### 3) IMPACT OF DIFFERENT FREQUENCIES

The effect of different frequencies (0.5 GHz, 1 GHz, 2 GHz) on the performance metrics of all proposed circuits is studied.

Simulation is done at power supply Vdd equals 0.9 V, and temperature equals 27°C as illustrated in Fig. 14 (c).

The comparison of the proposed TMUL demonstrates a notable reduction in PDP as shown in Fig. 14 (c). For frequency = 0.5 GHz, around 75.15%, 67.2%, and 50.38% compared to [13], [15], and [16] respectively. For frequency = 1 GHz, around 73.19%, 62.52%, and 43.19% compared to [13], [15], and [16] respectively.

For frequency = 2 GHz, around 73.31%, 61.97%, and 40.91% compared to [13], [15], and [16] respectively.

The **advantage** of all proposed circuits is that they have the lowest PDP among all investigated circuits for different supply voltages, temperatures, and frequencies. Therefore, they are more suitable for low-power portable electronics and embedded systems to save battery consumption.

**VI. CONCLUSION**

This paper proposed new designs for the Standard Ternary Inverter, Ternary NAND, Ternary Decoder, Ternary Half Adder, and Ternary Multiplier that aim to keep high-performance levels and energy efficiency.

The design process tried to optimize several circuit techniques such as reducing the number of used transistors,

utilizing energy-efficient transistor arrangements, and applying the dual supply voltages (V<sub>dd</sub> and V<sub>dd</sub>/2).

The proposed ternary circuits are compared to the latest fifteen ternary circuits, simulated and tested using HSPICE simulator under various operating conditions with different supply voltages, different temperatures, and different frequencies.

One hundred eighty simulations are performed to prove the efficiency of the proposed designs. The results prove the merits of the approach in terms of reduced energy consumption (PDP) compared to other existing designs.

Therefore, the proposed circuits can be implemented in low-power portable electronics and embedded systems to save battery consumption.

**APPENDIX  
INVESTIGATED CIRCUITS FROM THE LITERATURE**

See Figs. 15–19.

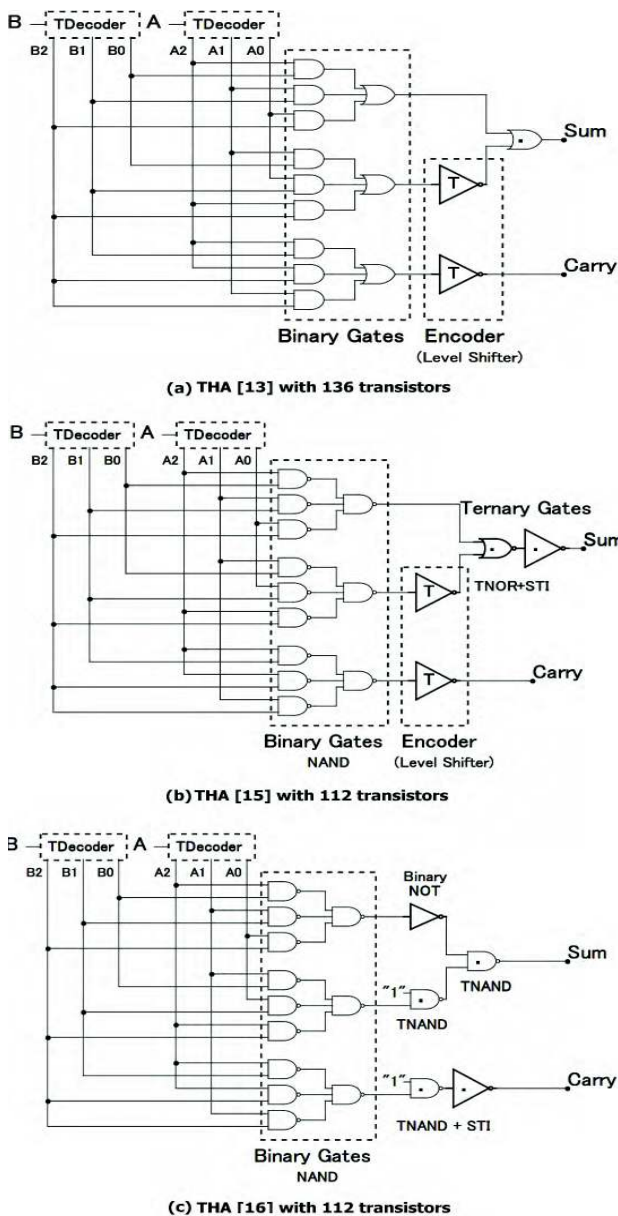


**FIGURE 18.** Existing THA in (a) [13], (b) [15], and (c) [16].

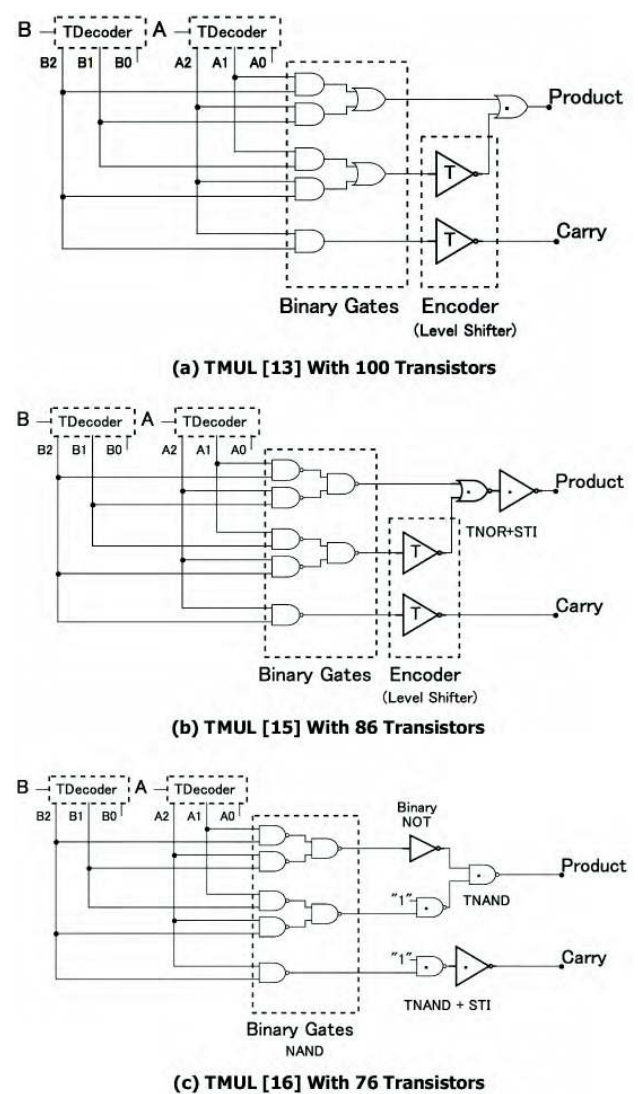


**FIGURE 19.** Existing TMUL in (a) [13], (b) [15], and (c) [16].

## REFERENCES

- [1] K. You and K. Nepal, "Design of a ternary static memory cell using carbon nanotube-based transistors," *IET Micro Nano Lett.*, vol. 6, no. 6, pp. 381–385, Jun. 2011. doi: [10.1049/mnl.2011.0168](https://doi.org/10.1049/mnl.2011.0168).
- [2] J.-M. Philippe, E. Kinvi-Boh, S. Pillement, and O. Sentieys, "An energy-efficient ternary interconnection link for asynchronous systems," in *Proc. IEEE Int. Symp. Circuits Syst. (ISCAS)*, Island of Kos, Greece, May 2006, pp. 1011–1014.
- [3] S. L. Hurst, "Multiple-valued logic—Its status and its future," *IEEE Trans. Comput.*, vol. C-33, no. 12, pp. 1160–1179, Dec. 1984. doi: [10.1109/TC.1984.1676392](https://doi.org/10.1109/TC.1984.1676392).
- [4] D. M. Miller and M. Soeken, "A spectral algorithm for ternary function classification," in *Proc. IEEE 48th Int. Symp. Multiple-Valued Log. (ISMVL)*, Linz, Austria, May 2018, pp. 198–203.
- [5] P. Reviriego, S. Pontarelli, and A. Ullah, "Error detection and correction in SRAM emulated TCAMs," *IEEE Trans. Very Large Scale Integr. (VLSI) Syst.*, vol. 27, no. 2, pp. 486–490, Feb. 2019. doi: [10.1109/TVLSI.2018.2877131](https://doi.org/10.1109/TVLSI.2018.2877131).
- [6] M. R. Khezeli, M. H. Moaiyeri, and A. Jalali, "Comparative analysis of simultaneous switching noise effects in MWCNT bundle and Cu power interconnects in CNFET-based ternary circuits," *IEEE Trans. Very Large Scale Integr. (VLSI) Syst.*, vol. 27, no. 1, pp. 37–46, Jan. 2019. doi: [10.1109/TVLSI.2018.2869761](https://doi.org/10.1109/TVLSI.2018.2869761).
- [7] H. Oseily and A. M. Haidar, "Hexadecimal to binary conversion using multi-input floating gate complementary metal oxide semiconductors," in *Proc. Int. Conf. Appl. Res. Comput. Sci. Eng. (ICAR)*, Beirut, Lebanon, Oct. 2015, pp. 1–6.
- [8] A. I. Khan, N. Nusrat, S. M. Khan, and M. Hasan, "Novel realization of quantum ternary Mux and Demux," in *Proc. Int. Conf. Elect. Comput. Eng.*, Dhaka, Bangladesh, Dec. 2006, pp. 153–156.
- [9] N. Saleh, A. Kassem, and A. M. Haidar, "Energy-Efficient architecture for wireless sensor networks in healthcare applications," *IEEE Access*, vol. 6, pp. 6478–6486, 2018. doi: [10.1109/ACCESS.2018.2789918](https://doi.org/10.1109/ACCESS.2018.2789918).
- [10] M. Irfan and Z. Ullah, "G-AETCAM: Gate-based area-efficient ternary content-addressable memory on FPGA," *IEEE Access*, vol. 5, pp. 20785–20790, 2017. doi: [10.1109/ACCESS.2017.2756702](https://doi.org/10.1109/ACCESS.2017.2756702).
- [11] R. Jaber, A. El-hajj, L. Nimri, and A. Haidar, "A Novel implementation of ternary decoder using CMOS DPL binary gates," in *Proc. Int. Arab Conf. Inf. Technol. (ACIT)*, Werdanye, Lebanon, Nov. 2018, pp. 1–3.
- [12] K. Jyoti and S. Narkhede, "An approach to ternary logic gates using FinFET," in *Proc. Int. Conf. Adv. Inf. Commun. Technol. Comput. (AICTC)*, Bikaner, India, 2016, p. 59.
- [13] S. Lin, Y. B. Kim, and F. Lombardi, "CNFET-based design of ternary logic gates and arithmetic circuits," *IEEE Trans. Nanotechnol.*, vol. 10, no. 2, pp. 217–225, Mar. 2011. doi: [10.1109/TNANO.2009.2036845](https://doi.org/10.1109/TNANO.2009.2036845).
- [14] K. Sridharan, S. Gurindagunta, and V. Pudi, "Efficient multiterinary digit adder design in CNFET technology," *IEEE Trans. Nanotechnol.*, vol. 12, no. 3, pp. 283–287, Mar. 2013. doi: [10.1109/TNANO.2013.2251350](https://doi.org/10.1109/TNANO.2013.2251350).
- [15] M. Muglikar, R. Sahoo, and S. K. Sahoo, "High performance ternary adder using CNFET," in *Proc. 3rd Int. Conf. Devices, Circuits Syst. (ICDCS)*, Coimbatore, India, Mar. 2016, pp. 236–239.
- [16] H. Samadi, A. Shahhoseini, and F. Aghaei-liavali, "A new method on designing and simulating CNFET-based ternary gates and arithmetic circuits," *Microelectron. J.*, vol. 63, pp. 41–48, May 2017. doi: [10.1016/j.mejo.2017.02.018](https://doi.org/10.1016/j.mejo.2017.02.018).
- [17] P. Wang, D. Gong, Y. Zhang, and Y. Kang, "Ternary 2-9 line address decoder realized by CNFET," U.S. Patent 20180182450 A1, Jun. 28, 2018.
- [18] S. Tabrizchi, M. R. Taheri, K. Navi, and N. Bagherzadeh, "Novel CNFET ternary circuit techniques for high-performance and energy-efficient design," *IET Circuits, Devices Syst.*, vol. 13, no. 2, pp. 193–202, Mar. 2019. doi: [10.1049/iet-cds.2018.5036](https://doi.org/10.1049/iet-cds.2018.5036).
- [19] G. Hills et al., "Understanding energy efficiency benefits of carbon nanotube field-effect transistors for digital VLSI," *IEEE Trans. Nanotechnol.*, vol. 17, no. 6, pp. 1259–1269, Nov. 2018. doi: [10.1109/TNANO.2018.2871841](https://doi.org/10.1109/TNANO.2018.2871841).
- [20] Stanford, CA, USA. *Stanford University CNFET Model Website*. Accessed: May 1, 2019. [Online]. Available: <http://nano.stanford.edu/model.php?id=23>
- [21] J. Deng and H.-S. P. Wong, "A compact SPICE model for carbon-nanotube field-effect transistors including nonidealities and its application—Part I: Model of the intrinsic channel region," *IEEE Trans. Electron Devices*, vol. 54, no. 12, pp. 3186–3194, Dec. 2007. doi: [10.1109/TED.2007.909030](https://doi.org/10.1109/TED.2007.909030).
- [22] J. Deng and H.-S. P. Wong, "A compact SPICE model for carbon-nanotube field-effect transistors including nonidealities and its application—Part II: Full device model and circuit performance benchmarking," *IEEE Trans. Electron Devices*, vol. 54, no. 12, pp. 3195–3205, Dec. 2007. doi: [10.1109/TED.2007.909043](https://doi.org/10.1109/TED.2007.909043).



**RAMZI A. JABER** (S'19) received the B.E. degree (Hons.) in computer and electrical engineering and the master's degree in computer engineering and informatics from Beirut Arab University (BAU), in 2001 and 2010, respectively, where he is currently pursuing the Ph.D. degree in computer and electrical engineering.

From 2002 to 2006, he taught at different high schools at Lebanon. From 2006 to 2010, he taught as a Lab Instructor in the Faculty of Computer Sciences, Lebanese University. From 2006 to 2019, he taught as a Lab Instructor and Lecturer in the Computer and Electrical Engineering Department, Beirut Arab University (BAU). He has been a Cisco Certified Network Associate (CCNA) Instructor, since 2011. His current research interests include high-performance and energy-efficient digital circuit design, as well as high-speed low-power very large-scale integrated (VLSI) circuit design and multiple-valued logic (MVL).



**ABDALLAH KASSEM** (S'98–M'02–SM'11) received the B.S. degree in microelectronics from the University of Quebec in Montreal, in 1992, and the M.Sc. and Ph.D. degrees in microelectronics from the École Polytechnique de Montréal, in 1996 and 2004, respectively. From 1996 to 2000, he taught some courses and laboratories as an Instructor in his field at AUB, LAU, Lebanon. He joined the Electrical and Computer Engineering Department, Notre Dame University, Lebanon,

as an Assistant Professor, where he was promoted to Associate Professor, in 2011. His research interests include microelectronics design and testing, VLSI, semiconductor device modeling and simulation, microprocessors, engineering education/management, ultrasonic applications, healthcare applications, biomedical system design, smart medical devices e-Health, and m-Health. He has published approximately 60 papers in reviewed journals and conference proceedings in Lebanon and around the world. He is an Associate Editor of the *IEEE Access* and a Guest Editor *AEU—International Journal of Electronics and Communications* (Elsevier). He was a member of the organizing committee of many international conferences sponsored or technically co-sponsored by IEEE (DINWC 2018, EBECEGC 2018, ICM, ICABME, MECBME, ACTEA, ICDIPC 2016, ECECA 2016, DICTAP 2015, TAECE 2015, ICABME 2015, ICeND2014, and MELECON). He was invited as a keynote speaker in some conferences and workshops.



**AHMAD M. EL-HAJJ** (S'05–M'16) received the B.E., M.E., and Ph.D. degrees in electrical and computer engineering from the American University of Beirut, in 2007, 2009, and 2014, respectively. He is currently an Assistant Professor in the communications and electronics program and the Coordinator of the biomedical engineering program with Beirut Arab University. His research interests include wireless network optimization, radio network planning, game theory,

neuro-engineering, biomimetics, and bioinformatics. He serves as a member of the Executive Committee of the IEEE-Lebanon Section and the Local Chapter of the IEEE Communications Society (IEEE ComSoc).



**LINA A. EL-NIMRI** received the Diploma degree in computer engineering from the Leningrad Electrotechnical Institute (LETI), in 1983, and the Ph.D. degree in technical sciences “computers, complexes, and systems” from Saint-Petersburg Electrotechnical University (ETU), in 1994. From 1983 to 1989, she was an Analyst, a Programmer, and a System Administrator in several companies, where she developed business applications and applications for production and analysis purposes.

While conducting her Ph.D. research, she was also working at the university’s computer laboratory, where she designed and programmed a parametric system for the simulation of processes and their interactions.

She has taught in Beirut Arab University (BAU), the Institute Supérieur des Sciences Appliquées et Économiques (ISAE-Cnam Liban), and the Islamic University of Lebanon (IUL), and since 1999, she has been, and continues to be, an Associate Professor with Lebanese University.

Her scientific interests and teaching experiences are focused on the following areas: simulation, logic design, operating systems, compilation theory, database theory, programming languages, system analysis and design, web development, web services, multimedia, big data, and information retrieval. Besides teaching, she has advised and supervised many students in their graduation projects and master’s theses.



**ALI MASSOUD HAIDAR** received the B.S. degree in electrical engineering (electronics and telecommunications) from Beirut Arab University, in 1986, the M.E. degree in computer and information engineering from the Faculty of Engineering, University of the Ryukyus, Japan, in 1992, and the Ph.D. degree in computer engineering from the Department of Computer and Information Engineering, Faculty of Engineering, Saitama University, Japan, in 1995. He joined Hiroshima City

University, in 1995, as an Assistant Professor. Then, he joined Beirut Arab University, in 1997, where he is currently a Professor with the Department of Electrical and Computer Engineering. His scientific interests include logic theory and its applications, neural networks, Petri nets, cloud computing, digital communication, and smart grids. He published approximately 100 papers in reviewed journals and conference proceedings. He has supervised around 25 graduate students (master’s and Ph.D.).

•••

## **Appendix B**

### **CNFET-Based Designs of Ternary**

### **Half-Adder using a Novel “Decoder-less”**

### **Ternary Multiplexer based on Unary**

### **Operators**



Contents lists available at ScienceDirect

## Microelectronics Journal

journal homepage: [www.elsevier.com/locate/mejo](http://www.elsevier.com/locate/mejo)

# CNFET-based designs of Ternary Half-Adder using a novel “decoder-less” ternary multiplexer based on unary operators

Ramzi A. Jaber<sup>a,\*</sup>, Ahmad M. El-Hajj<sup>a</sup>, Abdallah Kassem<sup>b</sup>, Lina A. Nimri<sup>c</sup>, Ali M. Haidar<sup>a</sup>

<sup>a</sup> *Depart. of Electrical & Computer Eng., Beirut Arab University (BAU), Debbieh, Lebanon*

<sup>b</sup> *Depart. of Electrical & Computer Eng., Notre Dame University (NDU), Louaize, Lebanon*

<sup>c</sup> *Department of Business Computer, Lebanese University, Beirut, Lebanon*

## ARTICLE INFO

## Keywords:

Carbon Nano-Tube Field Effect Transistors (CNFET)  
Combinational logic circuit  
Multi-Valued Logic (MVL)  
Noise immunity curve  
Process variations  
Ternary MUX  
Unary operators  
VLSI

## ABSTRACT

Multi-valued logic (MVL) has more than two-valued logic to decrease the interconnections and energy consumption. Also, the market has seen a significant increase in portable electronics and embedded systems, which depend on batteries. Therefore, this paper proposes 32 nm channel CNFET-Based a Ternary Half Adder (THA) and a “decoder-less” Ternary Multiplexer (TMUX) using the proposed Unary Operator aiming to decrease the power-delay product (PDP) to preserve battery consumption; Simulations performed using the HSPICE simulator for voltage variation, temperature variation, and frequency variation. The results demonstrate the advantage of proposed models with a reduction of 46.4% in transistors count for the THA and 57.3%, and 99.3% in energy consumption (PDP) for the TMUX, and THA, respectively. Moreover, the noise immunity curve (NIC) and Monte Carlo analysis for major process variations (TOX, CNT Diameter, CNT’s Count, and Channel length) were studied. The results confirmed that the proposed THA had higher robustness and higher noise tolerance, among other designs.

## 1. Introduction

Binary circuits suffer from high-power consumption because of a massive number of interconnections that increase power consumption. Whereas, Multi-Valued Logic (MVL) circuits have more than two-valued logic to reduce interconnections, chip area, and power consumption [1].

In addition, the authors of [2] has proven that the ternary system is the most efficient in circuit complexity and cost compared to other bases.

MVL has attracted researchers’ concern over binary logic. MVL can be implemented in communication system [3], cloud vehicular networks [4], wireless sensor networks [5], circuit designs such as Logic Gates, Memory, Memristor circuit [6–8], and software (algorithm) [9,10].

Carbon Nano-Tube Field Effect Transistors (CNFET) provides the best trade-off in terms of energy efficiency and circuit speed [11] compared to CMOS [12,13], and FinFet [14].

Thus, this paper uses CNFET technology to design the ternary com-

binational logic circuits and will compare to the CNFET-based designs in Refs. [15–18].

In particular, compared to our previous work in Ref. [16], the proposed ternary half adder (THA) significantly reduces the energy consumption (PDP) by adopting a new design paradigm relying on cascading of the proposed ternary multiplexer (TMUX) rather than utilizing a ternary decoder and basic logic gates as was done in Ref. [16].

In Ref. [15], presented CNFET-based ternary decoder (TDecoder) with 16 transistors, and ternary half adder (THA) with 136 CNFETs whereas in our previous work [16], proposed a novel TDecoder with 9 CNFETs, and THA with 85 CNFETs. Both papers [15,16], use TDecoder and basic logic gates like AND, OR, and NAND to design their THA.

However, in Ref. [17], the (3:1) ternary multiplexer (TMUX) based on a TDecoder proposed with 28 CNFETs, and THA with 168 CNFETs using cascading TMUXs while in Ref. [18], presented the (3:1) ternary multiplexer without using TDecoder with 18 CNFETs.

The above existing designs suffer from high-energy consumption either due to a large number of transistors [15,17,18] or transistor arrangement [16].

\* Corresponding author.

E-mail address: [r.jaber@ieee.org](mailto:r.jaber@ieee.org) (R.A. Jaber).

<https://doi.org/10.1016/j.mejo.2019.104698>

Received 1 August 2019; Received in revised form 13 December 2019; Accepted 29 December 2019

Available online XXX

0026-2692/© 2019 Published by Elsevier Ltd.

Thus, this paper proposes a novel “decoder-less” (3:1) TMUX with 15 CNFETs using unary operators of Ternary system, and THA with 90 CNFETs.

The new designs offer a considerable gain in terms of system performance compared to the designs in Refs. [15–18], as shown in the HSPICE-based simulation results and get the lowest PDP.

The rest of the paper is organized as follows: Section 2 provides a background of CNFETs and Unary Operators, while Section 3 and Section 4 describes the proposed Unary Operator and the proposed combinational logic circuits, respectively. Section 5 discusses the simulation results and comparisons, followed by the Conclusion.

## 2. Background

### 2.1. CNFET design

Details about the Stanford CNFET model used in this work can be found in Refs. [19–21]. However, it merits referencing that the CNFETs use a semiconducting single-walled CNT as a channel for conduction. Also, “CNFET demonstrates better performance based on the intrinsic CV/I gate-delay metric, fourteen times for P-FET, and six times for N-FET than the MOSFET, even with device nonidealities. Compared to CMOS circuits, the CNFET circuits with one to ten CNTs per device is about two to ten times faster, the energy consumption per cycle is about seven to two times lower, considering the realistic layout pattern and the interconnect capacitance.”

The angle of atom arrangement along the tube in a single-walled CNT (SWCNT) is a chirality vector represented by the integer pair  $(i, j)$ . This chirality vector measures if the CNT is metallic or semiconducting; if  $i = j$  or  $i - j = 3t$ , where  $t$  is an integer, then the nanotube is metallic else it is semiconducting.

The CNFET diameter can be calculated from the equation in (1):

$$D_{\text{cnt}} = \frac{\sqrt{3} \cdot a_0}{\pi} \sqrt{i^2 + j^2 + ij} \quad (1)$$

Where  $a_0 = 0.142$  nm is the inter-atomic distance between each carbon atom and its neighbor, and the integer pair  $(i, j)$  represents the chirality vector. The characteristics of the CNFET model are identical to MOSFETs. Except for the threshold voltage, which is calculated by the following equation (2):

$$V_{\text{th}} = \frac{E_g}{2 \cdot e} = \frac{\sqrt{3}}{3} \frac{a \cdot V\pi}{e \cdot D_{\text{cnt}}} \quad (2)$$

Where  $a = 2.49$  Å is the carbon to carbon atom distance,  $V\pi = 3.033$  eV is the carbon bond energy in the tight binding model,  $e$  is the electron charge unit, and  $D_{\text{cnt}}$  is the CNT diameter.

In general, three chiralities can be used in the ternary system. The relationship between the chirality, diameter, and threshold voltage are shown in Table 1.

### 2.2. Unary operators of ternary systems

To the best of our knowledge, the literature review about unary operators of MVL is limited. It was formally defined in Ref. [22] as the

**Table 1**  
The relation between the chirality, diameter, and threshold voltage, as calculated in Refs.: [15,16].

Chirality	CNT diameter	Threshold voltage	
		N-CNFET	P-CNFET
(19,0)	1.487 nm	0.289 V	- 0.289 V
(13,0)	1.018 nm	0.428 V	- 0.428 V
(10,0)	0.783 nm	0.559 V	- 0.559 V

**Table 2**  
Truth table of the selected Unary Operators.

Ternary Input A	PTI $A_p$	NTI $A_n$	STI $\bar{A}$	$A_1$
Logic 0 (0 V)	2	2	2	0
Logic 1 (0.45 V)	2	0	1	2
Logic 2 (0.9 V)	0	0	0	0

**Table 3**  
The Chirality, diameter, and threshold voltage of the CNTs used in the proposed Unary Operator.

CNFET Type	Chirality	Diameter	$V_{th}$
P-CNFET (T1)	(19,0)	1.487 nm	- 0.289 V
N-CNFET (T2)	(19,0)	1.487 nm	0.289 V
N-CNFET (T3)	(10,0)	0.783 nm	0.559 V

number of one-place, or unary, functions of a  $p$ -valued logic system is  $p^p$ .

For binary systems where  $p = 2$ , there are only four unary functions, the identity “01”, negation “10”, and the two constant functions “00” and “11”. Whereas, for ternary systems where  $p = 3$ , there are twenty-seven ( $3^3$ ) unary functions.

Ternary logic systems can be represented in two ways: balanced  $(-1, 0, 1)$  corresponding to  $(-V_{dd}, 0, V_{dd})$ , and standard  $(0, 1, 2)$  corresponding to  $(0, V_{dd}/2, V_{dd})$ .

The selected four unary operators are described in Table 2 and derived from (3) to be used later for designing TMUX in Section IV-A.

The first three unary functions are three types of ternary inverters, the first is a positive ternary inverter (PTI),  $A_p$ , the second is a negative ternary inverter (NTI),  $A_n$ , and the third one is a standard ternary inverter (STI), which is the complement of  $A$ ,  $\bar{A}$ . The fourth function is the Decisive literal,  $A_1$ .

$$\begin{aligned} A_p &= \begin{cases} 2, & \text{if } A \neq 2 \\ 0, & \text{if } A = 2 \end{cases} \\ A_n &= \begin{cases} 2, & \text{if } A = 0 \\ 0, & \text{if } A \neq 0 \end{cases} \\ \bar{A} &= 2 - A \end{aligned} \quad (3)$$

$$A_1 = \begin{cases} 2, & \text{if } A = 1 \\ 0, & \text{if } A \neq 1 \end{cases}$$

where  $A \in \{0, 1, 2\}$ .

### 3. Proposed unary operators of ternary systems

The existing Unary Operators designs in Ref. [15] is shown in Fig. 1. It shows three types of ternary inverters circuits and the three outputs of the proposed Ternary Decoder:  $A_p, A_n, \bar{A}, A_0 = A_n, A_1$ , and  $A_2$ .

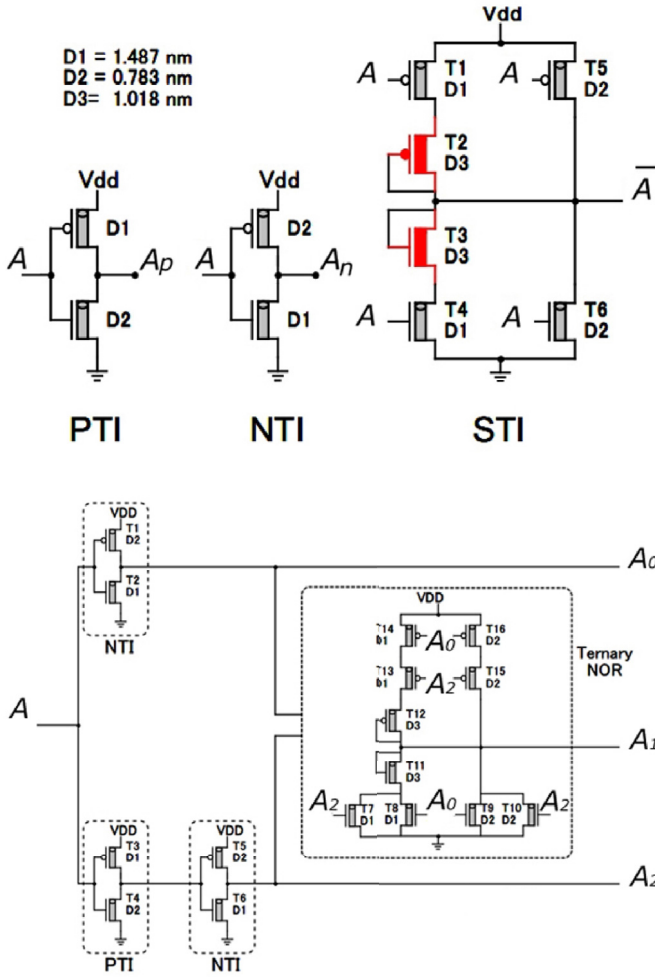
This paper will not use  $\bar{A}$ , and  $A_2$ , we will focus on  $A_1$ , which generates from Ternary NOR with ten transistors, as shown in Fig. 1.

This section proposes a new design for  $A_1$  with only three transistors, as shown in Fig. 2 with the transistor level design.

The chirality, diameter, and threshold voltage ( $V_{th}$ ) of the CNFETs used in Fig. 2 are shown in Table 3.

When the voltage of the gate varies (0 V, 0.45 V, 0.9 V), then the transistor will be turned ON or OFF. It depends on the type and the diameter of CNFET. The operation of CNFETs transistor for  $D1 = 1.487$  nm and  $D2 = 0.78$  nm describes in Table 4.

The operations of the proposed unary operators are summarised in Table 5.



The Outputs of Ternary Decoder are Unary Operators

Fig. 1. Existing unary operators in Ref. [15]:  $A_p, A_n, \bar{A}, A_0, A_1,$  and  $A_2$ .

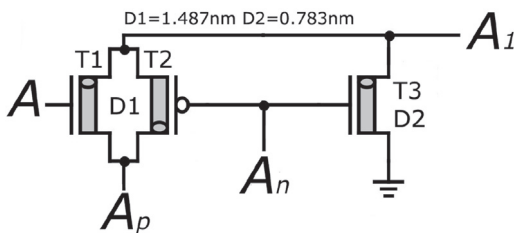


Fig. 2. The Transistor Level of the proposed Unary Operator  $A_1$ .

4. Proposed combinational circuits

This paper proposes some of the combinational circuits like TMUX and THA.

Table 4  
The State of CNFETs with  $D1 = 1.487$  nm and  $D2 = 0.783$  nm.

CNFET Type	Diameter	Voltage Gate		
		0 (0 V)	1 (0.45 V)	2 (0.9 V)
P-CNFET	D2	ON	OFF	OFF
	D1	ON	ON	OFF
N-CNFET	D2	OFF	OFF	ON
	D1	OFF	ON	ON

Table 5  
Operation of the proposed unary operator  $A_1$ .

A	$A_n$	$A_p$	Transistors Turned		Output $A_1$
			ON	OFF	
0	2	2	T3	T1,T2	0
1	0	2	T1,T2	T3	$A_p = 2$
2	0	0	T1,T2	T3	$A_p = 0$

4.1. Proposed ternary multiplexer

A Multiplexer (MUX) can select between several analog or digital input signals and forward it to a single output line.

The (3:1) Ternary Multiplexer (TMUX) is introduced with the general model as represented in Fig. 3, it has three inputs ( $I_0, I_1, I_2$ ), one selection ( $S$ ), and one output ( $Z$ ) which depends on ( $S$ ) as described in Equations (4) and (5).

$$Z = I_0 \cdot S_0 + I_1 \cdot S_1 + I_2 \cdot S_2 \tag{4}$$

$$Z = \begin{cases} I_0, & \text{if } S = 0 \\ I_1, & \text{if } S = 1 \\ I_2, & \text{if } S = 2 \end{cases} \tag{5}$$

The existing (3:1) TMUX in Ref. [17], and [18] are shown in Fig. 4.

Fig. 4 (a) shows the TMUX of [17] with 28 transistors, using the Ternary Decoder of [15] and Fig. 4 (b) shows the TMUX of [18] with 18 transistors without using the Ternary Decoder.

This section proposes the “decoder-less” (3:1) TMUX as shown in Fig. 5 with 15 transistors using unary operators,  $S_n, S_p, S_1$ , and the complement of  $S_1, \bar{S}_1$ .  $D1$  and  $D2$  are the selected diameters of CNTs used in the design.

The first nine transistors are:  $S_n$  (2 transistors),  $S_p$  (2 transistors),  $S_1$  (3 transistors), and  $\bar{S}_1$  (2 transistors), as described in Section 2 and Section 3. The detailed operation of the proposed (3:1) TMUX is shown in Table 6.

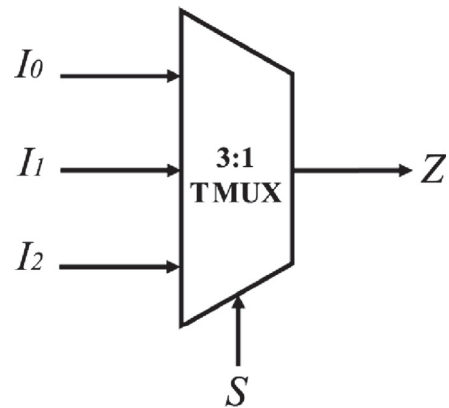


Fig. 3. The model of (3:1) TMUX.

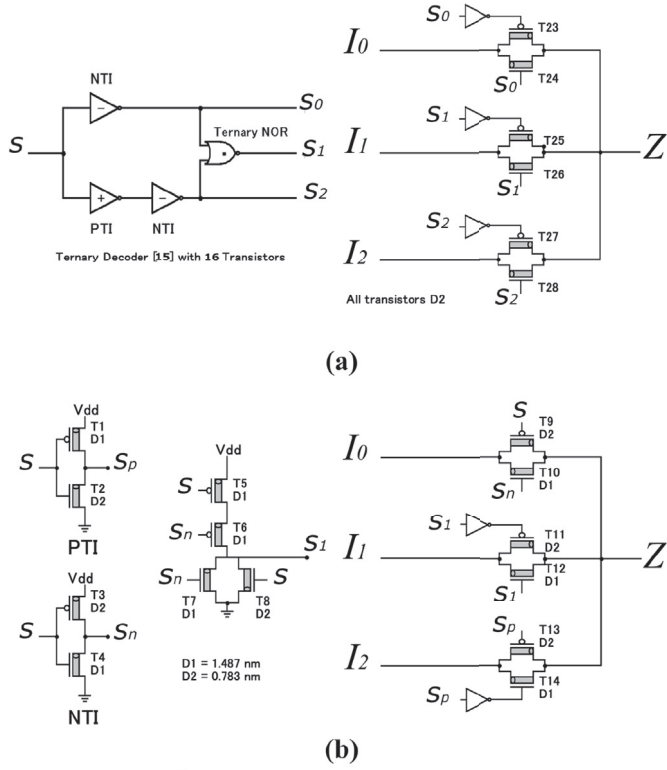


Fig. 4. Existing 3:1 TMUX: (a) In Ref. [17] with 28 transistors, (b) in Ref. [18] with 18 transistors.

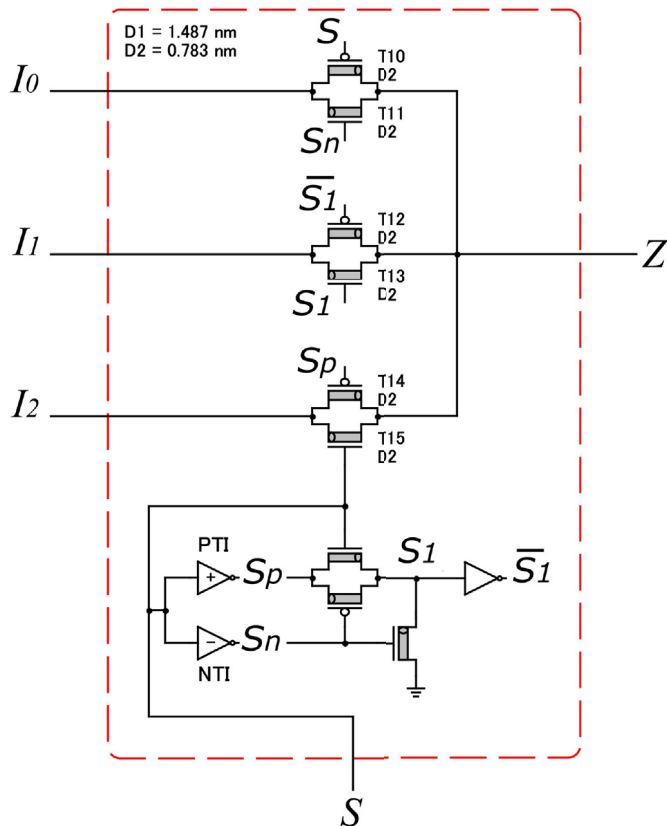


Fig. 5. Transistor Level of the proposed (3:1) TMUX with 15 CNFETs.

Table 6

The operation of the proposed (3:1) TMUX.

Selection (S)	0	1	2
$S_p$	2	2	0
$S_n$	2	0	0
$S_1$	0	2	0
$\bar{S}_1$	2	0	2
P-CNFET T10	ON	OFF	OFF
N-CNFET T11	ON	OFF	OFF
P-CNFET T12	OFF	ON	OFF
N-CNFET T13	OFF	ON	OFF
P-CNFET T14	OFF	OFF	ON
N-CNFET T15	OFF	OFF	ON
Output (Z)	$I_0$	$I_1$	$I_2$

Table 7

Truth table of THA.

A/B	$B_0(0)$	$B_1(1)$	$B_2(2)$
Sum			
$A_0(0)$	0	1	2
$A_1(1)$	1	2	0
$A_2(2)$	2	0	1
Carry			
A/B	$B_0(0)$	$B_1(1)$	$B_2(2)$
$A_0(0)$	0	0	0
$A_1(1)$	0	0	1
$A_2(2)$	0	1	1

When the selection S is logic 0 (0 V), then transistors (T10, T11) are turned ON, and (T12, T13, T14, T15) are turned OFF. Therefore, the output Z is equal to the value of the input  $I_0$ .

When the selection S is logic 1 (0.45 V), then transistors (T12, T13) are turned ON, and (T10, T11, T14, T15) are turned OFF. Therefore, the output Z is equal to the value of the input  $I_1$ .

Finally, when the selection S is logic 2 (0.9 V), then transistors (T14, T15) are turned ON, and (T10, T11, T12, T13) are turned OFF. Therefore, the output Z is equal to the value of the input  $I_2$ .

#### 4.2. Proposed ternary half adder

THA can add two ternary inputs and provides two outputs: the Sum and the Carry, as shown in Table 7.

The equations of the Sum and the Carry derived from Table 7 to design THA are:

1. Conventional design in Refs. [15,16] which uses Equation (6).
2. Cascading TMUXs design in Ref. [17] and in this work which uses Equation (7).

$$\begin{aligned} \text{Sum} &= 2 \cdot (A_0B_2 + A_1B_1 + A_2B_0) \\ &+ 1 \cdot (A_0B_1 + A_1B_0 + A_2B_2) \end{aligned} \quad (6)$$

$$\begin{aligned} \text{Carry} &= 1 \cdot (A_1B_2 + A_2B_1 + A_2B_2) \\ \text{Sum} &= A \cdot B_0 + (1.A_0 + 2.A_1 + 0.A_2) \cdot B_1 \\ &+ (2.A_0 + 0.A_1 + 1.A_2) \cdot B_2 \end{aligned} \quad (7)$$

$$\begin{aligned} \text{Carry} &= 0.B_0 + (0.A_0 + 0.A_1 + 1.A_2) \cdot B_1 \\ &+ (0.A_0 + 1.A_1 + 1.A_2) \cdot B_2 \end{aligned}$$

To derive equation (7), we start with equation (6), which is the conventional implementation of a Ternary Half-Adder:

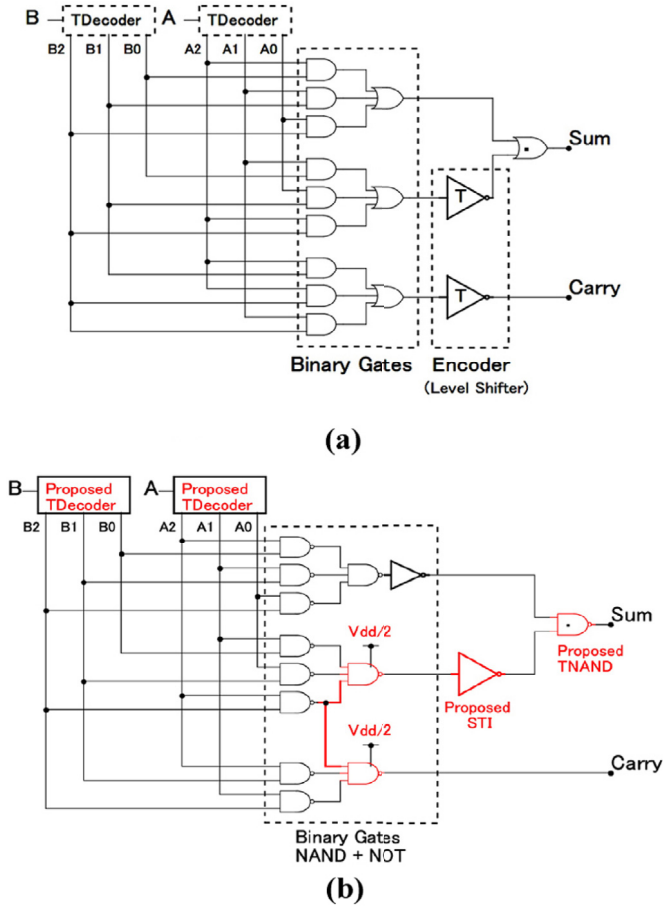


Fig. 6. Existing THA: (a) In Ref. [15] with 136 transistors, and (b) in Ref. [16] with 85 transistors.

$$\begin{aligned}
 Sum &= 2.A_0B_2 + 2.A_1B_1 + 2.A_2B_0 + 1.A_0B_1 + 1.A_1B_0 + 1.A_2B_2 \\
 &= B_0(1.A_1 + 2.A_2) + B_1(1.A_0 + 2.A_1) + B_2(2.A_0 + 1.A_2) \\
 &= B_0(0.A_0 + 1.A_1 + 2.A_2) + B_1(1.A_0 + 2.A_1 + 0.A_2) \\
 &\quad + B_2(2.A_0 + 0.A_1 + 1.A_2) \\
 Carry &= 1.A_1B_2 + 1.A_2B_1 + 1.A_2B_2 \\
 &= B_0(0) + B_1(0.A_0 + 0.A_1 + 1.A_2) + B_2(0.A_0 + 1.A_1 + 1.A_2)
 \end{aligned}$$

Where  $A_k$  and  $B_k$ ,  $k \in \{0,1,2\}$ , are the outputs of the Ternary Decoder from the inputs  $A$  and  $B$ .

The existing THAs in Refs. [15,16] are shown in Fig. 6 with 136, and 85, respectively.

Fig. 6 (a) shows the THA of [15] contains TDecoder (16 transistors), binary AND, binary OR, ternary encoder, and ternary OR.

Fig. 6 (b) shows the THA of [16] contains proposed TDecoder (9 transistors), binary NAND, binary Inverter, proposed STI, and proposed TNAND using De Morgan's Law and dual power supply ( $V_{dd}$  and  $V_{dd}/2$ ).

This section proposes THA using cascading proposed (3:1) TMUX with 90 (6\*15) transistors, as shown in Fig. 7.

The Existing THA design in Ref. [17] with 168 (6\*28) transistors is the same as Fig. 7 but with TMUX equals to 28 transistors;

The operation of the proposed THA in Fig. 7: Two ternary inputs  $A$  and  $B$  used as selection for the proposed TMUX.

When the selection  $B$  is logic 0, the output Sum will be equal to the values of  $A$  (0, 1, 2), and the output Carry will be equal to logic 0 for  $A$  (0, 1, 2), respectively.

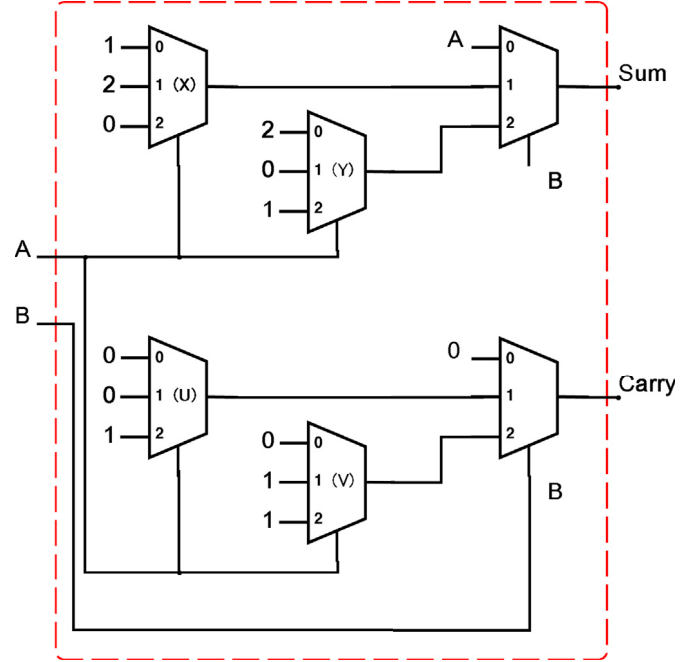


Fig. 7. Proposed THA with 90 transistors using proposed TMUX.

When the selection  $B$  is logic 1, the output Sum will be equal to the output of (X) TMUX (1, 2, 0) for  $A$  (0, 1, 2), respectively. The output Carry will be equal to the output of (U) TMUX (0, 0, 1) for  $A$  (0, 1, 2), respectively.

Finally, when the selection  $B$  is logic 2, the output Sum will be equal to the output of (Y) TMUX (2, 0, 1) for  $A$  (0, 1, 2), respectively. The output Carry will be equal to the output of (V) TMUX (0, 1, 1) for  $A$  (0, 1, 2), respectively.

The advantages of the proposed THA are:

1. The design does not use Ternary Decoder and basic logic gates such as "AND", "OR", and "NAND".
2. The design use the proposed Unary Operators and the proposed (3:1) TMUX.

All these advantages can reduce the transistors count and energy consumption.

### 5. Simulation results and comparisons

As mentioned in Section 1 that CNFET provides better energy efficiency compared to CMOS, FinFET, and other transistor technologies [11].

Therefore, the proposed (3:1) TMUX and THA are simulated and compared to CNFET-Based ternary circuits in Refs. [15–18].

Table 8 shows some essential parameters of the CNFET model used in all the circuits with brief descriptions.

The proposed THA are extensively simulated and tested using the HSPICE simulator with 32-nm channel length for power supply variation (from 0.8 V to 1 V), temperature variation (from 0 °C to 70 °C), frequency variation (from 0.5 GHz to 2 GHz), and manufacturing process variations (CNT diameter, CNT's count,  $T_{ox}$ , and channel length) by using Monte Carlo analysis.

All input signals have a fall and rise time of 15 ps The average power consumption, maximum propagation delay, and maximum PDP are obtained for all circuits.

The performance of the proposed circuits will be compared to other designs for the PDP (energy consumption).

**Table 8**  
Some of CNFET Model Parameters [19].

	Description	Value
$L_{ch}$	Physical channel length	32 nm
$L_{geff}$	The mean free path in the intrinsic CNT	100 nm
$L_{ss} (L_{dd})$	The length of doped CNT source-side (drain-side) extension region	10 nm
$E_{fi}$	The Fermi level of the doped tube	0.6 eV
$K_{gate}$	The dielectric constant of high-k top gate dielectric material (planer gate)	4
$T_{ox}$	The thickness of the high-k top gate dielectric material ( $HfO_2$ )	1 nm
$Pitch$	The distance between two adjacent CNTs within the same device	20 nm
$Tubes$	The number of tubes	1

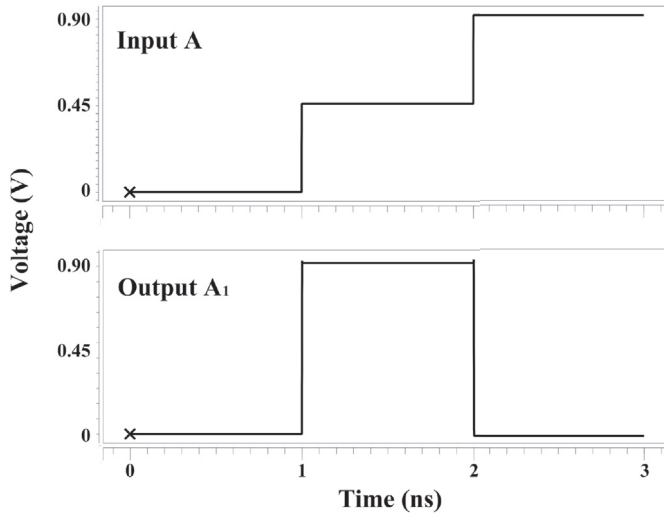


Fig. 8. Transient analysis of the proposed  $A_1$ .

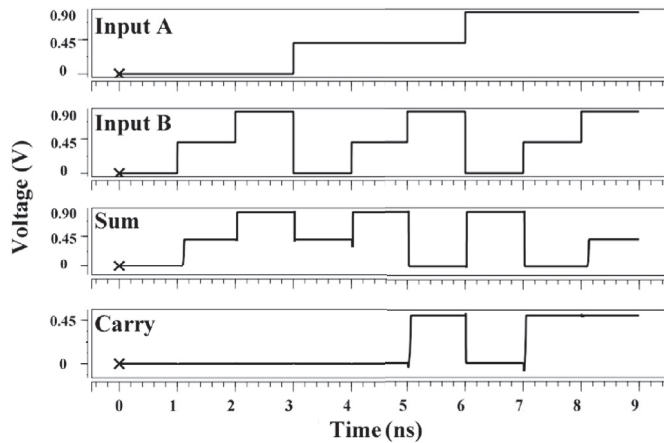


Fig. 9. Transient analysis of the proposed THA.

Fig. 8 and 9 illustrate the transient analysis of the proposed Unary Operator and THA.

### 5.1. Comparison of ternary multiplexers

The proposed TMUX is compared to the TMUX in Refs. [17,18]. The three circuits are simulated and tested using the HSPICE simulator with a frequency of 1 GHz, room temperature 27 °C, and a supply voltage 0.9 V (Vdd).

For a fair comparison, the three circuits are simulated using the same software, implementation techniques, CNFET model parameters,

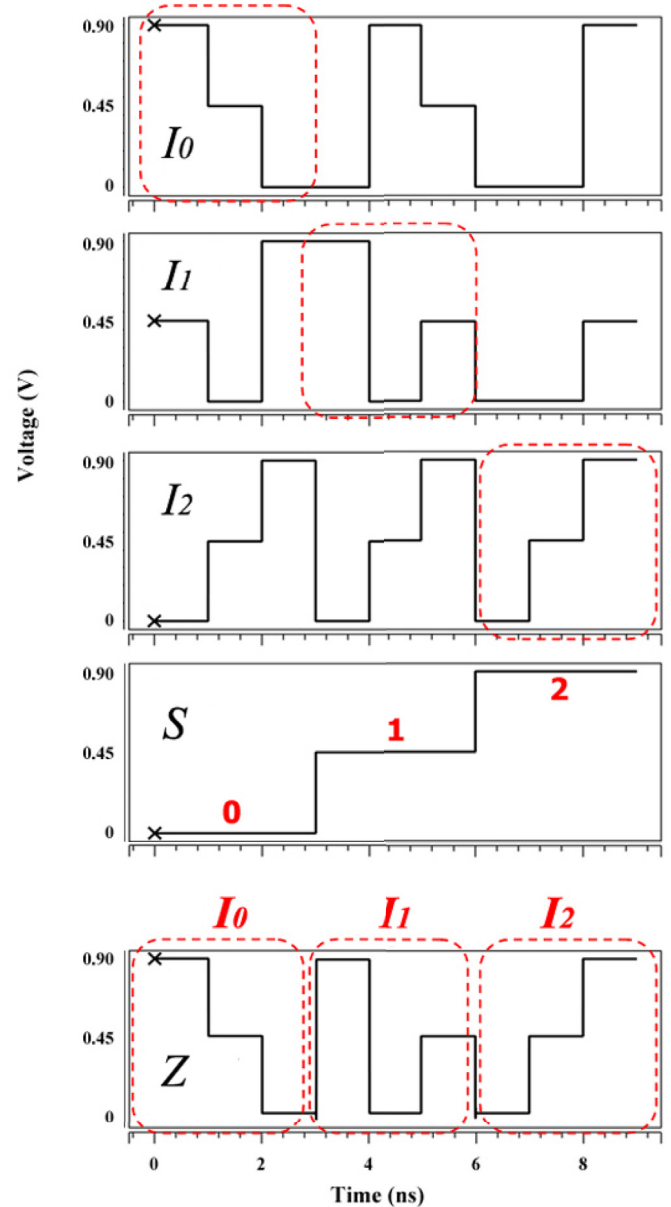


Fig. 10. Transient analysis of the proposed (3:1) TMUX (dotted rectangle corresponds to input selected according to S).

and the same values of  $(I_0, I_1, I_2, S)$  as follows:

$$I_0 = (210021002)_3, I_1 = (102201001)_3, I_2 = (012012012)_3 \text{ and } S = (000111222)_3.$$

Fig. 10 illustrates the transient analysis of the proposed (3:1) TMUX. The dotted rectangle for each of the three inputs  $(I_0, I_1, I_2)$  is selected according to the ternary selection (S) to get the output (Z).

**Table 9**  
Comparison of 3 TMUXs in terms of the transistors count at Vdd (0.9 V), temperature (27 °C), and frequency (1 GHz).

	CNFETs No.	Power ( $\mu$ W) AVG.	Delay (ps)		PDP ( $\times 10^{-20}$ J)	
			AVG.	Max.	AVG.	Max.
TMUX [17]	28	67.3	2.35	14.3	15.8	96.3
TMUX [18]	18	60.1	1.76	9.64	10.57	57.9
<b>Proposed TMUX</b>	<b>15</b>	<b>48.4</b>	<b>1.62</b>	<b>8.5</b>	<b>7.8</b>	<b>41.1</b>

**Table 10**  
Comparison of transistors count.

	THA
[15] Using TDecoder and Basic Logic Gates	136
[16] Using De Morgan’s Law	85
[17] Using Cascading TMUXs	168
<b>Proposed Using Cascading TMUXs</b>	<b>90</b>

Table 9 shows the comparison between the three TMUXs in terms of the transistors count, average power consumption, (average & maximum) propagation delay, and (average & maximum) PDP.

This comparison of the proposed “decoder-less” TMUX demonstrates a notable reduction in transistors count around 46.43%, and 16.67% compared to TMUX in Refs. [17,18], respectively. Also, a notable reduction in PDP of around 57.32%, and 29.02% compared to Ref. [17], and [18], respectively.

5.2. Comparison of transistors count for THAs

Albeit not being the only factor, minimizing the transistors’ count is a good metric to compare different circuit implementations.

Table 10 shows the comparison of transistors count for the THA of [15–17].

The proposed THA has a notable reduction in transistors count. Around 33.82%, –5.88%, and 46.43% compared to THA in Refs. [15–17], respectively.

5.3. Comparison of different THA circuits

5.3.1. Voltage variation

The effect of power supply variation (from 0.8 V to 1 V) on the performance metrics of all proposed circuits is studied.

Fig. 11 shows the comparison to the existing THA in Refs. [15–17] in terms of the average power consumption as shown in Fig. 11(a), maximum propagation delay as shown in Fig. 11(b), and maximum PDP as shown in Fig. 11(c) for a fixed frequency of 1 GHz, temperature of 27 °C, and by varying the supply voltages (from 0.8 V to 1 V).

The comparison of the proposed THA demonstrates a notable reduction in PDP, as shown in Fig. 11(c). For Vdd = 0.8 V, around 99.33%, 95.11%, and 95.54% compared to Refs. [15–17], respectively. For Vdd = 0.9 V, around 98.45%, 94.39%, and 94.67% compared to Refs. [15–17], respectively. For Vdd = 1 V, around 96.69%, 85.71%, and 88.53% compared to Refs. [15–17], respectively.

5.3.2. Temperature variation

Temperature noise is one of the most critical issues which negatively affect the performance of the circuit.

The effect of temperature variation (from 0 °C to 70 °C) on the performance metrics of all proposed circuits is studied.

Fig. 12 shows the comparison to the existing THA in Refs. [15–17] in terms of the average power consumption as shown in Fig. 12(a), maximum propagation delay as shown in Fig. 12(b), and maximum PDP as shown in Fig. 12(c) for a fixed frequency of 1 GHz, supply voltage of 0.9 V, and by varying the temperatures (from 0 °C to 70 °C).

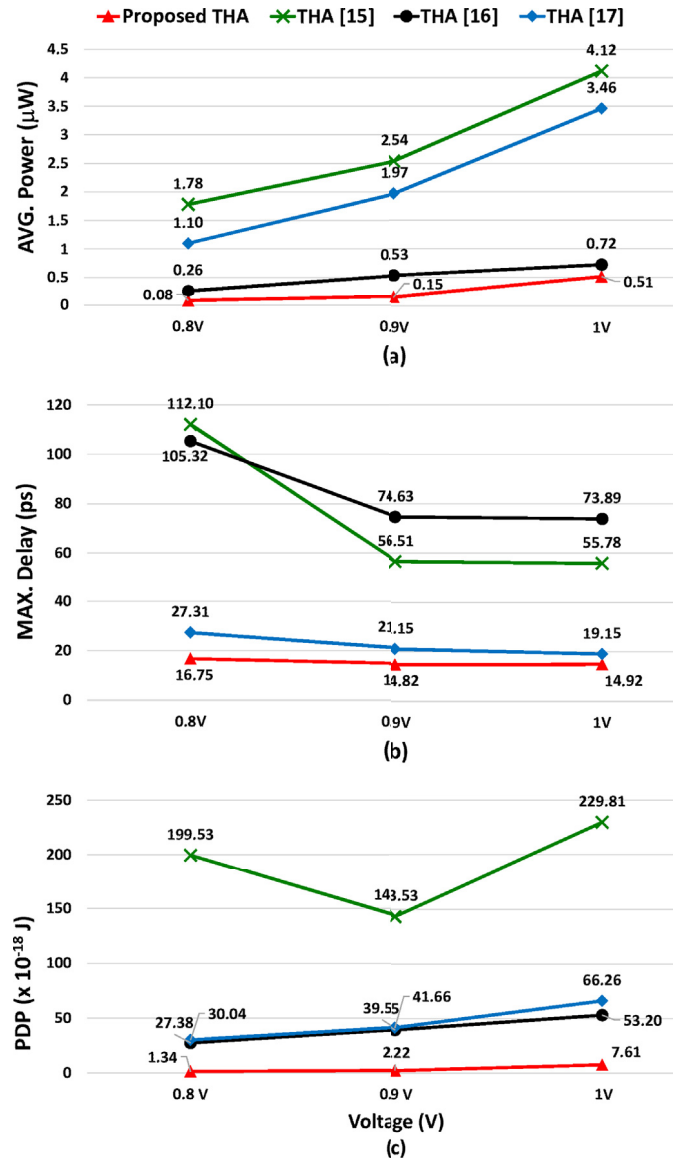


Fig. 11. Voltage variation of All THAs: (a) For Average Power, (b) for Maximum Delay, and (c) for PDP.

The comparison of the proposed THA demonstrates a notable reduction in PDP, as shown in Fig. 12(c). For Temperature = 0 °C, around 97.7%, 94.4%, and 91.96% compared to Refs. [15–17], respectively. For Temperature = 10 °C, around 98.2%, 94.15%, and 93.66% compared to Refs. [15–17], respectively. For Temperature = 27 °C, around 98.45%, 94.39%, and 94.67% compared to Refs. [15–17], respectively. For Temperature = 50 °C, around 98.26%, 94.27%, and 93.99% compared to Refs. [15–17], respectively. For Temperature = 70 °C, around 98.19%, 94%, and 93.45% compared to Refs. [15–17], respectively.

5.3.3. Frequency variation

Electronic circuits behave very differently at high frequencies due to a change in the behavior of passive components (resistors, inductors, and capacitors) and parasitic effects on active components and PCB tracks.

The effect of frequency variation (from 0.5 GHz to 2 GHz) on the performance metrics of all proposed circuits is studied.

Fig. 13 shows the comparison to the existing THA in Refs. [15–17] in terms of the average power consumption as shown in Fig. 13(a), maximum propagation delay as shown in Fig. 13(b), and maximum PDP

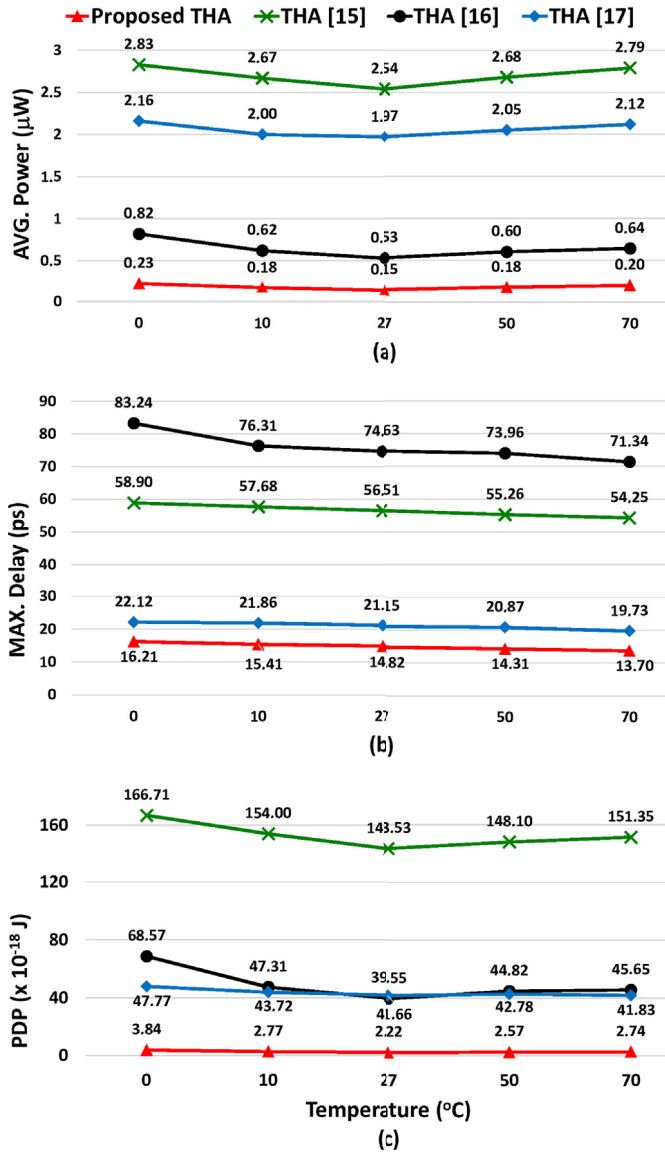


Fig. 12. Temperature variation of all THAs: (a) For average power, (b) for maximum delay, and (c) for PDP.

as shown in Fig. 13(c) for a fixed supply voltage of 0.9 V, temperature of 27 °C, and by varying the frequencies (from 0.5 GHz to 2 GHz).

The comparison of the proposed THA demonstrates a notable reduction in PDP, as shown in Fig. 13(c). For frequency = 0.5 GHz, around 98.8%, 95.23%, and 96.01% compared to Refs. [15–17], respectively. For frequency = 1 GHz, around 98.45%, 94.39%, and 94.67% compared to Refs. [15–17], respectively. For frequency = 2 GHz, around 97.76%, 91.94%, and 92.46% compared to Refs. [15–17], respectively.

### 5.3.4. Process variations

Process variations have a great impact on the performance and robustness of nanoscale devices and circuits. Hence, all THA circuits are tested in the presence of major process variations: TOX, CNT diameter, CNT's count, and channel length [23] (see Fig. 14).

#### TOX.

In the Stanford CNFET model, TOX is the oxide thickness of the Gate Dielectric  $k_1$  material ( $HfO_2$ ), as shown in 14. The variation in TOX will lead to leakage current. By decreasing TOX, the leakage current will increase, then the PDP will also increase and Vice Versa.

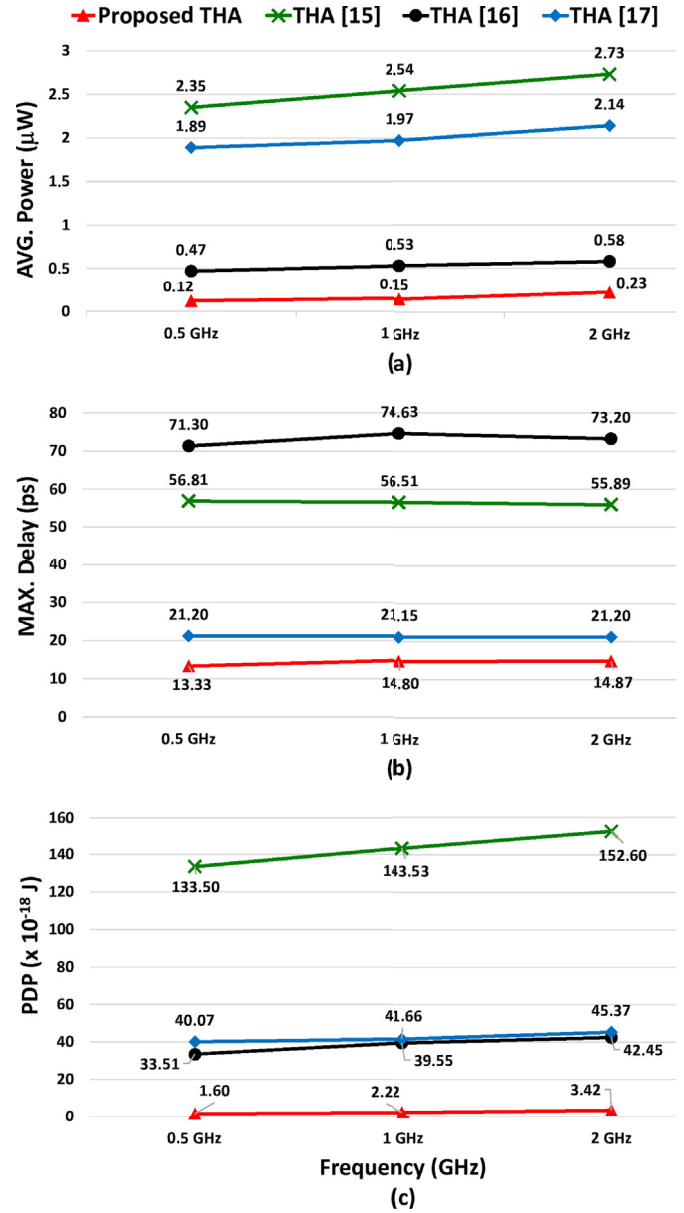


Fig. 13. Frequency variation of all THAs: (a) For average power, (b) for maximum delay, and (c) for PDP.

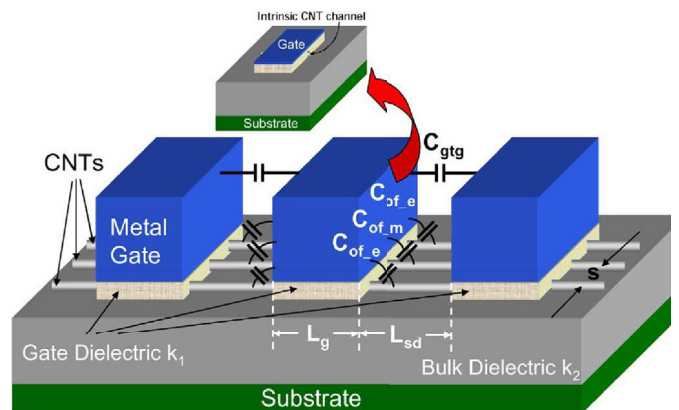


Fig. 14. Stanford CNFET model.

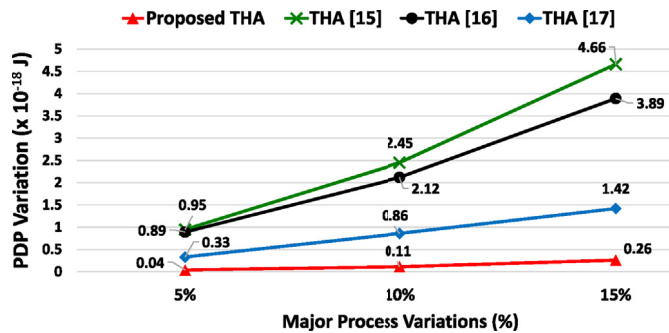


Fig. 15. Major Process Variations: TOX, CNT Diameter, CNT's Count, and Channel length.

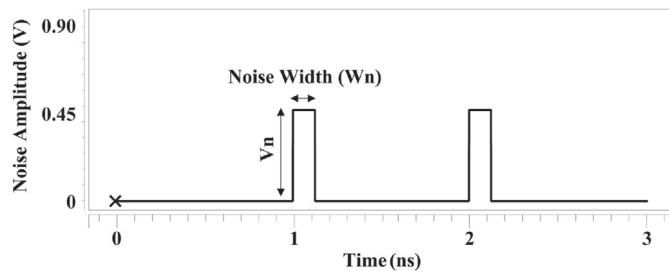


Fig. 16. Noise signal.

CNT Diameter.

The CNT diameter variation is one of the multiple problems of CNFET imperfections caused due to nonidealities in the CNT synthesis process, which negatively affects the performance of CNFET circuits because this variation will lead to variation in threshold voltage. This problem has more impact on MVL designs where transistors with different threshold voltages are applied.

CNT's Count.

Variation in the count of CNTs leads to a change in circuit parameters because it changes the output current of the transistor, which may cause a problem in the circuit functionality.

Channel Length.

Variation in channel length will lead to the variation of the channel between drain and source, which negatively affects the performance of CNFET circuits.

Therefore, this paper uses Monte Carlo analysis based on the Gaussian distributions with 5%, 10%, and 15% variations at the  $\pm 3\sigma$  level with the number of simulation running is equal to 1000.

Monte Carlo analysis is based on statistical distributions. It realistically simulates mismatching and process variations. In each simulation run, it calculates every parameter randomly according to a statistical distribution model.

The energy variations of all THA circuits in the presence of the major process variations are shown in Fig. 15.

As shown in Fig. 15, The proposed THA has lower sensitivity to process variations and is more robust in comparison with the other designs because the graph of the proposed THA is under all the investigated circuits.

### 5.3.5. Noise effect

Digital circuits are inherently noise-tolerant, and they are only affected by noises with high amplitude and wide width.

The Noise Immunity Curve (NIC) is used to determine the impact of noise inputs on all THAs circuits.

The noise signal, Fig. 16, is injected into inputs of THAs.

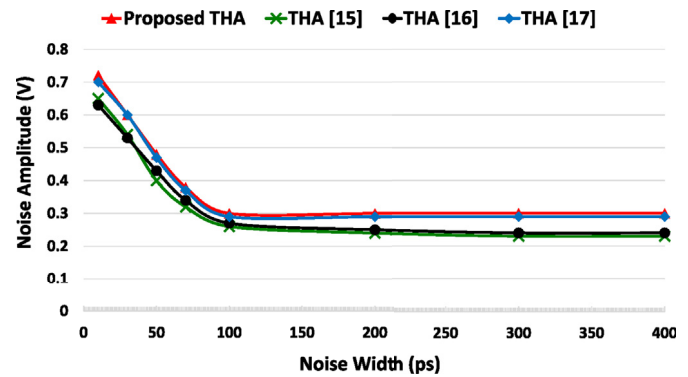


Fig. 17. Noise immunity curve (NIC).

As shown in Fig. 16, the noise signal has pulse width ( $W_n$ ) and pulse amplitude ( $V_n$ ).

Each point on the NIC curve is a pair of ( $W_n$ ,  $V_n$ ). Above that point, the circuit will produce an error on the output. The region above the NIC curve is an unsafe zone, whereas the region below the NIC curve is a safe zone against noise pulses.

Therefore, any circuit with higher NIC demonstrates a more noise-tolerant circuit [24].

As shown in Fig. 17, The proposed THA and the THA of [17] show higher noise immunity compared to our previous THA in Ref. [16] and the THA in Ref. [15] because their graphs are above of the others.

## 6. Conclusion

This paper proposed a Ternary Half Adder based on a proposed (3:1) Ternary Multiplexer using 32 nm channel CNFET, which aims to optimize the trade-off between performance and energy efficiency.

The comparison of the proposed approach to existing designs demonstrates notable performance gains for different simulation environments using HSPICE simulator with voltage variation, temperature variation, and frequency variation. Moreover, Monte Carlo analysis for major process variations (TOX, CNT Diameter, CNT's Count, and Channel length) was studied for all THAs models. The results confirmed that the proposed THA had higher robustness, among other designs. In addition, the noise immunity curve (NIC) showed that the proposed THA had a higher noise tolerance than other models.

Therefore, the proposed circuits can be implemented in low-power portable electronics and embedded systems to preserve battery consumption.

### Declaration of competing interest

None.

### Appendix A. Supplementary data

Supplementary data to this article can be found online at <https://doi.org/10.1016/j.mejo.2019.104698>.

### References

- [1] S. Hosseini, S. Etezadi, A novel very low-complexity multi-valued logic comparator in nanoelectronics, Springer Circuits, Systems, and Signal Processing 2 (June 2019) 1–22, <https://doi.org/10.1007/s00034-019-01158-2>.
- [2] S. Hurst, S. Etezadi, Multiple-valued logic its status and its future, IEEE Trans. Comput. 133 (1) (Dec. 1984) 1160–1179, <https://doi.org/10.1109/TC.1984.1676392>.
- [3] M. Abdelaziz, T. Gulliver, Ternary trellis coded modulation, IEEE Access 7 (April 2019) 49027–49038, <https://doi.org/10.1109/ACCESS.2019.2909707>.

- [4] Q. Yanq, B. Zhu, S. Wu, An architecture of cloud-assisted information dissemination in vehicular networks, *IEEE Access* 4 (May 2016) 2764–2770, <https://doi.org/10.1109/ACCESS.2016.2572206>.
- [5] N. Saleh, A. Kassem, A. Haidar, Energy-efficient architecture for wireless sensor networks in healthcare applications, *IEEE Access* 6 (Jan. 2018) 6478–6486, <https://doi.org/10.1109/ACCESS.2018.2789918>.
- [6] L. Sardinha, D. Silva, M. Vieira, L. Vieira, O. Neto, Tcam/cam-qca: (ternary) content addressable memory using quantum-dot cellular automata, *Microelectron. J.* 46 (7) (July 2015) 563–571, <https://doi.org/10.1016/j.mejo.2015.03.020>.
- [7] N. Soliman, M. Fouda, A. Alhurbi, L. Said, A. Madian, A. Radwan, Ternary functions design using memristive threshold logic, *IEEE Access* 7 (April 2019) 48371–48381, <https://doi.org/10.1109/ACCESS.2019.2909500>.
- [8] N. Soliman, M. Fouda, A. Radwan, Memristor-cntfet based ternary logic gates, *Microelectron. J.* 72 (Feb. 2018) 74–85, <https://doi.org/10.1016/j.mejo.2017.12.008>.
- [9] A spectral algorithm for ternary function classification; vol. 1 of 1, in: D. Miller, M. Soeken (Eds.), *IEEE 48th Int. Symp. On Multiple-Valued Logic (ISMVL)*, IEEE, Linz, Austria, 2018.
- [10] A. Basiri, S. Mahammad, High speed multiplexer design using tree based decomposition algorithm, *Microelectron. J.* 51 (May 2016) 99–111, <https://doi.org/10.1016/j.mejo.2016.02.009>.
- [11] G. Hills, M. Bardou, G. Doornbos, D. Yakimets, P. Schuddinck, R. Baert, D. Jang, L. Mattii, S. Sherazi, D. Rodopoulos, R. Ritzenthaler, C.S. Lee, A. Thean, I. Radu, A. Spessot, P. Debacker, F. Catthoor, P. Raghavan, M. Shulaker, H.S. Philip Wong, S. Mitra, Understanding energy efficiency benefits of carbon nanotube field-effect transistors for digital vlsi, *IEEE Trans. Nanotechnol.* 17 (6) (Nov. 2018) 1259–1269, <https://doi.org/10.1109/TNANO.2018.2871841>.
- [12] A Novel implementation of ternary decoder using CMOS DPL binary gates, in: R. Jaber, A. El-Hajj, L. Nimri, A. Haidar (Eds.), 2018 Int. Arab Conf. On Information Technology (ACIT), IEEE, Werdanye, Lebanon, 2018 <https://doi.org/10.1109/ACIT.2018.8672698>.
- [13] M. Jahangir, J. Mounika, Design and simulation of an innovative cmos ternary 3 to 1 multiplexer and the design of ternary half adder using ternary 3 to 1 multiplexer, *Microelectron. J.* 90 (Aug. 2019) 82–87, <https://doi.org/10.1016/j.mejo.2019.05.007>.
- [14] D. Kundu, S. Guin, G. Jyothi, S. Sridevi (Eds.), *High Speed FinFET Traff Comparator Based Function Generator*. Chennai, India: 2018 International Conference on Computation of Power, Energy, Information and Communication (ICCPEIC), 2018.
- [15] S. Lin, Y. Kim, F. Lombardi, Cntfet-based design of ternary logic gates and arithmetic circuits, *IEEE Trans. Nanotechnol.* 10 (March 2011) 217–225, <https://doi.org/10.1109/TNANO.2009.2036845>.
- [16] R. Jaber, A. Kassem, A. El-Hajj, L. Nimri, A. Haidar, High-performance and energy-efficient cnfet-based designs for ternary logic circuits, *IEEE Access* 7 (July 2019) 93871–93886, <https://doi.org/10.1109/ACCESS.2019.2928251>.
- [17] D. Das, A. Banerjee, V. Prasad (Eds.), *Design of Ternary Logic Circuits Using CNTFET*. Howrah, India: Int. Symp. On Devices, Circuits and Systems (ISDCS), March 2018.
- [18] D. Das, A. Banerjee, V. Prasad, Design of ternary logic circuits using cntfet, *IEEE Transactions on Circuits and Systems I: Regular Papers* 64 (8) (Aug. 2017) 2146–2159.
- [19] Stanford, , CA, , USA, . Stanford university cnfet model website. [online]. Accessed: July 1, 2019. . Available: <http://nano.stanford.edu/model.php?id= 23>
- [20] J. Deng, H.S. Wong, A compact spice model for carbon-nanotube field-effect transistors including nonidealities and its application - part i: model of the intrinsic channel region, *IEEE Trans. Electron Devices* 54 (12) (Dec. 2007) 3186–3194, <https://doi.org/10.1109/TED.2007.909030>.
- [21] J. Deng, H.S. Wong, A compact spice model for carbon-nanotube field-effect transistors including nonidealities and its application - part ii: full device model and circuit performance benchmarking, *IEEE Trans. Electron Devices* 54 (12) (Dec. 2007) 3195–3205, <https://doi.org/10.1109/TED.2007.909043>.
- [22] D. Miller, M. Thornton, *Multiple Valued Logic: Concepts and Representations*. 12, Morgan & Claypool, San Rafael, CA, USA, 2008 <https://doi.org/10.1016/j.mejo.2019.01.013>.
- [23] S. Ebrahimi, M. Reshadinezhad, A. Bohlooli, A new design method for imperfection-immune cnfet-based circuit design, *Microelectron. J.* 85 (2019) 62–71, <https://doi.org/10.1016/j.mejo.2019.01.013>.
- [24] G. Balamurugan, N. Shanbhag, The twin-transistor noise-tolerant dynamic circuit technique, *IEEE J. Solid State Circuits* 36 (2) (2001) 273–280, <https://doi.org/10.1109/4.902768>.

## **Appendix C**

# **A Novel Implementation of Ternary Decoder Using CMOS DPL Binary Gates**

# A Novel Implementation of Ternary Decoder Using CMOS DPL Binary Gates

Publisher: IEEE

**4 Author(s)** Ramzi Jaber ; Ahmad Elhajj ; Lina Nimri ; Ali Haidar [View All Authors](#)

1  
Paper  
Citation

44  
Full  
Text Views



## Abstract

### Document Sections

- I. Introduction
- II. Existing Ternary Decoder
- III. Double Pass-Transistor Logic (DPL)
- IV. Proposed Ternary Decoder
- V. Simulation Results & Comparisons

## Abstract:

This paper proposes a novel implementation of Ternary Decoder using CMOS DPL (Double Pass Logic) Binary logic gates, in digital CMOS technology. The physical design of the circuits is simulated and tested with Micro-Cap 10 SPICE simulator. The Proposed Ternary Decoder circuit can be used in VLSI design. The Proposed decoder circuit will be the basic circuit to create other Ternary Logic Circuits like Ternary Logic Gates, Ternary Memory, Adder, Multiplier, Multiplexer, and others. The simulation results demonstrate the merits of the approach in terms of reduced number of transistors by 25% compared to the existing ternary decoder.

**Published in:** 2018 International Arab Conference on Information Technology (ACIT)

**Date of Conference:** 28-30 Nov. 2018

**INSPEC Accession Number:** 18530437

**Date Added to IEEE Xplore:** 25 March 2019

**DOI:** 10.1109/ACIT.2018.8672698

# A Novel Implementation of Ternary Decoder Using CMOS DPL Binary Gates

Ramzi Jaber<sup>a</sup>, Ahmad ElHajj<sup>a</sup>, Lina Nimri<sup>b</sup>, Ali Haidar<sup>a</sup>

<sup>a</sup>Dept.of Electrical & Computer Eng., Beirut Arab University

<sup>b</sup>Dept. of Business Computer, Lebanese University

Beirut, Lebanon

[r.jaber@bau.edu.lb](mailto:r.jaber@bau.edu.lb) , [a.elhajj@bau.edu.lb](mailto:a.elhajj@bau.edu.lb) , [lnimri@ul.edu.lb](mailto:lnimri@ul.edu.lb) , [ari@bau.edu.lb](mailto:ari@bau.edu.lb)

**Abstract**—this paper proposes a novel implementation of Ternary Decoder using CMOS DPL (Double Pass Logic) Binary logic gates, in digital CMOS technology. The physical design of the circuits is simulated and tested with Micro-Cap 10 SPICE simulator. The Proposed Ternary Decoder circuit can be used in VLSI design.

The Proposed decoder circuit will be the basic circuit to create other Ternary Logic Circuits like Ternary Logic Gates, Ternary Memory, Adder, Multiplier, Multiplexer, and others. The simulation results demonstrate the merits of the approach in terms of reduced number of transistors by 25% compared to the existing ternary decoder.

**Keywords**— DPL, Ternary Circuit, Multi-Valued Logic, Ternary Decoder.

## I. INTRODUCTION

Almost all the digital devices have been designed using two-valued logic till date. In binary logic, each wire can hold two states: 0 and 1. The performances of digital devices rely mostly on how quickly the states can be changed, which determines the speed of the devices. Multiple-valued logic (MVL) systems are multi-voltage levels. Therefore, MVL circuits have the following advantages over binary circuits [1- 6].

(i) In MVL circuits, as each wire can hold more information than binary logic, then the number of interconnections in the circuit is reduced and hence, the complexity of the chip is also reduced. (ii) Therefore MVL circuit provides lower power dissipation.

When using MVL in CMOS binary logic design, the performance will be better [7, 8].

Base 3 system (ternary logic) shows better results in the efficiency and the complexity as compared to higher bases [9]. Ternary logic digit (trits) has three values (0, 1, 2) corresponding to (0 volt, Vdd/2, Vdd).

For example, a decimal number 234 is 11101010 (8-bits) in binary whereas, in ternary equivalent is 22200 (5-trits).

Thus the reduction in wires around 37.5% just for 8 bits, if more bits or wires the reduction will be more. That is why in the ternary circuit have lower interconnections, reducing the complexity, the power dissipation, and the propagation delay as compared to the binary circuit.

To the best of our knowledge, lot of research papers tries to design a ternary decoder using ternary logic gates like Standard Ternary Inverter (STI), Negative Ternary Inverter (NTI), Positive Ternary Inverter (PTI) and Ternary NOR logic gate [10,11,12] while the proposed Ternary Decoder only uses Binary AND logic gates, Binary NOR logic gate, MOSFET transistor , and resistor .

The Results from the proposed Ternary Decoder are less number of Transistors by 25% , therefore, gets a smaller chip area, reduced the energy consumptions, and decrease in the propagation delay.

The rest of the paper is organized as follows: Section II presents the existing Ternary Decoder, Section III presents the background of DPL, The proposed Ternary Decoder approach is presented in Section IV, Simulation results & Comparisons are discussed in Section V. Concluding remarks follow in Section VI.

## II. EXISTING TERNARY DECODER

The paper [12] presents three kinds of ternary inverters and ternary NOR to propose his Ternary Decoder. The first is Standard Ternary Inverter (STI), the second is Negative Ternary Inverter (NTI) and the third one is Positive Ternary Inverter (PTI). Table I shows their outputs.

Table I. Existing 3 ternary inverters truth table

Ternary Input	STI	NTI	PTI
0	2	2	2
1	1	0	2
2	0	0	0

The ternary decoder is one ternary input and three binary output circuit by generating unary functions for an input  $x$  is given by:

$$X^k = \begin{cases} 2 & \text{if } X = k \\ 0 & \text{if } X \neq k \end{cases} \quad (1)$$

Where k can take three logic values: logic 0, logic 1 and logic 2. The decoder outputs can take only two logic values i.e., logic 2 and logic 0, corresponding to logic 1 and logic 0 in binary logic.

The decoder consists of a PTI gate, two NTI gates, and a NOR gate, as shown in Fig. 1 and the truth table in Table II.

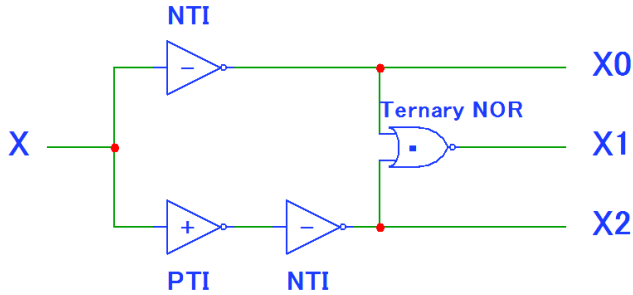


Fig. 1. Ternary Decoder [12]

Table II. The Ternary Decoder truth table

Ternary Inputs	X0	X1	X2
Logic 0	2	0	0
Logic 1	0	2	0
Logic 2	0	0	2

### III. DOUBLE PASS-TRANSISTOR LOGIC (DPL)

As shown in Fig.2 [14], Double Pass-transistor Logic (DPL) is a modified version of Complementary Pass-transistor Logic (CPL) by adding PMOS transistors in parallel with the NMOS transistors to eliminate the problems of noise margin and speed degradation at reduced voltages supply associated in CPL circuits.

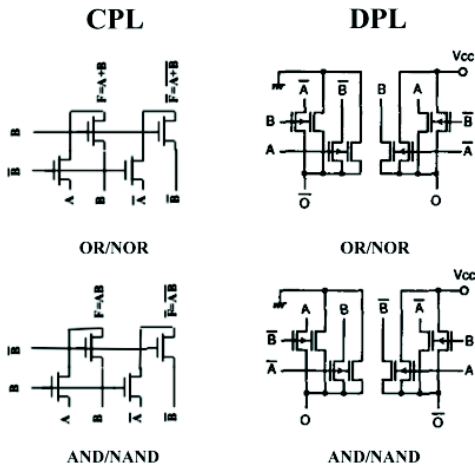


Fig.2. DPL Gates Design [14]

### IV. PROPOSED TERNARY DECODER

As seen in section II the Ternary Decoder using Ternary logic gates is used to design Half Adder [12], Full Adder, Multiplier [12] and Multiplexer [10].

When design it with Binary Logic Gates will be faster and simpler [13].

Therefore a novel circuit is designed to implement Ternary decoder using CMOS DPL Binary logic gates with power supply VDD equals 1.8 volts which can reduce the power consumption and decrease the propagation delay.

Fig .3 represents the proposed Ternary Decoder.

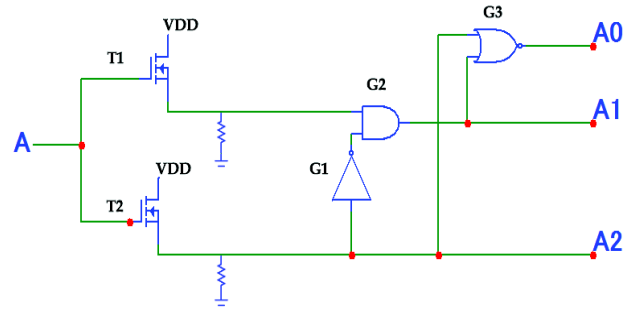


Fig. 3. The proposed Ternary Decoder

As shown in Fig.3. Two N-channels MOSFET, T1 with threshold voltage equals 0.7 volts and T2 with threshold voltage equals 1.4 volts, and three CMOS DPL Binary logic gates, G1 is "Inverter" logic gate, G2 is "AND" logic gate and G3 is "NOR" logic gate and two resistors 100 K Ω.

The explanation of Fig.3 is shown in Table III.

Table III. The proposed Ternary Decoder outputs

Ternary Input (A)	T1 Vth= 0.7v	T2 Vth= 1.4v	Binary Output		
			A0	A1	A2
Logic 0 (0v)	Open	Open	1(1.8V)	0	0
Logic 1 (0.9v)	Close	Open	0	1(1.8V)	0
Logic 2 (1.8v)	Close	Close	0	0	1(1.8V)

The proposed ternary decoder can implement almost all ternary logic circuits

### V. SIMULATION RESULTS & COMPARISONS

The proposed Ternary Decoder is analyzed using the Micro-cap 10 Spice simulator. The simulated circuits utilize an implementation of the AND and NOR DPL gates as shown in Fig.2 with a temperature 25°C, the power supply is set to 1.8 volts, the average propagation delay is 42.56 ps and the average power is 4.08 μw [16].

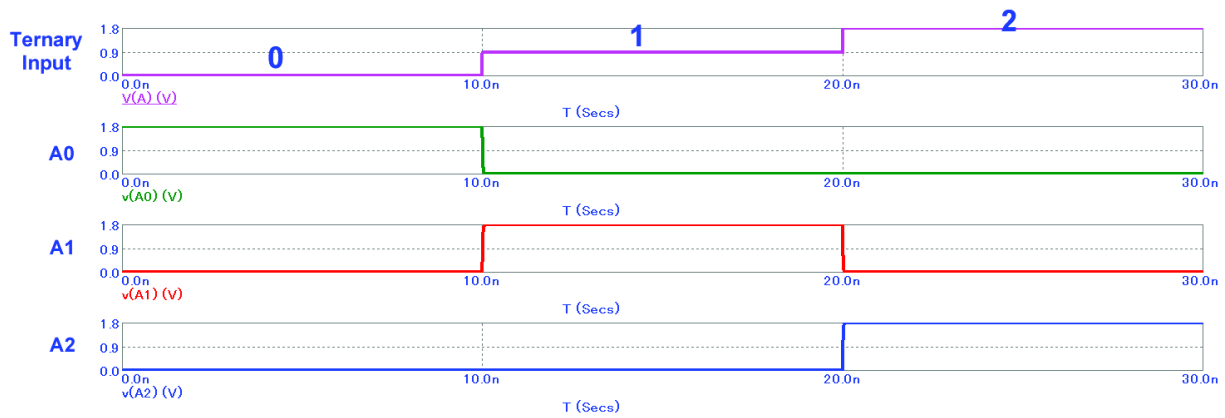


Fig.4. Transient Analysis of the Proposed Ternary Decoder

Fig. 4 shows the simulation transient analysis of the proposed circuit; The X-axis represents the time in 10 ns units and the Y-axis represents the voltage in 0.9 v units.

The Avg. power of the proposed Ternary Decoder is 13  $\mu$ w and the Max. Propagation delay is 0.14 ns

The existing Ternary Decoder [12] has 16 transistors while the proposed one has 12 transistors; therefore, the improvement of the proposed ternary decoder is 25% less number of the transistor.

## VI. CONCLUSION

In this paper, a new Ternary Decoder is proposed. The proposed approach takes one Ternary Digit (trits) and produces three Binary bits using a DPL (Double Pass Logic) CMOS Binary gates to design other Ternary Logic circuits like Ternary Logic Gates, Ternary Memory, Adder, Multiplier, Multiplexer, and others.

The simulation results demonstrate the merits of the approach in terms of reduced number of transistors by 25% compared to the existing ternary decoder and using binary logic gates.

## REFERENCES

- [1] M. H. Moaiyeri, K. Navi, O. Hashemipour, "Design and evaluation of CNTFET-based quaternary circuits," *Circuits, Systems, and Signal Processing*, vol. 31(5), pp. 1631-1652, Oct. 2012.
- [2] Vaibhav Jane, Sanjay Tembume, "Design Low Power Quaternary Adder Using Multi-Value Logic," *International Journal Of Advancement in Engineering Technology, Management and Applied Science (IJAETMAS)*, vol. 03(07), pp. 181-187, 2016.
- [3] M.H Moaiyeri, A. Doostaregan, K. Navi, "Design of energy efficient and robust ternary circuits for nanotechnology," *IET Circuits Devices Syst.* vol. 5(4), pp. 285-296, 2011.
- [4] Ramzi Jaber and Ali HAIDAR "Ternary Data Transmission between Hosts", the 23rd International Scientific Conference LAAS, 6 – 7 April 2017, Beirut, Lebanon.
- [5] Ouseily, H. and Haidar, A. M. "Hexadecimal to Binary Conversion Using Multi-Input Floating Gate Complementary Metal Oxide Semiconductors", the proceeding of International Conference on Applied Research in Computer Science and Engineering. ICAR 2015, 8 – 9 October 2015.
- [6] Haidar, A., N. El Ahdab, H. Shirahama, A. Alaeldine "Multiple-Valued Logic Neuron Clock Transformers", Proceeding of the ITC-CSCC'08 (The International Technical Conference on Circuit, Systems, Computers and Communications), Shimonoseki, Japan, July 2008.
- [7] D. A. Rich, "A Survey of Multivalued Memories," *IEEE Trans. Computer.*, vol. 35, pp. 99–106, Feb. 1986.
- [8] Y. Yasuda, Y. Tokuda, S. Zaima, K. Pak, T. Nakamura, and A. Yoshida, "Realization of Quaternary Logic Circuits by n-channel MOS Devices," *IEEE Journal of Solid-State Circuits*, vol. 21, pp. 162–168, Feb 1986.
- [9] Murotiya, S.L. and Gupta, A. (2014) 'Design of CNTFET-based 2-bit ternary ALU for nanoelectronics', *International Journal of Electronics*, Vol. 101, No. 9, pp.1244–1257
- [10] Chetan Vudadhaa, M.B.Srinivasb, "Design Methodologies for Ternary Logic Circuits", 2018 IEEE 48th International Symposium on Multiple-Valued Logic, 16-18 May 2018, Linz, Austria.
- [11] Debaprasad Das , Anirban Banerjee , Vikash Prasad, " Design of ternary logic circuits using CNTFET", 2018 International Symposium on Devices, Circuits and Systems (ISDCS), 29-31 March 2018, Howrah, India.
- [12] S. Lin, Y. B. Kim, and F. Lombardi, "CNTFET-Based Design of Ternary Logic Gates and Arithmetic Circuits," *IEEE Transactions on Nanotechnology*, vol. 10, pp. 217–225, March 2011.
- [13] E Daniai, I Michel, "Implementation of Ternary Circuits with Binary Integrated Circuits", *IEEE TRANSACTIONS ON COMPUTERS*, VOL. C-26, No. 12, December 1977.
- [14] M. Suzuki, N. Ohkubo, T. Shinbo, T. Yamanaka, A. Shimizu, K. Sasaki and Y. Nakagome, "A 1.5-ns 32-b CMOS ALU in Double Pass-Transistor Logic," *IEEE Journal of Solid-State Circuits*, vol. 28, no. 11, pp. 1145-1151, November 1993
- [15] Tony R. Kuphaldt "Lessons In Electric Circuits" Volume IV – Digital 2007 <https://www.allaboutcircuits.com/assets/pdf/digital.pdf>.
- [16] Saha Alope, Pal Dipankar, and Chandra Mahesh. Benchmarking of DPL Based 8b×8b Novel Wave-Pipelined Multiplier. In: *Int. J. of Electronics Letters (IJEL)*, Taylor & Francis. 2017; 5(1):115–128(doi: 10.1080/21681724.2016.1175031).

## **Appendix D**

### **A Novel Binary to Ternary Converter using Double Pass-Transistor Logic**



**ICM 2019**

[ABOUT](#)

[CALL FOR CONTRIBUTIONS](#)

[COMMITTEE](#)

[IMPORTANT DATES](#)

[REGISTRATION](#)

[TRAVEL & ACCOMMODATION](#)

# *The 31st International Conference on Microelectronics*

*(ICM 2019) December 15-18*

[CALL FOR PAPER pdf](#)

[SUBMISSION](#)

# A Novel Binary to Ternary Converter using Double Pass-Transistor Logic

Ramzi A. Jaber\*, Ahmad M. El-Hajj, Ali M. Haidar  
*Dept. of Electrical & Computer Engineering*  
*Beirut Arab University (BAU)*  
Debbieh, Lebanon  
{r.jaber\*, a.elhajj, ari}@bau.edu.lb

Abdallah Kassem  
*Dept. of Electrical & Computer Engineering*  
*Notre Dame University (NDU)*  
Louaize, Lebanon  
akassem@ndu.edu.lb

Lina A. Nimri  
*Department of Business Computer*  
*Lebanese University*  
Beirut, Lebanon  
lnimri@ul.edu.lb

**Abstract**—The ternary circuit has an advantage over the binary circuit concerning interconnect complexity, propagation delay, and energy consumption. This paper proposes a novel binary-to-ternary converter using Double Pass-Transistor (DPL) with four bits as input and three trits as output. The importance of this work is gained through its potential to increase the data rate, and reduce power consumption. Also, the proposed converter can be used as a bridge between binary and ternary circuits. The proposed circuit is simulated and tested using Micro-Cap V10 PSPICE simulator with CMOS process technology. It is then compared to different binary-to-ternary converters to conclude that significant improvement achieved.

**Index Terms**—CMOS, Double Pass-Transistor Logic (DPL), Logic circuit, Multi-Valued Logic (MVL), Ternary system.

## I. INTRODUCTION

The limitations in binary circuits are mainly due to a large number of connections, thus requiring a big chip area and a notable increase in energy consumption. Whereas, Multiple-Valued Logic (MVL), has more than two values, helps in reducing the interconnections and the chip area, and energy consumption [1].

For the past decade, MVL has attracted researchers' attention over binary logic, and it has used in several modern application areas such as Electronic Design Automation (EDA) tools to solve binary logic problems [2]. Moreover, MVL can be implemented in communication system [3], cloud vehicular networks [4], wireless sensor networks [5], circuit designs such as Logic Gates, Memory, Memristor circuit [6]–[10], and software (algorithm) [11].

Also, It has proven that radix three (ternary logic) is the most efficient radix in providing less complexity and cost efficiency as compared to other radices [12]. In addition two logic systems are available in ternary logic: balanced ternary logic (-1, 0, 1) correspond to (-V<sub>dd</sub>, 0, V<sub>dd</sub>), and simple ternary logic (0, 1, 2) correspond to (0, V<sub>dd</sub>/2, V<sub>dd</sub>). MVL enables much more data to store in a single digit, such as the decimal number 15 needs four binary digits (bits) to store

while four ternary digits (trits) are enough to store up to decimal number 80 ( $3^4-1$ ).

The design of binary-to-ternary converters has recently constituted an active area of research, and important papers are selected.

To illustrate, in [13], [14], a novel circuit that converts two binary bits to one ternary digit (trit) was proposed. In [15], the authors proposed a novel binary-to-ternary converter based on the Josephson junction (JJ). In [16], the designed converter circuit is characterized by a dual supply operation while in [17] the proposed circuit tailored in the context of Quantum-dot Cellular Automata. Finally, in [18], the authors proposed a novel binary-to-ternary converter based on DPL, which gives the best performance than all mentioned papers above.

All the aforementioned binary-to-ternary converters suffer from high power consumption [15], [16], large propagation delay [16], [18], complex circuit [16], [17] or even errors in the output when two binary inputs are set as high level voltage [13], [14].

Therefore, this paper proposes a novel binary-to-ternary converter which provides a drastic reduction in power consumption compared to circuits employing CMOS technology; also it lowers the propagation delay and provides a small, simple and error-free circuit implementation (for all possible inputs).

The proposed circuit converts four binary bits to three ternary trits by using Double Pass-Transistor Logic (DPL), and it is simulated using Micro-Cap V10 PSPICE simulator, demonstrates a notable reduction in devices count, propagation delay, and energy consumption.

The rest of the paper is organized as follows: A background of DPL presented in Section II. The proposed conversion approach described in Section III, Simulation results, and comparisons discussed in Section IV, followed by concluding remarks in section V.

## II. DOUBLE PASS-TRANSISTOR LOGIC (DPL)

As shown in Fig.1, DPL [19] is a modified version of complementary pass-transistor logic (CPL) by adding PMOS transistors in parallel with the NMOS transistors to eliminate the problems of noise margin and speed degradation at reduced supply voltages associated in CPL circuits. Besides, basic logic gates using DPL ideally have identical propagation delay so that it can use for time-equalized applications such as wave pipelining.

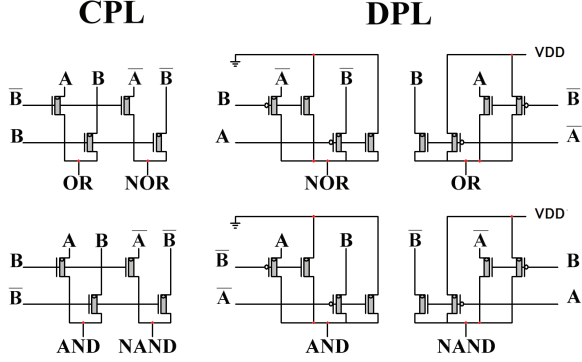


Fig. 1. DPL Gates Design [19]

## III. PROPOSED CONVERSION CIRCUIT

A novel four to three binary-to-ternary converter model is designed Fig.2.

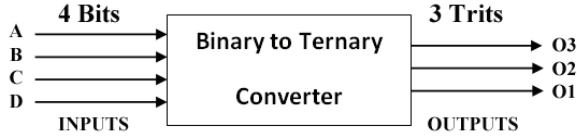


Fig. 2. binary-to-ternary model

As shown in Fig.2, four binary bits provide as input (A, B, C, D). The input “A” is the most significant bit (MSB), and the input “D” is the least significant bit (LSB). Three trits provided as output (O3, O2, O1). The output “O3” is the most significant trit (MST), and “O1” is the least significant trit (LST), using simple ternary logic (0, 1, 2).

Among the 27 trits combinations, only 16 used to represent all the four-bit combinations while the remaining 11 could be used for additional features such as error detection.

The 16 combinations that could produce in the converter circuit are shown in Table I. The voltage supply used in the proposed circuit is 1.8V to decrease power consumption. Therefore, DPL is used to eliminate the noise, as described in Section II.

Binary digits are (0: Low, and 1: High) and Ternary trits are (0: Low, 1: Medium, and 2: High). This paper will use, “0” represents low-level voltage (0V), “1” represents medium-level voltage (0.9V), and “2” represents high-level voltage (1.8V) for the both binary and ternary system.

TABLE I  
BINARY-TO-TERNARY TRUTH TABLE

Decimal	Binary Inputs				Ternary Outputs		
	A	B	C	D	O3	O2	O1
0	0	0	0	0	0	0	0
1	0	0	0	2	0	0	1
2	0	0	2	0	0	0	2
3	0	0	2	2	0	1	0
4	0	2	0	0	0	1	1
5	0	2	0	2	0	1	2
6	0	2	2	0	0	2	0
7	0	2	2	2	0	2	1
8	2	0	0	0	0	2	2
9	2	0	0	2	1	0	0
10	2	0	2	0	1	0	1
11	2	0	2	2	1	0	2
12	2	2	0	0	1	1	0
13	2	2	0	2	1	1	1
14	2	2	2	0	1	1	2
15	2	2	2	2	1	2	0

The procedure to build the proposed circuit starts with a novel technique by decomposition each ternary output in Table I to two intermediate binary outputs, as shown in Table II and Table III.

TABLE II

Decomposition O1 to two intermediate Binary Outputs		
Ternary Output	Intermediate Binary Outputs	
O1	O1a	O1b
Logic 0 (0V)	0	0
Logic 1 (0.9V)	0	2
Logic 2 (1.8V)	2	0

TABLE III  
DECOMPOSITION OF THE THREE TERNARY OUTPUTS

Binary Inputs				Ternary Outputs as Intermediate Binary				
A	B	C	D	O3	O2		O1	
				O3b	O2a	O2b	O1a	O1b
0	0	0	0	0	0	0	0	0
0	0	0	2	0	0	0	0	2
0	0	2	0	0	0	0	2	0
0	0	2	2	0	0	2	0	0
0	2	0	0	0	0	2	0	2
0	2	0	2	0	0	2	2	0
0	2	2	0	0	2	0	0	0
0	2	2	2	0	2	0	0	2
2	0	0	0	0	2	0	2	0
2	0	0	2	2	0	0	0	0
2	0	2	0	2	0	0	0	2
2	0	2	2	2	0	0	2	0
2	2	0	0	2	0	2	0	0
2	2	0	2	2	0	2	0	2
2	2	2	0	2	0	2	2	0
2	2	2	2	2	2	0	0	0

The second step involves using Karnaugh maps to get an optimized circuit for each intermediate outputs in Table III. The minimization process results in equations 1- 5.

$$O1a = \bar{A}\bar{B}C\bar{D} + \bar{A}B\bar{C}D + A\bar{B}\bar{C}\bar{D} + A\bar{B}C\bar{D} + A\bar{B}C\bar{D} \quad (1)$$

$$O1b = \bar{A}\bar{B}\bar{C}D + \bar{A}B\bar{C}\bar{D} + \bar{A}B\bar{C}D + A\bar{B}\bar{C}\bar{D} + A\bar{B}\bar{C}D \quad (2)$$

$$O2a = \bar{A}BC + \bar{A}B\bar{C}D + BCD + \bar{A}\bar{B}\bar{C}\bar{D} \quad (3)$$

$$O2b = \bar{B}\bar{C} + A\bar{B}\bar{D} + \bar{A}\bar{B}CD \quad (4)$$

$$O3b = AB + AC + AD \quad (5)$$

The resulting equations are implemented in the binary-to-ternary converter circuit shown in Fig. 3.

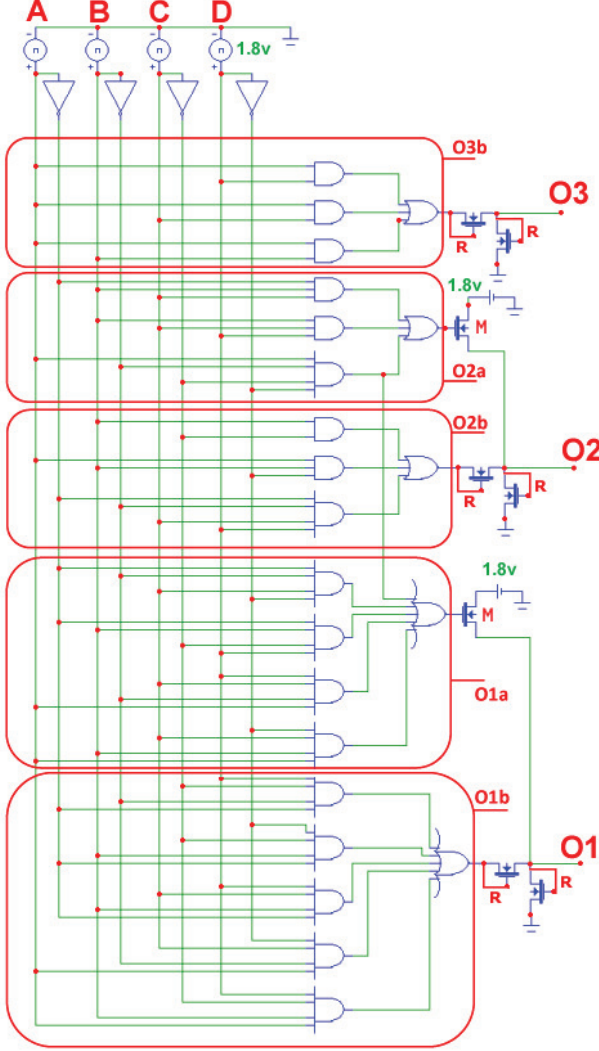


Fig. 3. Proposed binary-to-ternary Converter Circuit

Fig.3 represents the binary-to-ternary converter with four binary inputs (A, B, C, D) and three ternary outputs (O1, O2, O3). The intermediate binary outputs labeled as O1a, O1b, O2a, O2b, and O3b.

An enhancement MOSFET (M) used as a switch with its input (O1a, O2a). When O1a or O2a is at high-level voltage, then the transistor M will be turned "ON" to pass the 1.8 volts to final output O1, and it will be "OFF" when the O1a or O1b is a low-level voltage.

Similarity, two transistors (R) added after intermediate outputs (O1b, O2b, O3b), that act as a voltage divider. For

TABLE IV  
COMBINATION OF TERNARY OUTPUT O1

O1a	O1b	Transistor (M)	(2 Rs)	O1
0V	0V	OFF	Req	0V (Logic 0)
0V	1.8V	OFF	Divider	0.9V (Logic 1)
1.8V	0V	ON	Req	1.7V (Logic 2)
1.8V	1.8V	<b>This Case Does Not Exist*</b> <b>Whereas, in [13] and [14] have errors</b>		

example, when O1b is equal to 1.8V, then the output O1 is equal to 0.9V. When O1b is equal to 0V and O1a is equal to 1.8V, then the two transistors (Rs) will become two parallel resistors with equivalent resistance (Req) which will drop the output voltage O1 to 1.7V, as described in Table IV.

The same procedure will be done for output (O2) and (O3).

\* The proposed design has a notable advantage over previous converter designs in [13] and [14] since no error occurs for any input combination. As demonstrated in Tables III and IV, the intermediate binary outputs Oia, and Oib (i=1, 2) cannot be high at the same time which offers a significant advantage in simplifying the circuit.

The numbers count of devices in the proposed circuit calculated in Table V.

TABLE V  
DEVICE COUNT IN PROPOSED CIRCUIT (FIG.3)

Device Name	No. of devices	No. of Transistors	Subtotal
Inverter Gate	4	1 input *2 =2	8
2 inputs AND Gate	2	2 inputs *2 = 4	8
3 inputs AND Gate	3	3 inputs *2 = 6	18
4 inputs AND Gate	11	4 inputs *2 = 8	88
3 inputs OR Gate	3	3 inputs *2 = 6	18
5 inputs OR Gate	2	5 inputs *2 = 10	20
MOSFET	8	1	8
Internal Resistor (one per each gate Fig.1)			25
Internal Capacitor (one per each gate Fig. 1)			25
<b>Total No. ofDevices</b>			<b>218</b>

#### IV. SIMULATION RESULTS AND COMPARISONS

In [18], the authors proposed a novel binary-to-ternary converter based on DPL, which gives the best performance than binary-to-ternary converters in [13]–[17].

Therefore, the proposed converter will be compared to the latest converter circuit designs described in [18].

For fair comparisons, both circuits are implemented, simulated, and analyzed using the same software Micro-Cap V10 PSPICE Simulator with CMOS technology 0.18  $\mu\text{m}$ .

The simulated circuits utilize an implementation of the AND and OR DPL gates as previously described in [19] and shown in Fig.1. With a temperature of 25°C, average propagation delay (42.56 ps), and the average power (4.08  $\mu\text{w}$ ), as states in [20].

Fig.4 shows the simulation transient analysis of the proposed circuit with a temperature of 25°C, power supply (1.8V), and frequency (5GHz).

The following performance metrics will be used to compare to [18]: the frequency, the device count inside the circuit, the

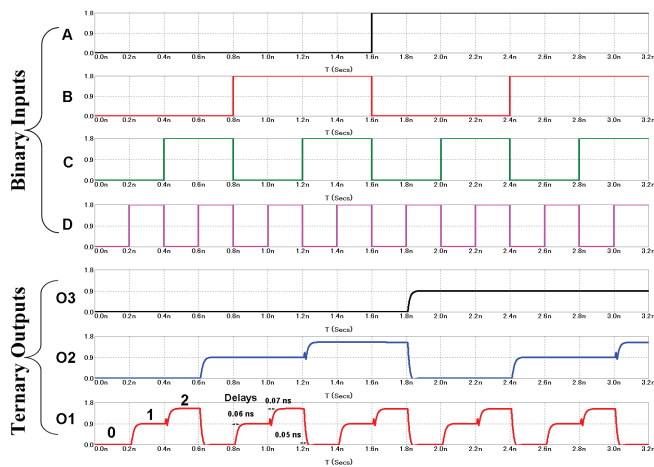


Fig. 4. The simulation transient analysis of proposed circuit

maximum propagation delay, the average power consumption, the maximum energy consumption, and the type of used logic gates.

The propagation delays in the proposed circuit are: From ternary “0” to “1” is 0.06 ns, from “1” to “2” is 0.07 ns and from “2” to “0” is 0.05 ns.

From the simulator, the average power consumption of the proposed circuit is 349.9  $\mu\text{W}$ .

Table VI summarizes that comparison.

TABLE VI  
COMPARISON TO THE LATEST NOVEL CONVERTER IN [18]

	Converter [18]	Proposed	Improvement
Frequency	0.33 GHz	5 GHz	1415%
Device Count	426	218	48.83%
MAX. Delay	0.91 ns	0.07 ns	92.31%
Avg. Power	270.42 $\mu\text{W}$	349.9 $\mu\text{W}$	-29.4%
MAX. Energy	246 $10^{-18}\text{J}$	24.5 $10^{-18}\text{J}$	90%
Type of used gates	Ternary & binary gates	binary gates	Faster, as [21]

The proposed (4:3) converter is bigger than the latest (3:2) converter in [18]. Despite that, the proposed converter gets better results compared to [18], as shown in Table VI.

## V. CONCLUSION

This paper proposes a binary-to-ternary converter with novel techniques. The proposed approach takes four bits and produces three trits using Double Pass-Transistor (DPL). The circuit designed and simulated using Micro-Cap V10 PSPICE simulator. Finally, logical analysis and simulation results demonstrate the merits of the approach in terms of reduced latency and energy consumption compared to other converters.

## REFERENCES

- [1] S. Hosseini, S. Etezadi, A novel very low-complexity multi-valued logic comparator in nanoelectronics, Springer Circuits, Systems, and Signal Processing 2 (June 2019) 1 – 22, <https://doi.org/10.1007/s00034-019-01158-2>.
- [2] D. Miller, M. Thornton, Multiple Valued Logic: Concepts and Representations., 12, Morgan & Claypool, San Rafael, CA, USA, 2008.
- [3] M. Abdelaziz, T. Gulliver, Ternary trellis coded modulation, IEEE Access 7 (April 2019) 49027 – 49038, <https://doi.org/10.1109/ACCESS.2019.2909707>.
- [4] Q. Yanq, B. Zhu, S. Wu, An architecture of cloud-assisted information dissemination in vehicular networks, IEEE Access 4 (May 2016) 2764 – 2770, <https://doi.org/10.1109/ACCESS.2016.2572206>.
- [5] N. Saleh, A. Kassem, A. Haidar, Energy-efficient architecture for wireless sensor networks in healthcare applications, IEEE Access 6 (Jan. 2018) 6478 – 6486, <https://doi.org/10.1109/ACCESS.2018.2789918>.
- [6] R. Jaber, A. El-Hajj, L. Nimri, A. Haidar (Eds.), A Novel implementation of ternary decoder using CMOS DPL binary gates, 2018 Int. Arab Conf. on Information Technology (ACIT), IEEE, Werdanye, Lebanon, 2018, <https://doi.org/10.1109/ACIT.2018.8672698>.
- [7] R. Jaber, A. Kassem, A. El-Hajj, L. Nimri, A. Haidar, High-performance and energy-efficient cnfet-based designs for ternary logic circuits, IEEE Access 7 (July 2019) 93871 – 93886, <https://doi.org/10.1109/ACCESS.2019.2928251>.
- [8] L. Sardinha, D. Silva, M. Vieira, L. Vieira, O. Neto, Tcam/cam-qca: (ternary) content addressable memory using quantum-dot cellular automata, Microelectronics Journal 46 (7) (July 2015) 563–571, <https://doi.org/10.1016/j.mejo.2015.03.020>.
- [9] N. Soliman, M. Fouda, A. Alhurbi, L. Said, A. Madian, A. Radwan, Ternary functions design using memristive threshold logic, IEEE Access 7 (April 2019) 48371–48381, <https://doi.org/10.1109/ACCESS.2019.2909500>.
- [10] N. Soliman, M. Fouda, A. Radwan, Memristor-cntfet based ternary logic gates, Microelectronics Journal 72 (Feb. 2018) 74–85, <https://doi.org/10.1016/j.mejo.2017.12.008>.
- [11] D. Miller, M. Soeken (Eds.), A spectral algorithm for ternary function classification, Vol. 1 of 1, IEEE 48th Int. Symp. on Multiple-Valued Logic (ISMVL), IEEE, Linz, Austria, 2018.
- [12] S. Hurst, S. Etezadi, Multiple-valued logic its status and its future, IEEE Transactions on Computers 133 (1) (Dec. 1984) 1160 – 1179, <https://doi.org/10.1109/TC.1984.1676392>.
- [13] T. Kurt M, “binary to ternary converter”, US Patent 3,217,316, <https://patents.google.com/patent/US3217316A/en> (12 1961).
- [14] Y. Nakanishi, T. Kawaguchi, M. Sekiya, “pulse synthesizing circuit”, US Patent 9,287,867, <https://patents.google.com/patent/US9287867B2/en> (2016).
- [15] F. Li, M. Morisue, T. Ogata, “a proposal of josephson binary-to-ternary converter”, IEEE Transactions on Applied Superconductivity Vol.5 (2) (1995) 2632–2635.
- [16] B. Zlatko, D. Bundalo, F. Softic, M. Kostadinovic (Eds.), “Interconnection of binary and ternary CMOS digital circuits and systems”, Vol. 1 of 1, The 33rd International Convention MIPRO, IEEE, Opatija, Croatia, 24-28 May 2010.
- [17] A. Mohsen M., M. Soryani, K. Navi, M. Tehrani (Eds.), “A novel ternary-to-binary converter in quantum-dot cellular automata”, Vol. 1 of 1, 2012 IEEE Computer Society Annual Symposium on VLSI, IEEE, Amherst, MA, USA, 19-21 Aug. 2012.
- [18] S. Aloke, P. Dipankar, “dpl-based novel binary-to-ternary converter on cmos technology”, AEU - International Journal of Electronics and Communications Vol.92 (1) (August 2018) 69–73.
- [19] M. Suzuk, N. Ohkubo, T. Shinbo, T. Yamanaka, K. Shimizu, Y. Nakagome (Eds.), “A 1.5 ns 32 b CMOS ALU in double pass-transistor logic”, Vol. 1 of 1, 1993 IEEE International Solid-State Circuits Conference Digest of Technical Papers, IEEE, San Francisco, CA, USA, 24-26 Feb. 1993.
- [20] S. Aloke, D. Pal, M. Chandra, “benchmarking of dpl-based 8b  $\times$  8b novel wave-pipelined multiplier”, International Journal of Electronics Letters Vol.5 (1) (2017) 115–128.
- [21] E. Danial, I. Michel, “implementation of ternary circuits with binary integrated circuits”, IEEE Transactions on Computers Vol.26 (12) (1977) 291 – 300.

## **Appendix E**

# **Ternary Data Transmission Between Hosts**

# LAAS

## 23rd International Scientific Conference

# Research and

# Science

# in the Service of

# Humanity

April 6-7, 2017

Faculty of Science  
Lebanese University

[www.fsciences.ul.edu.lb/laas23](http://www.fsciences.ul.edu.lb/laas23)

# Ternary Data Transmission Between Hosts

**Ramzi Ali JABER**

Depart.of Electrical & Computer Eng.  
Beirut Arab University  
Beirut, Lebanon  
[r.jaber@bau.edu.lb](mailto:r.jaber@bau.edu.lb)

**Lina Nimri**

Depart.of Business Computer  
Lebanese University  
Beirut, Lebanon  
[lnimri@ul.edu.lb](mailto:lnimri@ul.edu.lb)

**Ali Massoud Haidar**

Depart.of Electrical & Computer Eng.  
Beirut Arab University  
Beirut, Lebanon  
[ari@bau.edu.lb](mailto:ari@bau.edu.lb)

**Abstract**—there is limitation in Binary Data Transmission at Physical Layer in cable Connections between hosts (Computers, Hubs, Switches and Routers). In this paper we create a physical circuits to convert from Binary to Ternary and then from Ternary to Binary. After using these conversion the data is encrypted in transmission line and also the number of wires will reduce from 8 wires to 6 wires so we profit 25% from wires cost.

**Keywords**—Networking, Cabling, Physical Layer, Ternary, MVL, Multi-Valued Logic, Data Transmission.

## I- INTRODUCTION

Intel Company & Many researchers believe that the binary logic is *already doomed* because of: 1-Moore's Law 1965 (Transistors will double every two years); 2- we cannot shrink sizes of transistors indefinitely.

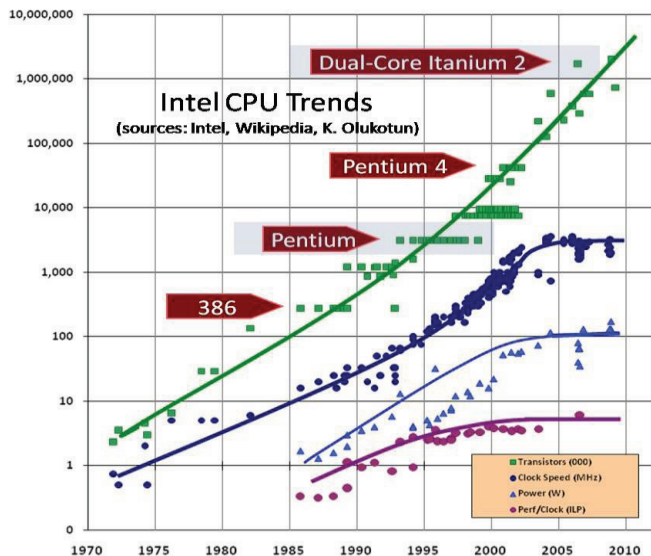


Fig. 1, Limitation of Clock Speed

For that reason we want to rethink to use Multi-Valued Logic system instead of binary system if we can. We use in this paper Ternary Data transmission at physical layer between hubs, switches and routers.

## II- HOW IT WORKS

In Cat 5 cable there are four twisted pairs, two pairs for sending data and two pairs to receiving data.

### A) Sender Side:

Four wires will send the data at physical layer so we have 16 ( $2^4$ ) combinations of binary digits : 0 for 0 volt, 1 for 5 volt. We mapping them to Ternary trits. We use karnaugh map to design logic circuits.

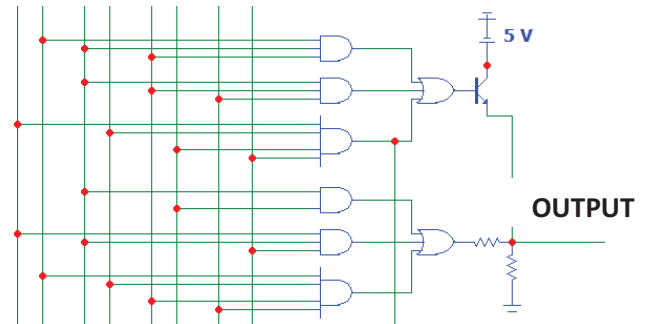


Fig. 2, portion from design model

We use 4 bits and their compliments entering logic AND Gates then OR Gates. At the above part there is transistor to pass only 5 volt state and open for 0 volt state.

At the lower part there is voltage divider to divide 5 volt into 2.5 volt. After this we will get ternary trits : 0 for 0 volt, 1 for 2.5 volt, 2 for 5 volt. So we get 3 wires instead of 4 wires.

### B) Receiver Side:

Now at each wire will be one of three states (0 or 1 or 2) (0 volt or 2.5 volt or 5 volt).

To convert them again to binary, we must do it into two steps (ie. Two circuits).

#### Step 1:

We create a circuit to convert 3 ternary wires into 5 binary wires.

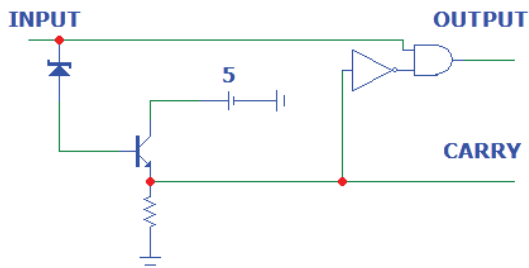


Fig. 3, Convert from ternary to binary

Ternary Wire	Binary	
	Carry	Output
0 (0 volt)	0	0
1 (2.5 volt)	0	1 (5 volt)
2 (5 volt)	1	0

TABLE 1, Conversion Table

We use 2.5 volt zener diode to filter the three voltages, when we have 0 or 2.5 volt as input the transistor will stay open so we get 0 or 5 volt at the output and if we have 5 volts as input then the transistor will operate and we get 0 for output and 5 volt for carry.

We have three wires as inputs, the first and the second wire have three states while the third wire has only two states 0 volt or 2.5 volt, so at final we will have 5 wires.

#### Step 2:

After we got 5 wires we will use five input karnaugh map to convert to 4 wires binary.

### III- Conclusion

In this paper a new concept has been proposed, Digital logic design based on binary system has been in use for long time. With phenomenal increase in circuit sizes, working with binary logic system is becoming increasingly complex. A Multiple-Valued Logic system reduces the significant amount of design effort, reduces the power consumption, increases the data transmission rate between devices and reduced the wires cost.

### REFERENCES

1. Y. Iijima and Y. Yuminaka, "Double-Rate Equalization Using Tomlinson-Harashima Precoding for Multi-Valued Data Transmission", ISMVL 2016 -46 th IEEE International Symposium on Multiple-Valued Logic
2. Yasushi Yuminaka, Masaaki Okui, "Efficient Data Transmission Using Multiple-Valued Pulse-Position Modulation 2012 IEEE 42nd International Symposium on Multiple-Valued Logic
3. A. M. Haidar, R. Dernaika, F. Shibani, "A Novel Ternary Quadrature Amplitude Modulation 2006 2nd IEEE International Conference on Information & Communication Technologies
4. A. M. Haidar, S. Ghabboura, N. Ahdab, "A Novel Multi-Valued Logic QAM" 2006 2nd IEEE International Conference on Information & Communication Technologies.

# Bibliography

- [1] D. E. Knuth. *The Art of Computer Programming: Seminumerical Algorithms*, volume 2. Addison-Wesley Pub (Sd), 2nd edition, 1981. ISBN 0201038226,9780201038224. pp. 190-193.
- [2] K. C. Smith. The prospects for multivalued logic: A technology and applications view. *IEEE Transactions on Computers*, 30(9):619–634, 1981. URL <https://doi.org/10.1109/TC.1981.1675860>.
- [3] S.A. Hosseini and S. Etezadi. A novel very low-complexity multi-valued logic comparator in nanoelectronics. *Springer Circuits, Systems, and Signal Processing*, 2:1–22, 2019. URL <https://doi.org/10.1007/s00034-019-01158-2>.
- [4] G. Ifrah. *The Universal History of Numbers. From Prehistory to the Invention of the Computer*. John Wiley & Sons, New York, 2000. ISBN 0-471-39340-1.
- [5] E.L. Post. Introduction to a general theory of elementary propositions. *Amer. J. Math*, 43:163–185, 1921. URL <https://doi.org/10.2307/2370324>.
- [6] N. Brusentsov and J.R. Alvarez. Ternary computers: The setun and the setun 70. pages 74–80, Berlin, Heidelberg, 2006. Springer, Perspectives on Soviet and Russian Computing (SoRuCom).
- [7] G. Moore. *Understanding Moore’s Law: Four Decades of Innovation (Chapter 7)*. Brock, David (ed.), New York, 2006. ISBN 978-0-941901-41-3.
- [8] D. Miller and M. Soeken. A spectral algorithm for ternary function classification. Linz, Austria, 2018. IEEE 48th Int. Symp. on Multiple-Valued Logic (ISMVL).

- [9] J. Chen, Y. Chen, C. Feng, Y. Huang, and R. Chen. Some new classes of entanglement-assisted quantum mds codes derived from constacyclic codes. *IEEE Access*, 7:91679 – 91695, 2019. URL <https://doi.org/10.1109/ACCESS.2019.2927294>.
- [10] N. Saleh, A. Kassem, and A.M. Haidar. Energy-efficient architecture for wireless sensor networks in healthcare applications. *IEEE Access*, 6:6478 – 6486, 2018. URL <https://doi.org/10.1109/ACCESS.2018.2789918>.
- [11] Q. Yang, B. Zhu, and S. Wu. An architecture of cloud-assisted information dissemination in vehicular networks. *IEEE Access*, 4:2764–2770, 2016. URL <https://doi.org/10.1109/ACCESS.2016.2572206>.
- [12] M. Abdelaziz and T.A. Gulliver. Ternary trellis coded modulation. *IEEE Access*, 7:49027 – 49038, 2019. URL <https://doi.org/10.1109/ACCESS.2019.2909707>.
- [13] M. Toulabinejad, M.R. Taheri, K. Navi, and N. Bagherzadeh. Toward efficient implementation of basic balanced ternary arithmetic operations in cnfet technology. *Microelectronics Journal*, 90:267–277, 2019. URL <https://doi.org/10.1016/j.mejo.2019.05.010>.
- [14] M. Abdelaziz and T.A. Gulliver. G-aetcam: gate-based area-efficient ternary content-addressable memory on fpga. *IEEE Access*, 5:20785 – 20790, 2017. URL <https://doi.org/10.1109/ACCESS.2017.2756702>.
- [15] N. Soliman, M.E. Fouda, A.G. Alhurbi, L.A. Said, A.H. Madian, and A.G. Radwan. Ternary functions design using memristive threshold logic. *IEEE Access*, 7:48371–48381, 2019. URL <https://doi.org/10.1109/ACCESS.2019.2909500>.
- [16] S.L. Hurst. Multiple-valued logic its status and its future. *IEEE Transactions on Computers*, 133(1):1160–1179, 1984. URL <https://doi.org/10.1109/TC.1984.1676392>.
- [17] J.R. Gordon. *Transistor circuit techniques: discrete and integrated*. CRC Press, 2003. ISBN 0748740759,9780748740758.

- [18] P. Valizadeh. *FET A COMPREHENSIVE OVERVIEW: From Basic Concepts to Novel Technologies*. John Wiley & Sons, Inc., Canada, 2016. ISBN 978-1-119-15549-2.
- [19] O.T. Rasit and H.-S. Philip. *Beyond-CMOS Technologies for Next Generation Computer Design*. Springer International Publishing, 2019. ISBN 978-3-319-90384-2;978-3-319-90385-9.
- [20] D. Sudeb, K. Brajesh, and K.P. Pankaj. *Spacer engineered FinFET architectures : high-performance digital circuit applications*. CRC Press, 2017. ISBN 9781351751049,1351751042,1498783597,978-1-4987-8359-0.
- [21] G. Hills, M.G. Bardon, G. Doornbos, D. Yakimets, P. Schuddinck, R. Baert, D. Jang, L. Mattii, S.Y. Sherazi, D. Rodopoulos, R. Ritzenthaler, C.-S. Lee, A. Thean, I. Radu, A. Spessot, P. Debacker, F. Catthoor, P. Raghavan, M. Shulaker, H.-S. Philip Wong, and S. Mitra. Understanding energy efficiency benefits of carbon nanotube field-effect transistors for digital VLSI. *IEEE Transactions on Nanotechnology*, 17(6):1259–1269, 2018. URL <https://doi.org/10.1109/TNANO.2018.2871841>.
- [22] Stanford university cnfet model website [online], Accessed: August, 16 2019. URL <http://nano.stanford.edu/model.php?id=23>.
- [23] J. Deng and H.-S. P. Wong. A compact spice model for carbon-nanotube field-effect transistors including nonidealities and its application - part i: model of the intrinsic channel region. *IEEE Transactions on Electron Devices*, 54(12):3186–3194, 2007. URL <https://doi.org/10.1109/TED.2007.909030>.
- [24] J. Deng and H.-S. P. Wong. A compact spice model for carbon-nanotube field-effect transistors including nonidealities and its application - part ii: full device model and circuit performance benchmarking. *IEEE Transactions on Electron Devices*, 54(12): 3195–3205, 2007. URL <https://doi.org/10.1109/TED.2007.909043>.
- [25] J.P. Deschamps, E. Valderrama, and L. Terés. *Digital Systems: From Logic Gates to Processors*. Springer International Publishing, 2017. ISBN 978-3-319-41198-9,978-3-319-41197-2.

- [26] D. M. Miller and M. A. Thornton. *Multiple Valued Logic: Concepts and Representations*. Morgan & Claypool, San Rafael, CA, USA, 2008. URL <https://doi.org/10.2200/S00065ED1V01Y200709DCS012>.
- [27] S. Lin, Y.B. Kim, and F. Lombardi. Cntfet-based design of ternary logic gates and arithmetic circuits. *IEEE Transactions on Nanotechnology*, 10:217–225, 2011. URL <https://doi.org/10.1109/TNANO.2009.2036845>.
- [28] M. Suzuki, N. Ohkubo, T. Shinbo, T. Yamanaka, K. Shimizu, and Y. Nakagome, editors. *A 1.5 ns 32 b CMOS ALU in double pass-transistor logic*, volume 1 of 1, San Francisco, CA, USA, 24-26 Feb. 1993. IEEE International Solid-State Circuits Conference Digest of Technical Papers, IEEE.
- [29] E. Shahrom and S. A. Hosseini. A new low power multiplexer based ternary multiplier using cntfets. *AEU - International Journal of Electronics and Communications*, 93(1): 191–207, 2018. URL <https://doi.org/10.1016/j.aeue.2018.06.011>.
- [30] A.L. Zimpeck, C. Meinhardt, L. Artola, G. Hubert, F.L. Kastensmidt, and R.A.L. Reisa. Impact of different transistor arrangements on gate variability. *Microelectronics Reliability*, 88:111–115, Sept. 2018. <https://doi.org/10.1016/j.microrel.2018.06.090>.
- [31] R.A. Jaber, A. Kassem, A.M. El-Hajj, L.A. Nimri, and A.M. Haidar. High-performance and energy-efficient cnfet-based designs for ternary logic circuits. *IEEE Access*, 7:93871 – 93886, July 2019. <https://doi.org/10.1109/ACCESS.2019.2928251>.
- [32] R.A. Jaber, A. Kassem, A.M. El-Hajj, L.A. Nimri, and A.M. Haidar. Cnfet-based designs of ternary half-adder using a novel "decoder-less" ternary multiplexer based on unary operators. *Microelectronics Journal*, 36, Feb. 2020. <https://doi.org/10.1016/j.mejo.2019.104698>.
- [33] H.T. Mouftah. A study on the implementation of three-valued logic. Logan, Utah, USA, 1976. MVL '76 Proceedings of the sixth international symposium on Multiple-valued logic.

- [34] A. Lloris, A. Prieto, and J. Velasco. C.m.o.s. circuit for implementation of unary operators in ternary logic. *IET-Electronics Letters*, 16(5):161–162, 1980. URL <https://doi.org/10.1049/el:19800115>.
- [35] A. Lloris, A. Cobo, and A. Prieto. Implementation of the unary operators in ternary logic : A universal cmos circuit. *International Journal of Electronics*, 52(4):307–311, 1982. URL <https://doi.org/10.1080/00207218208901433>.
- [36] B. Srinivasu and K. Sridharan. A synthesis methodology for ternary logic circuits in emerging device technologies. *IEEE Transactions on Circuits and Systems I: Regular Papers*, 64(8):2146–2159, 2017. URL <https://doi.org/10.1109/TCSI.2017.2686446>.
- [37] H. Samadi, A. Shahhoseini, and F. Aghaei-liavali. A new method on designing and simulating cntfet-based ternary gates and arithmetic circuits. *Microelectronics Journal, Elsevier*, 63:41–48, 2017. URL <https://doi.org/10.1016/j.mejo.2017.02.018>.
- [38] S. Tabrizchi, M.R. Taheri, K. Navi, and N. Bagherzadeh. Novel cnfet ternary circuit techniques for high-performance and energy-efficient design. *IET Circuits, Devices & Systems*, 13(2):193–202, 2019. URL <https://doi.org/10.1049/iet-cds.2018.5036>.
- [39] T. Ndjountche. *Digital Electronics, Volume 1: Combinational Logic Circuits*. Electronics Engineering. Wiley-ISTE, 1 edition, 2016. ISBN 1848219849,9781848219847.
- [40] K. Sridharan, S. Gurindagunta, and V. Pudi. Efficient multi-ternary digit adder design in cntfet technology. *IEEE Transactions on Nanotechnology*, 12(3):283–287, 2013. URL <https://doi.org/10.1109/TNANO.2013.2251350>.
- [41] P. Wang, D. Gong, Y. Zhang, and Y. Kang. Ternary 2 - 9 line address decoder realized by cnfet, 2018. U.S. Patent 20180182450.

- [42] D. Das, A. Banerjee, and V. Prasad. Design of ternary logic circuits using cntfet. Howrah, India, 2018. Int. Symp. On Devices, Circuits and Systems (ISDCS). URL <https://doi.org/10.1109/ISDCS.2018.8379661>. pp. 1-6.
- [43] R.A. Jaber, A.M. El-Hajj, L.A. Nimri, and A.M. Haidar, editors. *A Novel implementation of ternary decoder using CMOS DPL binary gates*, Werdanye, Lebanon, Nov. 2018. 2018 Int. Arab Conf. on Information Technology (ACIT), IEEE. <https://doi.org/10.1109/ACIT.2018.8672698>.
- [44] S. Alope, P. Dipankar, and C. Mahesh. Benchmarking of dpl based 8b×8b novel wave-pipelined multiplier. *Int. J. of Electronics Letters (IJEL)*, 5(1):115–128, 2017. URL <https://doi.org/10.1080/21681724.2016.1175031>.
- [45] T. Ndjountche. *Digital Electronics, Volume 2: Sequential and Arithmetic Logic Circuits*. Wiley-ISTE, 1st edition edition, 2016. ISBN 1119329779,9781119329770.
- [46] M. Muglikar, R. Sahoo, and S. K. Sahoo. High-performance ternary adder using cntfet. Coimbatore, India, 2016. 3rd Int. Symp. On Devices, Circuits and Systems (ISDCS). URL <https://doi.org/10.1109/ICDCSyst.2016.7570599>.
- [47] S.A. Ebrahimi, M.R. Reshadinezhad, and A. Bohlooli. A new design method for imperfection-immune cnfet-based circuit design. *Microelectronics Journal*, Jan. 2019. <https://doi.org/10.1016/j.mejo.2019.01.013>.
- [48] G. Balamurugan and N.R. Shanbhag. The twin-transistor noise-tolerant dynamic circuit technique. *IEEE Journal of Solid-State Circuits*, 36(2):273–280, 2001. <https://doi.org/10.1109/4.902768>.
- [49] M.L. Doelz, E.T. Heald, and D.L. Martin. Binary data transmission techniques for linear systems. *Proceedings of the IRE*, 45:656–661, 1957. ISSN 0096-8390. doi: 10.1109/jrproc.1957.278415. URL <http://doi.org/10.1109/jrproc.1957.278415>.

- [50] A. Simmonds. *Data Communications and Transmission Principles: An Introduction*. Macmillan New Electronics. Macmillan Education UK, 1997. ISBN 978-0-333-64689-2,978-1-349-13900-2.
- [51] W.Q. Yan. *Introduction to Intelligent Surveillance: Surveillance Data Capture, Transmission, and Analytics*. Texts in Computer Science. Springer International Publishing, 3rd ed. edition, 2019. ISBN 978-3-030-10712-3,978-3-030-10713-0.
- [52] H. Bidgoli. *The Handbook of Computer Networks, Key Concepts, Data Transmission, and Digital and Optical Networks (Volume 1)*, volume 1. Wiley, 2007. ISBN 0471784583,9780471784586.
- [53] M. Trampel. Binary to ternary converter. US Patent 3,217,316, 12 1961. <https://patents.google.com/patent/US3217316A/en>.
- [54] Y. Nakanishi, T. Kawaguchi, and M. Sekiya. Pulse synthesizing circuit. US Patent 9,287,867, 2016. <https://patents.google.com/patent/US9287867B2/en>.
- [55] F.Q Li, M. Morisue, and T. Ogata. A proposal of josephson binary-to-ternary converter. *IEEE Transactions on Applied Superconductivity*, 5(2):2632–2635, 1995.
- [56] B. Zlatko, D. Bundalo, F. Softic, and M. Kostadinovic, editors. *Interconnection of binary and ternary CMOS digital circuits and systems*, volume 1 of 1, Opatija, Croatia, 24-28 May 2010. The 33rd International Convention MIPRO, IEEE.
- [57] S. Aloke and P. Dipankar. Dpl-based novel binary-to-ternary converter on CMOS technology. *AEU - International Journal of Electronics and Communications*, 92(1): 69–73, August 2018.
- [58] G. Bowles. Ternary/binary converter circuit. US Patent 5,49,898, 1996. <https://patents.google.com/patent/US5498980A/en>.
- [59] V. Harish. Ternary and quaternary logic to binary bit conversion cmos integrated circuit design using multiple input floating gate mosfets, 2002. LSU Master’s Theses. <https://digitalcommons.lsu.edu/gradschooltheses/2548>.

- [60] S. Ratna. Ternary to binary converter design in cmos using multiple input floating gate mosfets, 2009. LSU Master's Theses. [digitalcommons.lsu.edu/gradschooltheses/3963](http://digitalcommons.lsu.edu/gradschooltheses/3963).
- [61] A. M. Haidar, H. Oseily, E. Nassar, and H. Shirahama, editors. *Quirmary Coded Decimal Conversion Techniques*, Bruges, Belgium, October 2005. The Proceeding of the NOLTA 2005.
- [62] H. Oseily and A. M. Haidar, editors. *Octal to Binary Conversion Using Multi-Input Floating Gate CMOS*, Iasi, Romania, June 30 – July 1 2011. The Proceeding of the 10-th International Symposium on Signals, Circuits and Systems. ISSCS 2011.
- [63] H. Oseily and A. M. Haidar, editors. *Hexadecimal to Binary Conversion Using Multi-Input Floating Gate Complementary Metal Oxide Semiconductors*, 8 – 9 October 2015. The proceeding of International Conference on Applied Research in Computer Science and Engineering (ICAR).
- [64] A. Mohsen, M. Soryani, K. Navi, and MA. Tehrani, editors. *A novel ternary-to-binary converter in quantum-dot cellular automata*, volume 1 of 1, Amherst, MA, USA, 19-21 Aug. 2012. 2012 IEEE Computer Society Annual Symposium on VLSI, IEEE.
- [65] H. Ito. Ternary valve input circuit, 2011. <https://www.google.com/patents/US8013630>.
- [66] R.A. Jaber, A. Kassem, A.M. El-Hajj, L.A. Nimri, and A.M. Haidar, editors. *A Novel Binary to Ternary Converter using Double Pass-Transistor Logic*, Cairo, Egypt, 15-19 Dec. 2019. 31st International Conference on Microelectronics (ICM 2019), IEEE. <https://doi.org/10.1109/ICM48031.2019.9021886>.
- [67] R.A. Jaber, L.A. Nimri, and A.M. Haidar, editors. *Ternary Data Transmission between Hosts*, Beirut, Lebanon, April 2017. 23rd International Scientific Conference LAAS.
- [68] A. Saha, P. Dipanka, and C. Mahesh. Benchmarking of dpl-based  $8b \times 8b$  novel wave-pipelined multiplier. *International Journal of Electronics Letters*, 5(1):115–128, Feb 2017.

- [69] E. Danial and I. Michel. Implementation of ternary circuits with binary integrated circuits. *IEEE Transactions on Computers*, 26(12):291 – 300, Dec. 1977.